SYNTHESIS, CHARACTERIZATION AND SENSING APPLICATIONS OF NOVEL SCHIFF BASE LIGANDS

Thesis submitted to
the University of Calicut for the award of

DOCTOR OF PHILOSOPHY IN CHEMISTRY

By

MUHAMMED ARSHAD

DEPARTMENT OF CHEMISTRY
UNIVERSITY OF CALICUT
KERALA-673635
MAY-2024

CERTIFICATE

This is to certify that the thesis entitled "**Synthesis, Characterization and Sensing Applications of Novel Schiff base Ligands"** submitted by **Muhammed Arshad** to the University of Calicut for the award of the degree of Doctor of Philosophy in Chemistry, is a record of precise research work carried out at the Department of Chemistry, University of Calicut under my guidance and supervision. The contents of the thesis have been checked for plagiarism using the software 'iThenticate' at C.H.M.K. Library, University of Calicut, and the similarity index falls under the permissible limit. I further certify that the thesis or part has not previously formed the basis for the award of any degree, diploma, or associateship of any other University or Institute.

The corrections/suggestions recommended by the adjudicators have been incorporated in the thesis and the content in the thesis and the soft copy are one and the same.

Dr. Abraham Joseph
Senior professor

University of Calicut

DECLARATION

I, **Muhammed Arshad**, hereby declare that the thesis entitled "**Synthesis, Characterization and Sensing Applications of Novel Schiff base Ligands"** submitted to the University of Calicut is a bonafide record of the research work done by me under the guidance and supervision of **Dr. Abraham Joseph**, Department of Chemistry, University of Calicut and it has not formed the basis for the award of any Degree/Diploma/Associateship/ Fellowship or other similar titles of any other University or Institution. The contents of the thesis have been checked for plagiarism using the software 'iThenticate' at C.H.M.K. Library, University of Calicut, and the similarity index falls under the permissible limit. I also declare that the thesis is free from AI generated contents.

Muhammed Arshad

University of Calicut

ACKNOWLEDGEMENT

It is my immense pleasure and a great privilege to express my sincere gratitude and obligation to my supervisor Dr. Abraham Joseph, Senior Professor, Department of Chemistry, University of Calicut, for his valuable guidance, wholehearted endless support, and suggestions throughout my research work.

I am extremely grateful to Dr. Rajeev S Menon Head of the Department of Chemistry and also to the former HOD Dr. Yahya A.I., for their support in providing research facilities in the department during my Ph.D. program. Also, I wish to express my gratitude to all the faculty members of the Department of Chemistry, University of Calicut for their support. Also, I would like to acknowledge all the non-teaching staff in the department for the valuable help and support.

I have immense pleasure in expressing my sincere gratitude and happiness to my friends Manu Gopinathan and Athira Ajayan for their valuable and positive suggestions that helped me in improving this research work. I also wish to express my heartful thanks to Mr. Shaju Cheriyan. A, Mr. Yusuff Arangoth, (University staff), and Mr. Mahesh. V for their valuable support during my research work. Without our fights, jokes, and vibrant camaraderie, my research life journey would have been dull and incomplete.

I would like to express my sincere thanks to all research scholars, and my research group members, especially to Sr. Asha Thomas, Dr.A.T. Jeeja Rani, Dr. Sowmya. P., Linda Williams, Anila Paul, Vismaya Joseph, A. Athira, T. Sreelakshmi, Anupriya, and Arunima for their support and useful suggestions. I also appreciate my labmates Deepak Joshy,

Anjitha.T, Dr. Jijil. C. P, Lijin Rajan, Shiva Krishna Prakash, and CSIF friends for their wholehearted support during the research period.

I am glad to thank my colleagues, non-teaching staff, and friends of GHSS Valayam and GGVHSS Feroke for their constant source of help and support they had given me throughout my research.

I am also thankful to CSIF - University of Calicut, STIC - Cochin University, NIT-Calicut, and *NIIST-Thiruvananthapuram for doing my analysis, which facilitated in completion of the research work on time.*

I am deeply indebted to my parents and family, especially my mother for their prayers, care, and support.

I also express my sincere gratitude to all those who have extended their support directly or indirectly for the successful completion of my work.

Above all, I bow to the God Almighty, the most merciful and beneficent for all the blessings for completing this research work successfully.

Muhammed Arshad

CONTENTS

Dedicated to

My Family

Preface

Environmental pollution, caused by a wide range of hazardous organic and inorganic compounds, is one of the most challenging problems facing the current generation and is probably going to be a problem for future generations as well. There is a great need for the precise and sensitive identification of pollutant species because environmental pollution is one of the main threats that eventually affect the health of people, animals, and vegetation. Growing human populations trying to achieve fast economic growth through industrialization, which necessitates massive resource exploitation through farming, fishing, forestry, mining, quarrying, oil and gas extraction, etc, are the main causes of environmental pollution. As a result of industrialization, different contaminants or pollutants present in soil, water, and air may reach a level that is hazardous to humans, animals, and plants. Currently, different traditional analytical and instrumental techniques have been employed for the detection of pollutant species, which demands expensive equipment, lack of portability, challenging multistep sample preparation procedures, difficult on-site operation or monitoring, and highly trained professionals for operation, etc.

Schiff bases are extensively used for the development of colourimetric and luminescence sensors for the detection of analyte species due to easy structural modification, complex formation ability, and attractive photophysical properties. Herein, we have designed and synthesized three different Schiff base receptors

namely, 1,1'-((1E,1'E)- ((2E,2'E)- (1,3-phenylenebis (methanylylide ne)) bis (hydrazine-2,1-diylidene)) bis (methanylylidene)) bis(naphthalen-2-ol)[PMB3], 1-((E)-((E)-(4-(benzyloxy)benzylide ne)hydrazono)methyl)naphthalen-2-ol [BBHN], and 1-((E)-((E)-(anthracen- 9-ylmethylene) hydrazono)methyl) naphthalen-2-ol [AHN], and their chemosensing activity through colourimetric and fluorescence responses have been explored, which offer great selectivity and sensitivity for different analytes of environmental significance.

The thesis is comprised of five chapters carrying a detailed account of the synthesis, characterization, and sensing applications of Schiff bases, excluding the summary and future outlook.

Chapter 1 presents a brief outline of the background of the study, the need for chemosensors, introduction to chemosensors, classification of chemosensors, signalling mechanisms, introduction of Schiff bases, structural and functional diversity of Schiff base and the mechanism of Schiff base formation, *etc*. This chapter also includes a brief review of previous studies related to Schiff bases used for the sensing of metal ions such as Zn^{2+}, Cu^{2+}, Ni^{2+}, and a highly explosive aromatic nitro compound, picric acid.

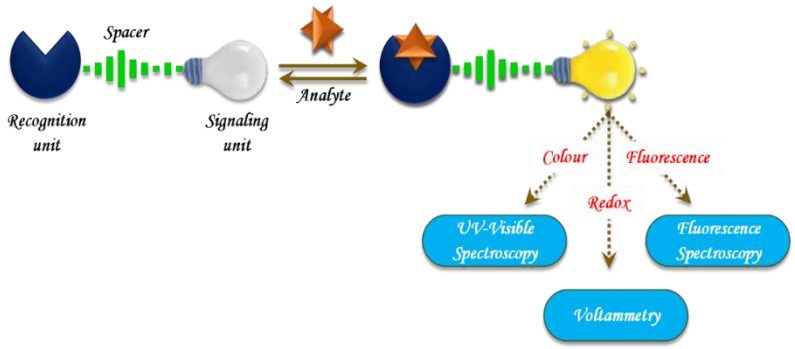

Chapter 2 describes a brief outline of the materials used, the experimental details for the synthesis of Schiff bases (**PMB3, BBHN, AHN**), the analytical procedure, methods of analysis, and instrumental techniques used to characterize the compounds.

The works included in **Chapter 3** are divided into four sections, **3.1, 3.2, 3.3 and 3.4** respectively. **Section 3.1** deals with a novel "OFF-ON-OFF" fluorescent sensor PMB3 for selective detection of Zn^{2+} ion and an *in-situ* produced complex PMB3-Zn^{2+} ensemble for the detection of picric acid (PA). The PMB3 exhibits a significant emission enhancement in intensity with Zn^{2+}, however, the intensity of emission of the *in-situ* produced complex PMB3-Zn^{2+} ensemble is quenched selectively upon the progressive addition of PA. PMB3 displays very selective, sensitive, and rapid changes in fluorescence in the presence of Zn^{2+}. The sensor efficiently binds with Zn^{2+} to form a 1:1 complex, which resulted in significant fluorescence enhancement upon gradual addition while other metal ions do not affect significantly the intensity of the emission. The limit of

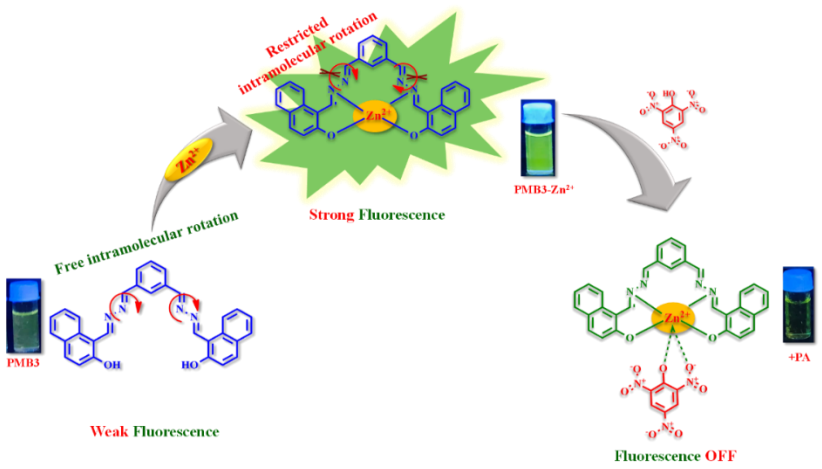

detection of bivalent zinc was 11.12×10^{-7}M. This *in-situ* produced complex PMB3-Zn^{2+} ensemble was observed to be extremely selective for picric acid up to femtomolar level, over other nitroaromatics. The detection limit for picric acid by utilizing the *in-situ* produced PMB3-Zn^{2+} ensemble complex was 42.40×10^{-15}M. This sensor is therefore quite effective in detecting picric acid via turn-off fluorescence.

Section 3.2 discusses the AIEE characteristics of PMB3 and its application for the selective detection of Cu^{2+} in aqueous medium. The PMB3 aggregates display a bright greenish fluorescence and show a fluorescence switch-off response to Cu^{2+} ion in the presence of diverse metal ions with a detection limit of 16.08 fM. These observations clearly divulge that PMB3 aggregates are highly selective to Cu^{2+} ions and hence can be extended for the instant naked-eye detection of Cu^{2+}.

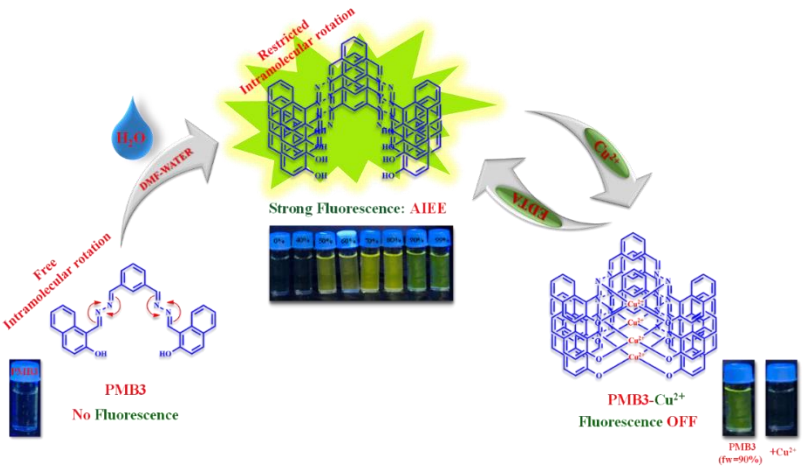

Section 3.3 also describes the AIEE characteristics of PMB3 and its application for the sensing of picric acid (PA). The PMB3 aggregate

was found to be highly selective for the detection of picric acid, over other nitroaromatics in aqueous medium with a detection limit of 2.43μM. The quenching of fluorescence emission intensity of PMB3 aggregates in the presence of PA was explained with a time-resolved emission study that follows a static quenching mechanism and the quenching constant value was found to be $2.33\times10^{6}\ M^{-1}$.

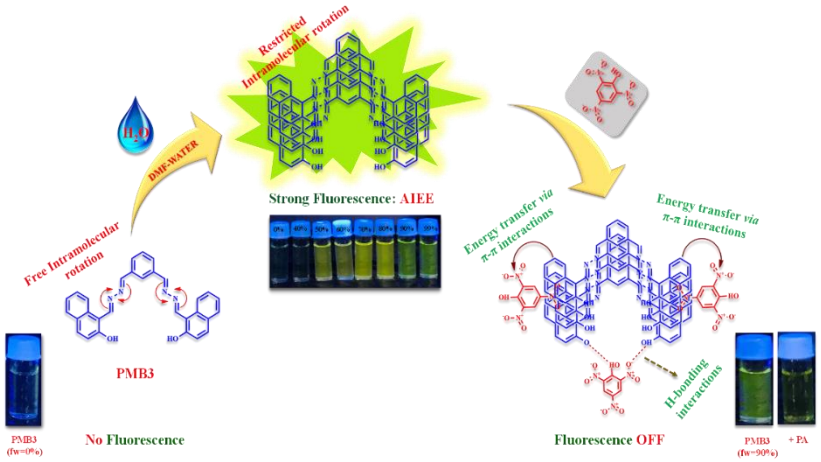

Section 3.4 deals with the colourimetric sensing of Cu^{2+} and Ni^{2+} using PMB3. The probe, PMB3, exhibited a sensitive colourimetric response to Cu^{2+} and Ni^{2+} ions among other competing metal ions, culminating in a prominent colour change from colourless to yellow. The stoichiometry of the ligand and metal complexes was ascertained to be 1:1 using Job's plot analysis. With detection limits of 4.56μM for Cu^{2+} and 2.68μM for Ni^{2+}, the method was effectively extended to real sample analysis, ensuring propitious results that closely aligned with the actual values.

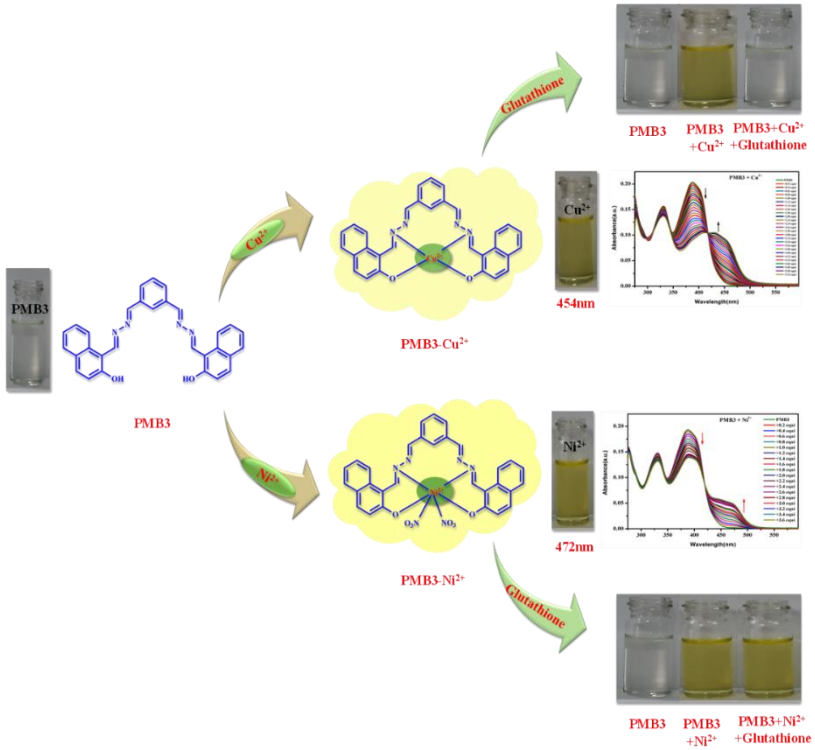

The works included in **Chapter 4** are divided into two sections, **4.1,** and **4.2** respectively. Section**.4.1** describes the AIEE characteristics of a novel Schiff base BBHN and its applications as a selective fluorescence "Turn off" sensor for copper ions in aqueous medium. The aggregate of BBHN shows relatively high Cu^{2+} ion selectivity and sensitivity among various metal ions through fluorescence "Turn off" response with a very high detection limit of 35.52 nM and a quenching constant value of 2.58×10^{8} M^{-1}. These observations suggest that the synthesized Schiff base, BBHN could effectively function as a nano sensor for the detection of Cu^{2+} ion in aqueous media, which could be very well applied for the instant "naked eye" detection of the metal ion. The fluorescence quenching behaviour of

BBHN in the presence of Cu^{2+} ions take place through dynamic quenching which was evident from the steady state fluorescence lifetime measurement study.

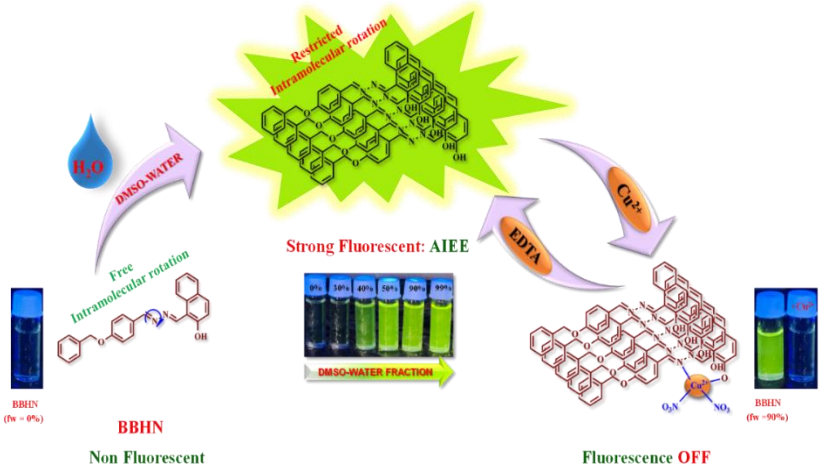

Section 4.2 also deals with the AIEE property of BBHN and its application for the sensing of picric acid (PA). The aggregates of BBHN showed a quick, highly selective, and sensitive fluorescence 'Turn off' response towards picric acid (PA) in aqueous medium among various other nitroaromatics. The limit of detection was 4.04μM with 2.03×10^{6} M^{-1} as the quenching constant. The

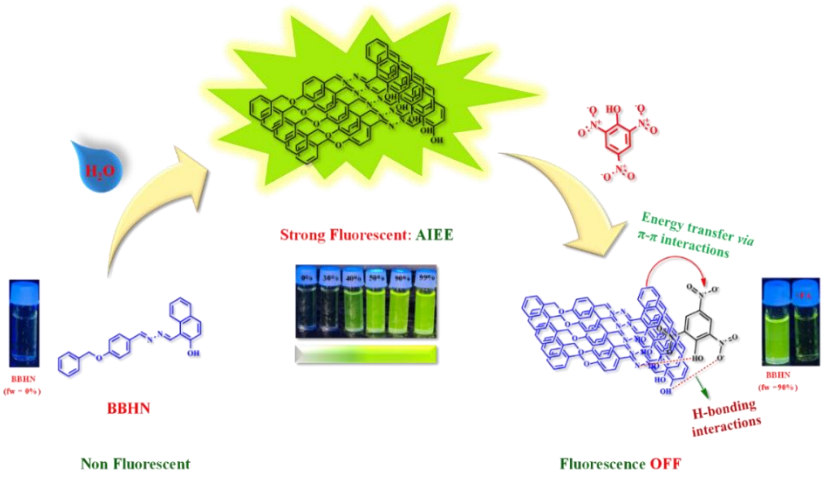

fluorescence "Turn off" response in the presence of PA is mainly due to π-π interactions, and other non-covalent interactions. Moreover, steady-state fluorescence lifetime measurement and Stern-Volmer plots reveal that the fluorescence quenching followed mixed quenching strategies.

Chapter 5 describes a novel Schiff base AHN, exhibiting multiple analytical responses comprising AIEE (Aggregation Induced Emission Enhancement) and colourimetric activity towards picric acid and cupric ion. The probe AHN with AIEE property acts as a fluorescent sensor for the selective detection of PA through fluorescence switch-off response and acts as a colourimetric sensor for Cu^{2+} in aqueous medium through a shift of colour from colourless to yellow. The multi-response characteristics of AHN propel its practical use for the naked-eye detection of these analytes. The addition of PA to the aggregate of AHN in DMSO with a 90% water fraction induces a quenching in the fluorescence intensity of the AHN aggregate and the limit of detection of PA was found to be 2.45μM with a quenching constant value of $6.21\times10^{7}M^{-1}$. Stern Volmer plots and lifetime measurements, clearly indicate that both static and dynamic processes were involved in the quenching mechanism. It is also evident that ground-state complexation between electron-rich fluorescent aggregates of AHN and electron-deficient PA takes place through π-π interactions and intramolecular hydrogen bonding interactions.

Further, AHN in DMSO exhibits a selective colourimetric response to bivalent copper among various metal ions with a detection limit of

3.16μM which is substantially below the permitted limit of copper recommended by WHO in drinking water. The mechanism of colorimetric response is the complexation of AHN with Cu^{2+} in the 2:1 stoichiometry, as confirmed by Job's plot method. Consequently, the versatility of probe AHN in detecting PA and Cu^{2+} through distinct mechanisms fosters its significance in the field of sensing and opens up promising avenues for practical applications.

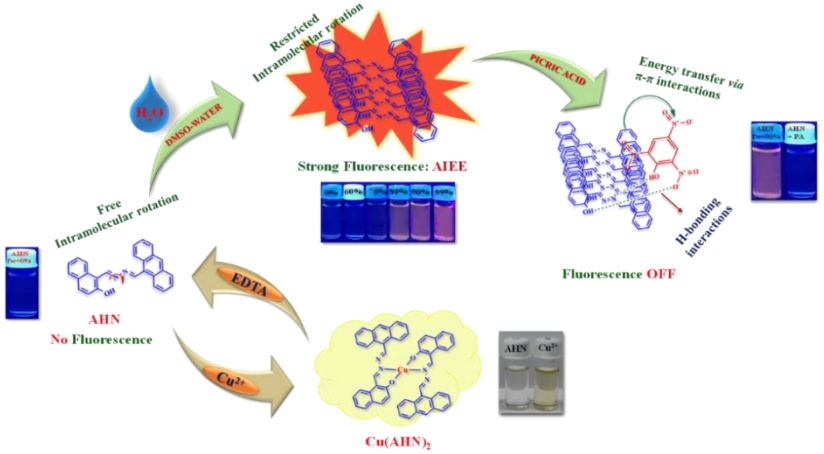

The last section of this thesis deals with a summary and future outlook.

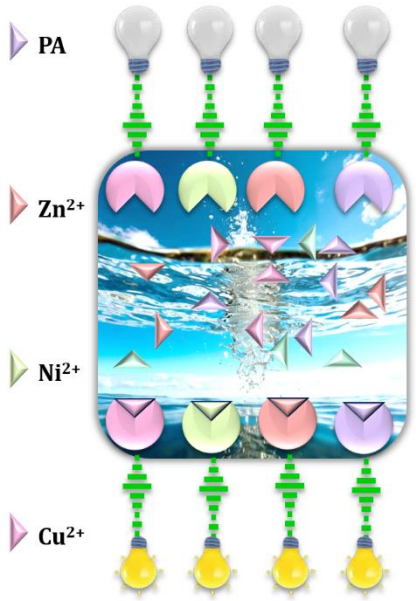

Chapter 1

Introduction and literature review

This chapter elucidates the significant threat posed by environmental pollution to human health, fauna, and flora, underscoring the necessity for precise and sensitive detection methods for pollutants. It provides an overview of chemosensors, their classifications, and signaling mechanisms, with a focus on Schiff bases due to their structural versatility and functional properties in sensor applications. The chapter reviews previous studies demonstrating the efficacy of Schiff bases in detecting metal ions such as Zn^{2+}, Cu^{2+}, and Ni^{2+}, as well as the explosive compound picric acid. This foundational discussion sets the stage for the comprehensive synthesis, characterization, and chemosensing applications of novel Schiff base receptors explored in the subsequent chapters.

One of the most challenging problems facing the current generation is environmental pollution, which is brought on by a variety of toxic and hazardous organic and inorganic compounds and will likely to continue be a problem for future generations also. Nowadays, environmental pollution increasingly becoming one of the foremost threats that ultimately affect human health, animals, and vegetation and hence there is a significant demand for specific and sensitive identification of pollutant species. The primary cause of environmental pollution is a growing human population that is attempting to achieve rapid economic growth through industrialization, which requires extensive natural resource exploitation through farming, fishing, forestry, mining, quarrying, oil and gas extraction, etc [1, 2]. As a result of industrialization, different contaminants or pollutants present in soil, water, and air may reach to a level that are hazardous to humans, animals, and plants. Moreover, various metal ions play vital roles in numerous environmental and biological processes such as transmission of nerve impulses, regulation of cell activity, muscle contraction, osmotic regulation, catalysis, biomineralization and metabolic process, etc [3]. Human body needs very little quantity of metal ions and excessive exposure has harmful effects, cause severe damages to human health and adversely affect the environment [4-6]. Therefore, the development and designing of a cost-effective chemosensor for the accurate qualitative and quantitative determination of these metal ions is very necessary and is a challenging goal.

Currently, different traditional analytical and instrumental techniques have been employed for the detection of hazardous metal ions, such as Atomic Absorption Spectroscopy (AAS), Atomic Emission Spectroscopy (AES), Inductively Coupled Plasma Mass Spectrometry (ICP-MS), Neutron Activation Analysis (NAA), and Stripping Voltammetry (SV), [7-14] etc., which demands expensive equipment, lack of portability, challenging multistep sample preparation procedures, difficult on-site operation or monitoring, and highly trained professionals for operation etc. Hence, it is important to develop an effective detection method that significantly overcomes the difficulties of the above-mentioned techniques. To limit this, significant attention has been paid to the methods of detection by colourimetric and fluorimetric approaches owing to their simplicity, selectivity, better sensitivity, direct visual perception, non-destructive methodology, economic viability, reproducibility, fast and quick real-time monitoring, etc [15-18].

Chemosensing, also referred as chemical sensing, is the process of detecting a specific analyte by using chemosensors. This field of study has been growing quickly in recent years owing to its wide applications in fields such as environmental monitoring, toxicological analysis, security systems, and medical diagnostics [19-21].

1.1 Chemosensors

A chemosensor is a chemical system which can bind with an analyte selectively and reversibly, followed by a change in at least one or more of its properties, such as colour, fluorescence, or redox

potential [22] (**Fig.1**). Chemical sensors can transform a chemical signal produced by the binding event of an analyte into a measurable analytical signal. Typically, a chemosensor consists of three parts: a receptor which is in charge of the specific analyte binding allowing the distinction, a photoactive unit or a signaling unit whose characteristics change upon the aforementioned binding of analyte, and a spacer, which has the ability to modify the geometry of the system so as to adjust the electronic interaction between the receptor and photoactive unit [23].

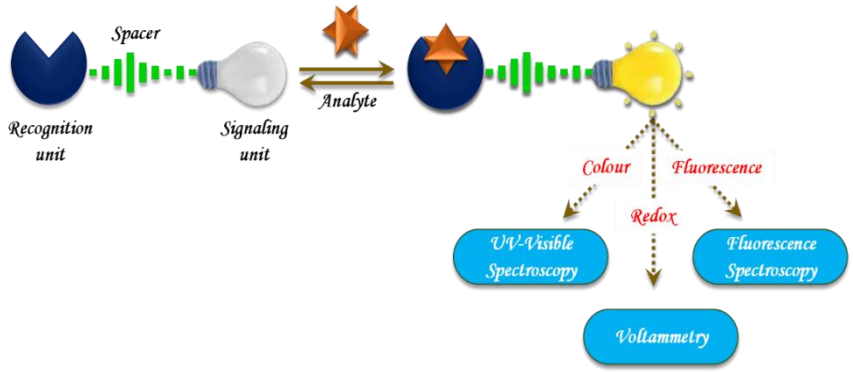

Fig.1 *Schematic representation of binding interactions of analyte by a chemosensor*

1.2 Classification of Chemosensors

Depending upon the nature of the signal that the signaling subunit emits, chemosensors are categorized into (1) Colourimetric sensors; (2) Fluorimetric sensors and (3) Electrochemical sensors.

1.2.1 Colourimetric Sensors (Chromogenic sensors)

Colourimetric sensors are those which measure changes in electronic characteristics of signaling subunits in association with Intra and Iintermolecular Charge Transfer (ICT) including Ligand-to-Metal Charge Transfer (LMCT) and Metal-to-Ligand Charge

Transfer (MLCT) transitions. In these kinds of sensors, a change in the colour of the signaling unit or a change in the UV-visible spectrum is observed because of the interaction between the analyte and the binding site. Furthermore, the colourimetric detection of metal is achieved by a chemosensor having a donor-π-acceptor(D-π-A) system. Hence, for that the electron-donating and electron-withdrawing groups can be introduced into the chemosensor molecule at the appropriate positions to make the D-π-A system. The HSAB concept of Pearson hold good with these binding sites and analyte that determines whether a specific metal ion will bind an electron donating (ED or D) or an electron withdrawing (EW or A) group. Generally binding of metal ion to electron donor site (ED) increases the chance for the LMCT transition which results in a blue

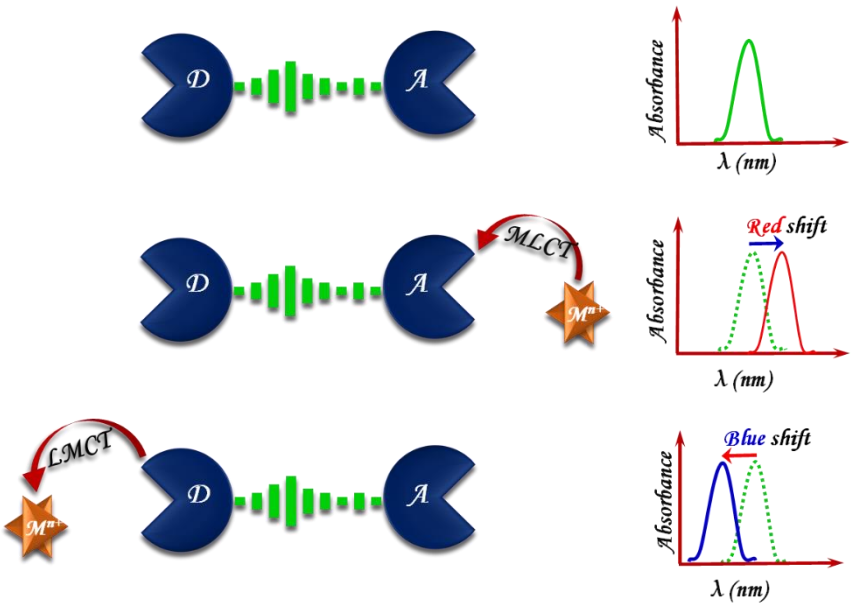

Fig.2 *Diagrammatic representation of metal binding effect on D-π-A system*

shift in the absorption spectrum and binding to electron withdrawing (EW) site will increase the chance of MLCT transitions which results in a red shift in absorption spectrum [24-26] (**Fig.2**).

1.2.2 Fluorimetric sensors (Fluorogenic sensors)

A fluorescent chemosensor is a molecular system whose physicochemical characteristics change in response to interaction with an analyte species, resulting a change in fluorescence [27]. Two integrated components typically used in the designing of fluorescent chemosensors are 1) a signaling fluorophore and 2) a guest binding receptor with recognition capabilities and they are connected by a spacer unit to form a fluorophore-spacer-receptor unit (**Fig.3**).

Two fundamental criteria which are to be fulfilled by an ideal fluorescent chemosensor are 1) the receptor needs to have the strongest binding selectivity to the relevant target analyte and 2) the fluorescence signal should also be free from environmental interference (signal-selectivity) based on strong binding selectivity, such as photobleaching, sensor molecule concentration, the environment around the sensor molecule like pH, polarity, temperature, etc., and stability under illumination.

Fig.3 *Schematic representation showing binding of analyte by a fluorescent chemosensor*

1.2.3 Electrochemical sensors

Electrochemical sensors are those which measure the changes in the electrochemical properties of signaling subunits in association with redox potential. The most widely used conventional methods, including cyclic voltammetry, differential pulse voltammetry, square wave voltammetry, and impedance spectroscopy, have been investigated in this area. The sensitivity of the sensor is influenced by surface modification, electrochemical transduction mechanisms, and the selection of the recognition receptor molecules.

1.3 Principles of designing Chemosensor

The three major ways of designing chemosensors are 1) Binding site-signaling subunit approach 2) Displacement approach and 3) Chemodosimeter approach

1.3.1 Binding site-signaling subunit approach

In this approach, the binding site and signaling subunit are connected by a covalent bond linker called spacer [28]. The change in electronic properties of the signaling subunit in association with the interaction of the binding site with the analyte results in the recognition of the target via colour or emission modulations (**Fig.4**).

Fig.4 *Diagrammatic representation of binding site-signaling subunit approach*

1.3.2 Displacement approach

In this approach, the binding site and the signaling subunit form a coordination type complex rather than being covalently bound. When the binding site coordinates with a specific analyte result in the release of the signaling subunit into the solution with a concurrent change in their optical properties [29] (**Fig.5**).

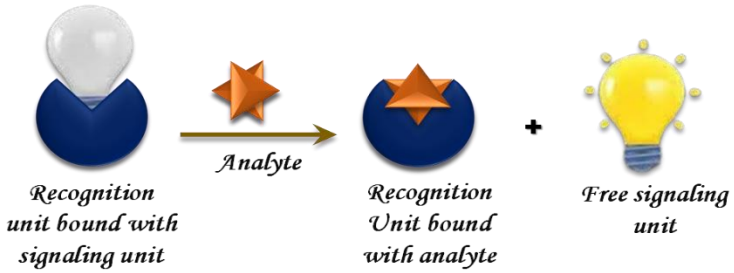

Fig.5 *Diagrammatic representation of displacement approach*

1.3.3 Chemodosimeter approach

In the chemodosimeter approach, a particular analyte-induced chemical reaction takes place which generates an optical signal (**Fig.6**). The binding of the analyte results in an irreversible change to the structure of the chemosensor [30, 31]. This approach usually results in remarkable spectroscopic modulations because the molecular probe undergoes a remarkable chemical modification upon reacting with the target molecule.

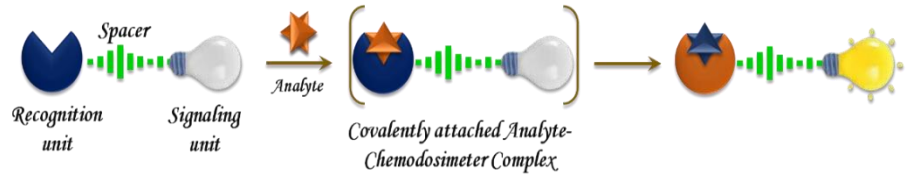

Fig.6 *Diagrammatic representation of the chemodosimeter approach*

1.4 Factors affecting chemosensor design

The size, shape, and binding energy of the receptor and analyte molecules play a significant role in the formation of a selective receptor-analyte complex. The following parameters need to be satisfied by the sensor molecule in order to function as an effective chemosensor [32, 33].

1.4.1 Sensitivity

The sensor must be sensitive to a specific analyte. The origin of the binding sites or receptors determines the sensitivity. The photophysical properties should change significantly with even a small change in the concentration of the analyte.

1.4.2 Selectivity

The sensor should be significantly selective on a specific analyte. Other competing molecules should not interfere with the binding interaction between the receptor and a specific analyte. The primary variables that determine selectivity are the binding strength and the solvent molecules.

1.4.3 Detection limit, response time and binding constant

An ideal sensor should possess the characteristics of a high binding constant, low limit of detection, and quick response time. The strength of the non-covalent interactions between the binding site and analyte influences the binding constant value.

1.4.4 Water solubility

Since most of the biological and environmental processes happen in an aqueous medium, the sensor should be soluble in water for

tracing the analyte such as metal ions, anions, and biomolecules involved in the process.

1.5 Signaling Mechanism: A pathway phenomena for absorption and fluorescence spectral changes

Chemosensors follow several sensing mechanisms which include,1) Intramolecular Charge Transfer mechanism (ICT), 2) Photo-induced Electron Transfer mechanism (PET), 3) Fluorescence Resonance Energy Transfer mechanism (FRET), 4) Excited State Intramolecular Proton Transfer mechanism (ESIPT), 5) Excimer-exciplex formation mechanism, 6) Inner Filter Effect (IFE), 7) C = N isomerization mechanism and 8) Aggregation-Induced Emission (AIE) process. These mechanisms result in a change in either the colour or fluorescence of the chemosensor with analyte binding.

1.5.1 Intramolecular Charge Transfer Mechanism (ICT)

Generally, colourimetric chemosensors follow an Intramolecular Charge Transfer mechanism (ICT). In Intramolecular Charge Transfer (ICT) sensors, the fluorophore and the receptor are linked directly by a π-conjugated system, forming a single entity. The two functionalities typically act as either an electron donor or an electron acceptor at opposite ends of the sensor molecule. The LUMO of the sensor has the highest electron affinity near the acceptor side, whereas the HOMO of the sensor has the highest electron density near the electron-donating moiety. As a result, upon excitation, a strong dipole with charge transfer from the donor to the acceptor is generated [34]. When an analyte is added, preferential bonding can occur at either the electron donor or acceptor regions.

This alters the dipole strength of the donor-acceptor couple, which is usually accompanied by changes in intensities and spectral shifts either blue or red region. Generally binding of an analyte to an electron donor site increases the chance for the LMCT transition which results in a blue shift in the spectrum whereas binding to an electron acceptor site (EW) will increase the chance of MLCT transition which results in a red shift in the spectrum [35] (**Fig.7**).

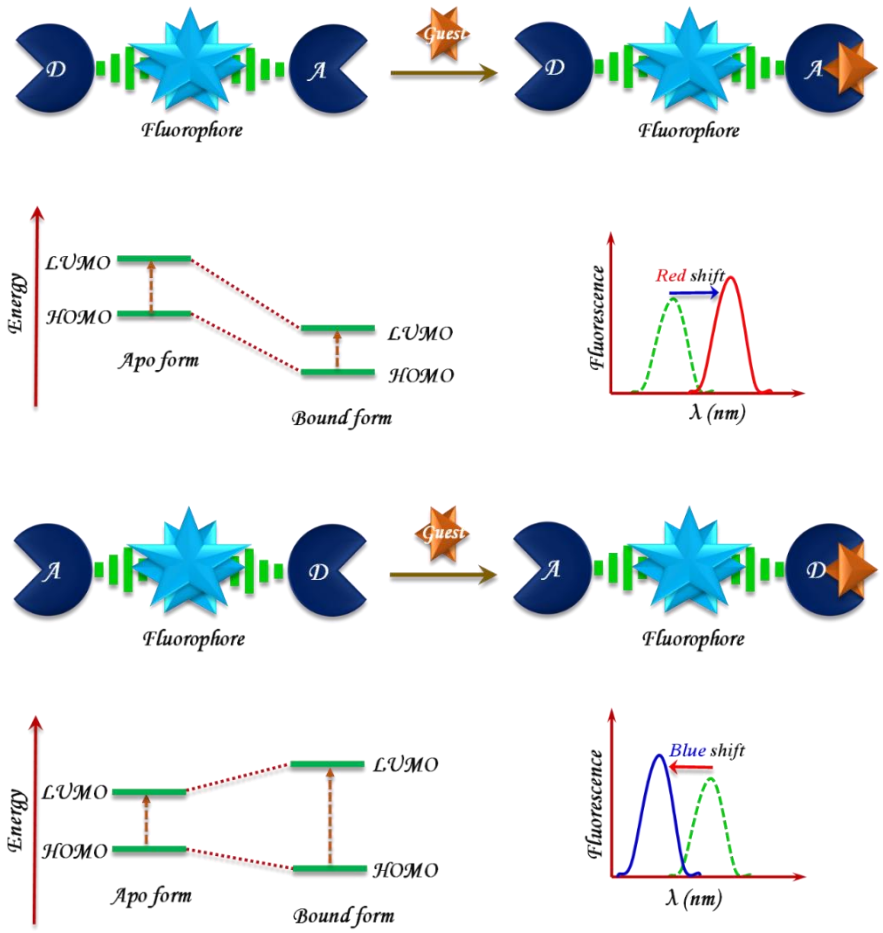

Fig.7 *Spectral changes of ICT based sensors when an analyte interact with acceptor site and with donor site*

1.5.2 Photo-induced Electron Transfer mechanism (PET)

In photo-induced electron transfer mechanism (PET) sensors, the fluorophore and the receptor are linked directly by a spacer. Photo-induced Electron Transfer (PET) is a type of quenching process, which involves an electron transfer from the receptor to the excited fluorophore in the absence of an analyte. This process occurs only when the energy level of the highest occupied molecular orbital (HOMO) of the receptor has to have an energy intermediate between the lowest unoccupied molecular orbital (LUMO) and the HOMO of the fluorophore. Up on excitation, the electron transfer process occurs followed by charge recombination by the transfer of an electron from the HOMO of the receptor to the HOMO of the fluorophore, *i.e.*, the process of photo-induced Electron Transfer (PET). Thus, when electrons are fully filled in the HOMO of the

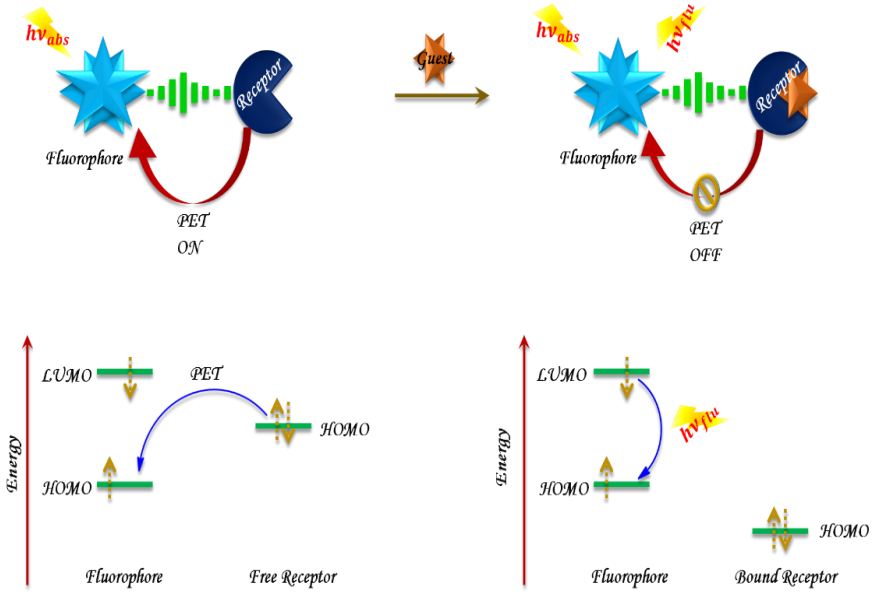

Fig.8 *Diagrammatic representation of the PET mechanism*

fluorophore, hinders the process of return of electrons from LUMO of the excited fluorophore to the ground state and thus prevents the fluorescence process. After binding with the analyte, the redox potential of the receptor is increased and hence the energy of the HOMO of the receptor is lowered than the energy of the HOMO of the fluorophore. Thus, the HOMO energy level of the receptor shifted outside the HOMO-LUMO gap of the fluorophore and the electron transfer from the HOMO of the receptor to the HOMO of the fluorophore becomes energetically unattainable and is blocked, resulting in the emission of photons in the form of fluorescence [36] (**Fig.8**).

1.5.3 Fluorescence Resonance Energy Transfer mechanism (FRET)

The Fluorescence Resonance Energy Transfer mechanism (FRET) is an electrodynamic non-radiative mechanism where the distance-dependent energy transfer between excited state donor fluorophore and ground state acceptor fluorophore through dipole-dipole interactions [37, 38] (**Fig.9**). The FRET process requires some degree of spectral overlap between the emission spectrum of the

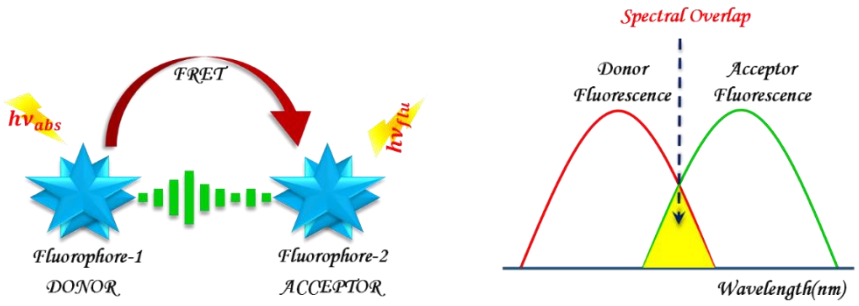

Fig.9 *Diagrammatic representation of the FRET mechanism*

donor and absorption spectrum of the acceptor and for an effective FRET to occur, the distance between the donor and acceptor needs to be between 10 and 100 A^0 [27, 39].

1.5.4 Excited State Intramolecular Proton Transfer mechanism (ESIPT)

Fluorophores with the ability to transfer protons between two sites of a molecule, *ie.,* in between proton donor and acceptor site are known as Excited State Intramolecular Proton Transfer (ESIPT) fluorophores[40]. These molecules are typically keto-enol tautomers [41]. For the effective ESIPT process, the proton donor and acceptor should be in proximity. Upon excitation, a proton is transferred from the donor site to the acceptor site leading to the formation of a tautomer in the excited state which differs from that in the ground state [34], and as a result, the fluorescence intensity of the system is suppressed [42]. Binding with analyte either through

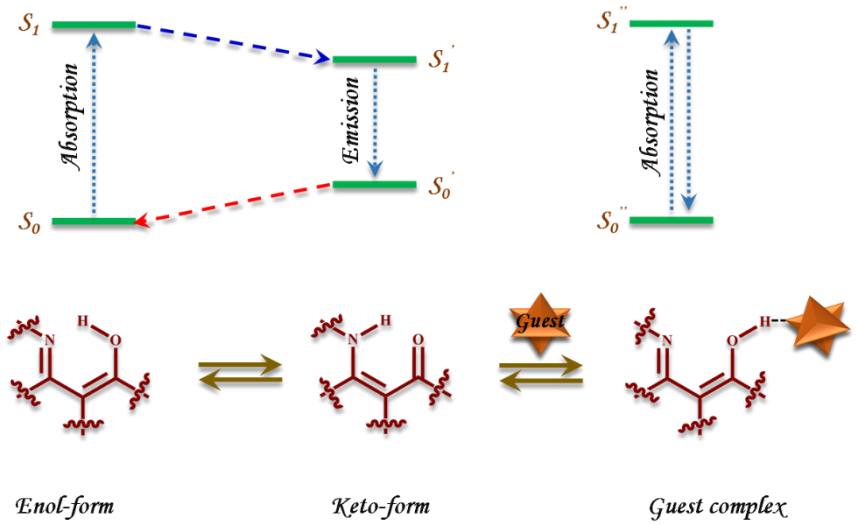

Fig.10 *Diagrammatic representation of the ESIPT mechanism*

proton donor or proton acceptor site or both inhibits the proton transfer by ESIPT process, resulting in radiative emission [43] (**Fig.10**).

1.5.5 Excimer-Exciplex formation mechanism

The interaction of a fluorophore in its excited state with a fluorophore having the same structure in its ground state results in the formation of a complex called an excimer. Likewise, the interaction of a fluorophore in its excited state with a fluorophore with a different structure in its ground state results in the formation of a complex called an exciplex [27]. As compared to the emission spectral profile of the monomer, the emission spectra of excimers and exciplex have a red shift which conforms to the formation of excimer and exciplex complex. As a result, a single spectral profile shows emission from both the monomer and the complex. Upon interaction with an analyte leads to the formation or deformation of the excimer/exciplex complex resulting the modifications in structure, and is analysed by observing the excimer/exciplex band in the emission spectrum recorded using spectroscopic method.

1.5.6 Inner Filter Effect mechanism (IFE)

The inner filter effect (IFE) mechanism is a phenomenon based on the non-irradiation energy conversion model. It is a radiative process which occur when the analyte (quencher or absorber) absorbs either emission or excitation energy of the fluorophore(sensor), leads to the exceptional quenching of the fluorescence of the fluorophore [44]. This mechanism works differently from the other mechanisms since there is no interaction

between the fluorophore (sensor) and the absorber (analyte). The IFE process requires some degree of spectral overlap between the absorbance of the quencher (analyte) and the excitation and or emission of the fluorophore (sensor) and the extent of spectral overlap determines the efficiency of the IFE process [4, 45] (**Fig.11**).

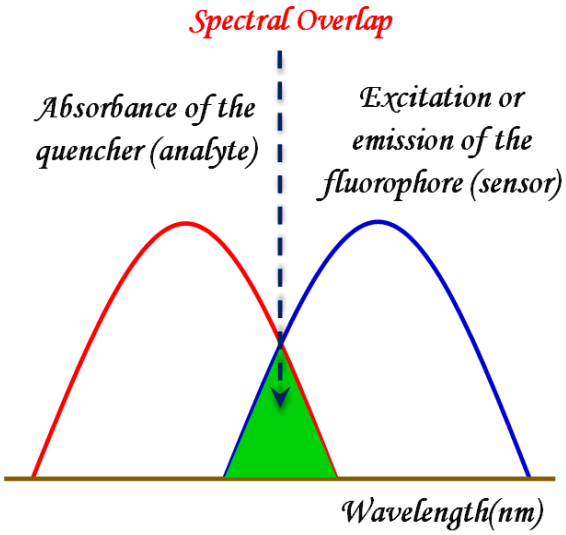

Fig.11 *Diagrammatic representation of the IFE mechanism*

1.5.7 C = N isomerization mechanism

A relatively new signalling mechanism and photophysical process involving C=N isomerization was reported in 2007 using conformationally restricted compounds. It has been found that unbridged C=N structured compounds are non-fluorescent due to C=N isomerization between E and Z isomeric forms, which is the predominant decay process in the excited state. As a result, the excited state energy is used for the isomerization process and leads to non-radiative decay emission. The suppression of C=N isomerization in the excited states by bridging with the C=N bond

results in drastic increase in the fluorescence of the compounds [46]. Hence, it is clear that the interaction of analyte species to unbridged C=N bond through complexation leads to inhibition of C=N isomerization and results in radiative emission [47]. Thus, the blocking or inhibition of C=N isomerization by analyte species is a useful mechanism for the recognition of analytes by a sensor (**Fig.12**).

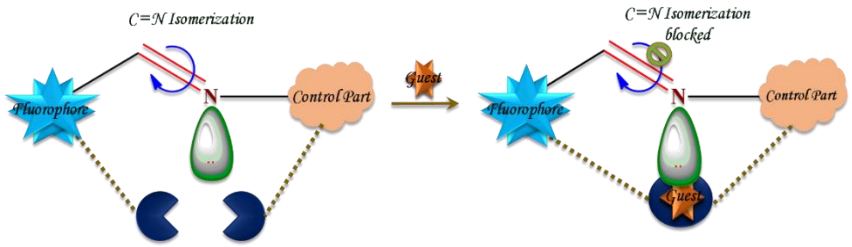

Fig.12 *Diagrammatic representation of the C=N isomerization mechanism.*

1.5.8 Aggregation-Induced Emission (AIE) mechanism

Aggregation Induced Emission (AIE), is one of the interesting fluorescent mechanisms and was first observed by Tang et al in 2001 in an organosilicon compound (hexaphenylsilole) which showed weak emission in solution state but strong emission upon aggregation phase [48, 49]. It has been found that some organic molecules that are almost non-fluorescent in a solution state become highly fluorescent when they are aggregated and this phenomenon is called Aggregation-Induced Emission (AIE). The non-fluorescent behaviour of a molecule(chromophore) in a solution state is due to its high degree of rotational freedom which leads to intramolecular rotations within the molecules. As in the aggregation process, the molecule or chromophore is locked in a rigid conformation that restricts the intramolecular bond rotation (RIR) leading to the

molecule being highly emissive one [50] (**Fig.13**). The restriction of intramolecular rotation (RIR), the restriction of intramolecular motion (RIM), and the restriction of intramolecular vibration (RIV) are the backbone processes behind the AIE phenomena [43, 51]. In addition to the above mechanism of restriction of intramolecular motion (RIM), there are some other mechanisms also proposed and used to explain AIE phenomena, such as j-aggregates [52], excimer formation [53], ESIPT [54], restriction of intramolecular rotation about the double bond [55], and inhibition of twisted intramolecular charge transfer (TICT) [56] process.

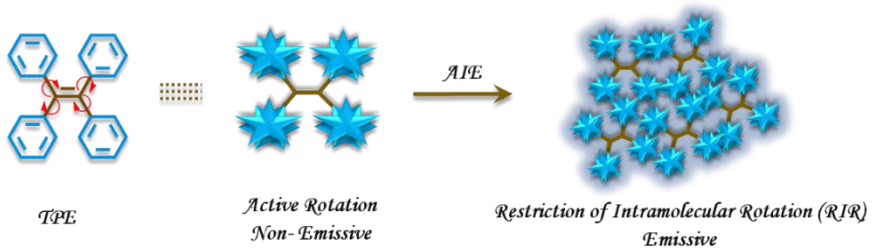

Fig.13 *Diagrammatic representation of the AIE mechanism*

A class of compounds with AIE activity phenomenon now has been applied in the chemosensing area for selective detection of environmentally and biologically important analytes such as metal ions, anions, explosives, *etc*. There is no common mechanism that applies to all AIE chemosensors, but each mechanism applies only to that system. Among the various mechanisms, the following are the specific main sensing mechanisms applied in AIE-based chemosensors [57], (1) Insoluble aggregates are produced when metal ions(analyte) coordinate with the sensor, which may limit

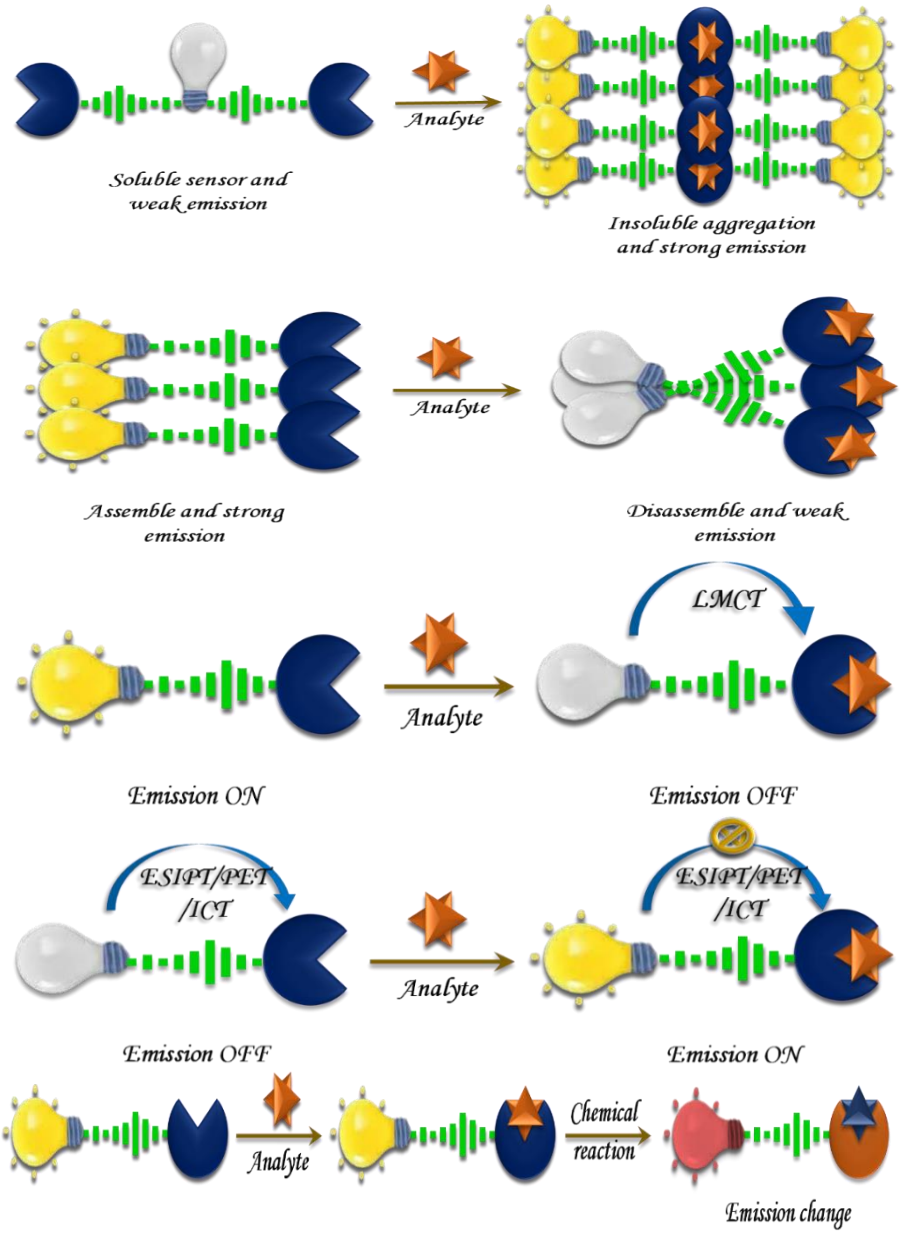

Fig.14 *Diagrammatic representation of various sensing mechanisms shown by an AIE based chemosensor*

intramolecular rotation and activate fluorescence emission. (2) Through a variety of noncovalent interactions, including electrostatic, hydrogen bonds, van der Waals, C-H interaction, and J-

type aggregates, the sensor itself self-assembles into a new pattern of fluorescence turning on and the aggregates will be disassembled by the added metal ions, which will quench the fluorescence of sensor. (3) The sensor on chelation with metal ion would induce or block some photophysical process involving Photo-induced Electron Transfer (PET), Intramolecular Charge Transfer (ICT) either through Metal-to-Ligand Charge Transfer (MLCT), or Ligand-to-Metal Charge Transfer (LMCT), Excited-State Intramolecular Proton Transfer (ESIPT), FRET, C=N isomerization, which either quenches or enhances the fluorescence emission. (4) The sensor binding with an analyte metal ion alters the structure of the chemosensor by irreversible chemical reaction resulting an impact on changes in its fluorescence behaviour (**Fig.14**).

1.6 Schiff bases as Chemosensor

Schiff bases, also referred as imines or azomethines, are the condensation products formed from primary amines and aldehydes or ketones[58] (**Scheme 1**). A German chemist, Hugo Schiff, who synthesized the first Schiff base in 1864 from primary amine with carbonyl compounds through a condensation process [59]. Schiff bases demonstrate exceptionally good performance for the identification of metal ions and have received great attention due to their ease of synthesis, low cost, high selectivity, and quick response

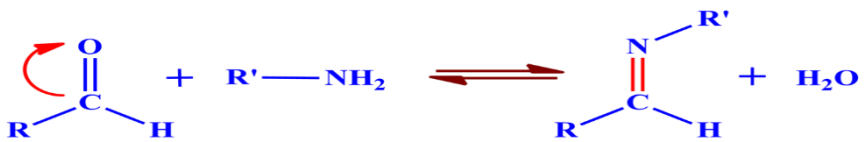

Scheme 1 *Schematic representation of Schiff base formation reaction*

with an ability to form stable chelates with almost all metals [21, 60, 61].

Schiff bases have been explored as a chemosensor for the successful determination of a wide variety of metal ions [62, 63]. The interaction between analyte metals and the Schiff base is crucial for generating a signal for sensing. Depending on the type of signal that the sensing materials emit, Schiff base chemosensors can be categorized into colourimetric sensors or fluorimetric sensors. Schiff bases can form complexes with almost all metals because the nitrogen atom in the imine bond has unpaired electrons, making them electron donors and basic in nature [64, 65]. The azomethine group, in which the nitrogen atom is linked by a double bond, can serve as a coordination site for d-metal ions is suitable for back bonding owing to its π-orbitals (**Fig.15**). Thus, the nitrogen atom in the azomethine group serves as both π-acceptor and σ-donor and hence gives extra stability to metal complexes formed from Schiff bases [66]. The distinct properties of Schiff bases make them useful in biological systems [67, 68], catalysis [69-71], medicine and pharmacy [72, 73], *etc*.

The selectivity of Schiff base structure towards specific analyte depends on both the size and charge of the ion, the hard-soft acid base(HSAB) nature of both metal ion and electron withdrawing or donating groups on the Schiff base, the electronic configuration of both metal and binding site of the ligand and the ring size of chelate system [74].

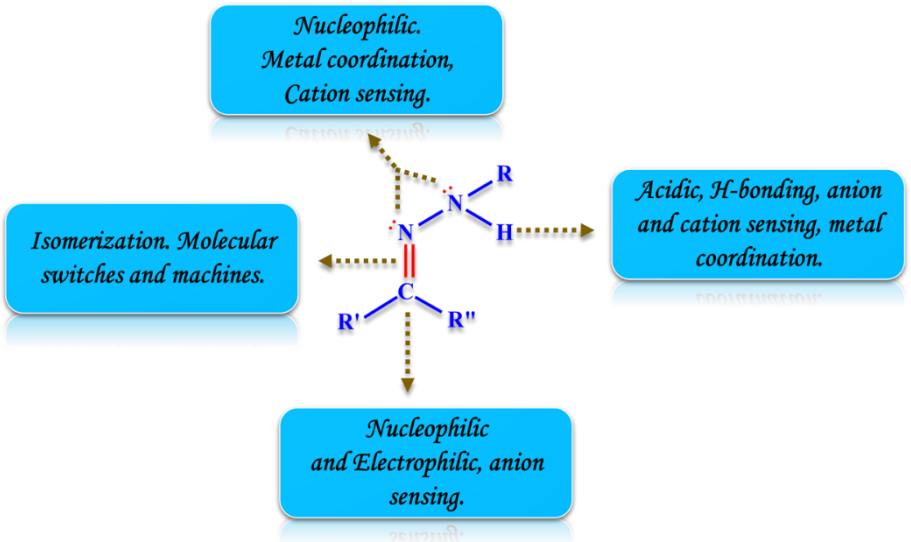

Fig.15 *Structural and functional diversity of a Schiff base*

1.7 Mechanism of Schiff base formation

Generally, imine formation happens in two stages. In the first stage, a nucleophilic attack of the amino group on the unsaturated carbon of the carbonyl compound results in the formation of a tetrahedral intermediate of carbinolamine, and in the second stage elimination of water from carbinolamine tetrahedral intermediate leads to the formation of imine bond (C=N bond) [75] (**Scheme 2**). Since the carbinolamine is a labile species, it is usually not isolated or determined[76].

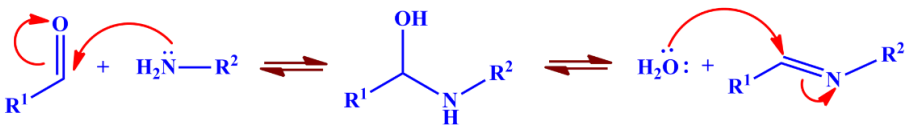

Scheme 2 *Mechanism of imine bond (C=N) formation*

Schiff base formation can happen either through acid-catalysed or base-catalysed reactions [77]. In acid catalysed reaction, the acidic

proton protonates the carbonyl oxygen which increases the electron deficiency on carbonyl carbon and the attack of a lone pair of electrons from the nitrogen atom of the amino group on the electron-deficient carbonyl carbon leading to the formation of carbinolamine intermediate. On subsequent heating eliminates water from the intermediate and Schiff base is generated (**Scheme 3**).

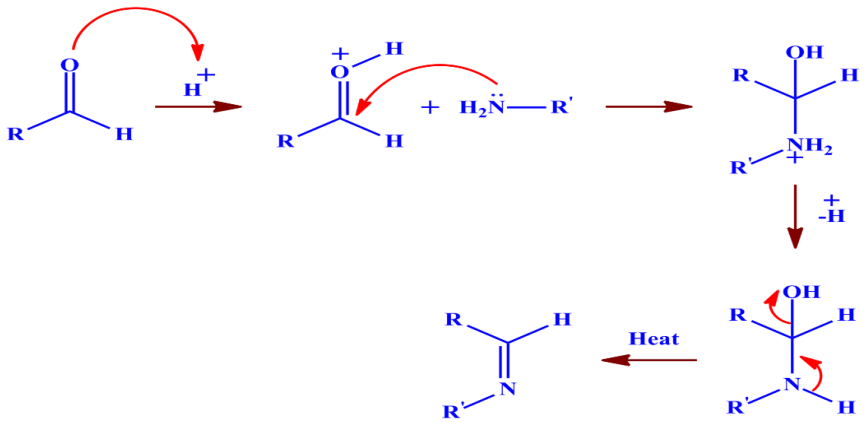

Scheme 3 *Mechanism of acid catalysed Schiff base formation*

In base catalysed reaction, the base increases the nucleophilicity of the amine group and attack the unsaturated carbon of carbonyl

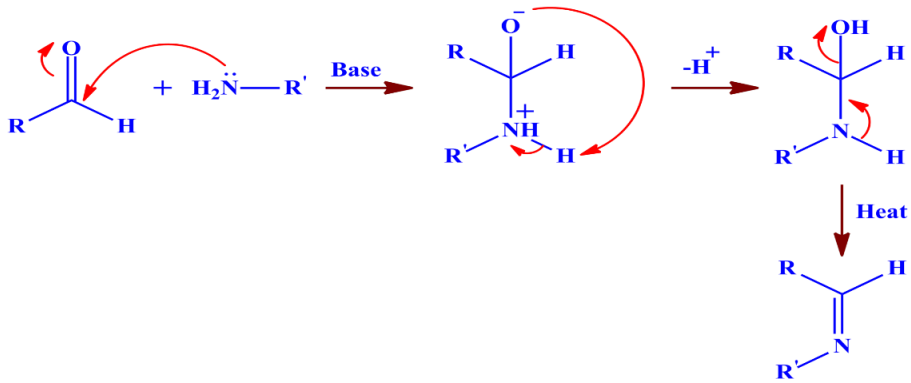

Scheme 4 *Mechanism of Base catalysed Schiff base formation*

compound by nucleophilic addition resulting in the formation of a carbinolamine intermediate. Elimination of water from the carbinolamine intermediate by heating generates Schiff base (**Scheme 4**).

1.8 Schiff base derived from 2-hydroxy-1-naphthaldehyde as a chemosensor

2-hydroxy-1-napthaldehyde is one of the frequently used fluorophores for the development of various fluorescent probes due to the presence of donor and acceptor sites on them. That is the OH group in the 2-position acts as a hydrogen bond donor site and the aldehyde group in the 1-position is transformed into an imine group which acts as an acceptor site [78]. Herein we utilized naphthaldehyde for the synthesis of a chemosensor due to its ability to act both as a donor and an acceptor, good photostability and biocompatibility, etc. The rotation of the C=N bond and hydrogen bonding through the hydroxyl group have crucial roles and provide an opportunity for chelation with metals. Moreover, due to the possibility of free rotation about the C=N bond, naphthaldehyde-based chemosensors may also show Aggregation-Induced Emission (AIE) phenomenon which will also increase its utility in the field of sensing studies.

1.9 Previous Studies-A Review

Scientific interest in the chemosensing properties of Schiff-base receptors and their applications is quite interesting and gets greater attention in recent times. Schiff-base ligands exhibit a wide variety of applications that extend their use in analytical chemistry,

biological, pharmacological, and medical fields. In this study, we focus on the chemosensing applications of Schiff-base ligands and their interactions with different analytes through colourimetric and fluorescence responses.

1.9.1 Schiff base sensors for Cu^{2+}

Copper is an essential trace element and the third most abundant metal present in the biological system which plays a vital role in physiological and biological processes [79, 80]. Copper plays an active role as a cofactor in various metalloenzymes including superoxide dismutase, cytochrome *c* oxidase, tyrosinase, nuclease, etc, [81-83] and is also needed for bone-tissue formation, cellular respiration, for maintaining good conditions of the central nervous system and cardiovascular system and so on in the human body [84]. Apart from these, a major concern has been given to copper, a non-biodegradable one becoming an important environmental pollutant due to its extensive use in various fields such as industry, agriculture, etc [85]. The major source of copper contamination is industrial waste, agriculture waste, decaying vegetation, and photovoltaics which will pose a threat to human health [86-88]. Moreover, over exposure and the extensive intake of copper to the human body leads to serious neurodegenerative diseases such as Parkinson's, Alzheimer's, Wilson disease, prion diseases, and liver and kidney disorders [89-94]. The World Health Organisation (WHO) has established the necessary regulations, which specify that the maximum amount of Cu^{2+} ions in drinking water should not exceed 31.5 μM [95, 96]. Therefore, in view of the above, it is highly

demanded a suitable cost-effective method for the detection of copper in different systems. In this context, Schiff-base sensors offering remarkable sensing properties have been used to detect copper ions, with remarkable limits of detection, good selectivity and sensitivity (**Table 1**).

1.9.2 Schiff base sensors for Ni^{2+}

Nickel is one of the essential ultra-trace elements in biological system as it plays an active role in some biological processes within the body like metabolism, respiration, and biosynthesis and is a vital component of many metalloenzymes, including hydrogenases, ureases, etc [97-100]. Furthermore, the modern industrial sector makes extensive use of metallic nickel and its compounds to produce nickel-cadmium batteries, electronic equipment, supercapacitors, in electroplating and electroforming [101-104]. Moreover, stainless steel is one of the alloys of nickel, which is widely used to produce tools, machinery, armaments, and appliances [105]. However, the extensive use of nickel in these sectors inevitably results in environmental pollution and adversely affects human health. Excessive exposure and intake of Ni^{2+} by human beings could cause major health issues, such as respiratory problems, lung cancer, pneumonitis, central nervous disorders, and kidney disorders [106-108]. Hence, great attention is needed to a cost-effective recognition method for the detection of nickel ions and is a challenging one and in this perspective, Schiff base colourimetric sensors have great significance. Till date, many Schiff base sensors have been reported

for the colourimetric determination of nickel with good selectivity and sensitivity and are summarised in **Table 2.**

1.9.3 Schiff base sensors for Zn^{2+}

Zinc is the second most abundant trace metal in the human body, as it plays an active role in some biological processes within the body like brain function, neural signal transmission, immune function, gene transcription, catalytic cofactors, the regulation of metalloenzymes, energy generation, and cellular metabolism [109-114]. Furthermore, industrial sectors make use of zinc for galvanizing processes with iron metals to prevent rusting and die-casting in the electrical, automobile, and hardware industries. However, the widespread use of zinc in these industries invariably leads to environmental pollution and has an adverse effect on human health [115, 116]. Even though zinc is a vital trace element indispensable for life, both excessive and inadequate levels of consumption lead to serious neurodegenerative disorders like Alzheimer's disease, Parkinson's disease, epilepsy, etc [117-123]. Since the d^{10} electronic configuration of Zn^{2+} makes them insensitive to many spectrophotometric detection methods [124, 125], it is a very challenging task to design a suitable selective and sensitive method for the detection of zinc in the presence of other metal ions. In this context, Schiff base fluorescent sensors have great significance and several Schiff base sensors have been reported as fluorimetric sensors for zinc ion with remarkable limit of detection, selectivity, and sensitivity which are summarised in **Table 3.**

1.9.4 Schiff base AIEE active sensors for Picric acid

Nitroaromatic compounds (NACs), with explosive properties, have been utilized for military operations and terrorist activities [126, 127]. Among the nitroaromatic compounds, picric acid (PA) is one of the most critical analytes and has paramount significance because of its explosive nature, non-biodegradability, higher water solubility, and is a harmful pollutant to human health and the ecosystem [128-131]. Besides its explosive nature, PA is widely used for rocket fuel manufacturing, dyes, paints, leather, and pharmaceutical industries, etc [132-134]. However, the widespread use of PA in these sectors leads to get into groundwater and soil which results in environmental pollution which hardly affects human health. Furthermore, extensive exposure to PA will lead to serious health problems like skin and eye irritation, anaemia, liver dysfunction, cancer, etc [135-137]. The existing analytical techniques for PA detection have some difficulties with on-site monitoring like expensive instrumental techniques, difficulties in handling, less sensitivity, and less portability [138, 139]. Therefore, it is essential and extremely important to develop a sensitive and selective method to identify PA. In this context**,** herein we have developed a few AIEE active Schiff-base sensors and in-site formed Schiff base-metal complexes which offer great selectivity and sensitivity for PA detection. Several AIEE active Schiff base and in-site formed Schiff base-metal complexes with a remarkable limit of detection, with good selectivity and sensitivity have been reported elsewhere for the detection of PA and are summarised in **Table 4**

Table 1 *Reported Schiff base chemosensors for the detection of Cu^{2+} ion*

Sensor	Sensor type	Sensing mechanism	Analyte	L:M	LOD [M]	Metrix/ Solvent	Ref
Probe-1	Colourimetric	ICT and LMCT	Cu^{2+}	2:1	5.80×10^{-6}	DMSO	[140]
Probe-2	Colourimetric	ICT	Cu^{2+}	1:1	28.0×10^{-6}	CH_3CN	[141]
Probe-3	Colourimetric & Fluorescent	Complex formation	Cu^{2+}	1:1	8.68×10^{-6}	DMSO-HEPES	[142]
Probe-4	Colourimetric & Fluorescent	Complex formation	Cu^{2+}	1:1	2.48×10^{-6}	DMF	[143]
Probe-5	Colourimetric	Complex formation &ICT	Cu^{2+}	2:1	2.85×10^{-6}	CH_3CN - H_2O	[144]
Probe-6	Colourimetric	ICT and LMCT	Cu^{2+}	1:1	$9.3x10^{-7}$	CH_3OH-H_2O	[83]
Probe-7	AIEE active Fluorescent	ESIPT& CHEQ	Cu^{2+}	1:1	2.10×10^{-6}	DMF-HEPES	[145]
Probe-8	Fluorescent	C=N isomerization & PET	Cu^{2+}	1:1	1.8×10^{-7}	CH_3CN	[146]
Probe-9	Fluorescent	PET	Cu^{2+}	1:1	0.26×10^{-6}	DMSO-H_2O	[147]

Probe-10	Fluorescent	C=N isomerization & CHEF	Cu^{2+}	2:1	1.80×10^{-6}	CH_3OH	[148]
Probe-11	Fluorescent	Complex formation	Cu^{2+}	1:1	1.01×10^{-7}	CH_3OH-H_2O	[149]
Probe-12	AIEE active Fluorescent	Complex formation	Cu^{2+}	2:1	5.0×10^{-9}	DMSO-H_2O	[150]
Probe-13	AIEE active Fluorescent	PET	Cu^{2+}	1:1	3.98×10^{-8}	DMSO-H_2O	[151]
Probe-14	AIEE active Fluorescent	CHEQ	Cu^{2+}	1:1	24.0×10^{-9}	DMSO-H_2O	[152]
Probe-15	AIEE active Fluorescent	ESIPT	Cu^{2+}	1:1	5.31×10^{-7}	EtOH-DMSO	[153]
Probe-16	Fluorescent	CHEQ	Cu^{2+}	2:1	2.80×10^{-6}	DCM-CH_3OH	[84]
Probe-17	Fluorescent	ICT & CHEF	Cu^{2+}	2:1	30.0×10^{-9}	DMSO-H_2O	[87]
Probe-18	AIEE active Fluorescent	Complex formation	Cu^{2+}	2:1	8.14×10^{-8}	CH_3CH_2OH-PBS	[154]
Probe-19	AIEE active Fluorescent	Complex formation	Cu^{2+}	1:1	17.0×10^{-9}	DMF-PBS	[155]
Probe-20	Fluorescent	C=N isomerization & CHEF	Cu^{2+}	1:1	1.54×10^{-9}	CH_3CN	[156]

Probe-21	Colourimetric & Fluorescent	Complex formation	Cu^{2+}	1:1	7.3×10^{-10}	CH_3OH-H_2O	[157]
Probe-22	Colourimetric	Complex formation	Cu^{2+}	2:1	1.8×10^{-6}	CH_3OH-H_2O	[158]
Probe-23	Colourimetric & Fluorescent	Complex formation	Cu^{2+}	2:1	2.40×10^{-8}	CH_3OH-H_2O	[159]
Probe-24	Colourimetric & Fluorescent	Complex formation	Cu^{2+}	1:1	4.9×10^{-7}	CH_3OH-Tris-HCl	[97]
Probe-25	Fluorescent	Complex formation	Cu^{2+}	1:1	0.35×10^{-6}	DMF	[160]
Probe-26	Colourimetric & Fluorescent	Complex formation	Cu^{2+}	1:1	20.0×10^{-6}	CH_3CN	[161]
Probe-27	Fluorescent	CHEF	Cu^{2+}	1:1	9.0×10^{-7}	CH_3CN	[162]
Probe-28	AIEE active Fluorescent	Aggregate disruption	Cu^{2+}	1:1	18.6×10^{-9}	H_2O	[163]

Table 2 *Reported Schiff base sensors for the detection of Ni^{2+} ion*

Sensor	Sensor type	Sensing mechanism	Analyte	L:M	LOD [M]	Metrix/ Solvent	Ref
Probe-1	Colourimetric	Complex formation	Ni^{2+}	2:1	0.14×10^{-6}	CH_3OH-PBS	[164]
Probe-2	Colourimetric & Fluorescent	Complex formation	Ni^{2+}	1:1	2.39×10^{-9}	CH_3CN-H2O	[165]
Probe-3	Colourimetric	Complex formation	Ni^{2+}	1:1	7.4×10^{-7}	CH_30H-Tris-HCl	[97]
Probe-4	Colourimetric & Fluorescent	C=N isomerization & PET	Ni^{2+}	1:1	1.71×10^{-6}	CH_30H-Tris-HCl	[166]
Probe-5	Colourimetric & Fluorescent	C=N isomerization & PET	Ni^{2+}	2:1	1.80×10^{-6}	CH_30H-Tris-HCl	[99]
Probe-6	Colourimetric & Fluorescent	CHEF & LMCT	Ni^{2+}	1:1	0.36×10^{-6}	CH_3CN	[167]
Probe-7	Colourimetric	ICT & Complex formation	Ni^{2+}	1:1	0.5×10^{-6}	Ethanol	[168]
Probe-8	Colourimetric	ICT	Ni^{2+}	1:1	1.0×10^{-7}	DMSO-H_2O	[169]
Probe-9	Colourimetric	Complex formation	Ni^{2+}	1:1	5.0×10^{-6}	DMSO-H_2O	[105]

Probe-10	Colourimetric	Complex formation	Ni^{2+}	2:1	1.47×10^{-6}	CH_3CN-HEPES	[170]
Probe-11	Colourimetric	Complex formation	Ni^{2+}	1:1	0.12×10^{-6}	CH_3CN	[171]
Probe-12	Colourimetric	Complex formation	Ni^{2+}	1:1	Not found	CH_3CN	[100]
Probe-13	Colourimetric & Fluorescent	Complex formation	Ni^{2+}	1:1	Not found	Ethanol-H_2O HEPES	[172]
Probe-14	Colourimetric	Complex formation	Ni^{2+}	1:1	6.96×10^{-7}	DMSO	[173]
Proe-15	Colourimetric	Complex formation	Ni^{2+}	1:1	1.10×10^{-6}	CH_3OH-H_2O	[26]
Probe-16	Colourimetric & Fluorescent	C=N isomerization &PET	Ni^{2+}	1:1	1.61×10^{-6}	CH_3OH-H_2O	[174]
Probe-17	Colourimetric & Fluorescent	d-d transition	Ni^{2+}	1:1	17.7×10^{-7}	DMSO	[175]
Probe-18	Colourimetric & Fluorescent	CHEF & ICT	Ni^{2+}	1:1	0.04×10^{-6}	Ethanol	[176]
Probe-19	Colourimetric & Fluorescent	C=N isomerization	Ni^{2+}	1:1	1.08×10^{-6}	CH_3OH-H_2O	[177]
Probe-20	Colourimetric & Fluorescent	d-d transition	Ni^{2+}	1:1	9.04×10^{-6}	CH_3OH-H_2O	[178]

Probe-21	Colourimetric & Fluorescent	C=N isomerization & PET	Ni^{2+}	1:1	3.3×10^{-7}	DMSO-H_2O	[179]
Probe-22	Fluorescent	Complex formation	Ni^{2+}	2:1	60.0×10^{-9}	DMF	[180]
Probe-23	Colourimetric	ICT	Ni^{2+}	1:1	50.0×10^{-6}	Ethanol	[181]
Probe-24	Colourimetric	ICT	Ni^{2+}	1:1	375×10^{-9}	CH_3OH-H_2O	[182]
Probe-25	Fluorescent	C=N isomerization	Ni^{2+}	2:1	2.1×10^{-11}	THF-PBS	[183]

Table 3 *Reported Schiff base sensors for the detection of Zn^{2+} ion*

Sensor	Sensor type	Sensing mechanism	Analyte	L:M	LOD [M]	Metrix/ Solvent	Ref
Probe-1	Fluorescent	C=N isomerization & ESIPT	Zn^{2+}	1:1	4.7×10^{-6}	CH_3CN-H_2O	[184]
Probe-2	Fluorescent	ESIPT	Zn^{2+}	1:1	1.6×10^{-7}	CH_3OH-H_2O	[185]
Probe-3	Fluorescent	Complex formation	Zn^{2+}	1:1	7.2×10^{-6}	CH_3OH	[186]
Probe-4	Fluorescent	CHEF	Zn^{2+}	1:1	1.51×10^{-7}	DMSO-H_2O	[187]
Probe-5	Fluorescent	Complex formation	Zn^{2+}	2:1	2.3×10^{-6}	DMSO-H_2O	[188]
Probe-6	Fluorescent	ESIPT	Zn^{2+}	1:1	2.93×10^{-5}	DMSO	[189]
Probe-7	Fluorescent	C=N isomerisation	Zn^{2+}	1:1	0.35×10^{-6}	DMF-H_2O	[190]
Probe-8	Fluorescent	Complex formation	Zn^{2+}	1:1	0.66×10^{-6}	CH_3OH-H_2O	[191]
Probe-9	Fluorescent	C=N isomerisation & PET	Zn^{2+}	1:1	1.73×10^{-7}	Ethanol	[192]
Probe-10	Fluorescent	CHEF & C=N isomerisation	Zn^{2+}	1:1	1.29×10^{-6}	DMF	[193]

Probe-11	Fluorescent	C=N isomerisation & PET	Zn^{2+}	1:1	10.0×10^{-6}	DMF	[194]
Probe-12	Fluorescent	CHEF	Zn^{2+}	1:1	11.9×10^{-6}	DMSO	[195]
Probe-13	Fluorescent	C=N isomerisation & PET	Zn^{2+}	1:1	2.5×10^{-4}	DMSO	[196]
Probe-14	Fluorescent	PET	Zn^{2+}	1:1	3.35×10^{-7}	Ethanol-HEPES	[197]
Probe-15	Fluorescent	C=N isomerisation & PET	Zn^{2+}	1:1	3.60×10^{-6}	Ethanol-H_2O	[198]
Probe-16	Fluorescent	C=N isomerisation & PET	Zn^{2+}	2:1	2.72×10^{-6}	DMF-H_2O	[199]
Probe-17	Fluorescent	ESIPT/ICT	Zn^{2+}	1:1	2.2×10^{-9}	CH_3CN-H_2O	[200]
Probe-18	AIEE active Fluorescent	CHEF and AIEE-activation	Zn^{2+}	1:1	1.1×10^{-7}	DMF-H_2O	[201]
Probe-19	Fluorescent	ESIPT & PET	Zn^{2+}	1:1	3.18×10^{-7}	Ethanol-H_20	[202]
Probe-20	Fluorescent	C=N isomerisation & PET	Zn^{2+}	2:1	5.03×10^{-7}	Ethanol-HEPES	[203]
Probe-21	Fluorescent	ESIPT & CHEF	Zn^{2+}	1:1	37.7×10^{-9}	CH_3OH-HEPES	[204]

Probe-22	Fluorescent	PET & CHEF	Zn^{2+}	1:1	5.50×10^{-9}	Ethanol-H_2O	[205]
Probe-23	Fluorescent	PET & CHEF	Zn^{2+}	1:1	21.2×10^{-9}	CH_3OH	[206]
Probe-24	Fluorescent	ESIPT & PET	Zn^{2+}	1:1	1.17×10^{-6}	CH_3CN-H_2O	[207]
Probe-25	Fluorescent	ESIPT & PET	Zn^{2+}	1:1	1.20×10^{-6}	CH_3CN-H_2O	[207]
Probe-26	Fluorescent	ESIPT & CHEF	Zn^{2+}	1:1	3.7×10^{-8}	CH_3OH-H_2O	[208]
Probe-27	Fluorescent	ESIPT & CHEF	Zn^{2+}	1:1	11.0×10^{-9}	CH_3CN-H_2O	[209]
Probe-28	Fluorescent	Complex formation	Zn^{2+}	1:1	8.73×10^{-7}	DMSO	[210]
Probe-29	Fluorescent	CHEF	Zn^{2+}	1:1	0.01×10^{-6}	DMSO-H_2O	[211]
Probe-30	Fluorescent	CHEF & C=N isomerisation	Zn^{2+}	1:1	0.14×10^{-6}	Ethanol-H_2O	[212]
Probe-31	Fluorescent	PET	Zn^{2+}	1:1	5.10×10^{-9}	CH_3CN-H_2O	[116]
Probe-32	Fluorescent	CHEF & C=N isomerisation	Zn^{2+}	1:1	39.0×10^{-9}	DMSO-H_2O	[213]

Probe-33	Fluorescent	CHEF	Zn^{2+}	1:1	1.12×10^{-6}	DMSO	[214]
Probe-34	AIEE active Fluorescent	Coordination polymerization induced emission [CPIE]	Zn^{2+}	1:1	2.8×10^{-7}	THF-H_2O	[215]
Probe-35	AIEE active Fluorescent	CHEF, C=N isomerisation & PET	Zn^{2+}	1:2	2.18×10^{-6}	DMSO-H_2O	[216]
Probe-36	Fluorescent	ESIPT	Zn^{2+}	1:1	0.01×10^{-6}	DMSO-H_2O	[217]

Table 4 *Reported Schiff base sensors for the detection of PA*

Sensor	Sensor type	Sensing mechanism	Analyte	Quenching constant [M^{-1}]	LOD [M]	Metrix/ Solvent	Ref
Probe-1	AIEE active fluorescent	Ground state complexation	PA	4.14×10^{5}	1.74×10^{-6}	THF-H_2O	[206]
Probe-2	Fluorescent	Static and dynamic quenching	PA	2.91×10^{4}	2.81×10^{-7}	DMF	[218]
Probe-3	AIEE active fluorescent	Ground state complexation	PA	70.1×10^{6}	72.6×10^{-9}	THF-H_2O	[219]
Probe-4	Fluorescent	PET	PA	6.45×10^{7}	96.3×10^{-9}	DMSO-H_2O	[220]
Probe-5	Fluorescent	strong -I and -R effect	PA	Not found	1.22×10^{-4}	DMSO-H_2O	[221]
Probe-6	Fluorescent	Static quenching	PA	1.16×10^{6}	20.1×10^{-9}	HEPES	[222]
Probe-7	Fluorescent	PA-Complex formation	PA	1.16×10^{6}	12.1×10^{-9}	DMSO-HEPES	[223]
Probe-8	Fluorescent	H-bonding & π-π interactions	PA	4.77×10^{4}	10.8×10^{-9}	CH_3OH-HEPES	[224]
Probe-9	Fluorescent	H-bonding & π-π interactions	PA	8.49×10^{4}	8.89×10^{-9}	Methanol- HEPES	[224]

Probe-10	Fluorescent	H-bonding & π-π interactions	PA	5.69×10^{6}	9.30×10^{-9}	CH_3OH-HEPES	[224]
Probe-11	Fluorescent	H-bonding interactions	PA	Not found	2.2×10^{-10}	CH_3OH-DMF	[225]
Probe-12	AIEE active fluorescent	PET	PA	2.1×10^{4}	0.77×10^{-6}	CH_3OH-H_2O	[226]
Probe-13	AIEE active fluorescent	Ground state complexation	PA	1.91×10^{5}	0.11×10^{-6}	CH_3OH-H_2O	[227]
Probe-14	AIEE active fluorescent	Inner filter effect [IFA]	PA	2.61×10^{5}	93.0×10^{-9}	THF-H_2O	[228]
Probe-15	AIEE active fluorescent	PET & Ground state complexation	PA	1.48×10^{4}	55.0×10^{-9}	Ethanol-Water	[229]
Probe-16	AIEE active fluorescent	static and dynamic mechanisms & PET	PA	2.21×10^{5}	9.50×10^{-6}	CH_3CN-H_2O	[141]
Probe-17	Fluorescent	H-bonding interactions	PA	2.29×10^{7}	19.0×10^{-9}	CH_3CN	[230]
Probe-18	Fluorescent	FRET, IFE & PET	PA	10.5×10^{3}	4.32×10^{-6}	CH_3CN-H_2O	[231]
Probe-19	Fluorescent	FRET, IFE & PET	PA	29.4×10^{3}	4.15×10^{-6}	CH_3CN-H_2O	[231]

Probe-20	Fluorescent	Static quenching	PA	1.20×10^{3}	Not found	DMSO-H_2O	[232]
Probe-21	AIEE active fluorescent	Static quenching	PA	7.81×10^{4}	0.77×10^{-6}	THF-H_2O	[233]
Probe-22	AIE active fluorescent	Ground state complexation	PA	4.70×10^{5}	16.0×10^{-9}	CH_3CN-H_2O	[234]
Probe-23	fluorescent	PET	PA	Not found	1.7×10^{-5}	CH_3CN-H_2O	[235]
Probe-24	Fluorescent	Resonance energy transfer RET-ICT	PA	Not found	1.50×10^{-6}	CH_3CN-H_2O	[236]
Probe-25	AIE active fluorescent	Destroying of the aggregation effect by PA insertion	PA	Not found	37.5×10^{-9}	DMSO-H_2O	[237]

1.10 The present investigation

Metals/ metal ions are necessary for vital life functions as they play key roles in a variety of essential biological processes. Apart from these, overuse of metals will also act as pollutants that affect human life and environment resulting serious health issues. Even though different analytical techniques have been proposed and used for metal ion monitoring, most of which needs sophisticated instrumentations, lacks on-site real-time monitoring and high cost. Since colourimetric and fluorimetric methods can provide naked eye detection without the use of very expensive equipment, the development of colourimetric and fluorimetric sensors is becoming a growing priority and has great significance in the field of sensing. Therefore, the focus of this research work will be on the design and development of cost-effective, highly sensitive, and selective chemosensors for selected metal ions and PA derived from different Schiff bases. A brief overview of the three Schiff base molecular probes designed and synthesised and their chemosensing behaviours studied are outlined below.

[1] 1,1'-((1E,1'E)((2E,2'E)(1,3-phenylenebis (methanylylidene) bis(hydrazine-2,1-diylidene))bis(methanylylidene))bis (naphthalen-2-ol) [PMB3]

(a) As an organo- fluorescent sensor for successive detection of bivalent zinc and picric acid

(b) As a AIEE active florescent probe for highly sensitive femtomolar level detection of copper in aqueous media.

(c) As an Aggregation-Induced Emission Enhancement (AIEE) active "turn-off" fluorescent sensor for the selective detection of picric acid in aqueous medium

(d) As a colourimetric sensor for simultaneous detection of Cu^{2+} and Ni^{2+} ions.

[2] 1-((E)-((E)-(4-(benzyloxy)benzylidene)hydrazono) methyl) naphthalen-2-ol [BBHN]

(a) As an aggregation-induced emission enhancement fluorescent sensor for nanoscale detection of copper.

(b) As an AIEE active "turn off" fluorescent probe for picric acid.

[3] 1-((E)-((E)-(anthracen-9-ylmethylene)hydrazono) methyl) naphthalen-2-ol [AHN]

(a) As an AIEE active "turn off" fluorescent probe for picric acid and as a colourimetric sensor for Cu^{2+} ion.

Detailed synthesis steps, characterization, sensing activity, and chemosensing mechanism are discussed in the following chapters.

References

1. Săcărescu, L., et al., Selective detection of metal ions, sulfites and glutathione with fluorescent pyrazolines: a review. Environmental Chemistry Letters, 2023. 21(1): p. 561-596.
2. Berhanu, A.L., et al., A review of the applications of Schiff bases as optical chemical sensors. TrAC Trends in Analytical Chemistry, 2019. 116: p. 74-91.
3. Al-Fartusie, F.S. and S.N. Mohssan, Essential trace elements and their vital roles in human body. Indian J Adv Chem Sci, 2017. 5(3): p. 127-136.
4. Goshisht, M.K., G.K. Patra, and N. Tripathi, Fluorescent Schiff base sensors as a versatile tool for metal ion detection: strategies, mechanistic insights, and applications. Materials Advances, 2022. 3(6): p. 2612-2669.
5. Egorova, K.S. and V.P. Ananikov, Toxicity of metal compounds: knowledge and myths. Organometallics, 2017. 36(21): p. 4071-4090.

6. Aragay, G., J. Pons, and A. Merkoçi, Recent trends in macro-, micro-, and nanomaterial-based tools and strategies for heavy-metal detection. Chemical reviews, 2011. 111(5): p. 3433-3458.
7. Pohl, P., Determination of metal content in honey by atomic absorption and emission spectrometries. TrAC Trends in Analytical Chemistry, 2009. 28(1): p. 117-128.
8. Caroli, S., et al., Determination of essential and potentially toxic trace elements in honey by inductively coupled plasma-based techniques. Talanta, 1999. 50(2): p. 327-336.
9. Townsend, A.T., et al., The determination of copper, zinc, cadmium and lead in urine by high resolution ICP-MS. Journal of Analytical Atomic Spectrometry, 1998. 13(11): p. 1213-1219.
10. Doner, G. and A. Ege, Determination of copper, cadmium and lead in seawater and mineral water by flame atomic absorption spectrometry after coprecipitation with aluminum hydroxide. Analytica Chimica Acta, 2005. 547(1): p. 14-17.
11. Lu, Y., et al., A review of the identification and detection of heavy metal ions in the environment by voltammetry. Talanta, 2018. 178: p. 324-338.
12. Siraj, K. and S.A. Kitte, Analysis of copper, zinc and lead using atomic absorption spectrophotometer in ground water of Jimma town of Southwestern Ethiopia. International Journal of Chemical and Analytical Science, 2013. 4(4): p. 201-204.
13. Das, D.D., N. Sharma, and P.A. Chawla, Neutron activation analysis: An excellent nondestructive analytical technique for trace metal analysis. Critical Reviews in Analytical Chemistry, 2023: p. 1-17.
14. Malik, L.A., et al., Detection and removal of heavy metal ions: a review. Environmental Chemistry Letters, 2019. 17: p. 1495-1521.
15. Lee, Y.J., et al., A multifunctional sensor: chromogenic sensing for Mn2+ and fluorescent sensing for Zn2+ and Al3+. Sensors and Actuators B: Chemical, 2014. 201: p. 535-544.
16. You, G.R., et al., A colorimetric sensor for the sequential detection of Cu 2+ and CN− in fully aqueous media: practical performance of Cu 2+. Dalton Transactions, 2015. 44(19): p. 9120-9129.
17. Liu, X., et al., A turn-on fluorescent sensor for zinc and cadmium ions based on perylene tetracarboxylic diimide. Analyst, 2013. 138(3): p. 901-906.
18. Kumar, A., et al., Colorimetric and fluorescent Schiff base sensors for trace detection of pollutants and biologically significant cations: A review (2010–2021). Microchemical Journal, 2022. 181: p. 107798.
19. Wei, T.-B., et al., A highly selective chemosensor for colorimetric detection of Fe3+ and fluorescence turn-on response of Zn2+. Dyes and Pigments, 2013. 97(2): p. 297-302.

20. Hou, J.-T., et al., Two birds with one stone: Multifunctional and highly selective fluorescent probe for distinguishing Zn2+ from Cd2+ and selective recognition of sulfide anion. Talanta, 2013. 116: p. 434-440.
21. Kim, K.B., et al., A cap-type Schiff base acting as a fluorescence sensor for zinc (II) and a colorimetric sensor for iron (II), copper (II), and zinc (II) in aqueous media. Dalton Transactions, 2013. 42(47): p. 16569-16577.
22. Kaur, N. and S. Kumar, Colorimetric metal ion sensors. Tetrahedron, 2011. 67(48): p. 9233-9264.
23. Kaur, B., N. Kaur, and S. Kumar, Colorimetric metal ion sensors–a comprehensive review of the years 2011–2016. Coordination chemistry reviews, 2018. 358: p. 13-69.
24. Caricato, M., et al., From red to blue shift: switching the binding affinity from the acceptor to the donor end by increasing the π-bridge in push–pull chromophores with coordinative ends. New Journal of Chemistry, 2013. 37(9): p. 2792-2799.
25. Hrishikesan, E. and P. Kannan, Azobenzene chemosensor based on nitrogen chelator for the detection of Cu (II) ion in aqueous medium. Inorganic Chemistry Communications, 2013. 37: p. 21-25.
26. Rani, R., K. Paul, and V. Luxami, An NBD-based two-in-one Cu 2+/Ni 2+ chemosensor with differential charge transfer processes. New Journal of Chemistry, 2016. 40(3): p. 2418-2422.
27. Wu, J., et al., New sensing mechanisms for design of fluorescent chemosensors emerging in recent years. Chemical Society Reviews, 2011. 40(7): p. 3483-3495.
28. Martínez-Máñez, R. and F. Sancenón, Chemodosimeters and 3D inorganic functionalised hosts for the fluoro-chromogenic sensing of anions. Coordination Chemistry Reviews, 2006. 250(23-24): p. 3081-3093.
29. Wiskur, S.L., et al., Teaching old indicators new tricks. Accounts of chemical research, 2001. 34(12): p. 963-972.
30. Martinez-Manez, R. and F. Sancenon, Fluorogenic and chromogenic chemosensors and reagents for anions. Chemical reviews, 2003. 103(11): p. 4419-4476.
31. Dujols, V., F. Ford, and A.W. Czarnik, A long-wavelength fluorescent chemodosimeter selective for Cu (II) ion in water. Journal of the American Chemical Society, 1997. 119(31): p. 7386-7387.
32. Sharma, H., et al., Optical chemosensors for water sample analysis. Journal of Materials Chemistry C, 2016. 4(23): p. 5154-5194.
33. Bell, T.W. and N.M. Hext, Supramolecular optical chemosensors for organic analytes. Chemical Society Reviews, 2004. 33(9): p. 589-598.
34. Jung, H.S., et al., Fluorescent and colorimetric sensors for the detection of humidity or water content. Chemical Society Reviews, 2016. 45(5): p. 1242-1256.

35. HeeáLee, M. and J. SeungáKim, Small molecule-based ratiometric fluorescence probes for cations, anions, and biomolecules. Chemical Society Reviews, 2015. 44(13): p. 4185-4191.
36. De Silva, A.P., T.S. Moody, and G.D. Wright, Fluorescent PET (Photoinduced Electron Transfer) sensors as potent analytical tools. Analyst, 2009. 134(12): p. 2385-2393.
37. Yuan, L., et al., Development of FRET-based ratiometric fluorescent Cu2+ chemodosimeters and the applications for living cell imaging. Organic letters, 2012. 14(2): p. 432-435.
38. Suresh, M., et al., Resonance energy transfer approach and a new ratiometric probe for Hg2+ in aqueous media and living organism. Organic Letters, 2009. 11(13): p. 2740-2743.
39. Zuo, Y., et al., Design strategies of logic gate sensors based on FRET mechanism. TrAC Trends in Analytical Chemistry, 2023: p. 117271.
40. Sedgwick, A.C., et al., Excited-state intramolecular proton-transfer (ESIPT) based fluorescence sensors and imaging agents. Chemical Society Reviews, 2018. 47(23): p. 8842-8880.
41. Zhao, J., et al., Excited state intramolecular proton transfer (ESIPT): from principal photophysics to the development of new chromophores and applications in fluorescent molecular probes and luminescent materials. Physical Chemistry Chemical Physics, 2012. 14(25): p. 8803-8817.
42. Iijima, T., et al., Excited-state intramolecular proton transfer of naphthalene-fused 2-(2′-hydroxyaryl) benzazole family. The Journal of Physical Chemistry A, 2010. 114(4): p. 1603-1609.
43. David, C.I., G. Prabakaran, and R. Nandhakumar, Recent approaches of 2HN derived fluorophores on recognition of Al3+ ions: A review for future outlook. Microchemical Journal, 2021. 169: p. 106590.
44. Chen, S., Y.-L. Yu, and J.-H. Wang, Inner filter effect-based fluorescent sensing systems: A review. Analytica chimica acta, 2018. 999: p. 13-26.
45. Panigrahi, S.K. and A.K. Mishra, Inner filter effect in fluorescence spectroscopy: As a problem and as a solution. Journal of Photochemistry and Photobiology C: Photochemistry Reviews, 2019. 41: p. 100318.
46. Wu, J.-S., et al., Fluorescence turn on of coumarin derivatives by metal cations: a new signaling mechanism based on C= N isomerization. Organic Letters, 2007. 9(1): p. 33-36.
47. Pandey, M.D., et al., Advancements in the Development of Fluorescent Chemosensors Based on C= N Bond Isomerization/Modulation Mechanistic Approach. Analytical Methods, 2024.
48. Tang, B.Z., et al., Efficient blue emission from siloles. Journal of Materials Chemistry, 2001. 11(12): p. 2974-2978.
49. Luo, J., et al., Aggregation-induced emission of 1-methyl-1, 2, 3, 4, 5-pentaphenylsilole. Chemical communications, 2001(18): p. 1740-1741.

50. Hong, Y., J.W. Lam, and B.Z. Tang, Aggregation-induced emission. Chemical Society Reviews, 2011. 40(11): p. 5361-5388.
51. Chua, M.H., et al., Recent advances in cation sensing using aggregation-induced emission. Materials Chemistry Frontiers, 2021. 5(2): p. 659-708.
52. Chung, J.W., et al., High-contrast on/off fluorescence switching via reversible E–Z isomerization of diphenylstilbene containing the α-cyanostilbenic moiety. The Journal of Physical Chemistry C, 2013. 117(21): p. 11285-11291.
53. Marsh, A.V., et al., Carborane-induced excimer emission of severely twisted bis-o-carboranyl chrysene. Angewandte Chemie, 2018. 130(33): p. 10800-10805.
54. Gupta, A.S., K. Paul, and V. Luxami, A fluorescent probe with "AIE+ ESIPT" characteristics for Cu2+ and F− ions estimation. Sensors and Actuators B: Chemical, 2017. 246: p. 653-661.
55. Xiong, J.-B., et al., Evidence for aggregation-induced emission from free rotation restriction of double bond at excited state. Organic letters, 2018. 20(2): p. 373-376.
56. Huang, S., et al., Insights into Optical Probes Based on Aggregation-Induced Emission: from Restriction of Intramolecular Motions to Dark State. Advanced Optical Materials, 2021. 9(21): p. 2100832.
57. Ye, F.-Y., M. Hu, and Y.-S. Zheng, Advances and challenges of metal ions sensors based on AIE effect. Coordination Chemistry Reviews, 2023. 493: p. 215328.
58. Da Silva, C.M., et al., Schiff bases: A short review of their antimicrobial activities. Journal of Advanced research, 2011. 2(1): p. 1-8.
59. Zafar, H., et al., Synthesis, characterization and antimicrobial studies of Schiff base complexes. Journal of Molecular Structure, 2015. 1097: p. 129-135.
60. Min, C.H., et al., A new Schiff-based chemosensor for chromogenic sensing of Cu 2+, Co 2+ and S 2− in aqueous solution: experimental and theoretical studies. New Journal of Chemistry, 2017. 41(10): p. 3991-3999.
61. Dai, Y., et al., Dinuclear Cu (II) complexes based on two flexible Schiff-base ligands and one unusual in situ formed diphenolate 2, 6-piperidin-4-one derivative. Dalton Transactions, 2014. 43(37): p. 13831-13834.
62. Hsieh, W.H., et al., A turn-on Schiff base fluorescence sensor for zinc ion. Tetrahedron letters, 2012. 53(44): p. 5848-5851.
63. Gupta, V.K., et al., Comparative study of colorimetric sensors based on newly synthesized Schiff bases. Sensors and Actuators B: Chemical, 2013. 182: p. 642-651.
64. Bariya, D., et al., AIEE active Cholyl Hydrazide Carbazole-Schiff base for selective detection of copper (II) ion. Journal of Photochemistry and Photobiology A: Chemistry, 2024: p. 115519.

65. Taha, A., et al., Recent developments in Schiff base centered optical and chemical sensors for metal ion recognition. Journal of Molecular Liquids, 2024: p. 124678.
66. Goel, A., et al., A multi-responsive pyranone based Schiff base for the selective, sensitive and competent recognition of copper metal ions. Spectrochimica Acta Part A: Molecular and Biomolecular Spectroscopy, 2021. 249: p. 119221.
67. Bsharat, I., et al., Synthesis, characterization, antibacterial and anticancer activities of some heterocyclic imine compounds. Journal of Molecular Structure, 2023. 1289: p. 135789.
68. Bensaber, S.M., et al., Chemical synthesis, molecular modelling, and evaluation of anticancer activity of some pyrazol-3-one Schiff base derivatives. Medicinal Chemistry Research, 2014. 23: p. 5120-5134.
69. Cozzi, P.G., Metal–Salen Schiff base complexes in catalysis: practical aspects. Chemical Society Reviews, 2004. 33(7): p. 410-421.
70. Sivagamasundari, M. and R. Ramesh, Luminescent property and catalytic activity of Ru (II) carbonyl complexes containing N, O donor of 2-hydroxy-1-naphthylideneimines. Spectrochimica Acta Part A: Molecular and Biomolecular Spectroscopy, 2007. 66(2): p. 427-433.
71. Venkatachalam, G. and R. Ramesh, Ruthenium (III) bis-bidentate Schiff base complexes mediated transfer hydrogenation of imines. Inorganic Chemistry Communications, 2006. 9(7): p. 703-707.
72. Adam, M.S.S., et al., Tailoring, structural inspection of novel oxy and non-oxy metal-imine chelates for DNA interaction, pharmaceutical and molecular docking studies. Polyhedron, 2021. 201: p. 115167.
73. Brawley, J., et al., Synthesis and evaluation of 4-hydroxycoumarin imines as inhibitors of class II myosins. Journal of medicinal chemistry, 2020. 63(19): p. 11131-11148.
74. Dudev, M., et al., Factors governing the metal coordination number in metal complexes from Cambridge Structural Database analyses. The Journal of Physical Chemistry B, 2006. 110(4): p. 1889-1895.
75. Ciaccia, M. and S. Di Stefano, Mechanisms of imine exchange reactions in organic solvents. Organic & Biomolecular Chemistry, 2015. 13(3): p. 646-654.
76. Kawamichi, T., et al., X-ray observation of a transient hemiaminal trapped in a porous network. Nature, 2009. 461(7264): p. 633-635.
77. Thakur, S. and A. Bhalla, Sustainable synthetic endeavors of pharmaceutically active Schiff bases and their metal complexes: A review on recent reports. Tetrahedron, 2024: p. 133836.
78. Das, A.K. and S. Goswami, 2-Hydroxy-1-naphthaldehyde: A versatile building block for the development of sensors in supramolecular chemistry and molecular recognition. Sensors and Actuators B: Chemical, 2017. 245: p. 1062-1125.
79. Myint, Z.W., et al., Copper deficiency anemia. Annals of hematology, 2018. 97: p. 1527-1534.

80. Ramdass, A., et al., Recent developments on optical and electrochemical sensing of copper (II) ion based on transition metal complexes. Coordination Chemistry Reviews, 2017. 343: p. 278-307.
81. Balamurugan, K. and W. Schaffner, Copper homeostasis in eukaryotes: teetering on a tightrope. Biochimica et Biophysica Acta (BBA)-Molecular Cell Research, 2006. 1763(7): p. 737-746.
82. Uauy, R., M. Olivares, and M. Gonzalez, Essentiality of copper in humans. The American journal of clinical nutrition, 1998. 67(5): p. 952S-959S.
83. Manna, A.K., et al., A new ICT based Schiff-base chemosensor for colorimetric selective detection of copper and its copper complex for both colorimetric and fluorometric detection of Cysteine. Journal of Photochemistry and Photobiology A: Chemistry, 2018. 367: p. 74-82.
84. Goswami, N., H.P. Gogoi, and P. Barman, A hydrazine-based unsymmetrical bis-imine-Schiff base as a chemosensor for turn-off fluorescence and naked-eye detection of Cu2+ ion: Application in aqueous media using test strips. Journal of Photochemistry and Photobiology A: Chemistry, 2024. 446: p. 115106.
85. Jang, Y.K., et al., A selective colorimetric and fluorescent chemosensor based-on naphthol for detection of Al3+ and Cu2+. Dyes and Pigments, 2013. 99(1): p. 6-13.
86. dos Santos Carlos, F., et al., A novel fluorene-derivative Schiff-base fluorescent sensor for copper (II) in organic media. Journal of Photochemistry and Photobiology A: Chemistry, 2017. 348: p. 41-46.
87. Sadia, M., et al., Synthesis and evaluation of a schiff-based fluorescent chemosensors for the selective and sensitive detection of Cu 2+ in aqueous media with fluorescence off-on responses. Journal of Fluorescence, 2018. 28: p. 1281-1294.
88. Patil, S.R., et al., A uracil nitroso amine based colorimetric sensor for the detection of Cu 2+ ions from aqueous environment and its practical applications. RSC advances, 2015. 5(28): p. 21464-21470.
89. Chopra, T., et al., A comprehensive review on recent advances in copper sensors. Coordination Chemistry Reviews, 2022. 470: p. 214704.
90. Shahid, M., H.M. Chawla, and P. Bhatia, A calix [4] arene based turn off/turn on molecular receptor for Cu2+ and CN− ions in aqueous medium. Sensors and Actuators B: Chemical, 2016. 237: p. 470-478.
91. Guo, Z.-Q., W.-Q. Chen, and X.-M. Duan, Highly selective visual detection of Cu (II) utilizing intramolecular hydrogen bond-stabilized merocyanine in aqueous buffer solution. Organic letters, 2010. 12(10): p. 2202-2205.
92. Scolari Grotto, F. and V. Glaser, Are high copper levels related to Alzheimer's and Parkinson's diseases? A systematic review and meta-analysis of articles published between 2011 and 2022. Biometals, 2023: p. 1-20.

93. Srishti, K., O. Negi, and P.K. Hota, Recent Development on Copper-Sensor and its Biological Applications: A Review. Journal of Fluorescence, 2024: p. 1-41.
94. Kozlowski, H., et al., Copper, zinc and iron in neurodegenerative diseases (Alzheimer's, Parkinson's and prion diseases). Coordination Chemistry Reviews, 2012. 256(19-20): p. 2129-2141.
95. Kim, P.A., et al., A chelated-type colorimetric chemosensor for sensing Co2+ and Cu2+. Inorganica Chimica Acta, 2020. 505: p. 119502.
96. Ryu, K.Y., et al., Colorimetric chemosensor for multiple targets, Cu 2+, CN− and S 2−. RSC advances, 2016. 6(20): p. 16586-16597.
97. Sahu, M., et al., A novel dihydro phenylquinazolinone-based two-in-one colourimetric chemosensor for nickel (II), copper (II) and its copper complex for the fluorescent colourimetric nanomolar detection of the cyanide anion. RSC advances, 2020. 10(73): p. 44860-44875.
98. Khan, R.I., A. Ramu, and K. Pitchumani, Design and one-pot synthesis of a novel pyrene based fluorescent sensor for selective “turn on”, naked eye detection of Ni2+ ions, and live cell imaging. Sensors and Actuators B: Chemical, 2018. 266: p. 429-437.
99. Manna, A.K., S. Chowdhury, and G.K. Patra, A novel hydrazide-based selective and sensitive optical chemosensor for the detection of Ni 2+ ions: Applications in live cell imaging, molecular logic gates and smart phone-based analysis. Dalton Transactions, 2019. 48(32): p. 12336-12348.
100. Chowdhury, B., et al., Salen type ligand as a selective and sensitive nickel (II) ion chemosensor: a combined investigation with experimental and theoretical modelling. Sensors and Actuators B: Chemical, 2018. 276: p. 560-566.
101. Chakraborty, S. and S. Rayalu, Detection of nickel by chemo and fluoro sensing technologies. Spectrochimica Acta Part A: Molecular and Biomolecular Spectroscopy, 2021. 245: p. 118915.
102. Feng, L., et al., Colorimetric filtrations of metal chelate precipitations for the quantitative determination of nickel (II) and lead (II). Analyst, 2011. 136(20): p. 4197-4203.
103. Khan, J., Optical Chemosensors Synthesis and Appplication for Trace Level Metal Ions Detection in Aqueous Media: A Review. Journal of Fluorescence, 2024: p. 1-22.
104. Kumar, M., et al., A Ni2+ selective chemosensor based on partial cone conformation of calix [4] arene. Dalton Transactions, 2010. 39(42): p. 10116-10121.
105. Liu, X., et al., A highly selective colorimetric chemosensor for detection of nickel ions in aqueous solution. New Journal of Chemistry, 2014. 38(4): p. 1418-1423.
106. Denkhaus, E. and K. Salnikow, Nickel essentiality, toxicity, and carcinogenicity. Critical reviews in oncology/hematology, 2002. 42(1): p. 35-56.

107. Kasprzak, K.S., F.W. Sunderman Jr, and K. Salnikow, Nickel carcinogenesis. Mutation Research/Fundamental and Molecular Mechanisms of Mutagenesis, 2003. 533(1-2): p. 67-97.
108. Lv, X.-L. and S.-Z. Luo, A fluorescence chemosensor based on peptidase for detecting nickel (II) with high selectivity and high sensitivity. Analytical and bioanalytical chemistry, 2012. 402: p. 2999-3002.
109. Arvas, B., et al., A new coumarin based Schiff base fluorescence probe for zinc ion. Tetrahedron, 2021. 88: p. 132127.
110. Park, G.J., et al., A highly selective turn-on chemosensor capable of monitoring Zn2+ concentrations in living cells and aqueous solution. Sensors and Actuators B: Chemical, 2015. 215: p. 568-576.
111. Falchuk, K.H., The molecular basis for the role of zinc in developmental biology. Molecular and cellular effects of nutrition on disease processes, 1998: p. 41-48.
112. Xue, J., L.-m. Tian, and Z.-y. Yang, A novel rhodamine-chromone Schiff-base as turn-on fluorescent probe for the detection of Zn (II) and Fe (III) in different solutions. Journal of Photochemistry and Photobiology A: Chemistry, 2019. 369: p. 77-84.
113. Xie, D.-X., et al., A simple fluorescent probe for Zn (II) based on the aggregation-induced emission. Dyes and Pigments, 2013. 96(2): p. 495-499.
114. Hong, Y., et al., Fluorogenic Zn (II) and chromogenic Fe (II) sensors based on terpyridine-substituted tetraphenylethenes with aggregation-induced emission characteristics. ACS applied materials & interfaces, 2011. 3(9): p. 3411-3418.
115. Mashraqui, S.H., et al., A simple 2, 6-bis (2-benzimidazole) pyridyl incorporated optical probe affording selective ratiometric targeting of biologically and environmentally significant Zn 2+ under buffer condition. Journal of Inclusion Phenomena and Macrocyclic Chemistry, 2016. 84: p. 129-135.
116. Rani, B.K. and S.A. John, A highly selective turn-on fluorescent chemosensor for detecting zinc ions in living cells using symmetrical pyrene system. Journal of Photochemistry and Photobiology A: Chemistry, 2021. 418: p. 113372.
117. Cuajungco, M.P. and G.J. Lees, Zinc metabolism in the brain: relevance to human neurodegenerative disorders. Neurobiology of disease, 1997. 4(3-4): p. 137-169.
118. Bush, A.I., Metals and neuroscience. Current opinion in chemical biology, 2000. 4(2): p. 184-191.
119. Cuajungco, M.P. and G.J. Lees, Zinc and Alzheimer's disease: is there a direct link? Brain research reviews, 1997. 23(3): p. 219-236.
120. Takeda, A., Zinc homeostasis and functions of zinc in the brain. Biometals, 2001. 14: p. 343-351.

121. Dos Santos, A.B., et al., Higher zinc concentrations in hair of Parkinson's disease are associated with psychotic complications and depression. Journal of Neural Transmission, 2019. 126: p. 1291-1301.
122. Baesler, J., et al., Zn homeostasis in genetic models of Parkinson's disease in Caenorhabditis elegans. Journal of Trace Elements in Medicine and Biology, 2019. 55: p. 44-49.
123. Kumar, V., et al., Alpha-synuclein aggregation, Ubiquitin proteasome system impairment, and L-Dopa response in zinc-induced Parkinsonism: Resemblance to sporadic Parkinson's disease. Molecular and cellular biochemistry, 2018. 444: p. 149-160.
124. Hagimori, M., et al., Fluorescence ON/OFF switching Zn2+ sensor based on pyridine–pyridone scaffold. Sensors and Actuators B: Chemical, 2013. 181: p. 823-828.
125. Hosseini, M., et al., Fluorescence "turn-on" chemosensor for the selective detection of zinc ion based on Schiff-base derivative. Spectrochimica Acta Part A: Molecular and Biomolecular Spectroscopy, 2010. 75(3): p. 978-982.
126. Liu, Y., et al., Diphenyl imidazole-based supramolecular self-assembly system for an efficient fluorometric detection of picric acid. Dyes and Pigments, 2022. 203: p. 110378.
127. Pang, C.-M., et al., A multifunctional probe based on the conjugate of four fused N-heterocycles: Detecting picric acid, Cu2+ and Al3+ in ethanol solution system. Journal of Photochemistry and Photobiology A: Chemistry, 2020. 403: p. 112835.
128. Nagarkar, S.S., et al., Highly selective detection of nitro explosives by a luminescent metal-organic framework. Angew. Chem., Int. Ed, 2013. 52(10): p. 2881-2885.
129. Li, Y.-J., et al., Tripodal naphthalimide assembled novel AIE supramolecular fluorescent sensor for rapid and selective detection of picric acid. Dyes and Pigments, 2020. 181: p. 108563.
130. Sathiyaraj, M., K. Pavithra, and V. Thiagarajan, Azine based AIEgens with multi-stimuli response towards picric acid. New Journal of Chemistry, 2020. 44(20): p. 8402-8411.
131. Jiang, K., et al., A functionalized fluorochrome based on quinoline-benzimidazole conjugate: From facile design to highly sensitive and selective sensing for picric acid. Dyes and Pigments, 2019. 162: p. 367-376.
132. Madhu, S., A. Bandela, and M. Ravikanth, BODIPY based fluorescent chemodosimeter for explosive picric acid in aqueous media and rapid detection in the solid state. RSC advances, 2014. 4(14): p. 7120-7123.
133. Kathiravan, A., et al., Pyrene-based chemosensor for picric acid—fundamentals to smartphone device design. Analytical chemistry, 2019. 91(20): p. 13244-13250.
134. Wang, L., et al., Dual mode detection of picric acid with fluorescence and smartphone colorimetry via AIE active

tetraphenylethylene derivatives. Dyes and Pigments, 2023. 220: p. 111743.
135. Huynh, T.-P., et al., Chemosensor for selective determination of 2, 4, 6-trinitrophenol using a custom designed imprinted polymer recognition unit cross-linked to a fluorophore transducer. Acs Sensors, 2016. 1(6): p. 636-639.
136. Seenan, S. and K.I. Sathiyanarayanan, A multisensing ratiometric fluorescent sensor for recognition of Al3+, Th4+ and picric acid. Inorganic Chemistry Communications, 2021. 132: p. 108825.
137. Cui, F., et al., Aggregation-induced emission enhancement (AIEE) active bispyrene-based fluorescent probe:"turn-off" fluorescence for the detection of nitroaromatics. Spectrochimica Acta Part A: Molecular and Biomolecular Spectroscopy, 2024: p. 124222.
138. Munir, F., et al., Synthesis of AIEE active triazine based new fluorescent and colorimetric probes: A reversible mechanochromism and sequential detection of picric acid and ciprofloxacin. Journal of Photochemistry and Photobiology A: Chemistry, 2022. 429: p. 113921.
139. Dhiman, S., et al., Protonation-and electrostatic-interaction-based fluorescence probes for the selective detection of picric acid (2, 4, 6-trinitrophenol)–an explosive material. Materials Advances, 2021. 2(20): p. 6466-6498.
140. Anbu Durai, W. and A. Ramu, Hydrazone Based Dual–Responsive Colorimetric and Ratiometric Chemosensor for the Detection of Cu 2+/F− Ions: DNA Tracking, Practical Performance in Environmental Samples and Tooth Paste. Journal of fluorescence, 2020. 30: p. 275-289.
141. Soufeena, P., T. Nibila, and K. Aravindakshan, Coumarin based yellow emissive AIEE active probe: A colorimetric sensor for Cu2+ and fluorescent sensor for picric acid. Spectrochimica Acta Part A: Molecular and Biomolecular Spectroscopy, 2019. 223: p. 117201.
142. Gao, C., et al., A retrievable and highly selective fluorescent sensor for detecting copper and sulfide. Sensors and Actuators B: Chemical, 2013. 185: p. 125-131.
143. Zhu, X., et al., A highly selective and instantaneously responsive Schiff base fluorescent sensor for the "turn-off" detection of iron (III), iron (II), and copper (II) ions. Analytical methods, 2019. 11(5): p. 642-647.
144. Aydin, Z. and M. Keles, Colorimetric Detection of Copper (II) Ions Using Schiff-Base Derivatives. ChemistrySelect, 2020. 5(25): p. 7375-7381.
145. Bhardwaj, K., et al., Improving copper (II) sensitivity by combined use of AIEE active and inactive schiff bases. Journal of Fluorescence, 2023: p. 1-10.

146. Wang, X., et al., A highly selective and sensitive Schiff-base based turn-on optical sensor for Cu2+ in aqueous medium and acetonitrile. Inorganic Chemistry Communications, 2017. 79: p. 50-54.
147. Arjunan, S., et al., A selective fluorescence chemosensor: pyrene motif Schiff base derivative for detection of Cu2+ ions in living cells. Journal of Photochemistry and Photobiology A: Chemistry, 2018. 364: p. 424-432.
148. Slassi, S., et al., A highly turn-on fluorescent CHEF-type chemosensor for selective detection of Cu2+ in aqueous media. Spectrochimica Acta Part A: Molecular and Biomolecular Spectroscopy, 2019. 215: p. 348-353.
149. Ghosh, S., et al., Dual mode selective chemosensor for copper and fluoride ions: a fluorometric, colorimetric and theoretical investigation. Dalton Transactions, 2016. 45(27): p. 11042-11051.
150. Bhosle, A.A., et al., Solvent-free mechanochemical synthesis of a novel benzothiazole-azine based ESIPT-coupled orange AIEgen for the selective recognition of Cu2+ ions in solution and solid phase. Journal of Photochemistry and Photobiology A: Chemistry, 2021. 413: p. 113265.
151. Sun, Y.-X., et al., A turn-off fluorescent probe for the detection of copper (II) ion based on a salicylaldehyde derivatives Schiff-base. Journal of Molecular Structure, 2023. 1291: p. 136069.
152. Padhan, S.K., et al., Ultrasensitive detection of aqueous Cu 2+ ions by a coumarin-salicylidene based AIEgen. Materials Chemistry Frontiers, 2019. 3(11): p. 2437-2447.
153. Bhardwaj, V., et al., An aggregation-induced emissive pyridoxal derived tetradentate Schiff base for the fluorescence turn-off sensing of copper (II) in an aqueous medium. New Journal of Chemistry, 2022. 46(7): p. 3248-3257.
154. Pan, W., et al., AIE-ESIPT based colorimetric and "OFF-ON-OFF" fluorescence Schiff base sensor for visual and fluorescent determination of Cu2+ in an aqueous media. Journal of Photochemistry and Photobiology A: Chemistry, 2021. 420: p. 113506.
155. Li, M., et al., Nopinone-based AIE-active dual-functional fluorescent chemosensor for Hg 2+ and Cu 2+ and its environmental and biological applications. Dalton Transactions, 2020. 49(43): p. 15299-15309.
156. Moghadam, F.N., et al., A new fluorene derived Schiff-base as a dual selective fluorescent probe for Cu2+ and CN−. Spectrochimica Acta Part A: Molecular and Biomolecular Spectroscopy, 2019. 207: p. 6-15.
157. Chandra, R., A. Ghorai, and G.K. Patra, A simple benzildihydrazone derived colorimetric and fluorescent 'on–off-on'sensor for sequential detection of copper (II) and cyanide ions in aqueous solution. Sensors and Actuators B: Chemical, 2018. 255: p. 701-711.
158. Manna, A.K., et al., A highly selective novel multiple amide based Schiff base optical chemosensor for rapid detection of Cu2+ and its

applications in real sample analysis, molecular logic gate and smart phone. Microchemical Journal, 2020. 157: p. 104860.
159. Wang, Z.-G., et al., The development of coumarin Schiff base system applied as highly selective fluorescent/colorimetric probes for Cu2+ and tumor biomarker glutathione detection. Dyes and Pigments, 2020. 175: p. 108156.
160. Torawane, P., et al., A new Schiff base as a turn-off fluorescent sensor for Cu2+ and its photophysical properties. Luminescence, 2017. 32(8): p. 1426-1430.
161. Rathod, R.V., et al., A colorimetric and fluorometric investigation of Cu (II) ion in aqueous medium with a fluorescein-based chemosensor. RSC advances, 2016. 6(41): p. 34608-34615.
162. Bhattacharyya, A., et al., Hydrazine appended self assembled benzoin-naphthalene conjugate as an efficient dual channel probe for Cu2+ and F−: A spectroscopic investigation with live cell imaging for Cu2+ and practical performance for fluoride. Journal of Photochemistry and Photobiology A: Chemistry, 2018. 353: p. 488-498.
163. Xu, Z.-H., et al., AIE active salicylaldehyde-based hydrazone: A novel single-molecule multianalyte (Al3+ or Cu2+) sensor in different solvents. Spectrochimica Acta Part A: Molecular and Biomolecular Spectroscopy, 2019. 212: p. 146-154.
164. Bawa, R., et al., A pyridine dicarboxylate based hydrazone Schiff base for reversible colorimetric recognition of Ni 2+ and PPi. RSC advances, 2023. 13(23): p. 15391-15400.
165. Singh, J., et al., Naphthaldehyde-Based Schiff Base Chemosensor for the Dual Sensing of Cu2+ and Ni2+ Ions. Journal of Fluorescence, 2024. 34(1): p. 149-157.
166. Manna, A.K., et al., A dual-mode highly selective and sensitive Schiff base chemosensor for fluorescent colorimetric detection of Ni 2+ and colorimetric detection of Cu 2+. Photochemical & Photobiological Sciences, 2019. 18: p. 1512-1525.
167. Kumar, G.G.V., et al., A Schiff base receptor as a fluorescence turn-on sensor for Ni 2+ ions in living cells and logic gate application. New Journal of Chemistry, 2018. 42(4): p. 2865-2873.
168. Jiang, J., et al., A novel highly selective colorimetric sensor for Ni (II) ion using coumarin derivatives. Inorganic Chemistry Communications, 2012. 15: p. 12-15.
169. Peralta-Domínguez, D., et al., A Schiff base derivative from cinnamaldehyde for colorimetric detection of Ni2+ in water. Sensors and Actuators B: Chemical, 2015. 207: p. 511-517.
170. Goswami, S., et al., A simple quinoxaline-based highly sensitive colorimetric and ratiometric sensor, selective for nickel and effective in very high dilution. Tetrahedron Letters, 2013. 54(37): p. 5075-5077.

171. Wang, L., D. Ye, and D. Cao, A novel coumarin Schiff-base as a Ni (II) ion colorimetric sensor. Spectrochimica Acta Part A: Molecular and Biomolecular Spectroscopy, 2012. 90: p. 40-44.
172. Li, H., et al., Novel coumarin fluorescent dyes: synthesis, structural characterization and recognition behavior towards Cu (II) and Ni (II). Dyes and Pigments, 2011. 91(3): p. 309-316.
173. Gupta, V.K., et al., An easily accessible switch-on optical chemosensor for the detection of noxious metal ions Ni (II), Zn (II), Fe (III) and UO2 (II). Sensors and Actuators B: Chemical, 2016. 222: p. 468-482.
174. Manna, A.K., et al., A benzohydrazide based two-in-one Ni2+/Cu2+ fluorescent colorimetric chemosensor and its applications in real sample analysis and molecular logic gate. Sensors and Actuators B: Chemical, 2018. 275: p. 350-358.
175. Kumar, A., et al., A highly selective ratiometric and colorimetric detection of Ni2+ and Cu2+ ions using Schiff base ligand. Journal of Molecular Structure, 2022. 1268: p. 133609.
176. Celestina, J.J., et al., One-pot green synthesis of optical fluorescent sensor for selective detection of Ni2+ ions and hydro gel studies. Optical Materials, 2020. 109: p. 110444.
177. Dhanushkodi, M., et al., A simple pyrazine based ratiometric fluorescent sensor for Ni2+ ion detection. Dyes and Pigments, 2020. 173: p. 107897.
178. Santhi, S., et al., Colorimetric and fluorescent sensors for the detection of Co (II), Ni (II) and Cu (II) in aqueous methanol solution. Research on Chemical Intermediates, 2019. 45: p. 4813-4828.
179. Murugan, A.S., et al., A Schiff's base receptor for red fluorescence live cell imaging of Zn 2+ ions in zebrafish embryos and naked eye detection of Ni 2+ ions for bio-analytical applications. Journal of materials chemistry B, 2017. 5(17): p. 3195-3200.
180. Liu, M., et al., A new acylhydrazine N'-(1, 3 dimethylbutylene)-3-hydroxy-naphthohydrazide based fluorescent sensor for the detection of Ni2+. Dyes and Pigments, 2020. 181: p. 108582.
181. Alqasaimeh, M.M., et al., Synthesis and characterization of a new Schiff-base derivative as an optical nickel (II) chemosensor and its antimicrobial activity. Journal of Photochemistry and Photobiology A: Chemistry, 2024. 447: p. 115277.
182. Patil, N., et al., N'-(4-(diethylamino)-2-hydroxybenzylidene) isonicotinohydrazide based chemosensor for nanomolar detection of Ni (II) ion. International Journal of Environmental Analytical Chemistry, 2023. 103(18): p. 7135-7151.
183. Lu, W., et al., An acylhydrazone coumarin as chemosensor for the detection of Ni2+ with excellent sensitivity and low LOD: synthesis, DFT calculations and application in real water and living cells. Inorganica Chimica Acta, 2021. 516: p. 120144.

184. Zhang, J., et al., An easy-to-synthesize multi-photoresponse smart sensor for rapidly detecting Zn 2+ and quantifying Fe 3+ based on the enol/keto binding mode. New Journal of Chemistry, 2019. 43(35): p. 14179-14189.
185. Gharami, S., et al., An ESIPT based chromogenic and fluorescent ratiometric probe for Zn 2+ with imaging in live cells and tissues. New Journal of Chemistry, 2019. 43(4): p. 1857-1863.
186. Wyss, K.M., E.E. Hardy, and A.E. Gorden, An example of enhanced emission of a pyridine containing schiff base zinc2+ complex. Inorganica Chimica Acta, 2019. 492: p. 156-160.
187. Mathew, M.M. and A. Sreekanth, Zn2+ ion responsive fluorescent chemosensor probe of Thiophene-diocarbohydrazide derivatives. Inorganica Chimica Acta, 2021. 516: p. 120149.
188. Upadhyay, Y., et al., Three-in-one type fluorescent sensor based on a pyrene pyridoxal cascade for the selective detection of Zn (II), hydrogen phosphate and cysteine. Dalton Transactions, 2018. 47(3): p. 742-749.
189. Qin, J.-c. and Z.-y. Yang, Fluorescent chemosensor for detection of Zn2+ and Cu2+ and its application in molecular logic gate. Journal of Photochemistry and Photobiology A: Chemistry, 2016. 324: p. 152-158.
190. Wang, Y., et al., A pyrrole-containing hydrazone and its Cu 2+ complex: an easily accessible optical chemosensor system for the successive detection of Zn 2+/Cu 2+ and pyrophosphate. Analytical methods, 2018. 10(48): p. 5790-5796.
191. Gao, L.-L., et al., Quinoline-based hydrazone for colorimetric detection of Co2+ and fluorescence turn-on response of Zn2+. Spectrochimica Acta Part A: Molecular and Biomolecular Spectroscopy, 2020. 230: p. 118025.
192. Yan, J., et al., A novel and resumable Schiff-base fluorescent chemosensor for Zn (II). Tetrahedron Letters, 2016. 57(26): p. 2910-2914.
193. Jung, J.M., et al., Selective chemosensor capable of sensing both CN− and Zn2+: Its application to zebrafish. Sensors and Actuators B: Chemical, 2019. 297: p. 126814.
194. Roy, N., et al., A new coumarin based dual functional chemosensor for colorimetric detection of Fe3+ and fluorescence turn-on response of Zn2+. Sensors and Actuators B: Chemical, 2016. 236: p. 719-731.
195. Kim, M.S., et al., A fluorescent and colorimetric Schiff base chemosensor for the detection of Zn2+ and Cu2+: Application in live cell imaging and colorimetric test kit. Spectrochimica Acta Part A: Molecular and Biomolecular Spectroscopy, 2019. 211: p. 34-43.
196. Hamzi, I., Y. Touati, and B. Mostefa-Kara, Benzil Bis-Hydrazone Based Fluorescence 'Turn-on'Sensor for Highly Sensitive and Selective

Detection of Zn (II) Ions. Journal of Fluorescence, 2023. 33(5): p. 1683-1693.
197. Liu, L.-m. and Z.-y. Yang, A rhodamine and chromone based "turn-on" fluorescent probe (RC1) for Zn (II) in aqueous solutions and its application. Journal of Photochemistry and Photobiology A: Chemistry, 2018. 364: p. 558-563.
198. Liu, C., et al., Development of a novel fluorescent probe for Zn2+/Cu2+/S2− in different solutions based on benzocoumarin derivative. Journal of Photochemistry and Photobiology A: Chemistry, 2019. 385: p. 112091.
199. Qin, J.-c., L. Fan, and Z.-y. Yang, A small-molecule and resumable two-photon fluorescent probe for Zn2+ based on a coumarin Schiff-base. Sensors and Actuators B: Chemical, 2016. 228: p. 156-161.
200. Budri, M., et al., An ESIPT blocked highly ICT based molecular probe to sense Zn (II) ion through turn on optical response: Experimental and theoretical studies. Journal of Photochemistry and Photobiology A: Chemistry, 2020. 390: p. 112298.
201. Shyamal, M., et al., Highly selective turn-on fluorogenic chemosensor for robust quantification of Zn (II) based on aggregation induced emission enhancement feature. ACS sensors, 2016. 1(6): p. 739-747.
202. Qin, J.-c., et al., Recognition of Al3+ and Zn2+ using a single Schiff-base in aqueous media. Synthetic Metals, 2015. 199: p. 179-186.
203. Zhu, J., et al., A Schiff base fluorescence probe for highly selective turn-on recognition of Zn2+. Tetrahedron letters, 2017. 58(4): p. 365-370.
204. Wu, Q., et al., Ratiometric sensing of Zn 2+ with a new benzothiazole-based fluorescent sensor and living cell imaging. Analyst, 2021. 146(13): p. 4348-4356.
205. Xu, Y., et al., A new multifunctional sensor for sequential recognizing of Zn2+ and PPi in acetonitrile solution and detection of In3+ in DMF solution. Journal of Photochemistry and Photobiology A: Chemistry, 2020. 392: p. 112348.
206. Dey, S., et al., An antipyrine based fluorescence "turn-on" dual sensor for Zn 2+ and Al 3+ and its selective fluorescence "turn-off" sensing towards 2, 4, 6-trinitrophenol (TNP) in the aggregated state. Photochemical & Photobiological Sciences, 2019. 18: p. 2717-2729.
207. Berrones-Reyes, J.C., et al., Quantum chemical elucidation of the turn-on luminescence mechanism in two new Schiff bases as selective chemosensors of Zn 2+: Synthesis, theory and bioimaging applications. RSC advances, 2019. 9(53): p. 30778-30789.
208. Patra, L., et al., A new multi-analyte fluorogenic sensor for efficient detection of Al 3+ and Zn 2+ ions based on ESIPT and CHEF features. New Journal of Chemistry, 2018. 42(23): p. 19076-19082.

209. Dey, S., et al., Highly selective and sensitive recognition of Zn (ii) by a novel coumarinyl scaffold following spectrofluorometric technique and its application in living cells. New Journal of Chemistry, 2018. 42(19): p. 16297-16306.
210. Anand, T., A.S. Kumar, and S.K. Sahoo, A novel Schiff base derivative of pyridoxal for the optical sensing of Zn2+ and cysteine. Photochemical & Photobiological Sciences, 2018. 17(4): p. 414-422.
211. Dong, Y., et al., A simple quinolone Schiff-base containing CHEF based fluorescence 'turn-on'chemosensor for distinguishing Zn 2+ and Hg 2+ with high sensitivity, selectivity and reversibility. Dalton Transactions, 2017. 46(20): p. 6769-6775.
212. Orhan, E., et al., A novel benzimidazole-based chemosensor for fluorometric determination of zinc ions. Journal of Fluorescence, 2021. 31: p. 1833-1842.
213. Xiang, D., et al., A novel naphthalimide-based "turn-on" fluorescent chemosensor for highly selective detection of Zn2+. Tetrahedron, 2022. 106: p. 132648.
214. Kim, S., et al., A benzyl carbazate-based fluorescent chemosensor for detecting Zn2+: Application to zebrafish. Spectrochimica Acta Part A: Molecular and Biomolecular Spectroscopy, 2020. 228: p. 117787.
215. Kauno, J.G., et al., Coordination polymerization-induced emission based on a salicylaldehyde hydrazone AIEgen toward Zn2+ detection. Crystal Growth & Design, 2022. 22(11): p. 6564-6574.
216. Das, B., et al., Acetate ion augmented fluorescence sensing of Zn2+ by Salen-based probe, AIE character, and application for picric acid detection. Analytical Science Advances, 2021. 2(9-10): p. 447-463.
217. Bhanja, A.K., et al., An efficient vanillinyl Schiff base as a turn on fluorescent probe for zinc (II) and cell imaging. RSC Advances, 2015. 5(61): p. 48997-49005.
218. Rajbanshi, M., et al., A ratiometric, turn-on chromo-fluorogenic sensor for sequential detection of aluminium ions and picric acid. Journal of Molecular Structure, 2023. 1284: p. 135357.
219. Shyamal, M., et al., Aggregation-induced emission–based highly selective 'turn-off'fluorogenic chemosensor for robust quantification of explosive picric acid in aqueous and solid states. Materials Today Chemistry, 2019. 14: p. 100193.
220. Kumar, R.S. and S.A. Kumar, Highly selective fluorescent chemosensor for the relay detection of Al3+ and picric acid. Inorganic Chemistry Communications, 2019. 106: p. 165-173.
221. Saha, S., et al., Pyridine-pyrazole based Al (III)'turn on'sensor for MCF7 cancer cell imaging and detection of picric acid. RSC advances, 2021. 11(17): p. 10094-10109.
222. Naskar, B., et al., A versatile chemosensor for the detection of Al 3+ and picric acid (PA) in aqueous solution. Dalton Transactions, 2018. 47(44): p. 15907-15916.

223. Sharma, S., et al., Fabrication of a Hydrazone-based Al (III)-selective "turn-on" fluorescent chemosensor and ensuing potential recognition of picric acid. ACS omega, 2019. 4(20): p. 18520-18529.
224. Ghosh, T.K., S. Jana, and A. Ghosh, Exploitation of the flexidentate nature of a ligand to synthesize Zn (II) complexes of diverse nuclearity and their use in solid-state naked eye detection and aqueous phase sensing of 2, 4, 6-trinitrophenol. Inorganic Chemistry, 2018. 57(24): p. 15216-15228.
225. Asthana, S.K., et al., Brightening quinolineimines by Al3+ and subsequent quenching by PPi/PA in aqueous medium: synthesis, crystal structures, binding behavior, theoretical and cell imaging studies. Inorganic Chemistry, 2017. 56(6): p. 3315-3323.
226. Dey, S., et al., Aggregation-induced emission-active hydrazide-based probe: selective sensing of Al3+, HF2–, and nitro explosives. ACS omega, 2019. 4(5): p. 8451-8464.
227. Maity, S., et al., Aggregation induced emission enhancement from antipyrine-based schiff base and its selective sensing towards picric acid. Sensors and Actuators B: Chemical, 2017. 248: p. 223-233.
228. Gowri, A., R. Vignesh, and A. Kathiravan, Anthracene based AIEgen for picric acid detection in real water samples. Spectrochimica Acta Part A: Molecular and Biomolecular Spectroscopy, 2019. 220: p. 117144.
229. Mondal, T., et al., Mechanistic Insight into Selective Sensing of Hazardous Hg2+ and Explosive Picric Acid by Using a Pyrene-Azine-Hydroxyquinoline Framework in Differential Media. ChemistrySelect, 2020. 5(30): p. 9336-9349.
230. Kundu, B.K., S.M. Mobin, and S. Mukhopadhyay, Mechanistic and thermodynamic aspects of a pyrene-based fluorescent probe to detect picric acid. New Journal of Chemistry, 2019. 43(29): p. 11483-11492.
231. Moral, R., O.A. Pegu, and G. Das, Probing the aggregation potential and picric acid recognition aptitude by altering aromatic core substitution in a series of cinnamaldehyde-based receptors. Dyes and Pigments, 2023. 218: p. 111502.
232. Rahman, Z., et al., A 4-aminophthalimide derive smart molecule for sequential detection of aluminum ions and picric acid. Journal of Photochemistry and Photobiology A: Chemistry, 2023. 439: p. 114593.
233. Mazumdar, P., et al., Proton triggered emission and selective sensing of picric acid by the fluorescent aggregates of 6, 7-dimethyl-2, 3-bis-(2-pyridyl)-quinoxaline. Physical Chemistry Chemical Physics, 2016. 18(10): p. 7055-7067.
234. Shyamal, M., et al., Synthesis of an efficient Pyrene based AIE active functional material for selective sensing of 2, 4, 6-trinitrophenol. Journal of Photochemistry and Photobiology A: Chemistry, 2017. 342: p. 1-14.

235. Ghosh, S., N. Baildya, and K. Ghosh, A new 1, 2, 3-triazole-decorated imino-phenol: selective sensing of Zn 2+, Cu 2+ and picric acid under different experimental conditions. New Journal of Chemistry, 2021. 45(24): p. 10923-10929.
236. Halder, S., et al., A quinoline-based compound for explosive 2, 4, 6-trinitrophenol sensing: experimental and DFT-D3 studies. New Journal of Chemistry, 2018. 42(11): p. 8408-8414.
237. Das, S., et al., Selective recognition of Zn (II) by a novel Schiff base chemosensor with the formation of an AIE active Zn (II) complex having picric acid detection ability: Application in live cell imaging study. Journal of Photochemistry and Photobiology A: Chemistry, 2024. 447: p. 115214.

Chapter 2

Synthesis, Characterization, and Methods

This chapter details the materials and experimental procedures used for the synthesis of Schiff bases PMB3, BBHN, and AHN. Additionally, it delves into the analytical techniques utilized for characterization, including spectroscopic methods such as NMR, FT-IR, and UV-Vis spectroscopy. This methodological foundation supports the subsequent evaluation of their chemosensing properties in later chapters.

This chapter describes a brief overview of the materials used, the experimental details for the synthesis of Schiff bases, the analytical procedures, the methods of analyses, and the instrumental techniques used to characterize the compounds.

2.1 Materials

All reagents used for the synthesis of Schiff bases including2-hydroxy-1-naphthaldehyde, 4-benzyloxybenzaldehyde, isophthalal dehyde, and 9-anthraldehyde were purchased from Sigma-Aldrich. Nitrate salts of metals such as Al^{3+}, Hg^{2+}, Zn^{2+}, Co^{2+}, Fe^{3+}, Cd^{2+}, Mn^{2+}, Mg^{2+}, Cr^{3+}, Cu^{2+}, Ni^{2+}, Ca^{2+}, Ag^{+}, Ba^{2+}, Pb^{2+}, Na^{+}, and K^{+} used for sensing studies were purchased from Sigma-Aldrich and Merck India Ltd. All nitroaromatic compounds (NACs) including 2,4,6-trinitro phenol (PA), 2,4- dinitrophenol (2,4-DNP), 2,4,6-trinitrotoluene (TNT), nitrobenzene (NB), 2-nitrophenol (2-NP), 4-nitrophenol (4-NP), 4-nitroaniline (4-NA), 2-nitrotoluene (2-NT), 4-nitrotoluene (4-NT), 3-nitroaniline (3-NA), 3-nitrobenzoic acid(3-NBA) 2-nitroaniline (2-NA), 3-nitrotoluene (3-NT), and 2,4-dinitroaniline (2,4-DNA) used for sensing studies were obtained from Merck India Ltd. The Tertiary butyl ammonium salts of different anions like CN^{-}, F^{-}, Cl^{-}, Br^{-}, I^{-}, NO_3^{-}, AcO^{-}, and $H_3PO_4^{-}$ used for anion sensing studies were purchased from Sigma-Aldrich.

Solvents such as methanol, ethanol, dimethyl formamide (DMF), dimethyl sulfoxide (DMSO), dichloromethane (DCM), acetonitrile, acetone, and chloroform used for the studies were of analytical grade and were used as received without further purifications.

Freshly prepared doubly distilled deionized water was used throughout the experiments.

2.2 Instrumental Techniques

The elemental analysis for carbon, hydrogen, and nitrogen was performed using the elemental analyser Vario EL III CHNS analyser. The Fourier Transform Infra-Red spectra were recorded using a KBr pellet on a Jasco FTIR 4100 spectrometer over the range of 400-4000cm^{-1}. ^{1}H NMR and ^{13}C NMR spectrum were recorded using JEOL JNM-ECZR 500 MHz spectrometer in d_6-DMSO solvent using tetramethyl silane (TMS) as the internal standard. The absorption and fluorescence spectral measurements were carried out using the Jasco UV-Visible spectrophotometer and the Agilent Technologies Cary Eclipse Fluorescence Spectrophotometer. The HRMS(ESI) spectrum analysis was performed on a Thermo Scientific Exactive Orbitrap mass spectrometer. Fluorescent images were taken on the Leica DM6 B System Microscope.

2.3 Synthesis of Schiff bases

2.3.1. Synthesis of (E) 1-(hydrazonomethyl) naphthalen-2-ol

One of the precursors (E) 1-(hydrazonomethyl) naphthalen-2-ol used for synthesis of [1, 1'-((1E, 1'E) - ((2E, 2'E) - (1, 3- phenylenebis (methanylylidene))bis(hydrazine-2,1diylidene))bis(methanylylide ne))bis(naphthalen-2-ol)] [**PMB3**], 1-((E)-((E)-(4-(benzyloxy) benzylidene) hydrazono) methyl) naphthalen-2-ol [**BBHN**], and 1-((E)-((E)-(anthracen-9-ylmethylene)hydrazono)methyl) naphthal en-2-ol [**AHN**] were synthesized from 2-hydroxy-1-naphthaldehyde as starting material using the method reported elsewhere [1-8].

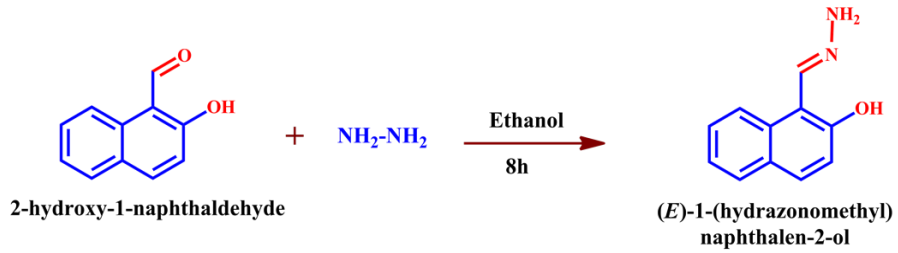

Scheme 1 *Synthetic route of (E) 1-(hydrazonomethyl) naphthalen-2-ol*

2.3.2. Synthesis of [1, 1'-((1E, 1'E) - ((2E, 2'E) - (1, 3-phenylenebis(methanylylidene))bis(hydrazine-2,1 diylidene)) bis (methanylylidene)) bis (naphthalen-2-ol)] [PMB3]

Ethanolic solution of (E) 1-(hydrazonomethyl) naphthalen-2-ol (0.372 g, 2 mmol), and isophthalaldehyde (0.314g, 1 mmol) were mixed in a 2:1 molar ratio with constant stirring with the addition of 2-3 drops of acetic acid. Following that, the mixture was refluxed for 8 h at 80°C. A yellow solid that precipitated was filtered and washed

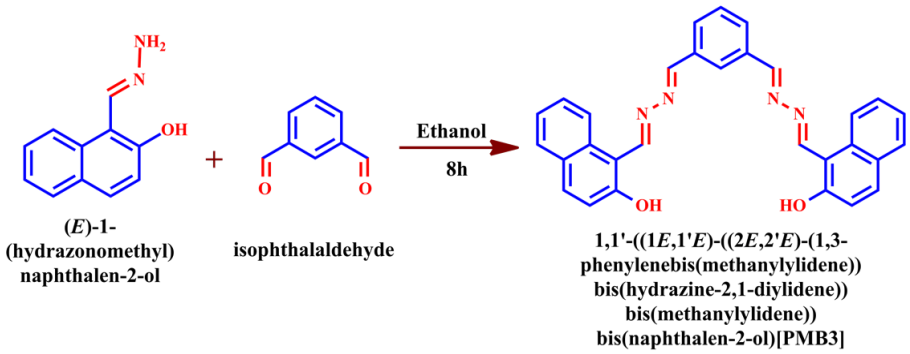

Scheme 2 *Synthetic route of PMB3*

with ethanol and then air-dried. Using column chromatography on alumina and a 1:1 mixture of ethyl acetate and hexane as eluents, the crude product was purified and recrystallized.

2.3.3 Synthesis of 1-((E)-((E)-(4-(benzyloxy)benzylidene) hydrazono) methyl) naphthalen-2-ol [BBHN]

Ethanolic solution of (E) 1-(hydrazonomethyl) naphthalen-2-ol (0.186 g, 1mmol) was added under vigorous stirring to an ethanolic solution of 4-benzyloxybenzaldehyde (0.212 g, 1 mmol) in a 1:1 molar ratio followed by the addition of 2-3 drops of glacial acetic acid, which was then refluxed for 8 h at 80 °C. The yellow solid precipitated was filtered, washed with ethanol and dried under reduced pressure, and purified by column chromatography on alumina using a 1:1 mixture of ethyl acetate and hexane as eluent.

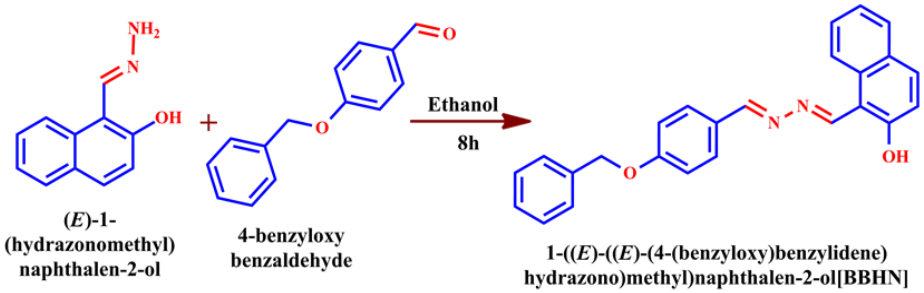

Scheme 3 *Synthetic route of BBHN*

2.3.4 Synthesis of 1-((E)-((E)-(anthracen-9-ylmethylene) hydrazono) methyl) naphthalen-2-ol [AHN]

The precursor (E) 1-(hydrazonomethyl) naphthalen-2-ol (0.186g,1mmol) dissolved in ethanol was added to one equivalent of 9-anthraldehyde (0.206g, 1mmol) with constant stirring and refluxed for 8 hours at 80 ^{0}C. The precipitated yellow solid was then filtered and washed with ethanol and purified by column chromatography on alumina using a 1:1 mixture of ethyl acetate and hexane as eluent.

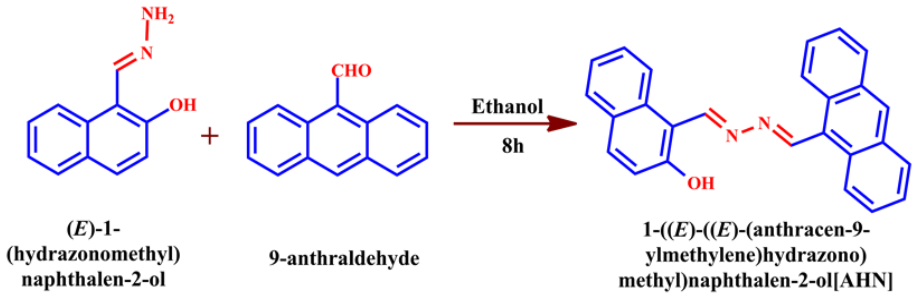

Scheme 4 *Synthetic route of AHN*

2.4 Characterization

The synthesized Schiff bases PMB3, BBHN, and AHN were characterized using methods such as CHNS,^{1}H NMR, ^{13}C NMR, and HRMS(ESI) analysis.

2.4.1 Characterization of PMB3

Chemical Formula: $C_{30}H_{22}N_4O_2$, Yellow solid, Yield: 90%; mp: 309 - 311^{0}C; Anal. Calculated (found) for $C_{30}H_{22}N_4O_2$; C-76.58(75.74), H-4.17(4.73), N-11.91(11.99). ^{1}H NMR (500 MHz, DMSO-d6) δ(ppm): 12.86(S,2H, OH), 9.97(S, 2H, HC=N), 8.64(S, 2H, HC=N), 8.03-8.01(d, 4H, J=9Hz, Ar.H), 7.91-7.90(d, 2H, J=8Hz, Ar.H), 7.62-7.5(m, 4H, J=8Hz, Ar.H), 7.45-7.42(m, 4H, J=10Hz, Ar.H), 7.28-7.26(d, 4H, J=9Hz, Ar.H). ^{13}CNMR (500 MHz, DMSO-d6) δ(ppm): 161.26, 151.20, 149.19, 138.87, 137.09, 131.64, 128.07, 125.4, 125.2, 123.2, 115.3, 109.6. FT-IR (KBr, cm^{-1}): 3437 (-OH), 1623,1596,1580,1540 (-CH=N), HRMS (ESI) $(M+H)^{+}$: calculated for $C_{30}H_{22}N_4O_2$ is 471.1700, found 471.1817. **Fig.1**, **Fig.2**, **Fig.3**, and **Fig.4** represent the FT-IR,^{1}H NMR,^{13}C NMR, and HRMS(ESI) spectrum of PMB3.

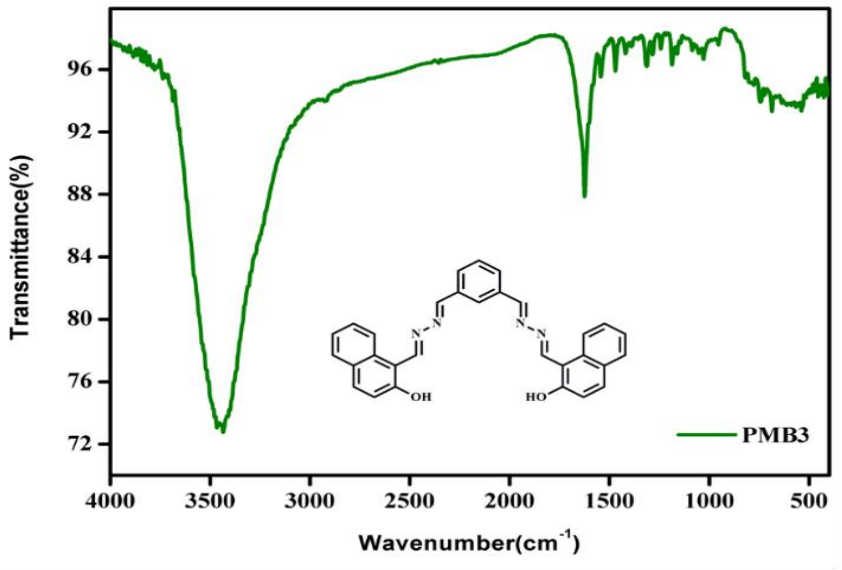

Fig.1 *FT-IR spectrum of PMB3*

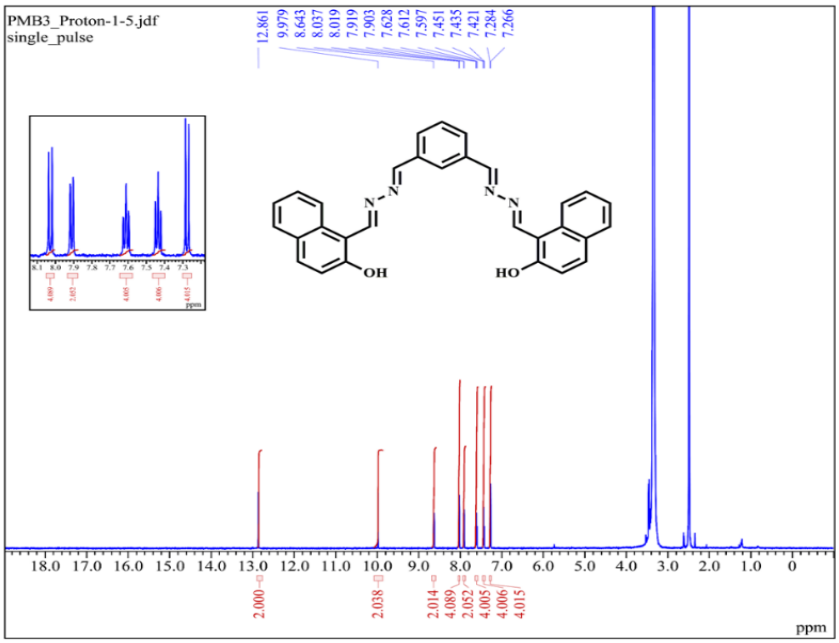

Fig.2 *^{1}H NMR spectrum of the PMB3 in d_6-DMSO solvent*

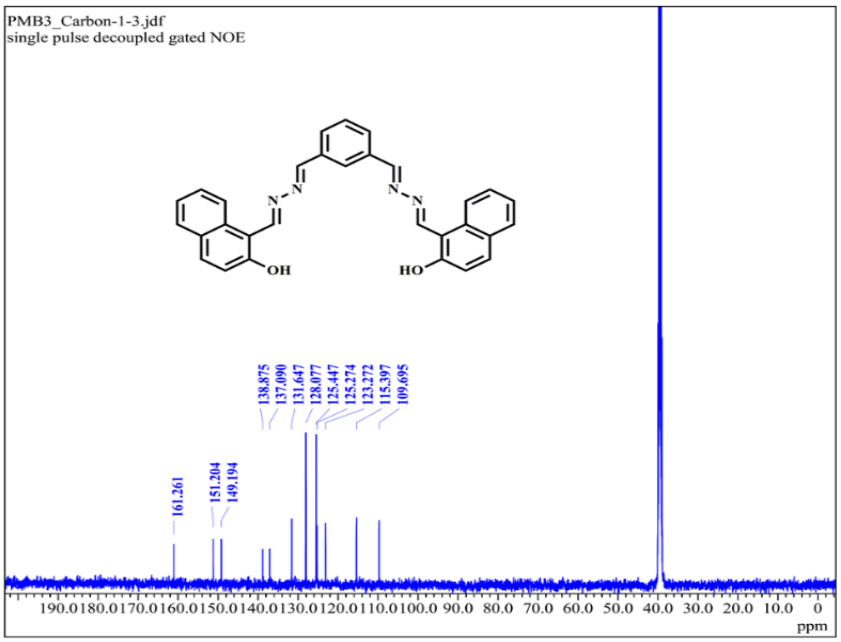

Fig.3 *^{13}C NMR spectrum of the PMB3 in d_6-DMSO solvent*

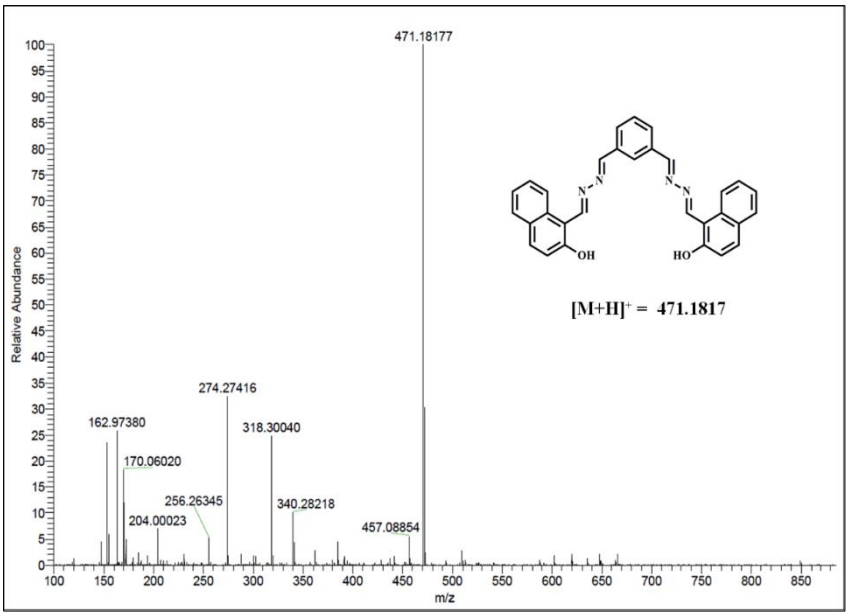

Fig.4 *HR-MS(ESI) spectrum of the PMB3 in acetonitrile solvent*

2.4.2 Characterization of BBHN

Chemical Formula: $C_{25}H_{20}N_2O_2$, Yellow solid, Yield: 87%; Mp: 295 – 297 ^{0}C; Anal. Calculated (found) for $C_{25}H_{20}N_2O_2$; C-78.93(78.62), H-5.30(5.28), N-7.36(7.38). ^{1}H NMR (500 MHz, DMSO-d6): 12.858(S, 1H, OH), 9.977(S, 1H, -HC=N), 8.609(S, 1H, -HC=N), 8.035-8.017(d, 1H, J=9Hz, Ar.H), 7.918-7.901(d, 1H, J=8.5Hz, Ar.H), 7.803-7.785(d, 3H, J=9Hz, Ar.H), 7.626-7.595(t, 2H, J=8.5Hz, Ar.H), 7.463-7.433(t , 2H, J=7.5Hz, Ar.H), 7.419-7.377(m, 1H, J=6Hz, Ar.H), 7.344-7.315(t, 1H, J=7Hz, Ar.H), 7.283-7.265(d, 1H, J=9Hz, Ar.H),7.126-7.108(d, 3H, J=9Hz, Ar.H), 5.171(S, 2H, -CH_2). ^{13}CNMR (500 MHz, DMSO-d6): 163.240, 159.081, 152.221, 149.521, 139.845, 137.182, 132.012, 128.014, 125.441, 125.268, 124.272, 118.092, 108.085, 66.913. FT-IR (KBr, cm^{-1}): 3444(-OH), 1621,1599 (-CH=N), 1161 (N-N) HRMS (ESI) $(M+H)^+$: calculated for $C_{25}H_{20}N_2O_2$ is 381.15, found 381.1601.

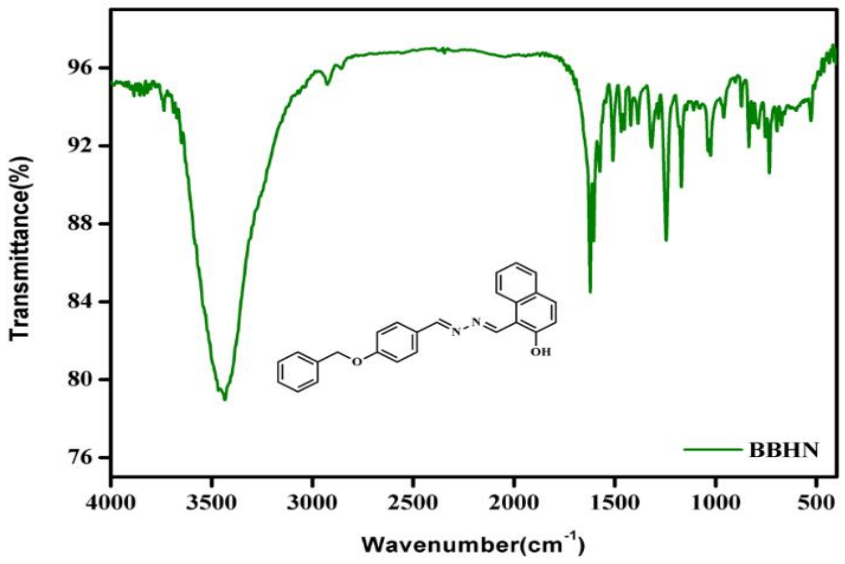

Fig.5 *FT-IR spectrum of BBHN*

Fig.5, **Fig.6**, **Fig.7**, and **Fig.8** represent the FT-IR,^{1}H NMR,^{13}C NMR, and HRMS(ESI) spectrum of BBHN.

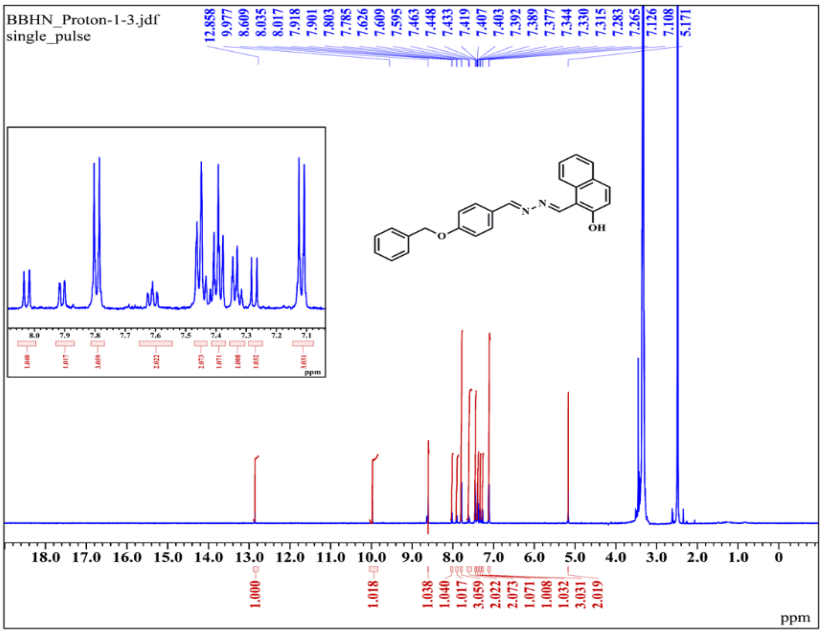

Fig.6 *^{1}H NMR spectrum of the BBHN in d_6-DMSO solvent*

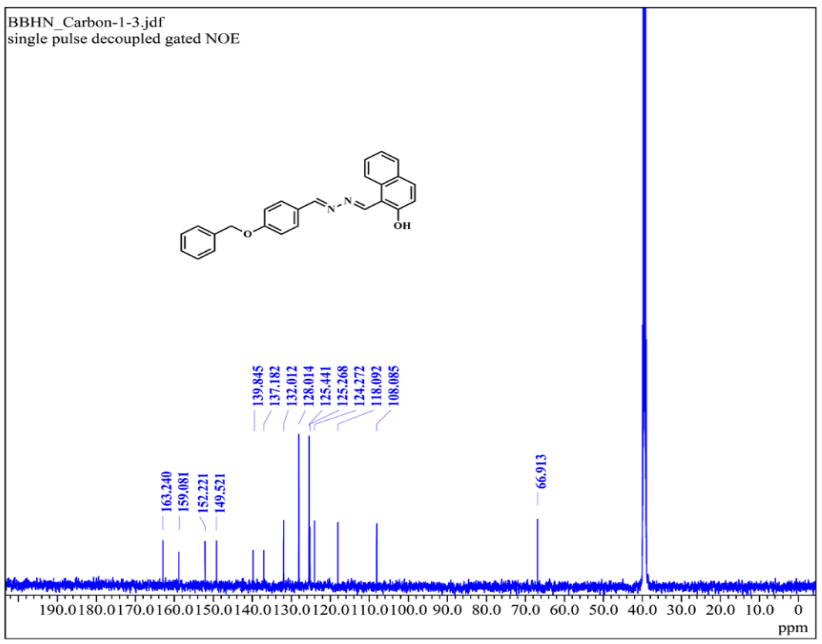

Fig.7 *^{13}C NMR spectrum of the BBHN in d_6-DMSO solvent*

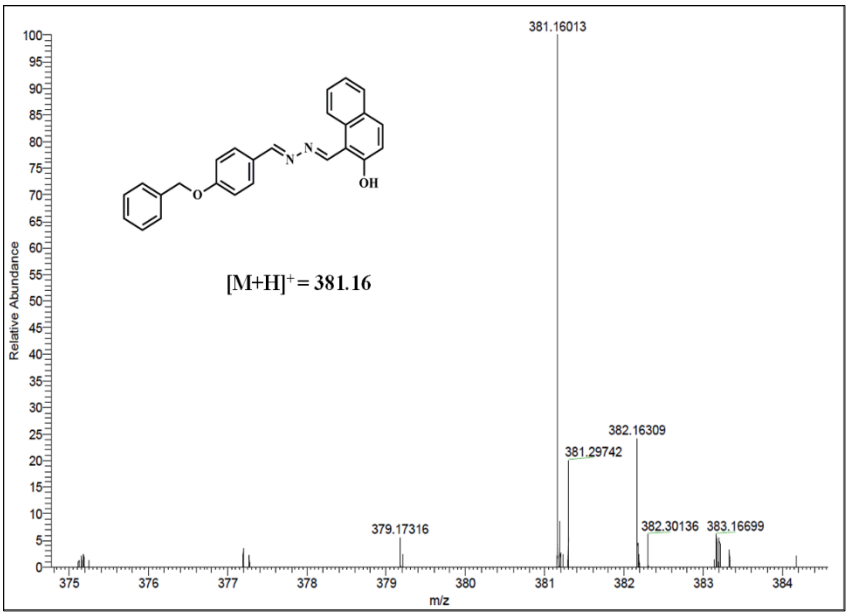

Fig.8 *HR-MS(ESI) spectrum of the BBHN in acetonitrile solvent*

2.4.3 Characterization of AHN

Chemical Formula: $C_{26}H_{18}N_2O$, Red solid, Yield: 87%; mp: 291-293 ^{0}C; anal. calculated (found) for $C_{26}H_{18}N_2O$; C-83.40(82.18), H-4.85(4.81), N-7.48 (7.30). ^{1}H NMR (500 MHz, DMSO-d_6):13.163(S, 1H, OH), 9.953(S, 1H, -CH=N), 9.725(S, 1H, -CH=N), 8.947-8.929(d, 2H, J=9Hz, Ar.H), 8.829(S, 2H, Ar.H), 8.627-8.610(d, 1H, J=8.5Hz, Ar.H), 8.203-8.186(d, 2H, J=8.5Hz, Ar.H), 8.061-8.043(d, 1H, J=9Hz, Ar.H), 7.935-7.919(d, 1H, J=8Hz, Ar.H), 7.705-7.672(t, 2H, J=10.5Hz, Ar.H), 7.635-7.603(t, 2H, J=10Hz, Ar.H), 7.457-7.426(t, 1H, J=9.5Hz, Ar.H),7.317-7.299(d, 1H, J=9Hz, Ar.H). ^{13}CNMR (500 MHz, DMSO-d_6): 161.144, 152.367, 150.778, 131.139, 130.908, 130.275, 129.056, 128.086, 127.626, 125.706, 125.322, 123.824, 121.598, 118.939. FT-IR (KBr, cm^{-1}): 3439 (-OH), 1622, 1586 (-CH=N), 1182 (N-N). HRMS (ESI) $(M + H)^+$: calculated for $C_{26}H_{18}N_2O$ is 375.1400,

found 375.1505. **Fig.9**, **Fig.10**, **Fig.11**, and **Fig.12** represent the FT-IR,^{1}H NMR,^{13}C NMR, and HRMS(ESI) spectrum of AHN.

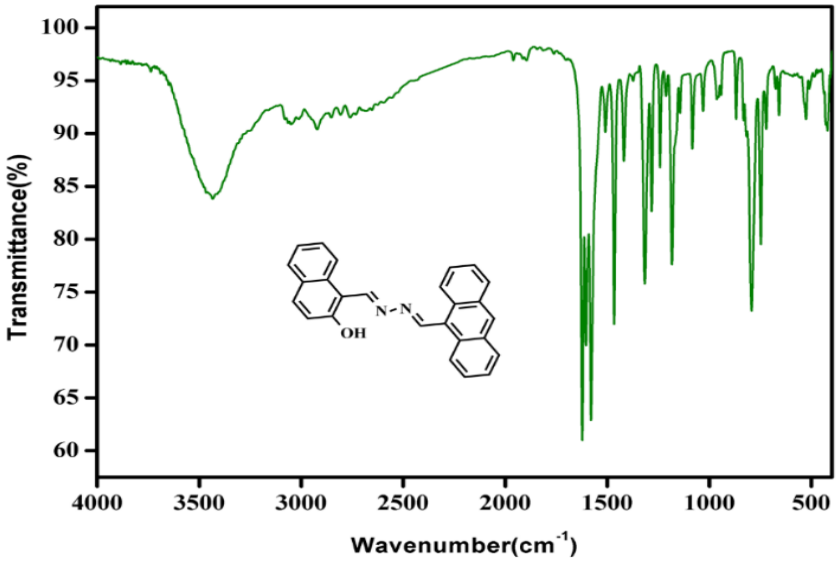

Fig.9 *FT-IR spectrum of AHN*

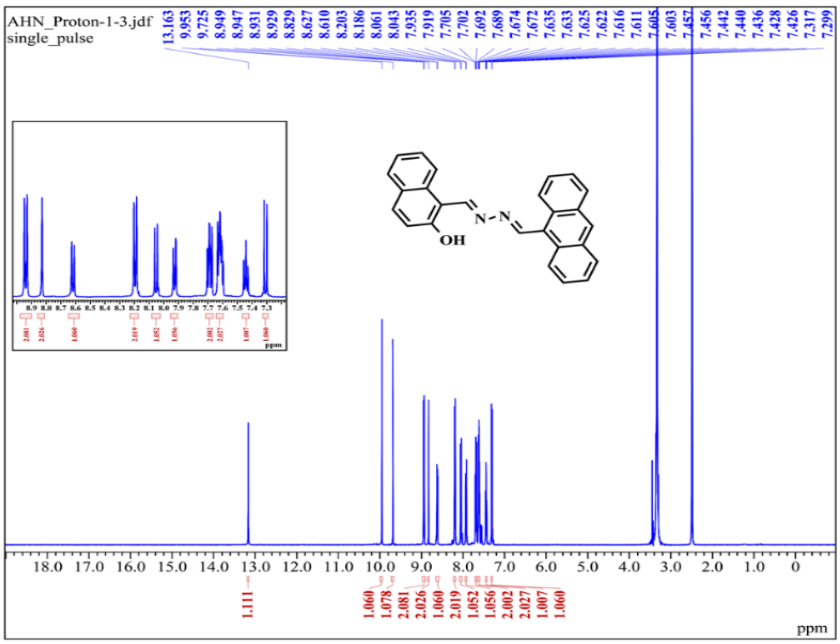

Fig.10 *^{1}H NMR spectrum of the AHN in d_6-DMSO solvent*

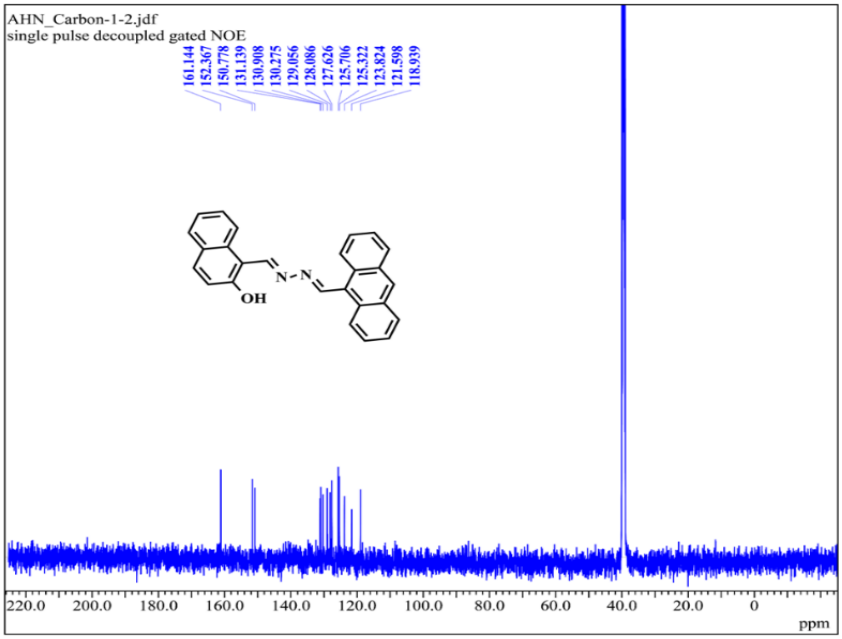

Fig.11 *^{13}C NMR spectrum of the AHN in d_6-DMSO solvent*

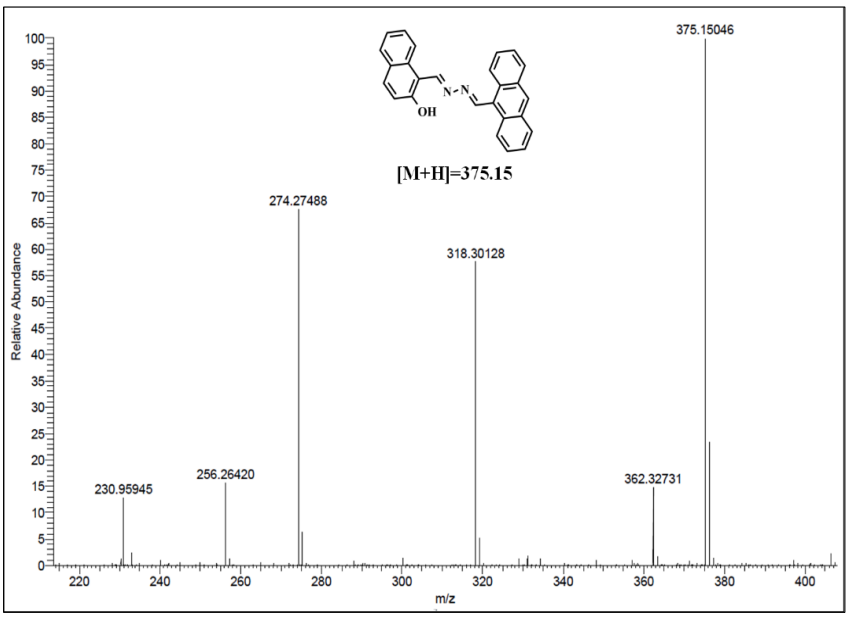

Fig.12 *HR-MS(ESI) spectrum of the AHN in acetonitrile solvent*

References

1. Xiao, H., et al., *Two novel aggregation-induced emission active coumarin-based Schiff bases and their applications in cell imaging.* New Journal of Chemistry, 2014. **38**(6): p. 2386-2393.
2. Ye, W., et al., *A fluorinated azine as a versatile scaffold for the development of Cu (II)-specific multi-functional imaging probes.* Sensors and Actuators B: Chemical, 2021. **343**: p. 130106.
3. Hu, Z., et al., *"AIE+ ESIPT" bis Schiff-base ligands with multicolor emission and their corresponding Eu (III) complexes: Synthesis and properties research.* Journal of Luminescence, 2020. **220**: p. 116929.
4. Singh, A. and D.R. Trivedi, *'Naked-eye'detection of biologically important anions in aqueous media by colorimetric receptor and its real life applications.* Spectrochimica Acta Part A: Molecular and Biomolecular Spectroscopy, 2017. **179**: p. 95-103.
5. Niu, Q., et al., *Highly sensitive and selective colorimetric/fluorescent probe with aggregation induced emission characteristics for multiple targets of copper, zinc and cyanide ions sensing and its practical application in water and food samples.* Sensors and Actuators B: Chemical, 2018. **266**: p. 730-743.
6. Chiter, C., et al., *Synthesis, crystal structure, spectroscopic and hirshfeld surface analysis, NCI-RDG, DFT computations and antibacterial activity of new asymmetrical azines.* Journal of Molecular Structure, 2020. **1217**: p. 128376.
7. Khanra, S., et al., *Subtle structural variation in azine/imine derivatives controls Zn 2+ sensitivity: ESIPT-CHEF combination for nano-molar detection of Zn 2+ with DFT support.* RSC advances, 2019. **9**(37): p. 21302-21310.
8. Guo, Z., et al., *A fast, highly selective and sensitive colorimetric and fluorescent sensor for Cu2+ and its application in real water and food samples.* Spectrochimica Acta Part A: Molecular and Biomolecular Spectroscopy, 2019. **213**: p. 97-103.

Chapter 3

Applications of PMB3 as sensor

Chapter 3 explores the versatile sensing capabilities of PMB3 across four distinct sections. PMB3 demonstrates a unique "OFF-ON-OFF" fluorescence behavior, enabling selective detection of bivalent Zn^{2+} ions and picric acid (PA) via turn-off fluorescence. Further, the Aggregation-Induced Emission Enhancement (AIEE) properties of PMB3 are investigated, revealing its effectiveness in selectively detecting Cu^{2+} ions in aqueous media and PA in aqueous medium with high sensitivity. Additionally, PMB3 exhibits colourimetric sensing abilities for Cu^{2+} and Ni^{2+} ions, offering a sensitive and selective response with potential for real sample analysis. Overall, Chapter 3 highlights its potential as a versatile and sensitive sensor for environmental pollutant detection and analysis.

SECTION 3.1

Successive detection of Zinc and Picric acid using an Organo-Fluorescent Sensor derived from 2-hydroxy-1-naphthaldehyde

3.1.1 Introduction

The design and development of an efficient, and simple method of determination of trace quantities of biologically and environmentally important species are of great significance in the field of environmental science, and analytical chemistry. The spectrofluorometric methods need to be extremely helpful for this purpose as they provide high selectivity, visual detection, non-destructive methodology, cost-effectiveness, fast, and quick real-time monitoring, etc [1-6]. The detection of metal ions using modern methods such as AAS [7], Chromatography [8], ICP-AES (Inductively coupled Plasma Atomic Emission Spectrometry) [9], ISE (Ion-Sensitive Electrodes) [10], and NAA (Neutron Activation Analysis) [11], etc., need sophisticated instrumentation. Therefore, finding new alternatives for the selective ion receptor systems with excellent optical responses towards a number of analytes [12-15] is an appreciable yet challenging goal. Hence developing fluorescent sensors for the detection of metal ions and other pollutants has received much attention. Schiff bases are very useful for this purpose, because of their easy method of synthesis, acceptable selectivity, relatively quick response time, and low cost [16]. The promising sensing response of Schiff bases towards metal ions is mainly due to their strong coordination ability and structural variations.

The detection of bivalent zinc has got extreme significance over other transition metal ions as it plays vital roles in biological processes [17-19]. Even though zinc is a vital trace element

indispensable for plants, animals, and microorganisms, both excessive and inadequate consumption can result in a number of health issues such as 'Alzheimer's disease', 'Parkinson's disease' [20-23], etc. Since the d^{10} electronic configuration of Zn^{2+} ion makes it spectroscopically silent, it is absolutely necessary to design easy and accessible alternative methods like fluorescent probes that selectively binds Zn^{2+} among the other metal ions under biological conditions.

For social and environmental safety, it is extremely significant to develop a more suitable and effective monitoring method for the trace-level detection of nitroaromatic explosives. Picric acid (PA), also known as 2,4,6-trinitrophenol (TNP), is one of the many nitroaromatic explosives quite important since it is the primary component of landmines and industrial explosives [24]. It is also widely used in the production of rocket fuels, pharmaceuticals, leather, and dye industries [25, 26]. PA has a higher water solubility than other nitroaromatics, which makes it more likely to pollute soil and groundwater. Picric acid is a non-biodegradable nitroaromatics and exposure to it can cause a number of health issues, including liver damage, anaemia, headaches, skin irritation, and other respiratory problems [27, 28]. Methods like Chromatography Coupled with Energy-Dispersive X-ray Diffraction [29], Surface-Enhanced Raman Spectroscopy [30], Mass Spectrometry [31-33], Nuclear Quadruple Resonance Spectroscopy [34], etc used today, are relatively complex and need expensive instrumentation. Therefore, the development of chemical sensors for the selective

detection of nitro compounds like picric acid with high selectivity in solution is still challenging and is highly desirable.

Herein this work, I present a novel "OFF-ON-OFF" fluorescent sensor PMB3 [1,1'- ((1E,1'E)- ((2E,2'E)- (1,3- phenylene bis (methanylylidene)) bis (hydrazine-2,1-diylidene)) bis (methanylylidene)) bis(naphthalen-2-ol)], for selective detection of bivalent zinc and an *in-situ* produced complex PMB3-Zn^{2+} ensemble for the detection of PA. The ligand PMB3 exhibits a significant emission enhancement in intensity with Zn^{2+}, however, the intensity of emission of the *in-situ* produced complex PMB3-Zn^{2+} ensemble is quenched selectively upon the progressive addition of PA.

3.1.2. Experimental

3.1.2.1. Fluorescence measurements

The stock solution of PMB3 with a concentration of 1 mM was prepared in DMF. The stock solutions of different metal salts and nitroaromatic compounds (NACs) of 1 mM concentration were prepared using freshly prepared double-distilled water. Emission spectra were obtained by excitation at 410 nm in DMF and sensing studies were carried out by recording the emission spectrum of the solution mixture consisting of 2.5ml of PMB3 with a concentration of 10μM and 1 equivalent of one of the metal ions stock solutions. The LOD was determined from emission spectral change using the formula, 3σ/k. where 'σ' is the standard deviation obtained from blank measurements and 'k' is the slope obtained from the calibration curve.

3.1.3. Results and Discussion

The fluorescent sensor (PMB3) was synthesized by the simple condensation of isophthalaldehyde and 1-(hydrazonomethyl) naphthalen-2-ol in ethanol medium under reflux conditions at room temperature (**Scheme 2** in chapter 2). The probe (PMB3) was easily soluble in DMF and DMSO.

3.1.3.1. The Sensing behaviour of PMB3 to Zn^{2+} in DMF solution

The ability of the Schiff base (PMB3) to sense a variety of different metal ions including Cd^{2+}, Al^{3+}, Hg^{2+}, Zn^{2+}, Ag^{+}, Pb^{2+}, Co^{2+}, Cr^{3+}, Ni^{2+}, Mn^{2+}, Ca^{2+}, Mg^{2+}, Ba^{2+}, Na^{+}, Cu^{2+}, Fe^{3+}, and K^{+} in a selective manner, was investigated by recording fluorescence spectra in DMF using an excitation wavelength at 410 nm as depicted in **Fig.1**. The ligand exhibited a weak emission at 512 nm because of an intra-molecular rotation. The intensity or wavelength of fluorescence did not significantly alter with the addition of metal ions, except for Zn^{2+}. However, when the Zn^{2+} ion was added, the emission peak intensity significantly increased and shifted to a shorter wavelength region of 507 nm. The enhancement in emission intensity of PMB3 with the addition of Zn^{2+} can be explained due to the structural rigidity of PMB3 that occurred in coordination with Zn^{2+}ion and suppression of C=N isomerization, which may be the mechanism that makes the free ligand to be a weak emissive system. No appreciable enhancement in fluorescence intensity was seen with the addition of other metal ions, which indicates that the Schiff base (PMB3) can function as an effective fluorescent sensor for bivalent zinc metal. The sensitive and selective detection of Zn^{2+} visually under a UV

lamp, making PMB3 as a promising optical sensor probe for the Zn^{2+}ion (**Fig.2**).

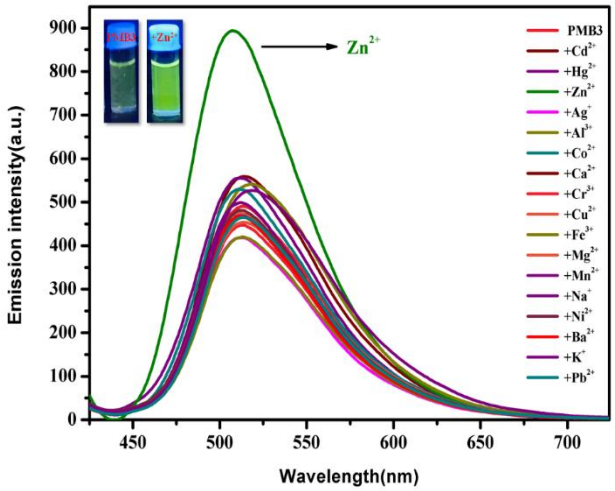

Fig.1 *Change in the fluorescence emission spectra of PMB3 (10 μM, λ_{ex}= 410 nm, λ_{em}= 512 nm) in DMF in the presence of different metal ions*

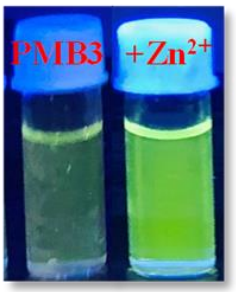

Fig.2 *The fluorescence colour change of PMB3 (10 μM) with 1 equivalent of Zn^{2+}ions*

For ascertaining the sensitivity of PMB3 towards bivalent Zn^{2+} ions, metal titration studies were performed with different zinc ion concentrations. When the Zn^{2+} ion concentration increases, the emission peak displays a little blue shift from 512nm to 507nm accompanied by the gradual enhancement of fluorescence intensity (**Fig.3**).

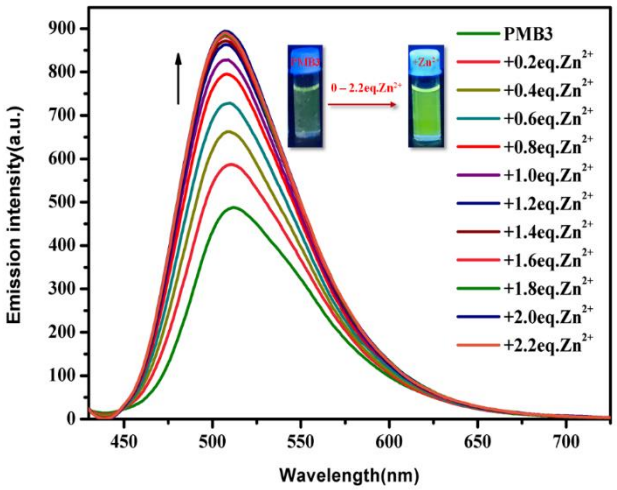

Fig.3 *Changes in the fluorescence emission spectra of PMB3 (10 μM, λ_{ex}= 410 nm, λ_{em}= 512 nm) in DMF up on the increase in the concentration of Zn^{2+} from 0- 2.2 equivalents*

3.1.3.2 The metal-ligand stoichiometry and Sensing mechanism

The reasons for the sensing response of fluorophore with analytes include the mechanisms like Photoinduced Electron Transfer (PET), Chelation Enhanced Fluorescence Transfer (CEFT), Intramolecular Charge Transfer (ICT), Twisted Intra-molecular/Intermediate Charge Transfer (TICT), C=N isomerization, etc. The fluorescence of the sensor gets quenched due to C=N isomerization process which has a significant influence on making the sensor into a weak emissive one. While the binding of metal ions to the sensor restricts the C=N isomerization and makes molecules more rigid, which enhances fluorescence emission. In this case, C=N isomerization processes are primarily responsible for the moderate fluorescence emission of PMB3 in the absence of bivalent Zn^{2+} ions. The blocking of the rotation about C=N of PMB3 by coordination with Zn^{2+} ions leads to restriction of C=N isomerization process and results in

enhancement in emission intensity[35]. Therefore, the effective suppression of the C=N isomerization process may be ascribed to the chelation between the nitrogen atom of the imine (C=N) group present in PMB3 and Zn^{2+}ions (**Scheme 1**). The binding stoichiometry of PMB3 with Zn^{2+} is established using, Job's method. The Job's plot given in **Fig.4** shows that maximum fluorescence intensity observed at 0.50 mol fraction for the PMB3-Zn^{2+} ensemble complex, suggesting that the stoichiometry of the metal complex is 1:1.

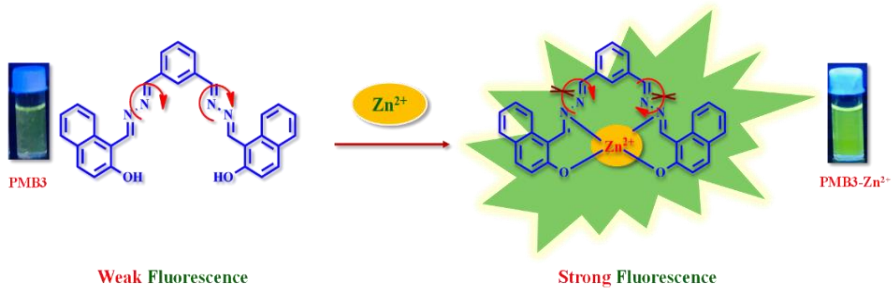

Scheme 1 *Proposed sensing mechanism for PMB3 with Zn^{2+}*

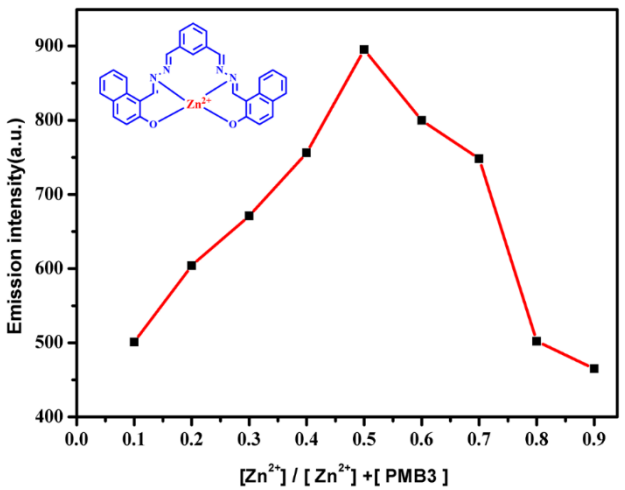

Fig.4 *Job's plot for the identification of metal-PMB3 ratio*

3.1.3.3. Detection limit and Association constant

The detection limit for the bivalent Zn^{2+} ion using PMB3 was determined from the emission spectral change using the equation,

$$\text{Limit of detection (LOD)} = 3\times \sigma/k$$

The LOD was determined to be 11.12×10^{-7}M (**Fig.5**). The association constant of PMB3 with Zn^{2+} was determined using fluorescence titration (Benesi-Hildebrand equation) to be $8.09 \times10^{5}M^{-1}$, indicating that the PMB3-Zn^{2+} complex is sufficiently stable and signifying the strong binding property between PMB3 and Zn^{2+}(**Fig.6**). The ability of a sensor to respond specifically to the target ion in the presence of complex background of more competitive analytes under biological pH is an essential requirement in sensor development. To confirm the selectivity of PMB3 towards bivalent Zn^{2+}, the competitive fluorescence studies were performed by recording the fluorescence spectra of PMB3 with the addition of 1 equivalent of Zn^{2+} and an equivalent quantity of other metal ions. The change in fluorescence intensity that occurred in the presence of other metal ions are shown in **Fig.7**. From the histogram, it is evident that no noticeable change or significant fluctuations occurred in the fluorescence emission intensity of ensemble complex PMB3-Zn^{2+} in the presence of other competing metal ions. This finding supports that the ligand system is highly specific for sensing bivalent Zn^{2+} ions. Furthermore, measurements of the luminescence lifetime were done to realize the stability at the excited state. The lifetime decay profile of PMB3 and PMB3-Zn^{2+} complex fits well with the single-exponential decay curve, and the

addition of Zn^{2+} increases the lifetime of PMB3 significantly from 1.002ns to 1.294ns (**Fig.8**).

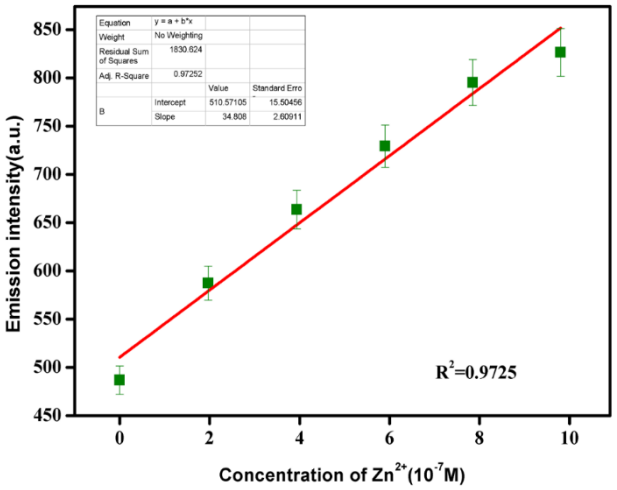

Fig.5 *Limit of detection (LOD) for bivalent Zn (II)*

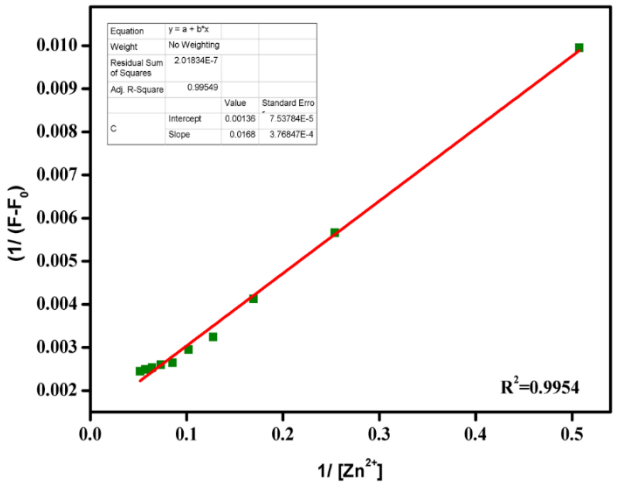

Fig.6 *Benesi-Hildebrand plot of PMB3 with* Zn^{2+}

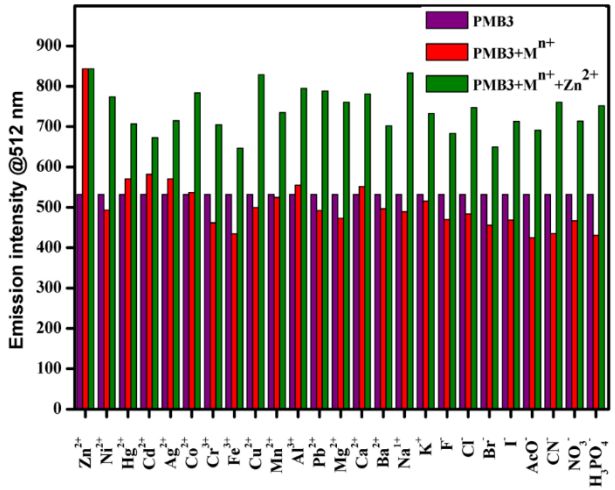

Fig.7 *Selectivity of PMB3 towards Zn(II). The selectivity of PMB3(10 μM, λ_{ex}= 410 nm, λ_{em}= 512 nm) in DMF towards Zn^{2+} (1 equivalent) in the presence of other metal ions (1 equivalent)*

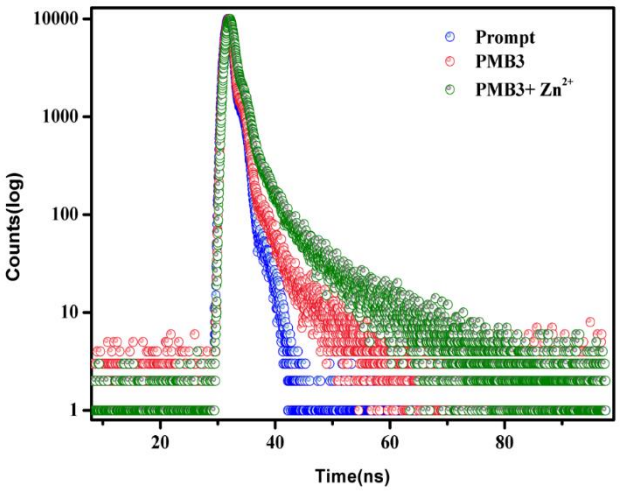

Fig.8 *Fluorescence decay profile of PMB3 in DMF (10μM) in the absence and presence of Zn^{2+}*

3.1.3.4. Reversibility of PMB3

Reversibility and reusability of the sensor molecules are very important in sensor development like sensitivity and selectivity. In reversibility experiments, the emission intensity of the ensemble

complex PMB3-Zn^{2+} was investigated with the addition of Na_2EDTA solution. As seen in **Fig.9**, with the addition of Na_2EDTA to the ensemble complex PMB3-Zn^{2+}, the fluorescence emission intensity decreased significantly and almost reversed to the original state of the free sensor which indicates the regeneration and recovery of the free PMB3. The findings demonstrated that the detection of Zn^{2+} ions was reversible by treatment with Na_2EDTA, allowing the sensor to be utilized again to detect Zn^{2+} ions in the presence of majority of competing metal ions.

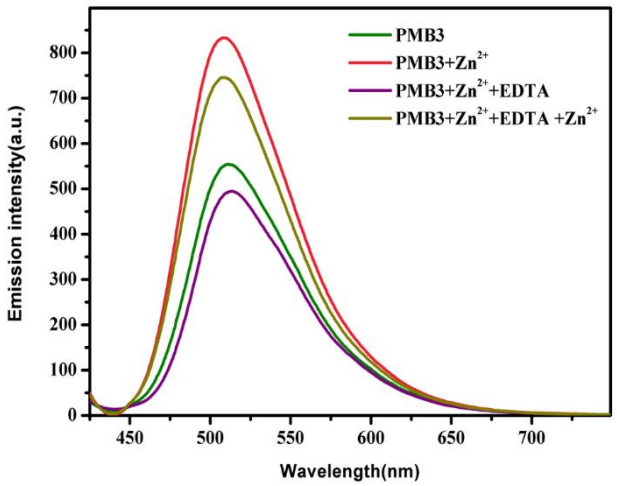

Fig.9 *Reversibility study of the PMB3 in DMF (10 μM, λ_{ex}= 410 nm, λ_{em}= 512 nm) towards Zn^{2+} with addition of EDTA*

3.1.3.5. The Effect of pH on Sensing

The influence of pH on the emission intensity of PMB3 in the absence and presence of bivalent Zn^{2+} ions was investigated. As illustrated in **Fig.10**, the emission intensity of PMB3 and ensemble complex PMB3-Zn^{2+} progressively increases when pH > 4, and is stable from the range 5 to 11, covering the biological pH range, showing the

potential use of PMB3 as a selective sensor for bivalent zinc in biological systems.

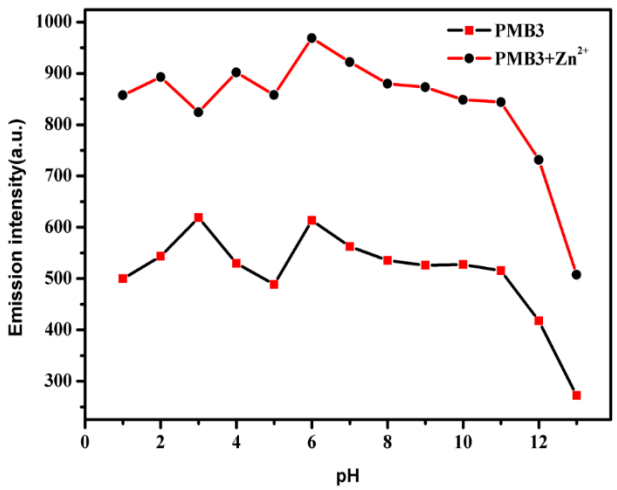

Fig.10 *pH effect on the determination of Zn (II) using PMB3(10 μM), λ_{ex}= 410 nm, λ_{em}= 512 nm) in DMF*

To explore the practical applications of PMB3 in biological systems, we have studied the cytotoxicity of PMB3 towards human cell lines (CHO K1). For this MTT cell viability assay was performed. The MTT assay is used to measure cellular metabolic activity as an indicator of cell viability, proliferation, and cytotoxicity. This colorimetric assay is based on the reduction of a yellow tetrazolium salt, the MTT (3–(4,5–dimethylthiazol–2–yl)–2,5–diphenyltetrazolium bromide), to purple formazan crystals by metabolically active cells. The viable cells contain NAD(P)H-dependent oxidoreductase enzymes which reduce the MTT to formazan. The insoluble formazan crystals will be dissolved using a solubilization medium and the resultant solution will be quantified by measuring absorbance at 570–630nm using a 96-well (microplate) spectrophotometer. The darker the solution, the greater the number of viable, metabolically active cells. The

result revealed that PMB3 was found to be highly biocompatible and cell viable within the concentration range 0-100 µg for 24h (**Fig.11** and **Table 1**).

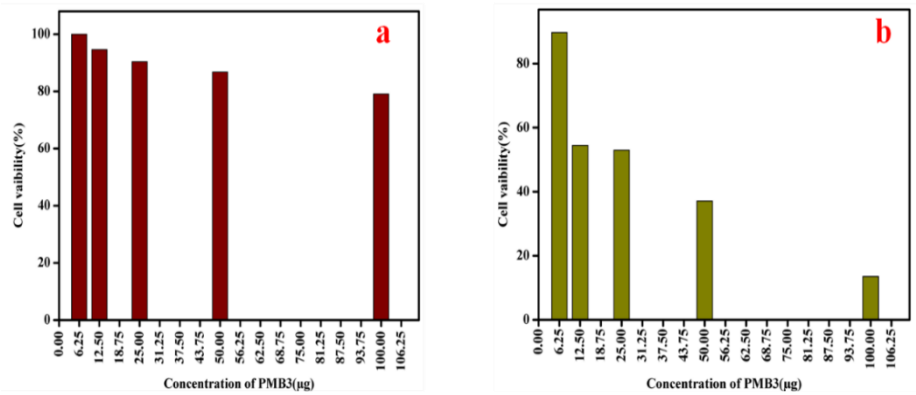

Fig.11 *Cytotoxicity study of PMB3 (**a**) cell with short-term exposure: 24h (**b**) cell with long-term exposure: 72h*

Table 1 *Results of cytotoxicity study of PMB3*

(**Short-term exposure: 24h**)

Conc. (µg)	***Absorbance (570 nm – 630 nm)***				***Cell viability (%)***
	1	*2*	*3*	*Mean*	
6.25	0.5984	0.5979	0.5988	0.5984	99.97
12.5	0.5661	0.5657	0.5665	0.5661	94.57
25	0.5402	0.5411	0.5407	0.5407	90.33
50	0.5193	0.5189	0.5190	0.5191	86.72
100	0.4738	0.4732	0.4736	0.4735	79.10
Control	0.5988	0.5984	0.5987	0.5986	

(**Long-term exposure: 72h**)

Conc. (µg)	***Absorbance (570 nm – 630 nm)***				***Cell viability (%)***
	1	*2*	*3*	*Mean*	
6.25	0.3611	0.3576	0.3421	0.3536	89.70
12.5	0.2152	0.2119	0.2173	0.2148	54.49
25	0.2088	0.2103	0.2076	0.2089	52.99
50	0.1477	0.1452	0.1464	0.1464	37.14
100	0.0527	0.0544	0.0529	0.0533	13.52
Control	0.3948	0.3937	0.3942	0.3942	

3.1.3.6. Picric acid Sensing

The sensing ability of ensemble complex PMB3-Zn^{2+} towards a number of nitro aromatic compounds including picric acid (PA), 2,4-dinitrophenol (2,4-DNP), 2,4,6-trinitrotoluene (TNT), nitrobenzene (NB), 2-nitrophenol (2-NP), 4-nitrophenol (4-NP), 4-nitroaniline (4-NA), 2-nitrotoluene (2-NT), 4-nitrotoluene (4-NT), 3-nitroaniline (3-NA), 3-nitrobenzoic acid(3-NBA) 2-nitroaniline (2-NA), 3-nitrotoluene (3-NT), and 2,4-dinitroaniline (2,4-DNA), was investigated by recording fluorescence spectra and the results are summarized in **Fig.12**. The fluorescence spectrum of the ensemble complex, PMB3-Zn^{2+}, shows a strong emission peak at 507 nm. The intensity of this peak decreases gradually upon the addition of PA without any change in the position of peak (**Fig.13**). The Stern-Volmer method is used for calculating the fluorescence quenching constant and is found to be 21.17×10^{15} M^{-1}. The I_0/I *vs* [PA] plot displays an upward curve, which indicates the efficiency of

quenching increases with PA concentration (**Fig.14**), besides that, at a higher PA concentration the plot bends upward, suggesting the "super amplified quenching process" [36]. Moreover, the percentage quenching efficiency was calculated using the equation [$(I_0-I)/I_0 \times 100$], where I_0 and I are fluorescence intensity of ensemble complex, PMB3-Zn^{2+}, before and after the addition of nitro compounds and the results obtained were given in **Fig.15**. Picric acid has much higher quenching efficiency than other nitro compounds. The fluorescence decay profile of the ensemble complex (**Fig.16**) both with and without PA fits well with the single-exponential decay curve and the lifetime of PMB3-Zn^{2+} complex is found to be 1.294ns which is almost unchanged in the presence of PA(1.289ns). This unchanged fluorescence lifetime value suggests that the interaction between ensemble complex PMB3-Zn^{2+} and PA takes place in the ground state and thus indicated the mechanism to be a static quenching.

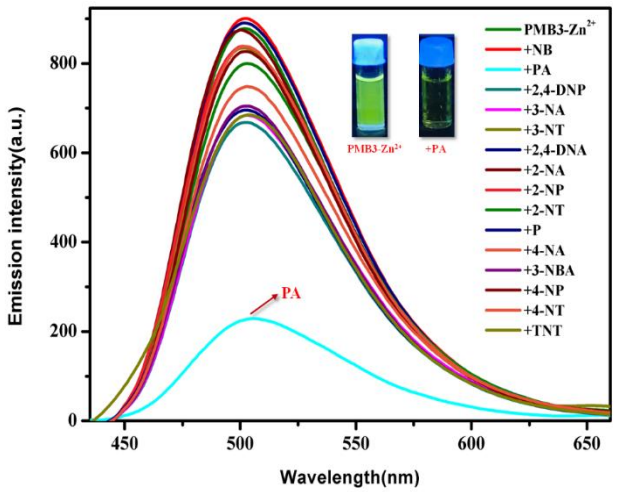

Fig.12 *Change in the fluorescence emission spectra of PMB3-Zn^{2+} in-situ complex in DMF (10 μM, λ_{ex}= 410 nm, λ_{em}= 507 nm) in the presence of different nitro compounds*

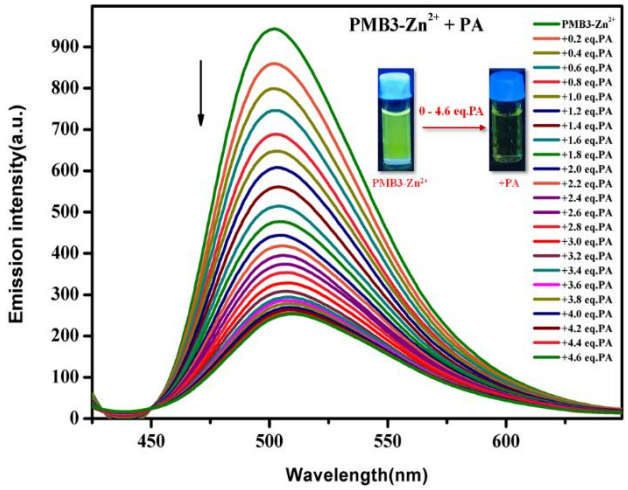

Fig.13 *Changes in the fluorescence emission spectra of PMB3-Zn^{2+} in-situ complex in DMF (10 μM, λ_{ex}= 410 nm, λ_{em}= 507 nm) up on the gradual increase in the concentration of PA from 0 - 4.6 equivalent*

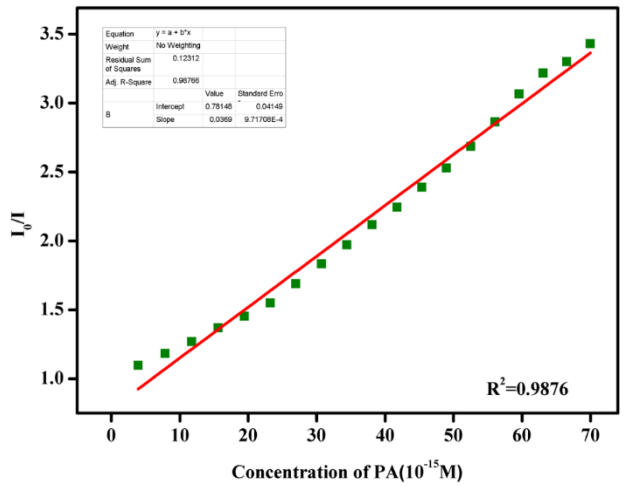

Fig.14 *Stern-Volmer plot of PMB3-Zn^{2+} in-situ complex in DMF (10 μM, λ_{ex}= 410 nm, λ_{em}= 507 nm) with PA*

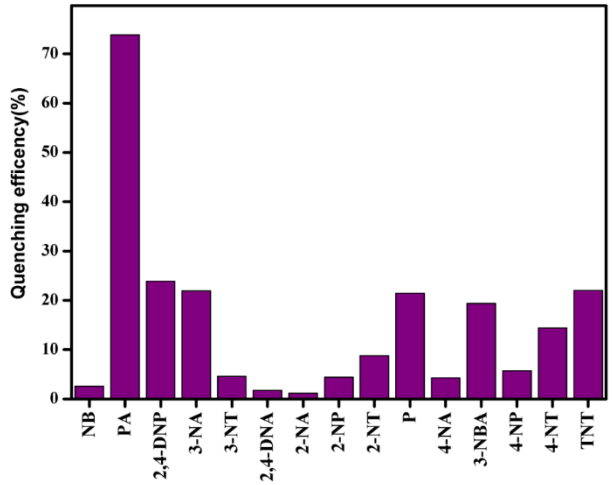

Fig.15 *Quenching efficiency of PMB3-Zn^{2+} in-situ complex in presence nitro compounds.*

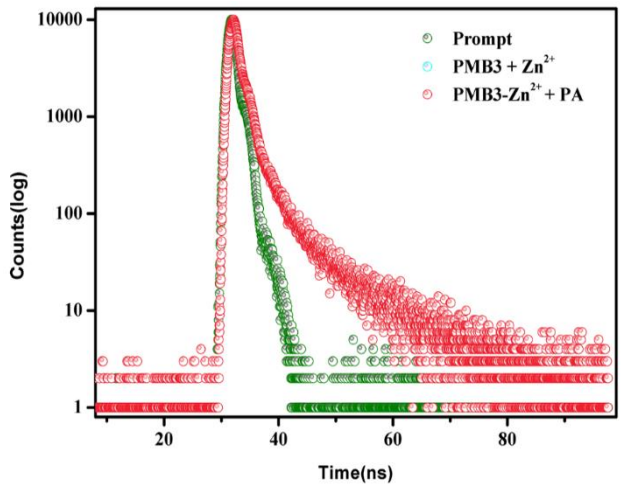

Fig.16 *Fluorescence decay profile of PMB3-Zn^{2+} in-situ complex in DMF in absence and presence of PA*

The most probable quenching mechanism was shown in **Scheme 2**. The bonding of nitrogen atom of the imine(C=N) group present in PMB3 with Zn^{2+} by chelation increases the structural rigidity of the molecule and thereby leading to enhancement in emission intensity

of the ensemble complex, PMB3-Zn^{2+}. However, as PA is added, the electron cloud is shifting towards PA due to the strong negative inductive effect (I) and resonance (R) effect, reducing the emission intensity of the whole complex. The strong electron-withdrawing property of three nitro groups (*i*.e., negative inductive effect) present in PA makes it more acidic and hence interacts with π-electron-rich part of the PMB3-Zn^{2+} complex. The lone pair of electrons present in the oxygen atom of the OH group got delocalized in the aromatic ring (negative R effect). This delocalization of electrons also makes it more acidic. Thus donor-acceptor interaction accompanied by proton transfer induces intermolecular charge transfer between PA and PMB3-Zn^{2+} complex followed by fluorescence quenching of PMB3-Zn^{2+} complex.

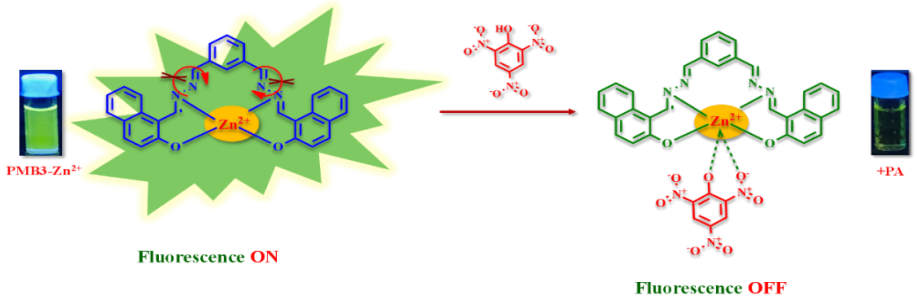

Scheme 2 *The proposed quenching mechanism*

The possibility of the inner-filter effect was investigated by taking the absorbance spectra of PA and excitation spectra of PMB3-Zn^{2+}. It was found that there was a significant overlap between the absorbance spectrum of PA and the excitation spectrum of PMB3-Zn^{2+}, indicating the possible existence of the Inner-Filter Effect (IFE). **Figure.17** shows the absorbance spectra of PA and excitation

spectra of PMB3-Zn^{2+}. Hence, the fluorescence quenching of PMB3-Zn^{2+} by the addition of PA is believed to be through inner-filter effect (IFE) and static quenching effect. The remarkable selectivity of ensemble complex PMB3-Zn^{2+} towards PA was examined by recording the emission spectra of ensemble complex, PMB3-Zn^{2+}, with PA in the presence of other aromatic nitro compounds. The **Fig.18** indicates the selectivity of ensemble complex towards PA and the data reveals that there is no significant guest-driven quenching of the fluorescence emission of the ensemble complex, PA system. The detection efficiency of PMB3 alone towards different nitro compounds was also investigated. The addition of PA and other nitro compounds does not show any detectable change in the emission spectra of PMB3 (**Fig.19**).

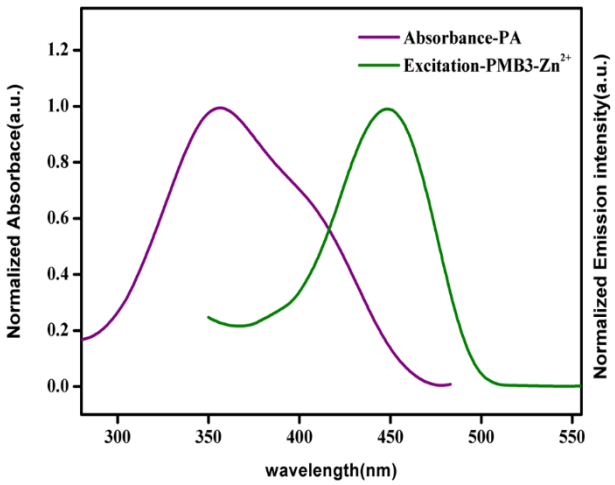

Fig.17 *The absorbance spectra of PA and excitation spectra of PMB3-Zn^{2+} in-situ complex in DMF*

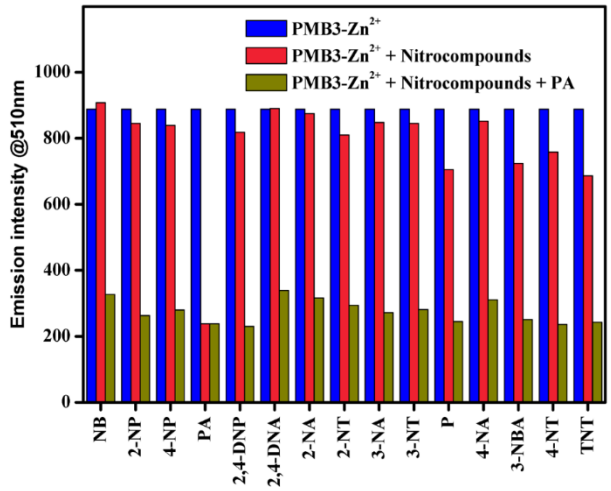

Fig.18 *The selectivity of PMB3-Zn²⁺ in-situ complex in DMF towards PA (10 μM) (1 equivalent) in the presence of other nitro compounds (10 μM) (1 equivalent)*

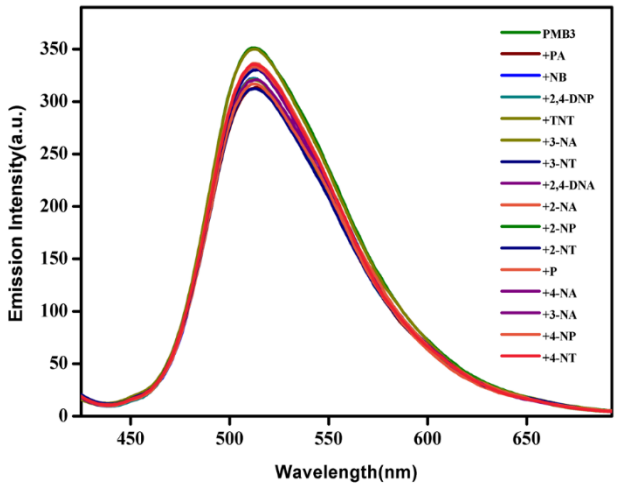

Fig.19 *Selectivity of PMB3 towards different nitro compound*

The limit of detection (LOD) of PA using the ensemble complex PMB3-Zn^{2+} was determined by the equation, "limit of detection (LOD) = 3× σ/k. The LOD was found to be 42.40×10^{-15}M (**Fig.20**). This result demonstrates that the ensemble complex PMB3-Zn^{2+} is a

powerful system for sensing picric acid at a femtomolar level. The change in emission intensity of the *in-situ* PMB3-Zn^{2+} ensemble complex with the concentration of PA is depicted in **Fig.21**.The comparison of PMB3 with other reported probes in the literature was done and the data are shown in **Table 2**.

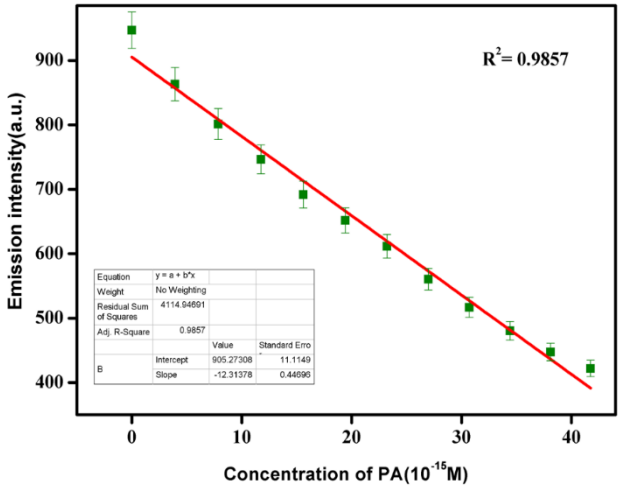

Fig.20 *Limit of detection (LOD) of PA using PMB3-Zn^{2+} in-situ complex*

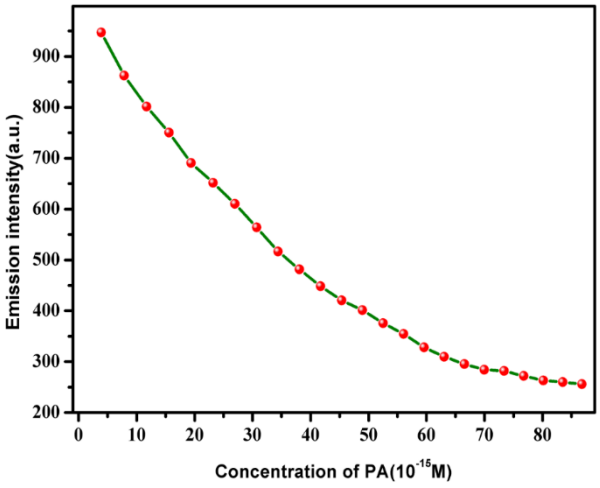

Fig.21 *The profile of fluorescence intensity vs PA concentration*

Table 2 *Comparison of PMB3 with other reported probes*

Probe	Sensing analyte	LOD	Interfering ions	Ref
Probe-1	Zn^{2+}	0.61μM	Cd^{2+}	[37]
Probe-2	Zn^{2+}	15.6 μM	Al^{3+}	[38]
Probe-3	Zn^{2+}	0.66μM	Fe^{3+}	[39]
Probe-4	Zn^{2+}	1.59μM	Al^{3+}	[40]
Probe-5	PA	10nM	No interfere	[41]
Probe-6	PA	0.11 μM	No interfere	[42]
PMB3 **PMB-Zn^{2+}**	**Zn^{2+}** **PA**	**Zn^{2+} = 1.11μM** **PA = 42.40fM**	**No interfere**	**Present work**

In practical applications, the reversibility and reusability of the sensor molecules are very important. We have done the cyclability experiment by adding zinc metal ions to the solution containing PMB3-Zn^{2+} and PA complex. As seen in **Fig.22**, with the addition of zinc ions, the fluorescence emission intensity increased significantly and almost reversed to the original state of the free PMB3-Zn^{2+}sensor which indicates the regeneration and recovery of the free ensemble complex. This may be due to the formation of zinc picrate salts i.e., the added zinc metal ion reacts with PA and form picrate salts. Due to this salt formation, the emission intensity of the PMB3-Zn^{2+} complex regenerated. The emission intensity decreases again with the addition of PA and the experiments can be repeated. The findings demonstrated that the detection of PA was reversible by treatment with Zn^{2+} ion, allowing the sensor to be utilized again to detect PA in the presence of majority of competing nitro compounds.

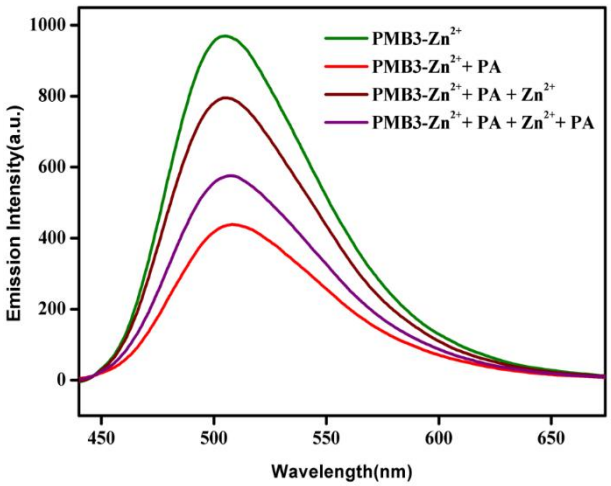

Fig.22 *Reversibility study of PMB3-Zn^{2+} in-situ complex in DMF (10 μM, λ_{ex}= 410 nm, λ_{em}= 507 nm) towards PA with addition of Zn^{2+}*

3.1.4. Conclusions

A novel simple and reusable organo-fluorescent sensor, PMB3, has been synthesized, which exhibits a very selective fluorescence emission response towards Zn^{2+}ions. Association constant was evaluated from the Bensi-Hildebrand relation and stoichiometry of the complex was established by Job's analysis (1:1). The binding of Zn^{2+} ions effectively increase the conformational rigidity and fluorescence of PMB3, due to the inhibition of C=N isomerization. The LOD was found to be 11.12×10^{-7}M. This ensemble complex PMB3-Zn^{2+} system was again used as a sensor for PA and the limit of detection goes down to femtomolar level for picric acid in solution. Using the ensemble complex PMB3-Zn^{2+}, the LOD for PA was calculated to be 42.40 fM. The fluorescence decay studies revealed that the generation of the complex takes place in ground-state and no change in the fluorescence lifetime was observed in the presence of PA indicating the mechanism to be the combination of static quenching and the Inner-Filter Effect (IFE).

References

1. Lee, S.Y., et al., Highly selective and sensitive colorimetric chemosensor for detection of Co2+ in a near-perfect aqueous solution. RSC Advances, 2016. 6(33): p. 28081-28088.
2. Guha, S., et al., n, MG Babashkina, MP Mitoraj, M. Bolte, Y. Garcia, SK Mukhopadhyay and D. Das. Dalton Trans, 2013. 42: p. 10198-10207.
3. Yang, Y.-K., K.-J. Yook, and J. Tae, A Rhodamine-Based Fluorescent and Colorimetric Chemodosimeter for the Rapid Detection of Hg2+ Ions in Aqueous Media. Journal of the American Chemical Society, 2005. 127(48): p. 16760-16761.
4. Ghorai, A., et al., Solvent-dependent fluorescent-colorimetric probe for dual monitoring of Al3+ and Cu2+ in aqueous solution: an application to bio-imaging. Dalton Transactions, 2016. 45(28): p. 11540-11553.
5. Köse, M., et al., A novel Schiff base: Synthesis, structural characterisation and comparative sensor studies for metal ion

detections. Spectrochimica Acta Part A: Molecular and Biomolecular Spectroscopy, 2015. 136: p. 1388-1394.
6. Bakker, E., P. Bühlmann, and E. Pretsch, Carrier-based ion-selective electrodes and bulk optodes. 1. General characteristics. Chemical reviews, 1997. 97(8): p. 3083-3132.
7. Mashhadizadeh, M., et al., Solid phase extraction of lead (II), copper (II), cadmium (II) and nickel (II) using gallic acid-modified silica gel prior to determination by flame atomic absorption spectrometry. Spectrochim. Acta B, 2008. 63: p. 885-888.
8. Harvey, D., Modern analytical chemistry. Vol. 1. 2000: McGraw-Hill New York.
9. Ferreira, A.C., M.d.G. Korn, and S.L. Ferreira, Multivariate optimization in preconcentration procedure for manganese determination in seawater samples by FAAS. Microchimica Acta, 2004. 146(3): p. 271-278.
10. Gupta, V., A. Singh, and B. Gupta, Schiff bases as cadmium (II) selective ionophores in polymeric membrane electrodes. Analytica chimica acta, 2007. 583(2): p. 340-348.
11. Mergu, N. and V.K. Gupta, A novel colorimetric detection probe for copper (II) ions based on a Schiff base. Sensors and actuators B: Chemical, 2015. 210: p. 408-417.
12. Kundu, A., et al., Developing new Schiff base molecules for selective colorimetric sensing of Fe3+ and Cu2+ metal ions: Substituent dependent selectivity and colour change. Sensors and Actuators B: Chemical, 2015. 206: p. 524-530.
13. Kumawat, L.K. and V.K. Gupta, Highly selective dual channel chemosensor based on benzo [d] thiazole for detection of Zn 2+ ions. Int. J. Electrochem. Sci, 2016. 11: p. 8861-8873.
14. Chen, C.-H., et al., A turn-on and reversible Schiff base fluorescence sensor for Al 3+ ion. Analyst, 2013. 138(9): p. 2527-2530.
15. Wang, L., G. Fang, and D. Cao, A novel phenol-based BODIPY chemosensor for selective detection Fe3+ with colorimetric and fluorometric dual-mode. Sensors and Actuators B: Chemical, 2015. 207: p. 849-857.
16. Hsieh, W.H., et al., A turn-on Schiff base fluorescence sensor for zinc ion. Tetrahedron letters, 2012. 53(44): p. 5848-5851.
17. Shellaiah, M., Y.-H. Wu, and H.-C. Lin, Simple pyridyl-salicylimine-based fluorescence “turn-on” sensors for distinct detections of Zn 2+, Al 3+ and OH− ions in mixed aqueous media. Analyst, 2013. 138(10): p. 2931-2942.
18. Li, K. and A. Tong, A new fluorescent chemosensor for Zn2+ with facile synthesis:“Turn-on” response in water at neutral pH and its application for live cell imaging. Sensors and actuators B: chemical, 2013. 184: p. 248-253.

19. Xu, Z., et al., An NBD-based colorimetric and fluorescent chemosensor for Zn2+ and its use for detection of intracellular zinc ions. Tetrahedron, 2009. 65(11): p. 2307-2312.
20. Liu, Y., et al., QD-Biopolymer-TSPP assembly as efficient BiFRET sensor for ratiometric and visual detection of zinc ion. ACS Applied Materials & Interfaces, 2017. 9(5): p. 4725-4732.
21. Guang, S., et al., A novel turn-on fluorescent probe for the multi-channel detection of Zn 2+ and Bi 3+ with different action mechanisms. Analyst, 2018. 143(2): p. 449-457.
22. An, M., et al., Fluorescence sensor for sequential detection of zinc and phosphate ions. Spectrochimica Acta Part A: Molecular and Biomolecular Spectroscopy, 2016. 169: p. 87-94.
23. Ding, Y., et al., Selective and sensitive "turn-on" fluorescent Zn 2+ sensors based on di-and tripyrrins with readily modulated emission wavelengths. Chemical Communications, 2011. 47(19): p. 5431-5433.
24. Germain, M.E. and M.J. Knapp, Optical explosives detection: from color changes to fluorescence turn-on. Chemical Society Reviews, 2009. 38(9): p. 2543-2555.
25. Hussain, S., et al., Ultrasensitive detection of nitroexplosive–picric acid via a conjugated polyelectrolyte in aqueous media and solid support. Chemical communications, 2015. 51(33): p. 7207-7210.
26. Ding, A., et al., Complex-formation-enhanced fluorescence quenching effect for efficient detection of picric acid. Chemistry–A European Journal, 2014. 20(38): p. 12215-12222.
27. Hou, X.-G., et al., A cationic iridium (III) complex with aggregation-induced emission (AIE) properties for highly selective detection of explosives. Chemical Communications, 2014. 50(45): p. 6031-6034.
28. Zhang, Y., et al., The locations of triphenylamine and tetraphenylethene on a cyclohexyl ring define a luminogen as an AIEgen or a DSEgen. Journal of Materials Chemistry C, 2022. 10(15): p. 6078-6084.
29. Walsh, M.E., Determination of nitroaromatic, nitramine, and nitrate ester explosives in soil by gas chromatography and an electron capture detector. Talanta, 2001. 54(3): p. 427-438.
30. Sylvia, J.M., et al., Surface-enhanced Raman detection of 2, 4-dinitrotoluene impurity vapor as a marker to locate landmines. Analytical chemistry, 2000. 72(23): p. 5834-5840.
31. Håkansson, K., et al., Low-mass ions observed in plasma desorption mass spectrometry of high explosives. Journal of mass spectrometry, 2000. 35(3): p. 337-346.
32. Yinon, J., Mass spectrometry of explosives: Nitro compounds, nitrate esters, and nitramines. Mass Spectrometry Reviews, 1982. 1(3): p. 257-307.
33. Mathurin, J., et al., High-pressure ion source combined with an in-axis ion trap mass spectrometer. 1. Instrumentation and applications. Analytical chemistry, 2000. 72(20): p. 5055-5062.

34. Luggar, R., et al., Multivariate analysis of statistically poor EDXRD spectra for the detection of concealed explosives. X-Ray Spectrometry: An International Journal, 1998. 27(2): p. 87-94.
35. Ding, A., et al., A α-cyanostilbene-modified Schiff base as efficient turn-on fluorescent chemosensor for Zn 2+. Journal of Chemical Sciences, 2015. 127: p. 375-382.
36. Wang, J., et al., Hyperbranched polytriazoles with high molecular compressibility: aggregation-induced emission and superamplified explosive detection. Journal of Materials Chemistry, 2011. 21(12): p. 4056-4059.
37. Roy, S.B., et al., A novel fluorene based "turn on" fluorescent sensor for the determination of zinc and cadmium: Experimental and theoretical studies along with live cell imaging. New Journal of Chemistry, 2016. 40(11): p. 9593-9608.
38. Choi, Y.W., et al., A single schiff base molecule for recognizing multiple metal ions: a fluorescence sensor for Zn (II) and Al (III) and colorimetric sensor for Fe (II) and Fe (III). Sensors and Actuators B: Chemical, 2014. 194: p. 343-352.
39. Tang, X., et al., A multifunctional Schiff base as a fluorescence sensor for Fe3+ and Zn2+ ions, and a colorimetric sensor for Cu2+ and applications. Spectrochimica Acta Part A: Molecular and Biomolecular Spectroscopy, 2017. 173: p. 721-726.
40. Kim, Y.S., et al., Multiple target chemosensor: a fluorescent sensor for Zn (II) and Al (III) and a chromogenic sensor for Fe (II) and Fe (III). RSC advances, 2015. 5(15): p. 11229-11239.
41. Panigrahi, A., et al., AIE active fluorescent organic nanoaggregates for selective detection of phenolic-nitroaromatic explosives and cell imaging. Journal of Photochemistry and Photobiology A: Chemistry, 2019. 374: p. 194-205.
42. Maity, S., et al., Aggregation induced emission enhancement from antipyrine-based schiff base and its selective sensing towards picric acid. Sensors and Actuators B: Chemical, 2017. 248: p. 223-233.

Sensors & Actuators: A. Physical 358 (2023) 114418

Contents lists available at ScienceDirect

Sensors and Actuators: A. Physical

journal homepage: www.journals.elsevier.com/sensors-and-actuators-a-physical

Successive detection of bivalent zinc and picric acid using an organo-fluorescent sensor derived from 2-hydroxy-1- naphthaldehyde

Muhammed Arshad [a], A.T. Jeejarani [a], Athira Ajayan [a], C.D. Sebastian [b], Abraham Joseph [a,*]

[a] Department of Chemistry, University of Calicut, Calicut University, P O-673635, India
[b] Department of Zoology, University of Calicut, Calicut University, P O-673635, India

ARTICLE INFO

Keywords:
Fluorescence
Femtomolar
Emission intensity
Sensor

ABSTRACT

A novel fluorescent sensor, PMB3 was designed, and synthesized from 2-hydroxy-1- naphthaldehyde and was characterized using FT-IR, CHNS elemental analysis, HR-MS, ^{1}H NMR, and ^{13}C NMR respectively. PMB3 displays very selective, sensitive, and rapid changes in fluorescence with the presence of Zn^{2+}. The sensor efficiently binds with bivalent zinc to form a 1:1 complex, which resulted in significant fluorescence enhancement upon gradual addition while other metal ions do not affect significantly in the intensity of the emission. The limit of detection of bivalent zinc was 11.12×10^{-7} M. The ligand can be easily regenerated using an EDTA solution. This zinc complex ensemble was observed to be extremely selective for picric acid up to femtomolar level detection, over other aromatic explosives. The detection limit for picric acid found by utilizing the zinc complex ensemble was 42.40×10^{-15} M. The developed sensor complex ensemble is therefore quite effective in detecting picric acid via turn-off fluorescence.

1. Introduction

The design and development of an efficient, easy, and quite simple determination method for the identification of trace quantities of biologically and environmentally important species are of great significance in the field of environmental science, and chemical sectors. The fluorescence spectroscopic methods need to be extremely helpful for this purpose as they provide a number of advantages, including ease of use, selectivity, visual detection, non-destructive methodology, cost-effective, fast, and quick real-time monitoring, etc. [1–6]. The detection of metal ions has been carried out using modern methods such as AAS [7], Chromatography [8], ICP-AES (Plasma Atomic Emission Spectrometry) [9], ISE (Ion-Sensitive Electrodes) [10], and NAA (Neutron Activation Analysis) [11], etc., which need sophisticated instrumentation. Therefore, finding new alternatives for the selective ion receptor systems with excellent optical responses towards a number of analytes [12–15] is an appreciable yet challenging goal. Hence developing fluorescent sensors for the detection of metal ions and other pollutants has received a lot of attention, due to their sensitivity, exceptional selectivity, and quite fast response time. Among the organic molecules, Schiff bases are very useful for this purpose, because of their easy synthesis procedure, acceptable selectivity, relatively quick response time, and low cost [16]. The promising sensing response of Schiff bases towards metal ions is mainly due to their strong coordination ability and structural variations.

The detection of bivalent zinc metal ion has got extreme significance over other transition metal ions since it plays vital roles in biological processes like structural, functional, Lewis acid, catalytic cofactors, signal transmitters, and agents that control apoptosis and gene expression [17–19]. Even though zinc is a vital trace element indispensable for plants, animals, and microorganisms, both excessive and inadequate consumption can result in a number of health issues such as 'Alzheimer's disease', 'Parkinson's disease' [20–23], etc. Since the d^{10} electronic configuration Zn^{2+} ion makes it spectroscopically silent, it is absolutely necessary to design easy and accessible methods like fluorescent sensors that selectively binds Zn^{2+} among the other metal ions under biological conditions.

For social and environmental safety, it is extremely significant to develop a more suitable and effective monitoring method for the trace-level detection of nitroaromatic explosives. Picric acid (PA), also known as 2,4,6-trinitrophenol, is one of the many nitroaromatic explosives quite important since it is the primary component of landmines and industrial explosives [24]. It is also widely used in the production of rocket fuels, pharmaceuticals, leather, and dye industries [25,26]. PA

* Corresponding author.
E-mail address: abrahamjoseph@uoc.ac.in (A. Joseph).

https://doi.org/10.1016/j.sna.2023.114418
Received 2 March 2023; Received in revised form 30 April 2023; Accepted 8 May 2023
Available online 9 May 2023

SECTION 3.2

Detection of copper in aqueous media using PMB3 as fluorescent probe

3.2.1. Introduction

The exploration of organic molecules exhibiting Aggregation-Induced Emission Enhancement (AIEE) has been a focal point in recent scientific investigations of luminescent materials. This interest is driven by the broad spectrum of potential applications, including the detection of biomolecules, the development of chemosensors for the highly sensitive identification of hazardous heavy metal ions, the advancement of Organic Light-Emitting Diodes (OLED), and their utilization in cancer theranostics [1-9]. In the pursuit of detecting biologically significant metal ions, researchers are developing cost-effective fluorescent chemosensors with AIEE activity, emphasizing simplicity, sensitivity, and selectivity [10-13].

Aggregation-Induced Enhancement (AIE) that transforms non-emissive organic molecules in pure solvents into highly emissive species upon aggregation, can be exploited for metal ion sensing. These AIEE active materials have the advantages of greater photostability, great selectivity, and high sensitivity making them useful sensors for real-time applications [14, 15].

A wide range of mechanisms governs AIEE activity, encompassing Restriction of Intramolecular Rotation (RIR) [16-18], Twisted Intramolecular Charge Transfer (TICT) [19-21], Restriction of Intramolecular Charge Transfer (ICT) [22], and Cis–Trans isomerization [23]. Each mechanism is system-specific, and there is no general mechanism applicable to all systems.

As the third most abundant essential trace metal ion in biochemical systems, after iron and zinc, bivalent copper exists in three forms:

Type I, Type II, and Type III. It functions as an oxygen management metalloprotein and as a catalytic cofactor for numerous metalloenzymes, including cytochrome c oxidase, plastocyanin, tyrosinase, ascorbic acid oxidase, and superoxide dismutase [24-29]. Even so, the abnormal level of accumulation of copper can lead to harmful health effects, such as gastrointestinal issues, neurodegenerative illnesses like Parkinson's and Alzheimer's, Amyotrophic Lateral Sclerosis, Wilson disease, prion diseases, and damage to the liver or kidney [30-34]. The widespread use and applications of Cu^{2+} ions in chemistry, and medicine have emerged as one of the most important environmental contaminants due to its excess accumulation in the environment, which create serious imbalance in the release and consumption cycle of the metal ion. The World Health Organisation (WHO) mandates that the concentration of Cu^{2+} ions in drinking water should not exceed 31.3μM [35]. Hence, the development of selective fluorescent chemosensors with a low detection limit and high sensitivity becomes imperative for the fast and precise detection of Cu^{2+} ions in environmental systems.

Compared to existing techniques fluorometric methods are superior and have great sensitivity, simplicity, and rapid response [36-40]. Numerous fluorophores, including quinoline, coumarin, fluorescein, naphthalimide, pyrene, pyrazine, and rhodamine-based fluorescent chemosensors [41-49], have been developed for the detection of cupric ions. However, a few of the probes have drawbacks, such as cumbersome procedure of synthesis, long response time, low fluorescence intensity, low selectivity and sensitivity, low stability,

less water solubility, etc. More importantly, very few fluorescent probes are available that are capable of detecting Cu^{2+} in both organic and aqueous systems. Therefore, the demand for a suitable fluorescent sensor for the quick and accurate detection of cupric ions at trace levels has paramount significance.

Herein this section, we report a Schiff base 1,1'- ((1E,1'E)- ((2E,2'E)- (1,3-phenylen bis (methanylylidene)) bis (hydrazine-2,1-diylidene)) bis (methanylylidene)) bis (naphthalen-2-ol) (PMB3) having AIEE activity for the selective detection Cu^{2+} in aqueous medium. The PMB3 aggregates display a bright greenish fluorescence and show a fluorescence switch-off response to Cu^{2+} ion with a detection limit of 16.08 fM. These observations clearly divulge that PMB3 aggregates are highly selective to Cu^{2+} ion and hence can be extended for the instant naked-eye detection of Cu^{2+}.

3.2.2. Results and Discussion

The sensor molecule PMB3 was synthesized through a two-step condensation reaction (**Scheme 2** in chapter 2) and is easily soluble in DMF, and DMSO and is insoluble in water.

3.2.2.1 AIEE activity of PMB3

The AIEE activity of PMB3 was investigated by leveraging its high solubility in DMF solvent and its insolubility in water. Fluorescence emission spectra were recorded in DMF containing varying volume percentage of water (0% to 99%) to assess the AIEE activity of PMB3 at an excitation wavelength of 410nm by keeping the concentration of PMB3 as 10μM at room temperature. PMB3 in DMF with 0% water fraction was feebly emissive at 512nm and the intensity of emission

increased with a light green emission at 536nm as the percentage of water fraction increased. The fluorescence spectra presented in **Fig.1** indicate that up to a 40% water fraction, there is no significant change in emission behaviour which is due to the active involvement of intramolecular rotation about C=N, N-N bonds [50]. Surprisingly, a light green emission at 536nm was observed on approaching the water fraction to 50% and intensity increased steadily with increase in the percentage of water fraction from 50 to 99. This drastic enhancement in the emission intensity as a function of volume percentage of water, **Fig.2,** indicates the AIEE effect. It was also clear from the emission profile (**Fig.1**) that despite of drastic emission enhancement, there was a 26nm red shift in emission and this redshift of the emission maxima divulged the process of transformation of a single organic molecule into aggregates by forming an intermolecular association between the organic

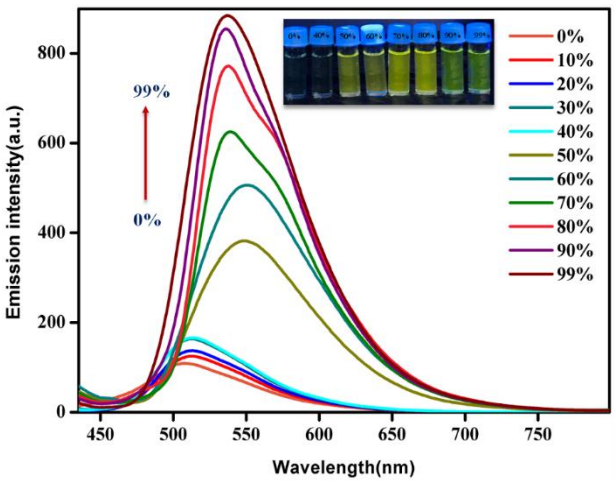

Fig.1 *Change in the fluorescence emission spectra of PMB3 in DMF (10μM, λ_{ex}=410 nm, λ_{em}= 536 nm) in presence of increasing water fraction(fw) from 0% to 99%*

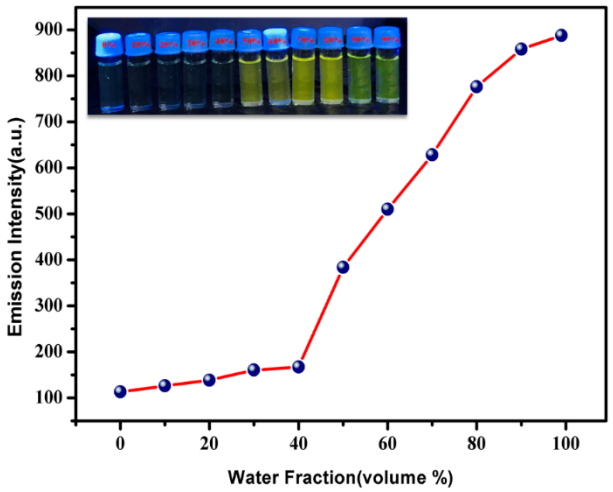

Fig.2 *Fluorescence emission intensity as a function of volume percentage of water*

molecules. Moreover, as the water fractions reaches 50%, aggregates start to form which blocks the intramolecular rotation about C=N and N-N bonds and hence leads to strong fluorescence emission (**Scheme 1**).

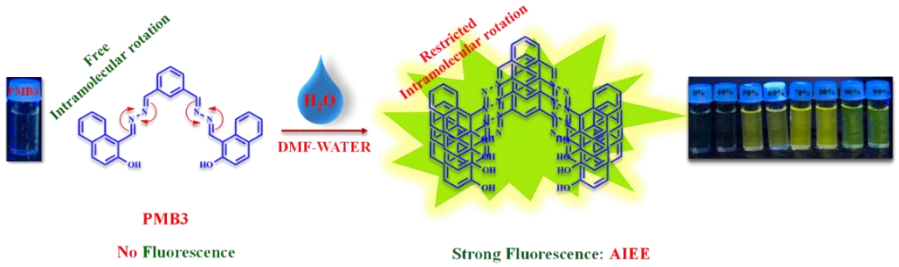

Scheme 1 *Proposed mechanism for AIEE behaviour of PMB3*

Apart from fluorescence measurements, the AIEE property of PMB3 was also studied using an optical microscope. The **Fig.3** represents the optical microscopic image of PMB3 in DMF with 0% water fraction and with 90% water fraction. It was clear from the image that, the particle with greenish-yellow fluorescence increased with

increase in the water fraction, supporting the formation of nanoparticle aggregates.

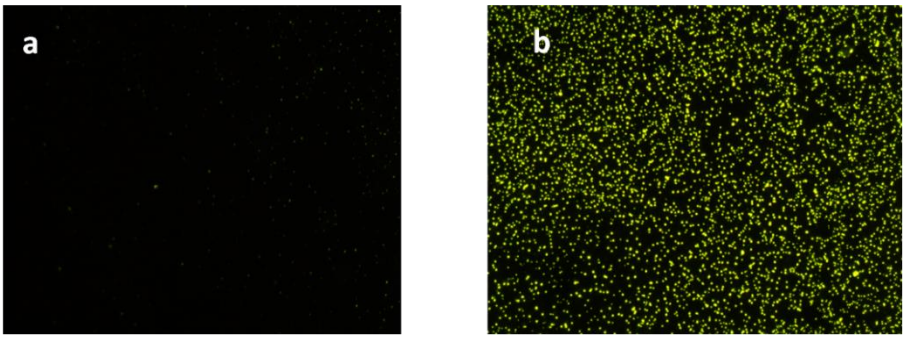

Fig.3 *Optical fluorescence microscopy images (under UV excitation) of (**a**) PMB3 in pure DMF with 0% water fraction(fw) in solution state (fw = 0%) and (**b**) PMB3 in DMF-Water mixed solvent with water fraction(fw) of 90% in the aggregated state (fw = 90%)*

Furthermore, the effect of viscosity on the AIEE activity of PMB3 was investigated. The solvent viscosity was varied by switching the glycerol percentage ratio to the methanol percentage ratio. It is clear from **Fig.4** that the emission intensity increases with increasing glycerol percentage which is the result of the viscosity effect and which hinder the C=N and N-N the intramolecular rotation [51] within PMB3. This observation validates the proposed mechanism of the enhancement of fluorescence emission intensity on aggregation and due to this restriction of intramolecular rotation the AIEE activity of PMB3 is significantly affected. Moreover, the photostability of PMB3 aggregates was examined by recording emission spectra of PMB3 aggregates periodically for 0 to 240 minutes as displayed in **Fig.5**. The stable emission intensity over a period of time proves its photostability and probable use as a sensor.

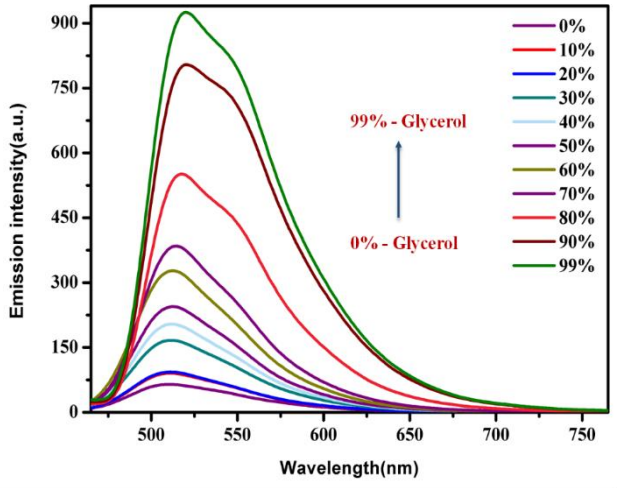

Fig.4 *Change in the fluorescence emission spectra of PMB3 in DMF (10 μM, λ_{ex}= 410 nm, λ_{em}= 536 nm) with change in viscosity of the solvent mixture by varying the solvent ratio of methanol to glycerol*

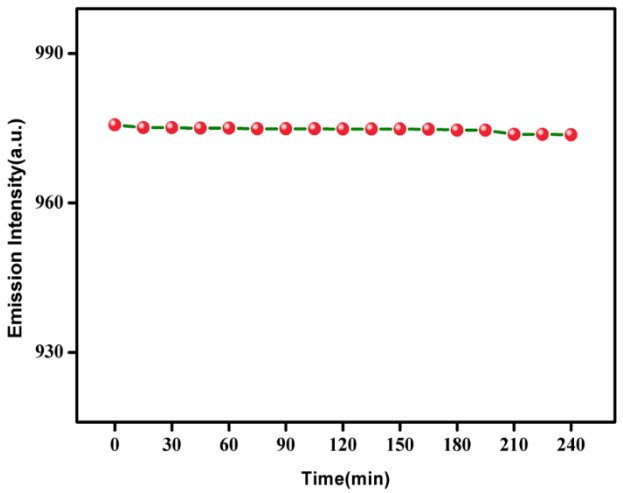

Fig.5 *Time-dependent emission intensity of PMB3 aggregates (fw = 90%)*

To get a vivid understanding of the AIEE activity of PMB3, the fluorescence lifetime was measured. The lifetime decay profile of PMB3 in DMF and in DMF-water mixed system with the percentage of water fraction 90 are depicted in **Fig.6**, which was well fitted with

a single exponential decay curve. PMB3 in DMF has a lifetime value of 1.032ns which significantly increases to 1.521ns with the increase of the percentage of water fraction due to the formation of PMB3 aggregates. The suppression of intermolecular rotation brought on by PMB3 aggregates is the cause of the increased fluorescence lifetime in the DMF-Water mixture having a 90% water fraction.

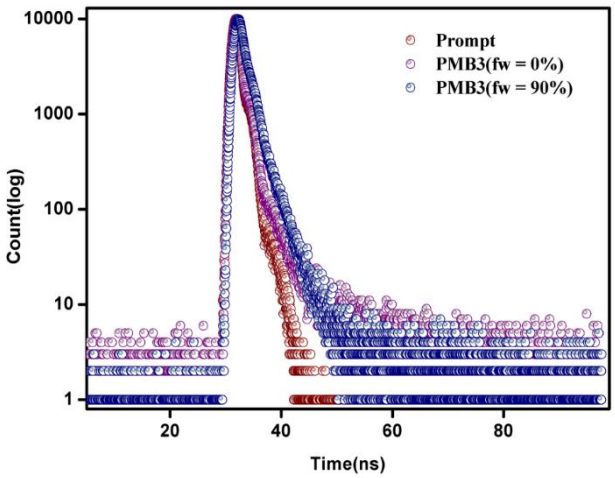

Fig.6 *Fluorescence decay profile of PMB3 (10 μM) in pure DMF with 0% water fraction(fw) in solution state (fw = 0%) and in DMF-Water mixed solvent with 90% water fraction(fw) in the aggregated state (fw = 90%)*

The pH dependence on the emission intensity of aggregates of PMB3 was investigated by recording the emission intensity of aggregates of PMB3 formed in DMF-Water mixture with water percentage 90 at different pH. It was clear from **Fig.7**, that the emission intensity of PMB3 aggregates increased as the pH increased from 2 to 7, and above pH 7 emission intensity decreased. The emission intensity was almost stable over the physiological pH range of 2-7, which increases potential application of the sensor in biological field.

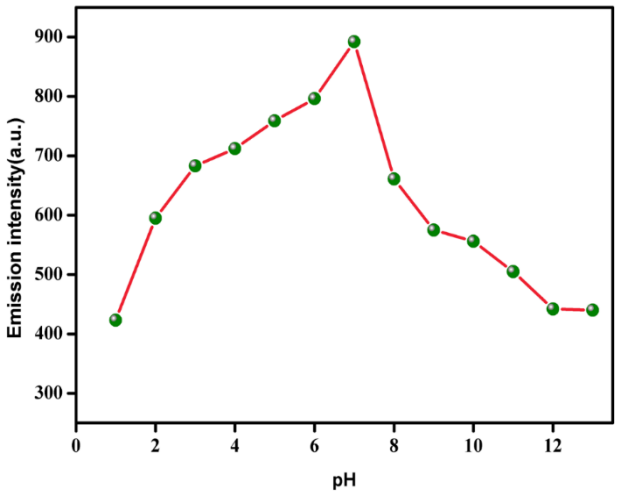

Fig.7 *Change in the emission intensity of PMB3 (10 μM), λ_{ex}= 410 nm, λ_{em}= 536nm) in DMF-Water mixture with water fraction 90% (fw = 90%) at different pH*

To gather more insight into the AIEE activity of PMB3 aggregate, UV-visible absorption spectral changes was also examined. **Fig.8** represents the UV-visible absorption spectra of PMB3 in DMF with 0% water fraction and in DMF-Water mixture solvent with 90%

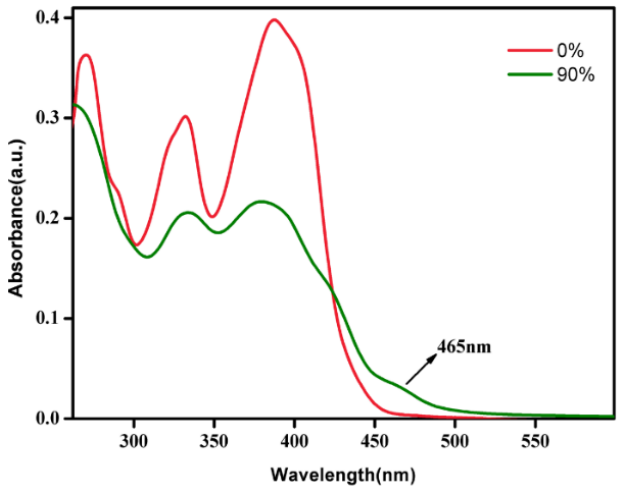

Fig.8 *UV-Visible spectra of PMB3 (10μM) in solution state in pure DMF and in DMF-Water mixed solvent with water fraction of 90% (aggregated state)*

water fraction. The two broad bands at 332nm and 387nm in the absorption spectra of PMB3 in DMF (0% water fraction) observed were attributed to π-π* transitions and n-π* transitions in the 2-hydroxy-1-naphthaldehyde moiety. Interestingly, as the percentage of water fraction increases from 0 to 99 the absorption profile shows significant changes, and the intensity of the absorption band at 387nm was decreased with a slight red shift which reveals the formation of PMB3 aggregates. The presence of an additional peak observed at 465nm with levelled-off tails in the visible region was

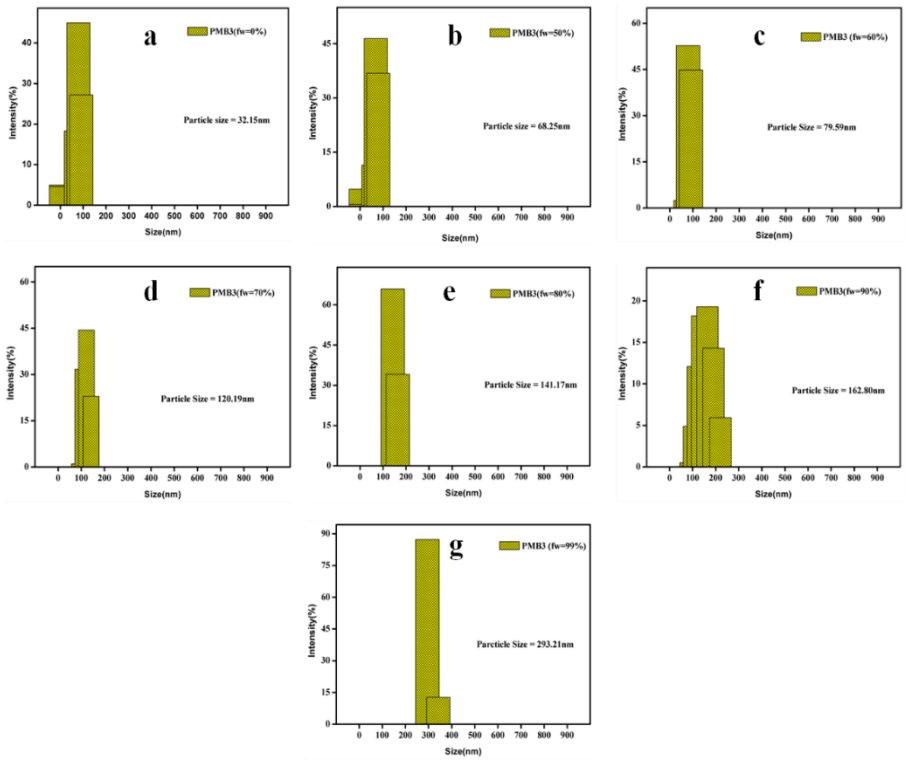

Fig. 9 *The dynamic light scattering (DLS) measurements of PMB3 (**a**) with 0% water fraction, (**b**) with 50% water fraction, (**c**) with 60% water fraction, (**d**) with 70% water fraction, (**e**) with 80% water fraction, (**f**) with 90% water fraction, (**g**) with 99% water fraction*

attributed to the Mie scattering caused by nanoparticle aggregates of PMB3 [52, 53]. The red shift in absorption spectra was the result of the formation of J-type aggregates (head-tail type) which resulted in the enhancement in emission intensity [54, 55]. Additionally, dynamic light scattering (DLS) measurement of PMB3 supports the size of PMB3 aggregates in the nano range (**Fig.9**).

3.2.2.2. Sensing of Cu^{2+} ion

The sensing characteristics of PMB3 aggregates, derived from DMF-water mixture with a water percentage of 90, were evaluated for various metal ions, including Zn^{2+}, Hg^{2+}, Cd^{2+}, Cu^{2+}, Ni^{2+}, Co^{2+}, Cr^{3+}, Al^{3+}, Mn^{2+}, Fe^{3+}, Mg^{2+}, Pb^{2+}, Ba^{2+}, Na^{+}, and K^{+}. Fluorescence spectra were recorded at an excitation wavelength of 410 nm (**Fig.10)**. The addition of Cu^{2+} ion results in a significant decrease in the fluorescence emission profile of the PMB3 aggregate, whereas no discernible response was shown for other metal ions, suggesting

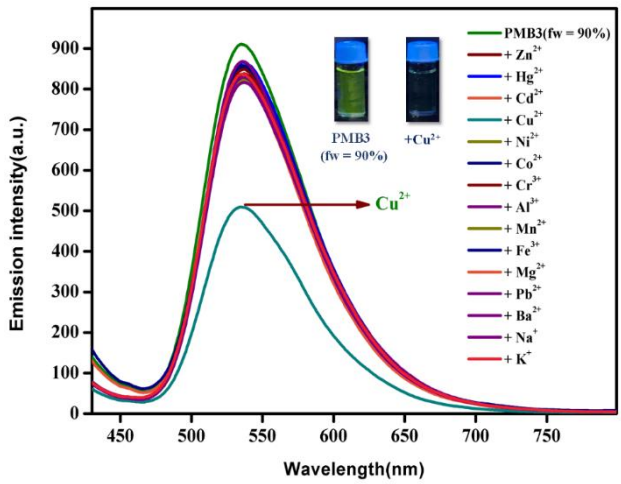

Fig.10 *Change in the fluorescence emission spectra of PMB3 in DMF (10 μM, λ_{ex}= 410 nm, λ_{em}= 536 nm) with water fraction 90% (fw = 90%) in the presence of different metal ions*

that the aggregate of PMB3 is selectively detecting Cu^{2+} in aqueous medium.

Through the incremental addition of Cu^{2+} ions to PMB3 aggregates, the fluorescence titration experiments were conducted to assess the sensing ability and selectivity of the aggregate of PMB3 towards Cu^{2+} ion. **Figure 11** reveals that the stepwise addition of Cu^{2+} ions to PMB3 aggregates led to an effective quenching of the fluorescence emission of PMB3 aggregates. Upon reaching a concentration of 3.2 equivalents of Cu^{2+}, the fluorescence completely ceased, suggesting a robust associative interaction between Cu^{2+} and PMB3 aggregates.

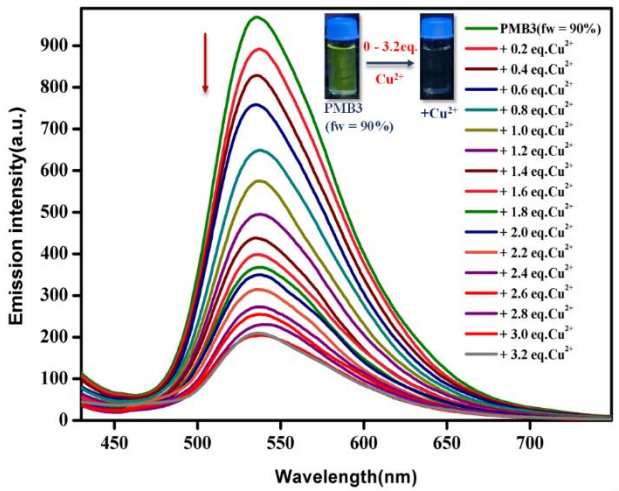

Fig.11 *Changes in the fluorescence emission spectra of PMB3 in DMF (10 μM, λ_{ex}= 410 nm, λ_{em}= 536 nm) with water fraction 90% (fw = 90%) up on the gradual increase in the concentration of Cu^{2+} from 0 - 3.2 equivalent*

Using the Stern-Volmer plot (**Fig.12**), the efficiency of fluorescence quenching was calculated and the value is $3.75\times10^{15}M^{-1}$. The detection limit calculated was $16.08\times10^{-15}M$ (16.08fM) based on the equation $3\sigma/k$ (**Fig.13**). This limit of detection acquired is much

lower than the value recommended by WHO in drinking water samples(31.5μM). A comparison was carried out between the obtained LOD of PMB3 aggregates with some of the chemosensors that have already been reported (**Table 1**). Even at lower concentration levels, PMB3 aggregates possess comparatively better Cu^{2+} ion sensitivity than many of the reported probes.

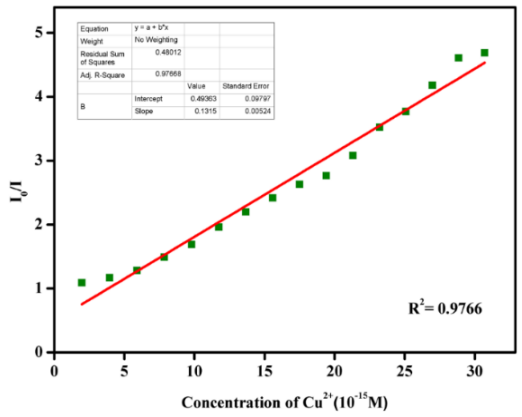

Fig. 12 *Stern-Volmer plot of PMB3 in DMF (10 μM, λ_{ex}= 410 nm, λ_{em}= 536 nm) aggregate with water fraction 90% (fw = 90%)*

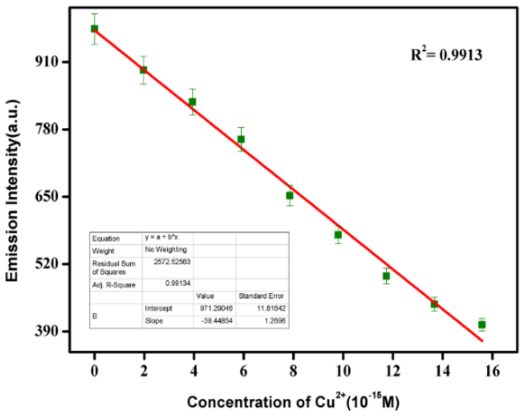

Fig.13 *Limit of detection (LOD) of PMB3 in DMF with water fraction 90% with Cu^{2+}*

Table 1 *Comparison of PMB3 with other reported probes*

Probe	Sensing Analyte	LOD [M]	Quenching constant [M^{-1}]	AIEE Property	Ref
Probe-1	Cu^{2+}	1.32×10^{-7}	Not Found	Yes	[56]
Probe-2	Cu^{2+}	4.5×10^{-9}	2.27×10^{6}	Yes	[14]
Probe-3	Cu^{2+}	7.84×10^{-9}	Not Found	No	[57]
Probe-4	Cu^{2+}	1.3×10^{-8}	1.45×10^{5}	No	[58]
Probe-5	Cu^{2+}	2.40×10^{-8}	3.77×10^{5}	No	[59]
Probe-6	Cu^{2+}	2.80×10^{-6}	Not Found	No	[60]
PMB3	**Cu^{2+}**	**16.08×10^{-15}**	**3.75×10^{15}**	**Yes**	**Present Study**

The excited state fluorescence lifetime measurements have been used to examine the strong fluorescence quenching behaviour of PMB3 aggregates in the presence of Cu^{2+}. The fluorescent lifetime decay profile of PMB3 aggregates in the presence and absence of Cu^{2+} is displayed in **Fig.14**. PMB3 aggregates with a lifetime value of 1.521ns exhibit single exponential decay in the absence of Cu^{2+}. The lifetime value of the PMB3 aggregates changed to 1.288ns after Cu^{2+} was added. This shift in the value of the fluorescence lifetime indicates that the dynamic quenching process is involved.

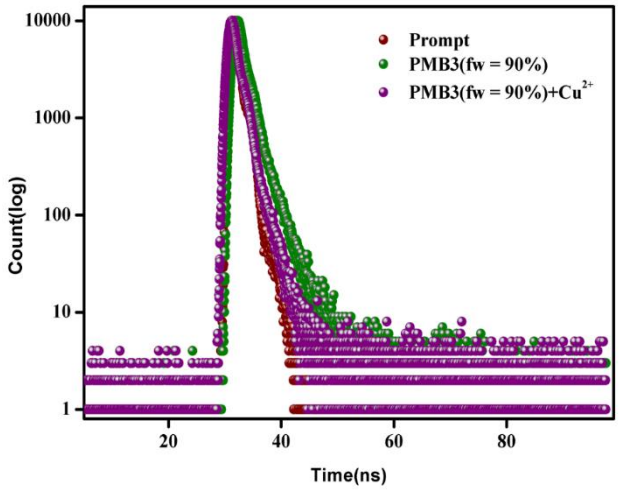

Fig.14 *Fluorescence decay profile of PMB3 in DMF (10μM) with water fraction(fw) percentage of 90 in aggregated state (fw = 90%) in absence and presence of* Cu^{2+}.

Additionally, chelation between the imine-N atom, and phenolic-O atom of PMB3 aggregates with Cu^{2+} ion will lead to disassembling of PMB3 aggregates, which may be responsible for the fluorescence quenching process (**Scheme 2**) of PMB3 aggregates in the presence of Cu^{2+}[61]. Job's plot analysis was used to investigate the

stoichiometry of complex formation between PMB3 and Cu^{2+} and the results showed that the binding stoichiometry was 1:1 (**Fig.15**).

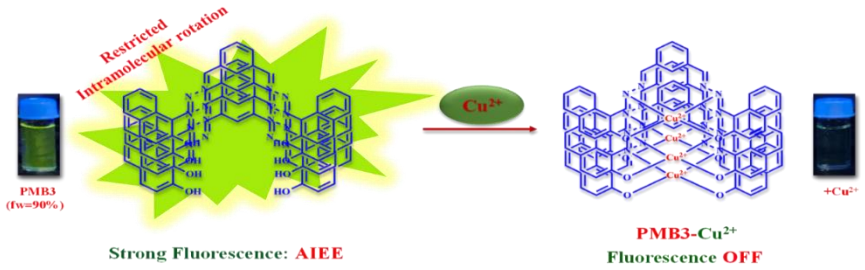

Scheme 2 *Proposed mechanism of interaction of PMB3 aggregate (fw = 90%) with* Cu^{2+}

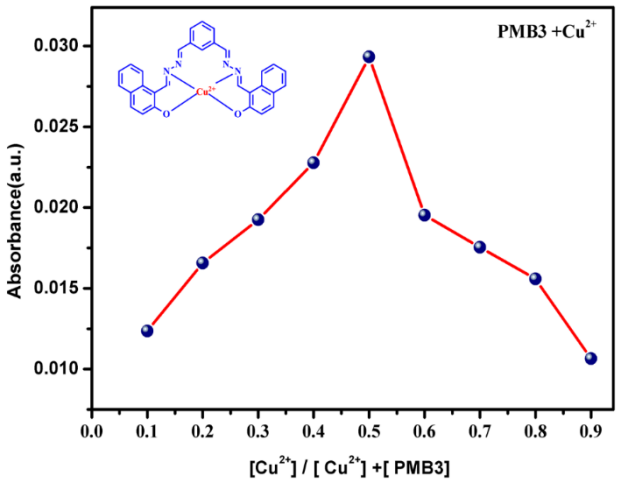

Fig.15 *Job's plot of PMB3 in DMF solvent*

Metal competitive analysis was conducted to ascertain selectivity of PMB3 aggregates to Cu^{2+}(**Fig.16**). This was accomplished by recording the fluorescence spectra of PMB3 aggregates in the presence of one equivalent of Cu^{2+} and an equivalent quantity of other metal ions and observed that the spectral properties of Cu^{2+} remains unchanged. Photographs of PMB3 aggregates with various metal ions exposed to a UV lamp, is shown in **Fig.17**. These results

indicate that the PMB3 aggregate possesses remarkable sensitivity and selectivity to Cu^{2+} and can be extended to the biological and environmental samples containing Cu^{2+} ions.

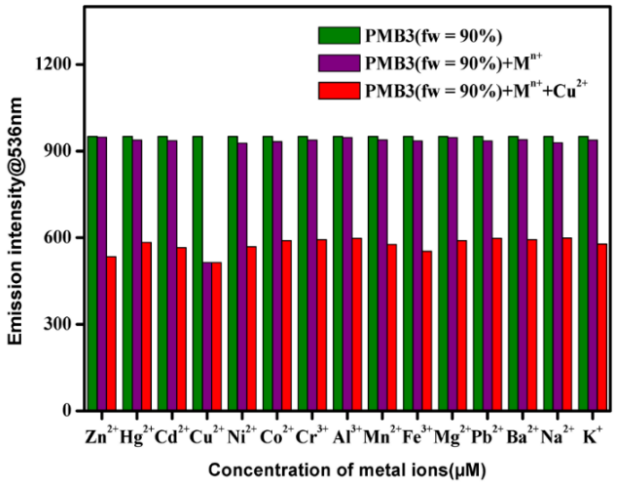

Fig.16 *The selectivity of PMB3 in DMF (10 μM, λ_{ex}= 410 nm, λ_{em}= 536 nm) with water fraction 90% (fw = 90%) towards Cu^{2+} (1 equivalent) in the presence of other metal ions (1 equivalent)*

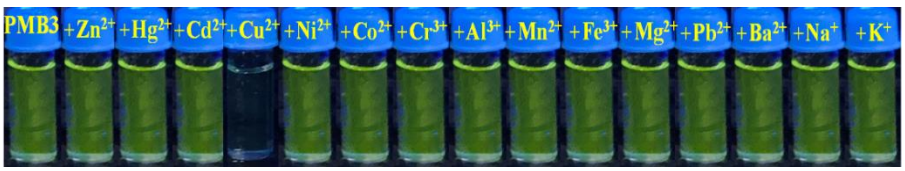

Fig.17 *Fluorescence emission of PMB3 in DMF (10 μM) with water fraction 90% (fw =90%) in the presence of fixed concentration (10 μM) of different metal ions under UV lamp*

Anion competitive analysis of PMB3 aggregates was conducted in the presence of CH_3COO^-, CN^-, NO_3^-, F^-, Cl^-, Br^-, I^-, and $H_3PO_4^-$. It is clear from **Fig.18**, that these anions do not alter the fluorescence emission profile of PMB3-Cu^{2+} system.

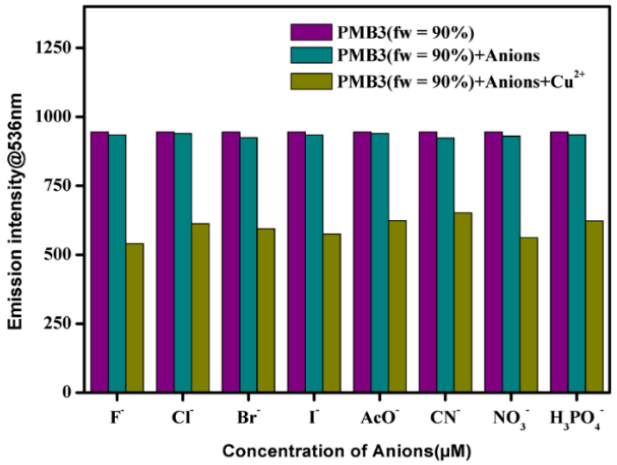

Fig.18 *The selectivity of PMB3 in DMF (10 μM, λ_{ex}= 410 nm, λ_{em}= 536 nm) with water fraction 90% (fw = 90%) towards Cu^{2+} (1 equivalent) in the presence of other anions (1 equivalent)*

The reversibility and reusability of the sensor system is studied using Na_2EDTA solution as a potent chelating ligand. The addition of Na_2EDTA solution to the PMB3-Cu^{2+} system restored the fluorescence of free PMB3 aggregates (**Fig.19**) which again

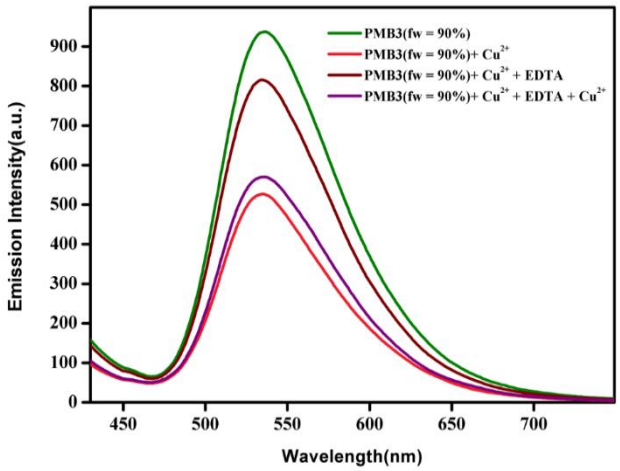

Fig.19 *Reversibility study of the PMB3 in DMF (10 μM, λ_{ex}= 410 nm, λ_{em}= 536 nm) with water fraction 90% (fw = 90%) towards Cu^{2+} with addition of EDTA*

quenched on adding Cu^{2+} into the system. This observation suggests

that the PMB3 free aggregates are regenerating, and the binding of PMB3 aggregates with Cu^{2+} is reversible and hence can be used as a suitable reusable sensor for detecting the Cu^{2+} ion.

3.2.2.3. Application of PMB3 aggregates in real sample analysis

To explore the fluorescence property of PMB3 aggregates in real samples analysis well water, tap water, and river water samples were studied using the standard spiking method. The data generated are given in **Table 2**. The percentage recoveries varied from 100.16 to 105.07. The spiked data obtained was again compared with ICPMS data.

3.2.2.4. PMB3 aggregates coated test strips

Since the on-site detection of Cu^{2+} has received a lot of attention, a strip sensor for Cu^{2+} has been developed using PMB3 aggregates. To explore this method, we have prepared two filter paper that has been coated with PMB3 aggregates. The Cu^{2+} solution was then dropped into one of the coated filter papers. **Fig.20** show the changes that were produced. The changes in emission colour are easily visible to the naked eye on exposure to UV light. Thus, this technique can be extended to the development of highly sensitive paper strip sensors for Cu^{2+}.

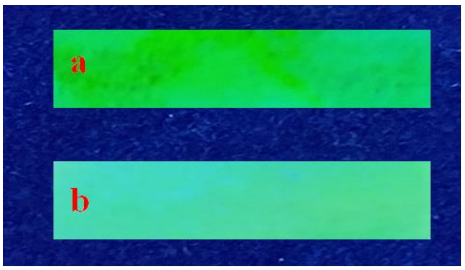

Fig.20 *Photographic image under UV-lamb* ***(a)*** *PMB3 aggregates formed in DMF-Water mixture of water fraction 90% (fw =90%) coated on filter paper* ***(b)*** *PMB3 aggregates coated filter paper dropped with* Cu^{2+} *ion*

Table 2 *Detection of Copper in Real samples*

Water sample	Added Cu^{2+} (μM)	Found (μM)	Recovery (%)	Error (%)	SD (%)	RSD (%)	ICPMS (μM)	ICPMS (SD) (%)	ICPMS (RSD) (%)
Well Water	1.97	1.98	100.50	0.50	0.74	0.37	1.98	0.83	0.41
	3.94	3.97	101.79	0.76	0.83	0.20	3.96	0.83	0.20
	5.90	5.91	100.16	0.16	1.58	0.26	5.93	0.54	0.09
Tap Water	1.97	2.01	102.03	2.03	0.54	0.26	1.99	1.14	0.57
	3.94	3.99	101.26	1.26	0.54	0.13	3.98	0.83	0.20
	5.90	5.96	101.01	1.01	2.06	0.34	5.94	0.59	0.09
River Water	1.97	2.07	105.07	5.07	0.54	0.26	1.98	0.89	0.45
	3.94	4.02	102.03	2.03	0.54	0.13	3.97	0.54	0.13
	5.90	6.03	102.20	2.20	1.00	0.16	5.96	0.89	0.14

3.2.3. Conclusions

A novel Schiff base PMB3 having AIEE activity and excellent sensitivity and selectivity for Cu^{2+} in the presence of diverse metal ions was designed and synthesized. The PMB3 aggregates show a greenish emission in DMF-Water mixture having a switch-off fluorescence response to Cu^{2+} ion, which makes the PMB3 aggregates a suitable sensing probe for the naked eye detection of Cu^{2+} under UV lamp. The detection limit was calculated to be 16.08×10^{-15} M (16.08 fM) range and the quenching constant value obtained from the Stern-Volmer plot was 3.75×10^{15} M^{-1}. The measurements of fluorescence lifetime indicate the involvement of the dynamic quenching process. The quenching of PMB3 aggregates is mainly due to the disassembling of PMB3 aggregates by chelation between the imine-N atom and phenolic -O atom of PMB3 and Cu^{2+} ion. The method was extended to real sample analysis and the result are quite promising and hence can be developed as real time Cu^{2+} sensor.

References

1. Würthner, F., *Aggregation-induced emission (AIE): a historical perspective.* Angewandte Chemie International Edition, 2020. **59**(34): p. 14192-14196.
2. Zhao, Z., et al., *Aggregation-induced emission: new vistas at the aggregate level.* Angewandte Chemie International Edition, 2020. **59**(25): p. 9888-9907.
3. Cai, X. and B. Liu, *Aggregation-induced emission: recent advances in materials and biomedical applications.* Angewandte Chemie International Edition, 2020. **59**(25): p. 9868-9886.
4. Hu, F., S. Xu, and B. Liu, *Photosensitizers with aggregation-induced emission: materials and biomedical applications.* Advanced materials, 2018. **30**(45): p. 1801350.

5. Wan, H., et al., *AIE-based fluorescent sensors for low concentration toxic ion detection in water.* Journal of Hazardous Materials, 2021. **403**: p. 123656.
6. Alam, P., et al., *AIE-based luminescence probes for metal ion detection.* Coordination Chemistry Reviews, 2021. **429**: p. 213693.
7. Tu, L., et al., *Aggregation-induced emission: red and near-infrared organic light-emitting diodes.* SmartMat, 2021. **2**(3): p. 326-346.
8. Wang, J., et al., *Effective design strategy for aggregation-induced emission and thermally activated delayed fluorescence emitters achieving 18% external quantum efficiency pure-blue OLEDs with extremely low roll-off.* ACS Applied Materials & Interfaces, 2021. **13**(48): p. 57713-57724.
9. Gao, M. and B.Z. Tang, *AIE-based cancer theranostics.* Coordination Chemistry Reviews, 2020. **402**: p. 213076.
10. Feng, H.-T., et al., *Tuning push–pull electronic effects of AIEgens to boost the theranostic efficacy for colon cancer.* Journal of the American Chemical Society, 2020. **142**(26): p. 11442-11450.
11. La, D.D., et al., *Tetraphenylethylene-based AIE-active probes for sensing applications.* ACS applied materials & interfaces, 2017. **10**(15): p. 12189-12216.
12. Wu, M., et al., *A multi-binding site hydrazone-based chemosensor for Zn (II) and Cd (II): a new strategy for the detection of metal ions in aqueous media based on aggregation-induced emission.* Dalton Transactions, 2021. **50**(4): p. 1507-1513.
13. Zhang, R., et al., *AIEgens for real-time naked-eye sensing of hydrazine in solution and on a paper substrate: structure-dependent signal output and selectivity.* Journal of Materials Chemistry C, 2016. **4**(14): p. 2834-2842.
14. Bai, J., et al., *A tetraphenylethene-based Schiff base AIEgen with a large Stokes shift as probe for highly sensitive and selective detection of aqueous Cu2+ ions and its application in cell imaging.* Spectrochimica Acta Part A: Molecular and Biomolecular Spectroscopy, 2023. **290**: p. 122190.
15. Wang, D., et al., *ESIPT-Active 8-Hydroxyquinoline-Based Fluorescence Sensor for Zn (II) Detection and Aggregation-Induced Emission of the Zn (II) Complex.* ACS omega, 2022. **7**(21): p. 18017-18026.
16. He, Z., C. Ke, and B.Z. Tang, *Journey of aggregation-induced emission research.* Acs Omega, 2018. **3**(3): p. 3267-3277.
17. Chen, J., et al., *Synthesis, light emission, nanoaggregation, and restricted intramolecular rotation of 1, 1-substituted 2, 3, 4, 5-tetraphenylsiloles.* Chemistry of materials, 2003. **15**(7): p. 1535-1546.

18. Zheng, H.-W., et al., *ESIPT-AIE active Schiff base based on 2-(2′-hydroxyphenyl) benzo-thiazole applied as multi-functional fluorescent chemosensors.* Dalton Transactions, 2021. **50**(11): p. 3916-3922.
19. Hu, Y., et al., *Towards white-light emission of fluorescent polymeric nanoparticles with a single luminogen possessing AIE and TICT properties.* Journal of Materials Chemistry C, 2020. **8**(2): p. 734-741.
20. Upamali, K.A., et al., *Carbazole-based cyano-stilbene highly fluorescent microcrystals.* Langmuir, 2011. **27**(5): p. 1573-1580.
21. Hu, R., et al., *Twisted intramolecular charge transfer and aggregation-induced emission of BODIPY derivatives.* The Journal of Physical Chemistry C, 2009. **113**(36): p. 15845-15853.
22. Xu, J., et al., *Morphology transition and aggregation-induced emission of an intramolecular charge-transfer compound.* Langmuir, 2008. **24**(8): p. 4231-4237.
23. Yu, X., et al., *Trans/cis-stereoisomers of triterpenoid-substituted tetraphenylethene: aggregation-induced emission, aggregate morphology, and mechano-chromism.* Nanoscale, 2021. **13**(36): p. 15257-15266.
24. Ridge, P.G., Y. Zhang, and V.N. Gladyshev, *Comparative genomic analyses of copper transporters and cuproproteomes reveal evolutionary dynamics of copper utilization and its link to oxygen.* PLoS One, 2008. **3**(1): p. e1378.
25. Boal, A.K. and A.C. Rosenzweig, *Structural biology of copper trafficking.* Chemical reviews, 2009. **109**(10): p. 4760-4779.
26. Uauy, R., M. Olivares, and M. Gonzalez, *Essentiality of copper in humans.* The American journal of clinical nutrition, 1998. **67**(5): p. S952-S959.
27. Peers, G. and N.M. Price, *Copper-containing plastocyanin used for electron transport by an oceanic diatom.* Nature, 2006. **441**(7091): p. 341-344.
28. Xie, X., et al., *Study on a highly selective colorimetric chemosensor for Cu2+ detection and its indirect sensing for hypochlorite.* Dyes and Pigments, 2013. **98**(3): p. 422-427.
29. Zhang, L., et al., *Determination of Cu 2+ and biothiols by novel red fluorescent hybrid nanoparticles.* Analytical Methods, 2018. **10**(22): p. 2560-2566.
30. Witt, B., et al., *Characterizing effects of excess copper levels in a human astrocytic cell line with focus on oxidative stress markers.* Journal of Trace Elements in Medicine and Biology, 2021. **65**: p. 126711.
31. Lener, M.R., et al., *Serum concentrations of selenium and copper in patients diagnosed with pancreatic cancer.* Cancer Research and Treatment: Official Journal of Korean Cancer Association, 2016. **48**(3): p. 1056-1064.

32. Desai, V. and S.G. Kaler, *Role of copper in human neurological disorders.* The American journal of clinical nutrition, 2008. **88**(3): p. 855S-858S.
33. Bull, P.C., et al., *The Wilson disease gene is a putative copper transporting P–type ATPase similar to the Menkes gene.* Nature genetics, 1993. **5**(4): p. 327-337.
34. Rossi, L., et al., *Mitochondrial dysfunction in neurodegenerative diseases associated with copper imbalance.* Neurochemical research, 2004. **29**: p. 493-504.
35. Kumar, M. and A. Puri, *A review of permissible limits of drinking water.* Indian journal of occupational and environmental medicine, 2012. **16**(1): p. 40.
36. Becker, J.S., et al., *Quantitative imaging of selenium, copper, and zinc in thin sections of biological tissues (Slugs– Genus Arion) measured by laser ablation inductively coupled plasma mass spectrometry.* Analytical chemistry, 2007. **79**(16): p. 6074-6080.
37. Otero-Romaní, J., et al., *Evaluation of commercial C18 cartridges for trace elements solid phase extraction from seawater followed by inductively coupled plasma-optical emission spectrometry determination.* Analytica chimica acta, 2005. **536**(1-2): p. 213-218.
38. Gonzales, A., et al., *Peat as a natural solid-phase for copper preconcentration and determination in a multicommuted flow system coupled to flame atomic absorption spectrometry.* Analytica chimica acta, 2009. **636**(2): p. 198-204.
39. Xiang, G., et al., *Determination of trace copper in food samples by flame atomic absorption spectrometry after solid phase extraction on modified soybean hull.* Journal of hazardous materials, 2010. **179**(1-3): p. 521-525.
40. Pathirathna, P., et al., *Fast-scan deposition-stripping voltammetry at carbon-fiber microelectrodes: real-time, subsecond, mercury free measurements of copper.* Analytical chemistry, 2012. **84**(15): p. 6298-6302.
41. Sawminathan, S., et al., *A simple quinazolinone-isophorone based colorimetric chemosensor for the reversible detection of copper (II) and its application in real samples.* Journal of Molecular Structure, 2022. **1257**: p. 132633.
42. Wu, C., et al., *A colorimetric quinoline-based chemosensor for sequential detection of copper ion and cyanide anions.* Tetrahedron, 2017. **73**(38): p. 5715-5719.
43. Jung, H.S., et al., *Coumarin-derived Cu2+-selective fluorescence sensor: synthesis, mechanisms, and applications in living cells.* Journal of the American Chemical Society, 2009. **131**(5): p. 2008-2012.

44. Ge, F., et al., *A new fluorescent and colorimetric chemosensor for Cu (II) based on rhodamine hydrazone and ferrocene unit.* Sensors and Actuators B: Chemical, 2013. **181**: p. 215-220.
45. Hu, J., et al., *Benzimidazole-quinoline-based copper complexes: Exploration for their possible antitumor mechanism.* Polyhedron, 2022. **211**: p. 115563.
46. Udhayakumari, D., S. Naha, and S. Velmathi, *Colorimetric and fluorescent chemosensors for Cu 2+. A comprehensive review from the years 2013–15.* Analytical Methods, 2017. **9**(4): p. 552-578.
47. Sarkar, S., et al., *A pyrene-based simple but highly selective fluorescence sensor for Cu 2+ ions via a static excimer mechanism.* Analyst, 2013. **138**(23): p. 7119-7126.
48. Li, J., et al., *A colorimetric and fluorimetric chemodosimeter for copper ion based on the conversion of dihydropyrazine to pyrazine.* Chemistry–An Asian Journal, 2016. **11**(1): p. 136-140.
49. Karakuş, E., *A rhodamine based fluorescent chemodosimeter for the selective and sensitive detection of copper (II) ions in aqueous media and living cells.* Journal of Molecular Structure, 2021. **1224**: p. 129037.
50. Soufeena, P., T. Nibila, and K. Aravindakshan, *Coumarin based yellow emissive AIEE active probe: A colorimetric sensor for Cu2+ and fluorescent sensor for picric acid.* Spectrochimica Acta Part A: Molecular and Biomolecular Spectroscopy, 2019. **223**: p. 117201.
51. Wang, C., et al., *A simple chalcone molecular rotor for specific fluorescence imaging of mitochondrial viscosity changes in living cells.* Dyes and Pigments, 2021. **194**: p. 109593.
52. Arshad, M., A. Paul, and A. Joseph, *Nanoscale detection of copper using an aggregation induced emission enhancement fluorescent sensor derived from hydroxy naphthaldehyde and benzyloxy benzaldehyde.* Journal of Photochemistry and Photobiology A: Chemistry, 2023: p. 114983.
53. Zhao, J., et al., *Excited state intramolecular proton transfer (ESIPT): from principal photophysics to the development of new chromophores and applications in fluorescent molecular probes and luminescent materials.* Physical Chemistry Chemical Physics, 2012. **14**(25): p. 8803-8817.
54. Irshad, H., et al., *AIEE active J-aggregates of naphthalimide based fluorescent probe for detection of Nitrobenzene: Combined experimental and theoretical approaches for Non-covalent interaction analysis.* Spectrochimica Acta Part A: Molecular and Biomolecular Spectroscopy, 2023. **290**: p. 122273.
55. Zhao, J.-S., et al., *Memory of chirality in J-type aggregates of an achiral perylene dianhydride dye created in a chiral asymmetric catalytic synthesis.* Chemical Science, 2011. **2**(5): p. 937-944.

56. Wang, D., et al., *AIE-active TPA modified Schiff base for successive sensing of Cu 2+ and His via an on–off–on method and its application in bioimaging.* Dalton Transactions, 2023. **52**(2): p. 434-443.
57. Kumar, S.M., et al., *Rationally constructed imidazole derivatized Schiff-base based fluorescent sensor for reversible identification of copper ions and its applications in fingerprint imaging.* Journal of Molecular Liquids, 2023. **373**: p. 121235.
58. Deng, L., et al., *A coumarin based ratiometric fluorescent probe for the detection of Cu2+ and mechanochromism as well as application in living cells and vegetables.* Spectrochimica Acta Part A: Molecular and Biomolecular Spectroscopy, 2023: p. 123479.
59. Wang, Z.-G., et al., *The development of coumarin Schiff base system applied as highly selective fluorescent/colorimetric probes for Cu2+ and tumor biomarker glutathione detection.* Dyes and Pigments, 2020. **175**: p. 108156.
60. Goswami, N., H.P. Gogoi, and P. Barman, *A hydrazine-based unsymmetrical bis-imine-Schiff base as a chemosensor for turn-off fluorescence and naked-eye detection of Cu2+ ion: Application in aqueous media using test strips.* Journal of Photochemistry and Photobiology A: Chemistry, 2024. **446**: p. 115106.
61. Shellaiah, M., Y.C. Rajan, and H.-C. Lin, *Synthesis of novel triarylamine-based dendrimers with N 4, N 6-dibutyl-1, 3, 5-triazine-4, 6-diamine probe for electron/energy transfers in H-bonded donor–acceptor–donor triads and as efficient Cu 2+ sensors.* Journal of Materials Chemistry, 2012. **22**(18): p. 8976-8987.

Sensors & Actuators: A. Physical 373 (2024) 115436

Contents lists available at ScienceDirect

Sensors and Actuators: A. Physical

journal homepage: www.journals.elsevier.com/sensors-and-actuators-a-physical

Highly sensitive detection of copper in aqueous media using a fluorescent probe developed from isophthaldehyde and (*E*)-1-(hydrazonomethyl) naphthlen-2-ol

Muhammed Arshad, Athira Ajayan, Vismaya Joseph, Abraham Joseph *

Department of Chemistry, University of Calicut, Calicut University, PO-673 635, India

ARTICLE INFO

Keywords:
AIEE
PMB3
Dynamic quenching
Chelation

ABSTRACT

A highly selective Schiff base PMB3 with AIEE activity was synthesized and characterized for detecting Cu^{2+} in aqueous media. The PMB3 aggregates exhibit a green fluorescence in the DMF-water mixed solvent, demonstrating a switch-off response specifically to Cu^{2+} ions over various other biologically significant metal ions. The quenching of fluorescence in PMB3 aggregates is likely attributed to the disassembly caused by the chelation of the imine-N atom and phenolic -O atom of PMB3 aggregates with Cu^{2+} ions. The molar ratio of the complex formed as per Job's plot method was 1:1 between PMB3 and Cu^{2+}. The fluorescence lifetime measurements confirmed the involvement of the dynamic quenching process in the reaction cycle. The analysis of the Stern-Volmer plot divulged a quenching constant of 3.75×10^{15} M^{-1}. Remarkably, the limit of detection was determined to be 16.08×10^{-15} M (16.08fM), demonstrating a sensitivity far exceeding the permissible limit set by the World Health Organization.

1. Introduction

The exploration of organic molecules exhibiting aggregation-induced emission enhancement (AIEE) has been a focal point in recent scientific investigations of luminescent materials. This interest is driven by the broad spectrum of potential applications, including the detection of biomolecules, the development of chemosensors for the highly sensitive identification of hazardous heavy metal ions, the advancement of organic light-emitting diodes (OLED), and their utilization in cancer theranostics [1–11]. In the pursuit of detecting biologically significant metal ions, researchers are developing cost-effective fluorescent chemosensors with AIEE activity, emphasizing simplicity, sensitivity, and selectivity [12–15]. The emphasis is on achieving simplicity, sensitivity, and selectivity in these sensing platforms, aligning with the overarching goal of addressing diverse applications in biosensing and advanced materials.

Aggregation-induced enhancement (AIE) that transforms non-emissive organic molecules in pure solvents into highly emissive species upon aggregation, can be exploited for metal ion sensing. These AIEE active materials have the advantages of greater photostability, great selectivity, and high sensitivity making them useful sensors for real-time applications [16,17].

A wide range of mechanisms governs AIEE activity, encompassing restriction of intramolecular rotation (RIR) [18–20], twisted intramolecular charge transfer (TICT) [21–23], restriction of intramolecular charge transfer (ICT) [24], and cis-trans isomerization [25]. Each mechanism is system-specific, and there is no universal mechanism applicable to all systems.

As the third most abundant essential trace metal ion in biochemical systems, after iron and zinc, bivalent copper exists in three forms: Type I, Type II, and Type III. It functions as an oxygen management metalloprotein and as a catalytic cofactor for numerous metalloenzymes, including cytochrome c oxidase, plastocyanin, tyrosinase, ascorbic acid oxidase, and superoxide dismutase [26–32]. Even so, the abnormal level of accumulation of copper can lead to harmful health effects, such as gastrointestinal issues, neurodegenerative illnesses like Parkinson's and Alzheimer's, Amyotrophic Lateral Sclerosis, Wilson disease, prion diseases, and damage to the liver or kidney [33–40]. The widespread use and applications of Cu^{2+} ions in chemistry, and medicine have emerged as one of the most important environmental contaminants due to its excess accumulation in the environment, which creates a serious imbalance in the release and consumption cycle of the metal ion. The World Health Organisation (WHO) mandates that the concentration of Cu^{2+} ions in drinking water should not exceed 31.3 μM [41]. Hence, the

* Corresponding author.
E-mail address: abrahamjoseph@uoc.ac.in (A. Joseph).

https://doi.org/10.1016/j.sna.2024.115436
Received 21 February 2024; Received in revised form 13 April 2024; Accepted 28 April 2024
Available online 30 April 2024

SECTION 3.3

Selective detection of picric acid in aqueous media using PMB3 as a “turn-off” fluorescent sensor

3.3.1. Introduction

Design, synthesis and development of AIE active simple and multi-functional organic compounds in an easy way for the selective detection of chemical species of multiple significance have a great attraction in luminescence materials research. Luminescent methods of detection have great interest in chemical and life sciences because of its simplicity, selectivity, sensitivity, economic viability, and quick responses [1-3]. Many organic molecules in their dilute solution state are highly emissive but loss their activity by Aggregation Caused Quenching effect (ACQ) [4, 5]. Since most organic molecules possess a π-conjugated chromophore system, the ACQ effect reduces its practical applications. To overcome the ACQ effect, a new photophysical phenomenon called Aggregation Induced Emission (AIE), was reported by Tang and co-workers [6, 7]. Molecules which are non-emissive in the free state becomes highly emissive in their aggregated form and is referred to as the aggregation induced emission effect [8-11]. This distinctive characteristic increases the utility of such systems in optical sensor developments. The AIEE characteristics are quite useful in the development of light-emitting diodes using organic molecules (OLEDs), electroluminescent materials, photo emitters, and sensors [12-19]. The AIEE property of such systems can be explained by Restriction of Interamolecular Rotation (RIR) [20], formation of Excited-State Proton Transfer [21], Intramolecular Charge-Transfer (ICT) [22, 23], and intramolecular hydrogen bonds [24], etc.

Selective recognition of traces of aromatic nitro explosives has great significance and considerable importance in recent times due to their devastating effects on environmental safety. Picric acid is one among them to be detected in very low level as it is used in landmines and industrial sectors commonly [25]. Since picric acid is more water soluble than other nitro compounds, it contaminates soil and groundwater more. Prolonged exposure to picric acid may cause health issues in humans, including skin irritation, anaemia, headache, respiratory problems, and liver damage [26-28]. Considering these adverse effects of picric acid, it is necessary to develop a simple and suitable method for the real-time monitoring for PA. Methods such as gas chromatography coupled with energy-dispersive X-ray diffraction [29], surface-enhanced Raman spectroscopy[30], mass spectrometry[31], nuclear quadruple resonance spectroscopy [32], are applied to detect explosives, but such methods need expensive instrumentation and trained personals. Thus, a highly sensitive and quick fluorescence sensor development is still challenging and is highly desirable for the efficient detection of picric acid in the aqueous medium.

Herein, we introduce a AIEE fluorescent sensor, 1,1'-((1E,1'E)-((2E,2'E)- (1,3-phenylenebis (methanylylidene)) bis (hydrazine-2,1-diylidene)) bis (methanylylidene)) bis (naphthalen-2-ol) [PMB3] for the selective detection of PA in low level in aqueous medium.

3.3.2. Experimental section

3.3.2.1. Method of Preparation of PMB3 aggregates

A 1mM solution of PMB3 in DMF was prepared. An aliquot of 100µl of PMB3 stock solution was then added to 10ml standard flask and diluted to a concentration of 10µM with an appropriate ratio of a DMF-Water mixture. The above solution was then sonicated for 20 minutes and absorption and emission spectrum recorded immediately.

3.3.2.2. Fluorescence and its Measurement

A stock solution of PMB3 (1mM) was prepared using DMF and the stock solutions of nitroaromatic compounds (NACs) of 1mM concentration were prepared in double-distilled water. The fluorescent spectra were recorded by excitation at 410 nm in DMF and fluorescent sensing analysis was performed by recording the fluorescence spectra of PMB3 aggregates in DMF/water mixture (1:9) and 1 equivalent of the nitro compounds at room temperature. The limit of detection was calculated using the formula 3σ/slope from the fluorescence titration profile.

3.3.3. Results and discussion

The Schiff base PMB3 was synthesized through the condensation reaction of isophthalaldehyde with 1-(hydrazonomethyl) naphthalen-2-ol in an ethanol medium under reflux conditions at room temperature (**Scheme 2** in chapter 2). PMB3 was readily soluble in DMF and DMSO.

3.3.3.1 Emission Enhancement due to Molecular Aggregation

The AIEE characteristics of PMB3 were studied at room temperature by recording the emission spectrum with the addition of different volumes of double distilled water to PMB3 solution prepared in

DMF. The amount of water fraction percentage (fw) in the DMF-Water mixture changed from 0 to 99 and emission characteristics were recorded by using 410 nm as the excitation wavelength. PMB3 of concentration 10 μM was weakly emissive in DMF solution at 512nm. However, the emission intensity increases with an increase in the percentage of water fraction and light green emission is observed at 536nm. It is evident from the fluorescence spectra in **Fig.1** that there is no noticeable change in the emission behaviour as the percentage of water fraction increases from 0 to 40. Surprisingly, as the percentage of the water fraction reaches 50, the emission intensity increases drastically and light green emission is observed at 536nm. As the percentage of water fraction increased to 60,70, 80, and 90, the intensity of emission increased steadily and at 99%, a drastic increase in fluorescence emission intensity was observed, indicating the AIEE effect. It was also observed from the emission

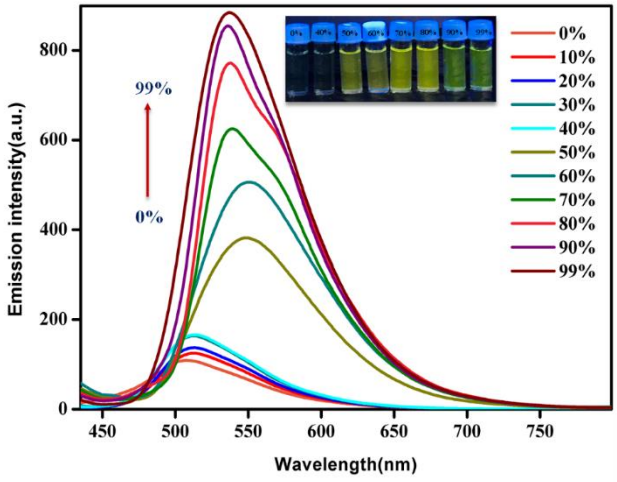

Fig.1 *Fluorescence emission spectra of PMB3in DMF (10μM) in presence of increasing water fraction(fw) from 0% to 99%*

profile that along with emission enhancement, there was a 26 nm red shift and the red shift of emission maxima revealed the transformation of a single organic molecule into aggregates by forming an intermolecular association between them.

3.3.3.2. Absorption Studies

Fig.2 displays the UV-visible spectra of PMB3 in pure DMF and DMF/water mixture with a 90% water content. The absorption spectra of PMB3 in DMF consisted of two broad bands at 332nm and 387nm respectively and were assigned to π-π* transitions and n-π* transitions in the 2-hydroxy-1-naphthaldehyde moiety. However, the absorption spectral profile significantly changed as the percentage of water fraction increased. As the water fraction increases, the intensity of absorption maxima of the PMB3 at 387nm decreases with a slight red shift, indicating the formation of aggregates. The appearance of a new peak with low intensity with levelled-off tails formed at 465 nm in the visible region was

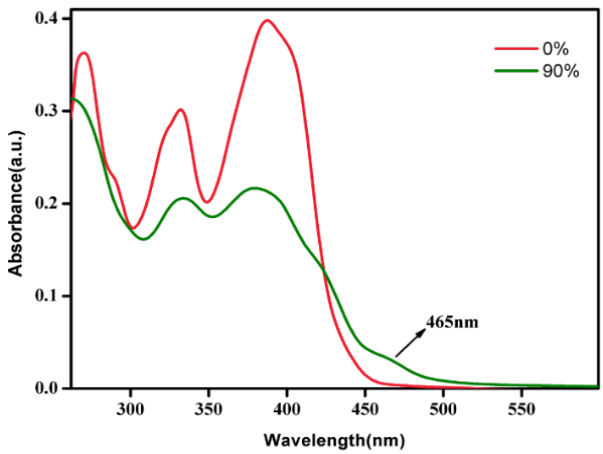

Fig.2 *UV-Visible spectra of PMB3 (10μM) in solution state in pure DMF and in DMF-Water mixed solvent with water fraction of 90% (aggregated state)*

attributed to the Mie scattering of nanoparticles [33, 34]. On the other hand, the ligand PMB3 exhibits a weak charge transfer band in pure DMF, and as the percentage of water increases in the mixture, PMB3 begins to aggregate, and the weak charge transfer band gets intensified as a result of the higher concentration of charge transfer excitons in the aggregated state. Generally, the red shift of the absorption in the UV-Visible spectrum originated from J-type (head-tail type) aggregates and which results in a significant enhancement of the emission intensity.

3.3.3.3 Optical microscopic study

Optical microscopic images of PMB3 obtained in the isolated states (**a**) and in the aggregated states (**b**) are shown in **Fig.3.** Particles in their isolated states have no fluorescence, while upon aggregation exhibit a greenish yellow emission. Optical image supports the formation of nanoparticles in the aggregated states, which is responsible for the fluorescence emission behaviour. The size of the PMB3 aggregates was analysed using the FE-SEM image (**Fig.4**) and

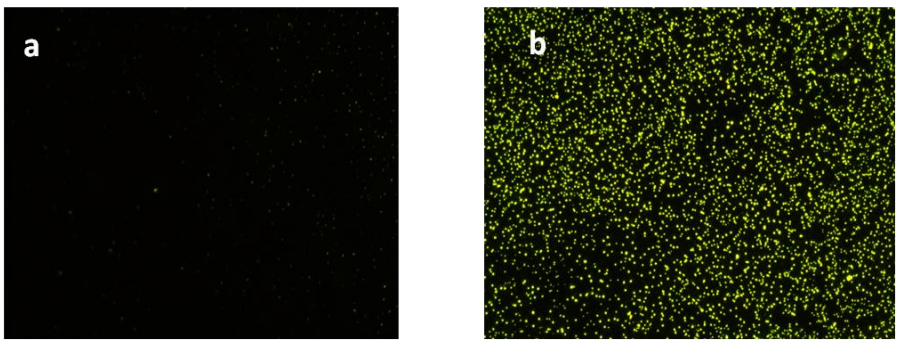

Fig.3 *Optical fluorescence microscopy images (under UV excitation) of (**a**) PMB3 in solution state (fw = 0%) and (**b**) PMB3 in aggregated state (fw = 90%)*

was found to be 54.95nm. FE-SEM image showed the presence of spherical shaped nano aggregates.

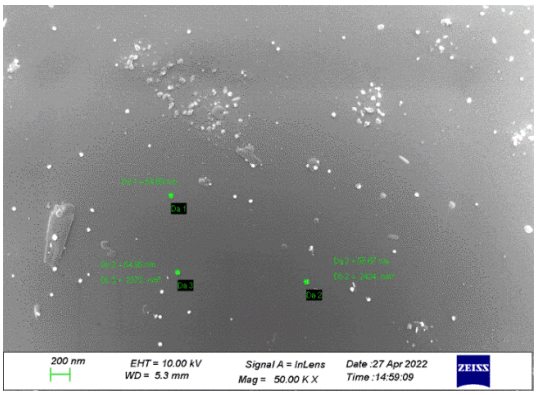

Fig.4 *FE-SEM image of PMB3 in aggregated state (fw = 90%)*

3.3.3.4 Fluorescence decay study

The luminescence lifetime measurement was carried out to gather more insights into the aggregation phenomenon and consequent emission enhancement. The results of lifetime decay measurements

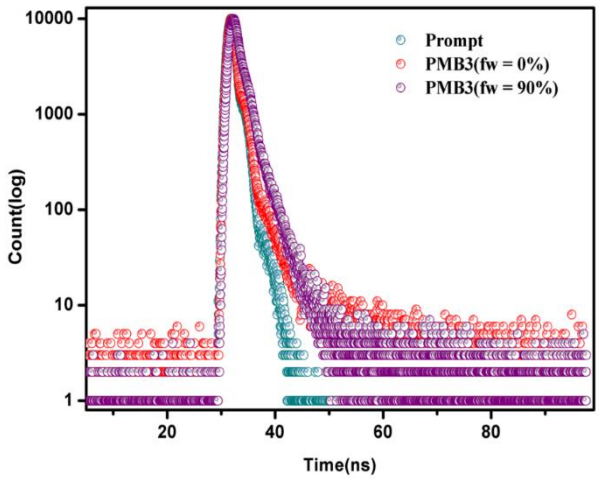

Fig.5 *Fluorescence decay profile of PMB3(10 μM) in pure DMF (fw = 0%) and in DMF-Water mixture (1:9) (fw = 90%)*

of PMB3 in pure DMF and DMF/water mixture with 90% water content are well fit by a single-exponential decay curve (**Fig.5**). The lifetime value for PMB3 in pure DMF is 1.032ns which is significantly increased to 1.521ns on aggregation. This increase in the lifetime of the system in DMF-Water mixture with a relatively greater percentage of water content (90%) is attributed to the decrease of radiation-less decay in the aggregated state.

3.3.3.5 The Effect of Viscosity on Fluorescence Emission

To validate the mechanism of the enhancement of fluorescence emission intensity on aggregation, the effect of viscosity was examined by integrating methanol with glycerol, and the solvent viscosity was adjusted by changing the glycerol percentage ratio to the methanol percentage ratio. As the glycerol fraction is increased, the intensity of emission maxima also increased (**Fig.6**) and this emission enhancement is the result of the change in the viscosity of the medium and associated restriction of intramolecular rotation.

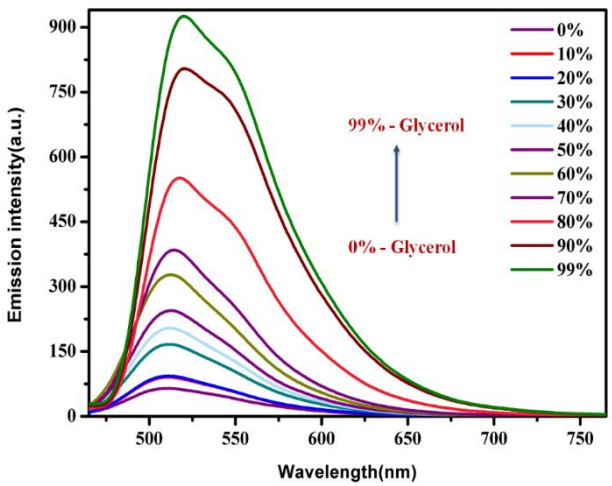

Fig.6 *Fluorescence emission spectra of aggregates of PMB3 (10 μM) with change in viscosity of the solvent mixture by varying the solvent ratio of glycerol to methanol*

As it is clear from **Fig.1**, the emission spectral profile changed with increasing the percentage of water fraction, and up to 40%, the active participation of N-N and C-N intramolecular rotation persists which reduces the emission intensity. When the water fraction reaches 50%, aggregation starts and because of physical constraints, the intramolecular motion was inhibited, and strong emission happens (**Scheme 1**).

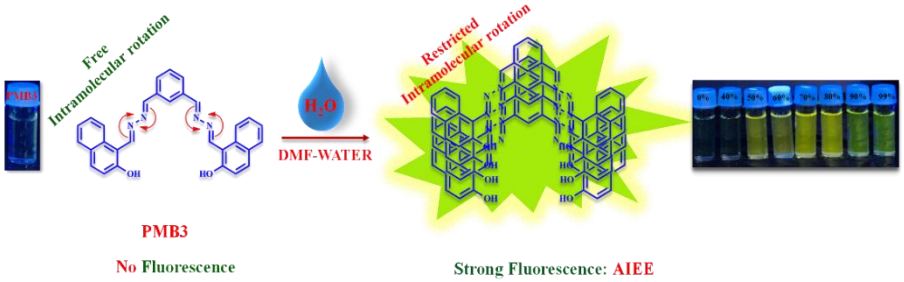

Scheme 1 *Proposed mechanism for AIEE behaviour of PMB3*

3.3.3.6 The effect of pH on emission intensity

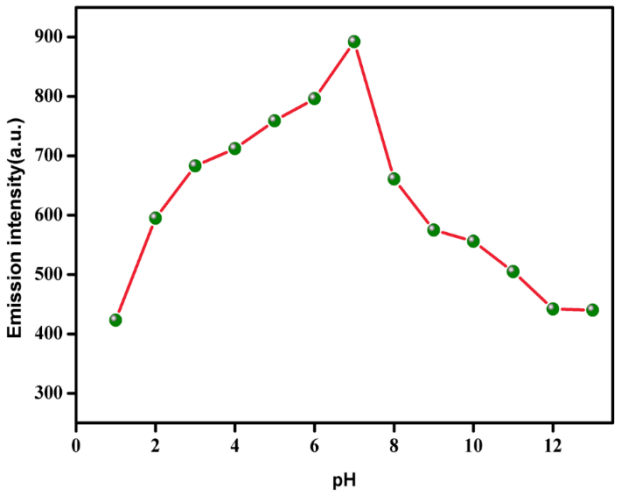

Fig.7 *Variation of emission intensity of PMB3 (10 μM) in DMF-Water mixture (1:9 v/v) at different pH.*

For practical applications, the influence of pH on the intensity of emission of PMB3 aggregate in DMF-Water mixture with a water fraction of 90% using 4-(2-hydroxyethyl)-1-piperazineethanesulfonic acid (HEPES) buffer was studied. As shown in **Fig.7**, the fluorescence intensity of PMB3 aggregate increased from pH 2 to 7 and then decreased. No appreciable variations in the emission intensity were observed over the physiological pH range of 2-7, indicating the potential applications of PMB3 aggregate in the biological environments.

3.3.3.7 Picric acid sensing

The sensing ability of the PMB3 aggregates formed in DMF /water mixture (1:9) towards various nitro derivatives including picric acid (PA) has been investigated by recording fluorescence spectra (**Fig.8**). PMB3 aggregates exhibit a prominent emission peak at 536nm in its fluorescence spectra and the emission intensity

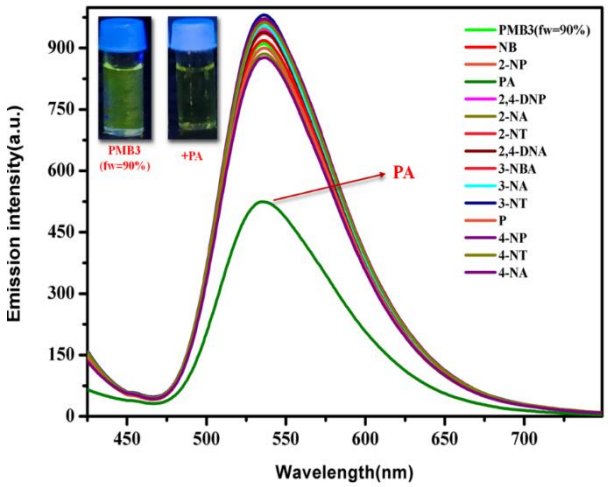

Fig.8 *Fluorescence emission spectra of aggregate of PMB3 (10 μM) with water fraction 90% (fw = 90%) in presence of different nitro compounds*

decreases gradually with the addition of PA without any change in the position of peak (**Fig.9**). This decrease in emission intensity indicates that the quenching efficiency increases with increase in concentration of PA.

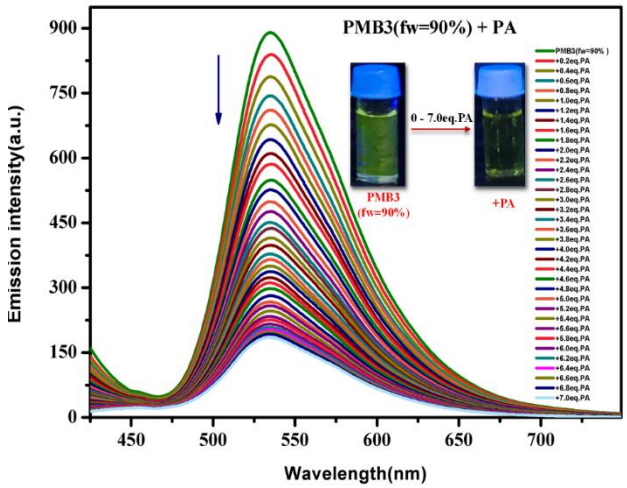

Fig.9 *Fluorescence emission spectra of aggregate of PMB3 in presence of increasing concentration of PA*

There was a considerable 'turn-off' fluorescence response for PA among all other tested nitro compounds, which indicates that the fluorescence quenching is caused by ground-state complexation between electron-rich PMB3 aggregates and electron-deficient picric acid through charge transfer process (**Scheme 2**). In addition, the strong electron-withdrawing property of three nitro groups present in PA makes it more acidic and make the phenyl group to an electron-deficient π-system. The naphthyl group present in PMB3 aggregates is an electron rich π -system and hence PA could bind with this group through donor-acceptor π-π interactions[35-37]. This donor-acceptor π-π interaction and proton transfer induced intermolecular charge transfer between PA and PMB3 aggregates,

induces fluorescent quenching of PMB3 aggregate. The Stern-Volmer plot was used to determine the fluorescence quenching constant, which was found to be 2.33× 10^6 M^{-1} (**Fig.10**).

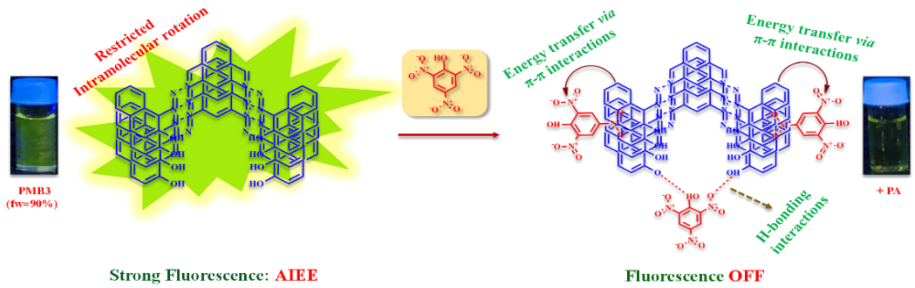

Scheme 2 *Proposed mechanism of interaction of PMB3 aggregates with PA*

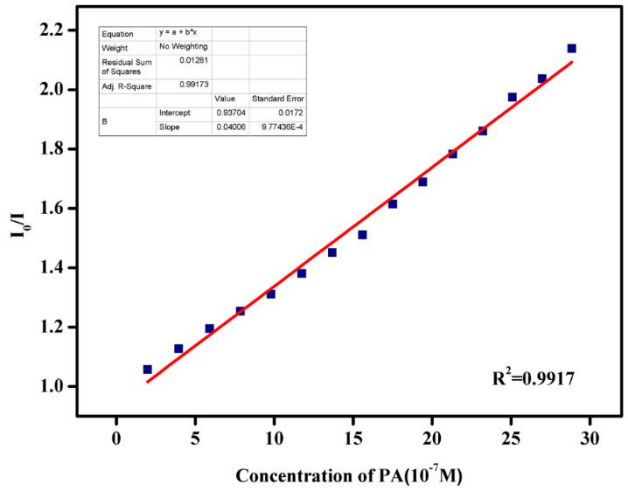

Fig.10 *Stern-Volmer plot for the interaction of PMB3 aggregates with PA*

The strong quenching in the fluorescence intensity of PMB3 aggregates with the addition of PA may be attributed to the static or dynamic or combinations thereof which was confirmed from the excited state fluorescence lifetime measurements. For that, the lifetime decay profile of PMB3 aggregates with and without PA was

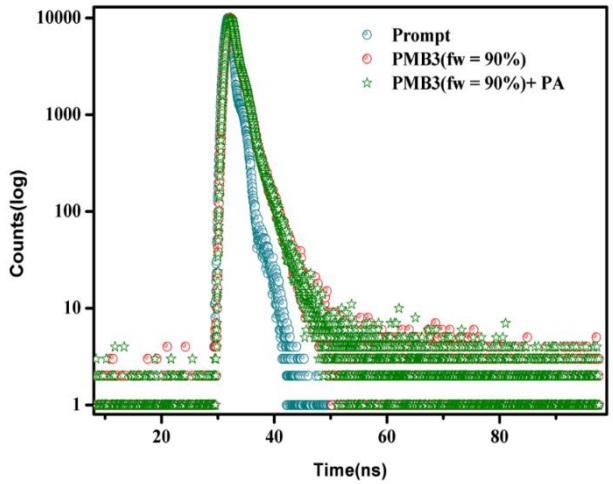

Fig.11*.Fluorescence decay profile of PMB3 in DMF (10μM) with water fraction (fw) percentage of 90 in aggregated state (fw = 90%) in absence and presence of PA*

recorded (**Fig.11**). The lifetime value of aggregates of PMB3 was found to be 1.521ns and remains unchanged after the addition of PA. This unchanged fluorescence lifetime value suggests the involvement of the static quenching process. Moreover, the non-

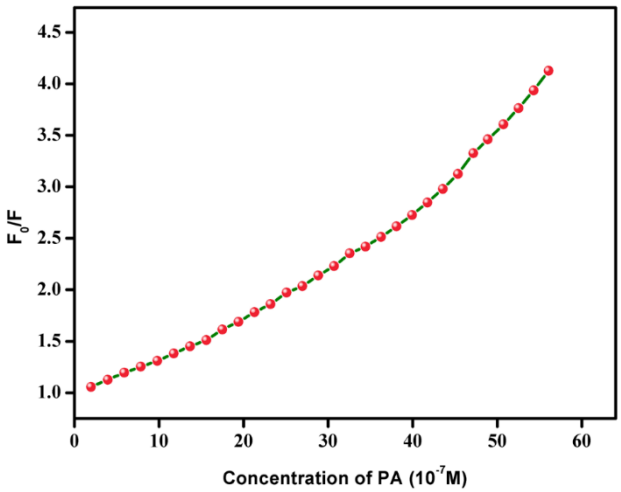

Fig.12 *Stern-Volmer plot of aggregate of PMB3 with increasing concentration of PA*

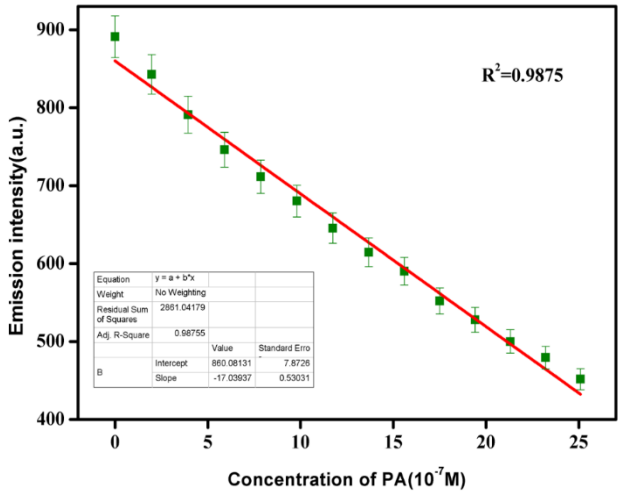

Fig.13 *Limit of detection (LOD)*

linearity observed in the Stern-Volmer plot further supports the combined effect of both static and dynamic quenching processes (**Fig.12**). The linearity of the plot in the lower concentration of PA

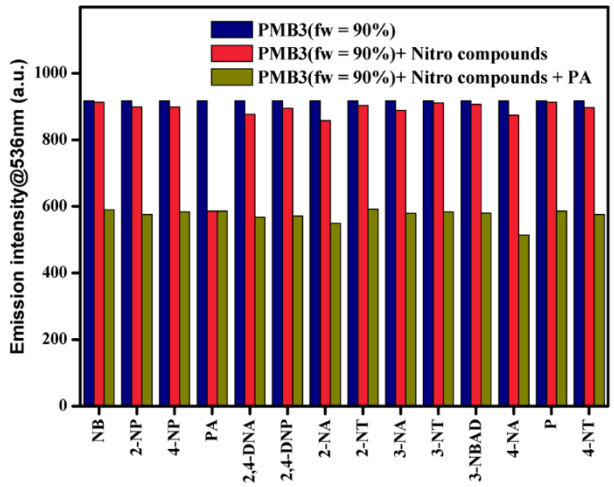

Fig.14 *The selectivity of aggregate of PMB3 (10 μM) towards PA (1 equivalent) in the presence of other nitro compounds (1 equivalent)*

indicated the static quenching process which was confirmed by excited state lifetime measurements and an upward bending at a higher concentration of PA indicated a dynamic quenching process. The limit of detection was calculated using the formula, 3σ / k, and the detection limit was found to be 2.43μM (**Fig. 13**).

To confirm the high selectivity of PMB3 aggregates with PA, the fluorescence competitive experiments were also studied by recording the emission spectra of PMB3 aggregates in the addition of 1 equivalent of PA and an equivalent amount of other nitro compounds. It was observed from the bar diagram depicted in **Fig.14** that PA has a significantly higher quenching efficiency than other nitro compounds.

3.3.3.8 Analysis of Real Sample

The method of using PMB3 aggregates for the analysis of PA was extended to real samples made from natural resources such as well water, tap water, and river water samples respectively by the standard addition method. The results obtained are presented in **Table 1**. The recoveries varied in 99-101% range, which demonstrates the applicability and reliability of PMB3 aggregates in PA detection in real samples.

3.3.3.9 PMB3 aggregates coated paper sensor

This method has been further extended to the development of a paper sensor for PA. To explore this, we have prepared a TLC plate coated with PMB3 aggregates and PA solution dropped onto the test plate. The changes obtained are depicted in **Fig. 15**. The changes in the emission colour can be easily visualized when exposed to UV

light with the naked eye. So, this method can be well extended to the development of paper sensor for PA.

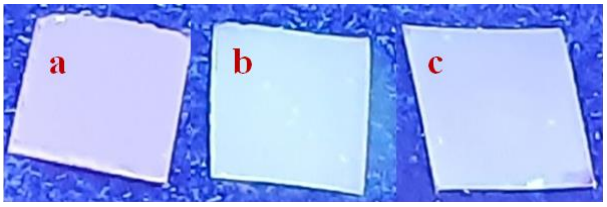

Fig. 15. *Photographs of TLC plate containing (**a**) TLC plate only (**b**) TLC plate coated with PMB3 aggregates (**c**) TLC plate coated with PMB3 aggregates and PA.*

Table 1 *Detection of Picric acid (PA) in real samples*

Water sample	Added PA (μM)	Found (μM)	Error (%)	Recovery (%)
Well Water	3.98	4.0	0.50	100.50
	5.96	5.98	0.33	100.33
	7.93	7.92	0.12	99.57
Tap Water	3.98	3.96	0.50	99.49
	5.96	5.94	0.66	99.33
	7.93	7.89	0.50	99.49
River Water	3.98	4.01	0.75	100.75
	5.96	6.01	0.83	100.83
	7.93	7.97	0.50	100.53

3.3.4. Conclusions

A novel fluorescent sensor based on naphthaldehyde, PMB3, have been designed and synthesized for the first time. The feeble emissive characteristics of PMB3 in the solution state display strong emission in the aggregated state, exhibiting AIEE properties. This strong

emission behaviour in the aggregated state is due to the restricted intramolecular rotation of the molecules. The AIEE properties of PMB3 have been explained using UV-visible spectra, fluorescence decay study, and optical microscopic study. The utility of AIEE active property of PMB3 aggregate was further used for the selective sensing of PA and the detection limit was 2.43μM with a quenching constant value of 2.33×10^{6} M^{-1}. Moreover, the quenching fluorescence emission intensity of PMB3 aggregates in presence of PA was explained with the steady-state fluorescence lifetime measurement and Stern-Volmer plots which confirm that the fluorescence quenching follows both static and dynamic processes.

References

1. Peng, Y., et al., *A colorimetric and fluorescent chemosensor for the detection of an explosive—2, 4, 6-trinitrophenol (TNP).* Chemical communications, 2011. **47**(15): p. 4505-4507.
2. Dinda, D., et al., *Highly selective detection of trinitrophenol by luminescent functionalized reduced graphene oxide through FRET mechanism.* ACS applied materials & interfaces, 2014. **6**(13): p. 10722-10728.
3. Sun, X., Y. Wang, and Y. Lei, *Fluorescence based explosive detection: from mechanisms to sensory materials.* Chemical Society Reviews, 2015. **44**(22): p. 8019-8061.
4. Jenekhe, S.A. and J.A. Osaheni, *Excimers and exciplexes of conjugated polymers.* Science, 1994. **265**(5173): p. 765-768.
5. Hong, Y., J.W. Lam, and B.Z. Tang, *Aggregation-induced emission.* Chemical Society Reviews, 2011. **40**(11): p. 5361-5388.
6. Tang, B.Z., et al., *Efficient blue emission from siloles.* Journal of Materials Chemistry, 2001. **11**(12): p. 2974-2978.
7. Luo, J., et al., *Aggregation-induced emission of 1-methyl-1, 2, 3, 4, 5-pentaphenylsilole.* Chemical communications, 2001(18): p. 1740-1741.
8. Hong, Y., J.W. Lam, and B.Z. Tang, *Aggregation-induced emission: phenomenon, mechanism and applications.* Chemical communications, 2009(29): p. 4332-4353.
9. An, B.-K., et al., *Enhanced emission and its switching in fluorescent organic nanoparticles.* Journal of the American Chemical Society, 2002. **124**(48): p. 14410-14415.

10. Mei, J., et al., *Aggregation-induced emission: the whole is more brilliant than the parts.* Advanced materials, 2014. **26**(31): p. 5429-5479.
11. Yin, Y., et al., *Highly Emissive Multipurpose Organoplatinum(II) Metallacycles with Contrasting Mechanoresponsive Features.* Inorganic Chemistry, 2022. **61**(6): p. 2883-2891.
12. Kasahara, T., et al., *Multi-color microfluidic organic light-emitting diodes based on on-demand emitting layers of pyrene-based liquid organic semiconductors with fluorescent guest dopants.* Sensors and Actuators B: Chemical, 2015. **207**: p. 481-489.
13. Yang, B., et al., *Shape-controlled micro/nanostructures of 9, 10-diphenylanthracene (DPA) and their application in light-emitting devices.* The Journal of Physical Chemistry C, 2011. **115**(16): p. 7924-7927.
14. Li, G., et al., *Synthesis, characterization, physical properties, and OLED application of single BN-fused perylene diimide.* The Journal of organic chemistry, 2015. **80**(1): p. 196-203.
15. Mazumdar, P., et al., *Proton induced green emission from AIEE active 2, 2′ biquinoline hydrosol and its selective fluorescence turn-on sensing property towards Zn2+ ion in water.* Sensors and Actuators B: Chemical, 2017. **238**: p. 1266-1276.
16. Shyamal, M., et al., *Highly selective turn-on fluorogenic chemosensor for Zn2+ based on chelation enhanced fluorescence.* ACS Sens., 2016. **1**(6): p. 739-747.
17. Shyamal, M., et al., *Highly selective turn-on fluorogenic chemosensor for robust quantification of Zn (II) based on aggregation induced emission enhancement feature.* ACS sensors, 2016. **1**(6): p. 739-747.
18. Li, J. and Q. Zhang, *Linearly fused azaacenes: novel approaches and new applications beyond field-effect transistors (FETs).* ACS Applied Materials & Interfaces, 2015. **7**(51): p. 28049-28062.
19. Zhang, M.-X., et al., *Synthesis, structure and mechanofluorochromic properties of phenothiazine-S-oxide and phenothiazine-S, S-dioxide derivatives.* Spectrochimica Acta Part A: Molecular and Biomolecular Spectroscopy, 2023. **292**: p. 122427.
20. Chen, J., et al., *ID 835 Williams, D. Zhu and BZ Tang.* Chem. Mater, 2003. **15**: p. 1535-1546.
21. He, T., et al., *Aggregation-induced emission enhancement of polycyclic aromatic alkaloid derivatives and the crucial role of excited-state proton-transfer.* Chemical Communications, 2011. **47**(10): p. 2907-2909.
22. Xu, J., et al., *Morphology transition and aggregation-induced emission of an intramolecular charge-transfer compound.* Langmuir, 2008. **24**(8): p. 4231-4237.
23. Liang, X. and Q. Zhang, *Recent progress on intramolecular charge-transfer compounds as photoelectric active materials.* Science China Materials, 2017. **60**(11): p. 1093-1101.

24. Upamali, K.A., et al., *Carbazole-based cyano-stilbene highly fluorescent microcrystals.* Langmuir, 2011. **27**(5): p. 1573-1580.
25. Germain, M.E. and M.J. Knapp, *Optical explosives detection: from color changes to fluorescence turn-on.* Chemical Society Reviews, 2009. **38**(9): p. 2543-2555.
26. Hussain, S., et al., *Ultrasensitive detection of nitroexplosive–picric acid via a conjugated polyelectrolyte in aqueous media and solid support.* Chemical communications, 2015. **51**(33): p. 7207-7210.
27. Davidson, A.J., et al., *Explosives under pressure—the crystal structure of γ-RDX as determined by high-pressure X-ray and neutron diffraction.* CrystEngComm, 2008. **10**(2): p. 162-165.
28. Ashbrook, P.C. and T.A. Houts, *Top ten institutional ways to minimize laboratory waste.* Chemical Health and Safety, 2001. **6**(8): p. 27.
29. Luggar, R., et al., *Multivariate analysis of statistically poor EDXRD spectra for the detection of concealed explosives.* X-Ray Spectrometry: An International Journal, 1998. **27**(2): p. 87-94.
30. Sylvia, J.M., et al., *Surface-enhanced Raman detection of 2, 4-dinitrotoluene impurity vapor as a marker to locate landmines.* Analytical chemistry, 2000. **72**(23): p. 5834-5840.
31. Håkansson, K., et al., *Low-mass ions observed in plasma desorption mass spectrometry of high explosives.* Journal of mass spectrometry, 2000. **35**(3): p. 337-346.
32. Anferov, V., G. Mozjoukhine, and R. Fisher, *Pulsed spectrometer for nuclear quadrupole resonance for remote detection of nitrogen in explosives.* Review of Scientific Instruments, 2000. **71**(4): p. 1656-1659.
33. Zhao, J., et al., *Excited state intramolecular proton transfer (ESIPT): from principal photophysics to the development of new chromophores and applications in fluorescent molecular probes and luminescent materials.* Physical Chemistry Chemical Physics, 2012. **14**(25): p. 8803-8817.
34. Auweter, H., et al., *Supramolecular structure of precipitated nanosize β-carotene particles.* Angewandte Chemie International Edition, 1999. **38**(15): p. 2188-2191.
35. Yin, Y., et al., *Ligand-Triggered Platinum(II) Metallacycle with Mechanochromic and Vapochromic Responses.* Inorganic Chemistry, 2021. **60**(13): p. 9387-9393.
36. Ahmed, M.B., et al., *Sorption of hydrophobic organic contaminants on functionalized biochar: Protagonist role of π-π electron-donor-acceptor interactions and hydrogen bonds.* Journal of Hazardous Materials, 2018. **360**: p. 270-278.
37. Qu, X., L. Xiao, and D. Zhu, *Site-Specific Adsorption of 1, 3-Dinitrobenzene to Bacterial Surfaces: A Mechanism of n–π Electron-Donor-Acceptor Interactions.* Journal of environmental quality, 2008. **37**(3): p. 824-829.

Journal of Luminescence 258 (2023) 119818

Contents lists available at ScienceDirect

Journal of Luminescence

journal homepage: www.elsevier.com/locate/jlumin

Full Length Article

Selective detection of picric acid in aqueous medium using a novel naphthaldehyde-based aggregation induced emission enhancement (AIEE) active "turn-off" fluorescent sensor

Muhammed Arshad, Jeeja Rani AT, Vismaya Joseph, Abraham Joseph *

Department of Chemistry, University of Calicut, Calicut University, P O-673 635, India

ARTICLE INFO

Keywords:
Fluorescent sensor
Picric acid
Aggregation
Quenching

ABSTRACT

A new aggregation induced emission enhancement (AIEE) fluorescent sensor derived from hydroxy naphthaldehyde (PMB3), was synthesized, and used as a switch-off sensor for 2,4,6-trinitrophenol (PA) in an aqueous medium after detailed characterization. The detection limit of and quenching constant was estimated to be 2.43 μM and 2.33 × 10^6 M^{-1}respectively. The static quenching mechanism of the fluorescence of PMB3 aggregates in the presence of PA was monitored and confirmed using a time-resolved emission study. The selectivity of the PMB3 aggregate for picric acid over nitro aromatic explosives in the aqueous medium is confirmed by a series of detections carried out under different experimental conditions. We, therefore, report in this paper that the newly developed AIEE active PMB3 sensor is highly efficient and selective for the detection of PA in the aqueous medium.

1. Introduction

Design and synthesis and development of AIE active simple and multi-functional organic compounds in an easy way for the selective detection of chemical species of multiple significance have a great attraction in luminescence materials research. Luminescent methods of detection have great interest in chemical and life sciences because of its simplicity, selectivity, sensitivity, economic viability, and quick responses [1–3]. Many organic molecules in their dilute solution state are highly emissive but loss their activity by aggregation caused quenching effect (ACQ) [4,5]. Since most organic molecules possess a π-conjugated chromophore system, the ACQ effect reduces its practical applications. To overcome the ACQ effect, a new photophysical phenomenon called aggregation induced emission (AIE), was reported by Tang and co-workers [6,7]. Molecules which are non-emissive in the free state becomes highly emissive in their aggregated form and is referred to as the aggregation induced emission effect [8]. There are many other classes of compounds that are feebly emissive in pure solvent are transformed to strong luminescent emitters in aggregated state. This phenomenon is described by using the term aggregation induced emission enhancement (AIEE) [9–11]. This distinctive characteristic of course increases the utility of such systems in optical sensor developments. The AIEE characteristics are quite useful in the development of light-emitting diodes using organic molecules (OLEDs), electroluminescent materials, photo emitters, and sensors [12–19]. The AIEE property of such systems can be explained by restriction of intermolecular rotation (RIR) [20], formation of excited-state proton transfer [21], intramolecular charge-transfer (ICT) [22,23], and intramolecular hydrogen bonds [24], etc.

Selective recognition of traces of aromatic nitro explosives has great significance and considerable importance in recent times due to their devastating effects on environmental safety. Picric acid is one among nitro explosives to be detected in very low level as it is used in landmines and industrial sectors commonly [25]. Since picric acid is more water soluble as compared to other nitro compounds, it contaminates soil and groundwater more than others. Prolonged exposure to picric acid may experience a number of health issues in humans, including skin irritation, anaemia, headache, respiratory problems, and liver damage [26–28]. Considering these adverse effects of picric acid, it is necessary to develop a sensor suitable method for the real-time monitoring for PA. Methods such as gas chromatography coupled with energy-dispersive X-ray diffraction [29], surface-enhanced Raman spectroscopy [30], mass spectrometry [31], nuclear quadruple resonance spectroscopy [32], are applied to detect explosives, but such methods need expensive

* Corresponding author.
E-mail address: abrahamjoseph@uoc.ac.in (A. Joseph).

https://doi.org/10.1016/j.jlumin.2023.119818
Received 11 February 2023; Received in revised form 12 March 2023; Accepted 20 March 2023
Available online 25 March 2023

SECTION 3.4

Simultaneous detection of bivalent Copper and Nickel in aqueous media using PMB3 as a Colourimetric probe

3.4.1. Introduction

A colourimetric sensor is an ingenious device that undergoes a visible colour change immediately when it detects specific substances, facilitating swift and simple sensing without the demand for intricate apparatus. The primary allure of colourimetric strategies lies in their simplicity, combined with sensitivity and selectivity (SSS). This method perpetually carves out a unique niche on account of its distinctive characteristics, including naked eye detection under visible light, rapid response, and inexpensive instrumental facilities. Formulating a colorimetric sensor with exceptional selectivity for the detection and estimation of cations has consistently been an acute challenge for researchers. The achievement of efficient and simultaneous detection of multiple target ions with a single sensor seems more appealing and cost-effective than one-to-one testing methods, as it alleviates the hurdles associated with using multiple indicators [1-3].

Considering the multifaceted significance of copper in diverse physiological and pathological contexts, and its crucial role in maintaining human organs and functions, the development of a selective colourimetric sensor for Cu^{2+} is quite imperative.

Nickel is another indispensable metal that finds applications in both industrial and biological domains. In industry, it is widely used for stainless steel production and other alloy formulations, while it plays a key role in biological processes such as enzyme protein development, cytohormone regulation, and pigment metabolism[4, 5]. However, excessive Ni^{2+} ions can be detrimental to human health,

as they can readily accumulate in the liver, spleen, and kidneys, triggering 'lung cancer' and 'nasopharyngeal carcinoma'[6, 7]. In 1990, "International Agency for Research on Cancer" (IARC) proclaimed nickel compounds as Group 1 human carcinogens, emphasizing their proclivity to cause human cancer[8]. Hence, ensuring social and environmental safety necessitates the development and deployment of a robust monitoring system and a proficient technique for nickel detection, which indeed poses an intriguing and formidable endeavour.

The determination of copper and nickel currently relies on conventional methods, such as spectroscopic techniques. However, the high cost and complexity of these techniques make them quixotic for rudimentary testing laboratories. Thus, it is essential to explore novel alternatives for selectively detecting bivalent copper and nickel with superior responses in the presence of several heavy and trace metal ions.

Herein, I have acquainted a novel colourimetric sensor, 1,1'-((1E,1'E)-((2E,2'E)-(1,3-phenylenebis(methanylylidene))bis(hydrazine-2,1-diylidene)) bis (methanylylidene)) bis (naphthalen-2-ol) [PMB3] synthesized from (E)-1-(hydrazonomethyl)naphthalen-2-ol and isophthalaldehyde for the synchronous and selective detection of Cu^{2+} and Ni^{2+} with a very low limit of detection. The PMB3 sensor exhibits an evident colour change, thus rendering it suitable for naked-eye detection of bivalent copper and nickel ions and facilitating real sample analysis.

3.4.2. Experimental section

3.4.2.1. Colourimetric Measurements

A 1mM stock solution of PMB3 was prepared in dimethylformamide (DMF), while 1mM stock solutions of diverse metal ions were prepared from their nitrate salts, using double-distilled water. The experimental protocol of colourimetric sensing involved recording absorption spectra for mixtures formed by combining 2.5mL of a 10μM PMB3 solution with an equimolar quantity of metal ion stock solutions. The detection limit (LOD) was determined from the UV-visible spectral titration curve utilizing the formula 3σ/slope. Furthermore, the Benesi-Hildebrand equation was applied to ascertain the association constant.

3.4.3. Results and Discussion

The sensor PMB3 was synthesized through a two-step condensation reaction, as outlined **Scheme 2** in chapter.2. PMB3 demonstrated pronounced solubility in organic solvents like dimethyl sulfoxide (DMSO) and dimethylformamide (DMF).

3.4.3.1 Colourimetric analysis

The sensing efficacy of PMB3 was systematically evaluated using a visual assessment in the presence and absence of diverse metal ions. Upon the addition of Cu^{2+} and Ni^{2+} ions, an immediate colour change of the PMB3 solution in DMF was observed, transitioning from colourless to yellow (**Fig.1**). On another hand the addition of other metal ions (Al^{3+}, Hg^{2+}, Zn^{2+}, Co^{2+}, Fe^{3+}, Cd^{2+}, Ag^{+}, Mn^{2+}, Mg^{2+}, Ba^{2+}, Ca^{2+}, Cr^{3+}, Pb^{2+}, and Na^{+}) yielded no discernible effect on the colour. This remarkable finding underscores the ability of PMB3 for visual

detection, specifically demonstrating its selectivity for divalent copper and nickel ions.

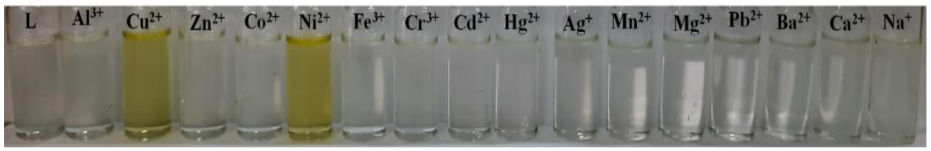

Fig.1 *Colour changes of PMB3(10μM) before and after addition of respective metal ions.*

3.4.3.2. UV-Visible Absorption studies

Fig.2 depicts the UV-visible absorption spectrum of PMB3 in DMF in the presence of diverse metal ions. The DMF solution of PMB3 exhibited two broad bands at 332nm and 387nm, corresponding respectively to the π-π* and n-π* transitions of the 2-hydroxy-1-naphthaldehyde moiety. The addition of Cu^{2+} and Ni^{2+} induced substantial alterations in the absorption spectral profile. Specifically, the introduction of bivalent copper led to a reduction in the peak intensity at 387nm and the emergence of a new peak at

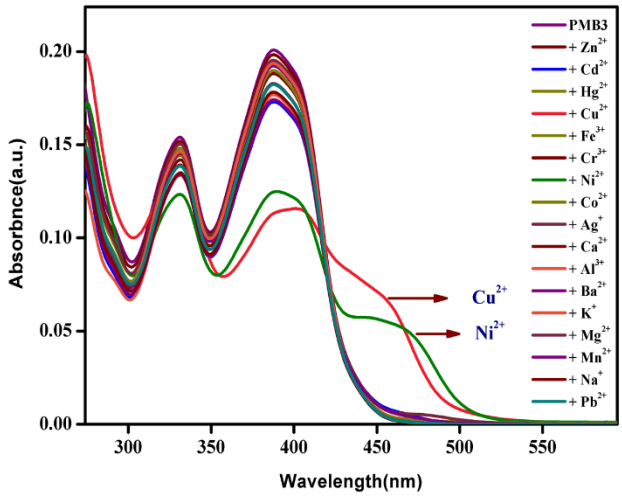

Fig.2 *UV–Visible spectra of PMB3 (10μM) in presence of various metal ions*

454nm. Similarly, the addition of bivalent nickel resulted in a diminished intensity of the peak at 387nm, accompanied by the appearance of a new peak at 472nm. Notably, the position or intensity of the absorption peaks remained relatively unaffected with the introduction of other metal ions under investigation.

3.4.3.3 UV -Visible absorption titration on Cu^{2+} and Ni^{2+} ions

The sensitivity of the PMB3 sensor to Cu^{2+} and Ni^{2+} is delineated in **Fig. 3a and b**. Regarding Cu^{2+} ions, with increasing concentration, the absorption band at 387nm gradually attenuated, concomitant with the emergence of a new absorption band at 454nm, and a distinct isosbestic point was observed at 416nm, indicating the formation of the PMB3-Cu^{2+} complex in the solution state. Furthermore, the initially colourless solution underwent a transition to a pale-yellow hue, intensifying with higher concentrations of Cu^{2+}, and the absorption peak exhibited a red shift. In assessing the specificity of PMB3 towards Ni^{2+}, the absorption

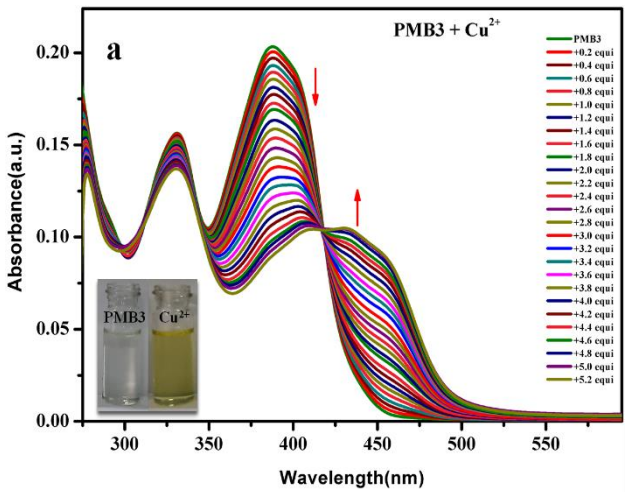

Fig.3a *UV -Visible absorption titration spectra of PBM3(10μM) with Cu^{2+}*

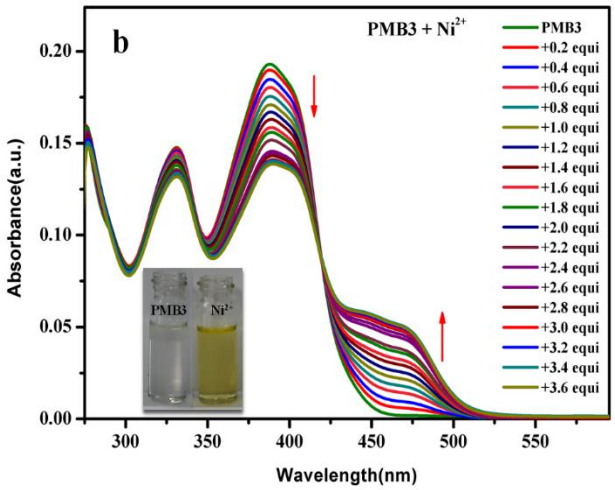

Fig.3b *UV -Visible absorption titration spectra of PBM3(10μM) with* Ni^{2+}

peak of PMB3 at 387nm systematically shifted downwards with the gradual addition of Ni^{2+} ions and subsequently, an additional intense peak is registered at 472nm. This spectral alteration, coupled with a distinct isosbestic point at 418nm, confirms the formation of the PMB3-Ni^{2+} complex.

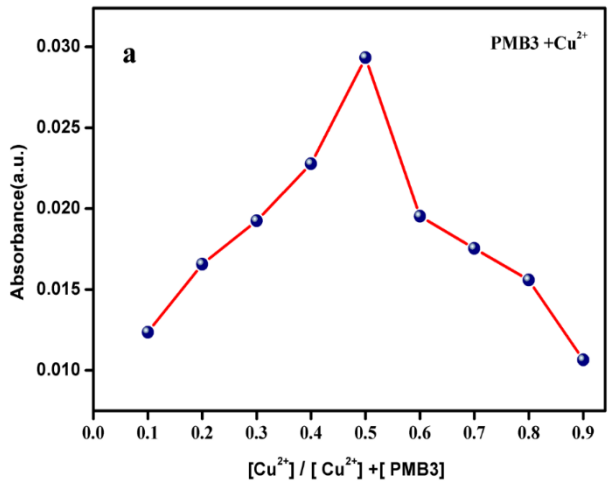

Fig.4a *Job's plot of PMB3 (10μM) with* Cu^{2+}

3.4.3.4 Stoichiometry of metal complexes

The Job's plot, given in **Fig.4 a and b**, illustrates the variation in the maximum absorption at 454nm and 472nm concerning the mole fraction. This analysis reveals that in PMB3-Cu^{2+} and PMB3-Ni^{2+} complexes have1:1 binding ratio.

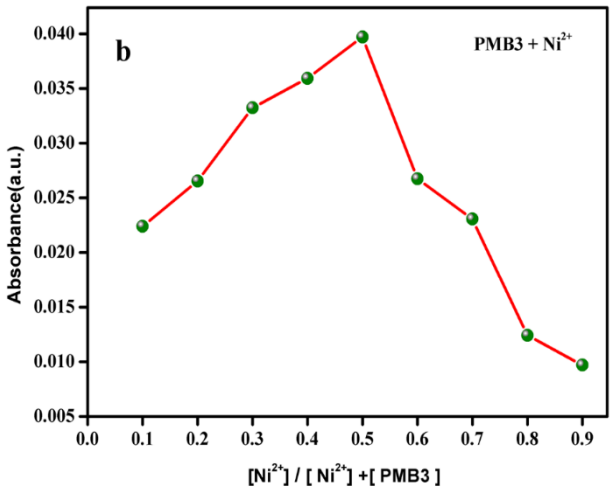

Fig.4b *Job's plot of PMB3 (10μM) with* Ni^{2+}

3.4.3.5 Limit of Detection (LOD)

The determination of detection limits for these metal ions was conducted by employing standard deviation method, as provided in **Fig. 5**. The detection limits were found to be 4.56μM for PMB3-Cu^{2+} and 2.68μM for PMB3-Ni^{2+}. A comparison was carried out between the obtained LOD value of PMB3 and some of the colourimetric probes that have been already reported (**Table 1**). Even at lower concentration levels, PMB3 found to have better Cu^{2+} and Ni^{2+} ion sensitivity than many of the other reported probes, which is a desired quality of an effective colourimetric probe. The assessment of binding interactions between the metal ions and PMB3 was done

using the Benesi-Hildebrand equation, disclosing association constants of $3.47\times10^{4}M^{-1}$ and $8.02\times10^{4}M^{-1}$ for the PMB3-Cu^{2+} and PMB3-Ni^{2+} complexes respectively (**Fig.6**).

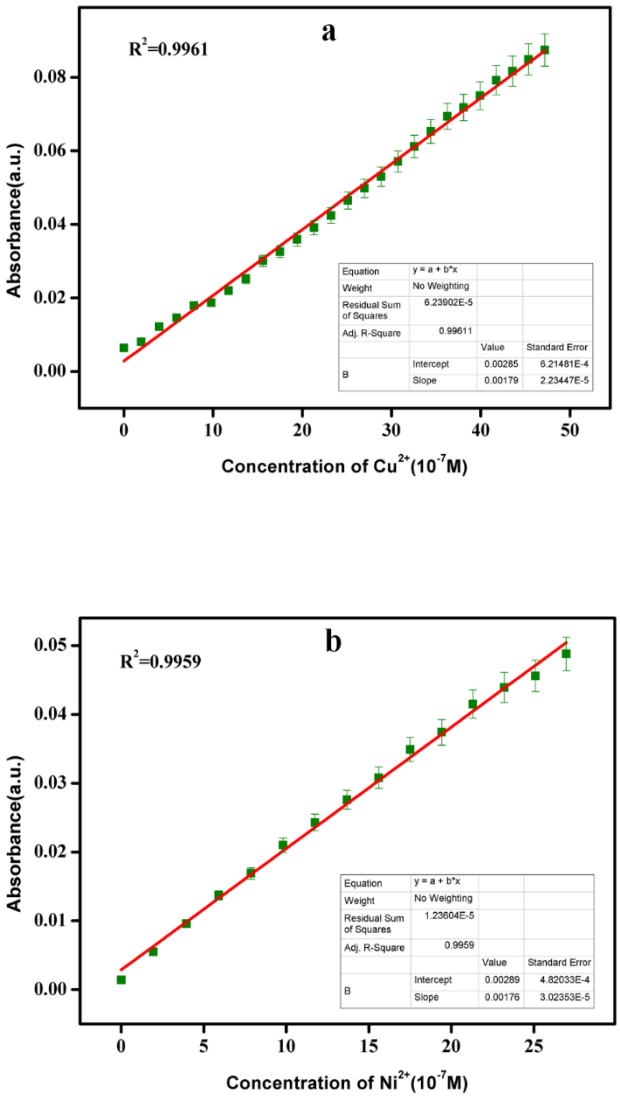

Fig.5 *Limit of detection (LOD) for (**a**) Cu^{2+} (**b**) Ni^{2+} metal ions.*

Table 1 *Comparison of PMB3 with other reported colourimetric probes*

Probe	Sensing Analyte	LOD [M]	Binding constant [M^{-1}]	Mode of detection	Ref
Probe-1	Cu^{2+}	0.66×10^{-6}	1.90×10^{4}	Colourimetric	[9]
Probe-2	Cu^{2+}	5.80×10^{-6}	1.20×10^{4}	Colourimetric	[10]
Probe-3	Cu^{2+}	8.0×10^{-6}	4.49×10^{2}	Colourimetric	[11]
Probe-4	Cu^{2+}	28.0×10^{-6}	1.87×10^{4}	Colourimetric	[12]
Probe-5	Cu^{2+}	8.77×10^{-6}	2.70×10^{3}	Colourimetric	[13]
Probe-6	Ni^{2+}	0.5×10^{-6}	2.343×10^{4}	Colourimetric	[8]
Probe-8	Ni^{2+}	1.71×10^{-6}	1.10×10^{4}	Colourimetric	[14]
Probe-9	Ni^{2+}	1.8×10^{-6}	1.45×10^{3}	Colourimetric	[15]
Probe-10	Ni^{2+}	1.47×10^{-6}	2.5×10^{5}	Colourimetric	[16]
Probe-11	Ni^{2+}	0.14×10^{-6}	3.07×10^{3}	Colourimetric	[17]
PMB3	**Cu^{2+}** **Ni^{2+}**	**45.63×10^{-7}** **26.85×10^{-7}**	**3.47×10^{4}** **8.02×10^{4}**	**Colourimetric**	**Present Work**

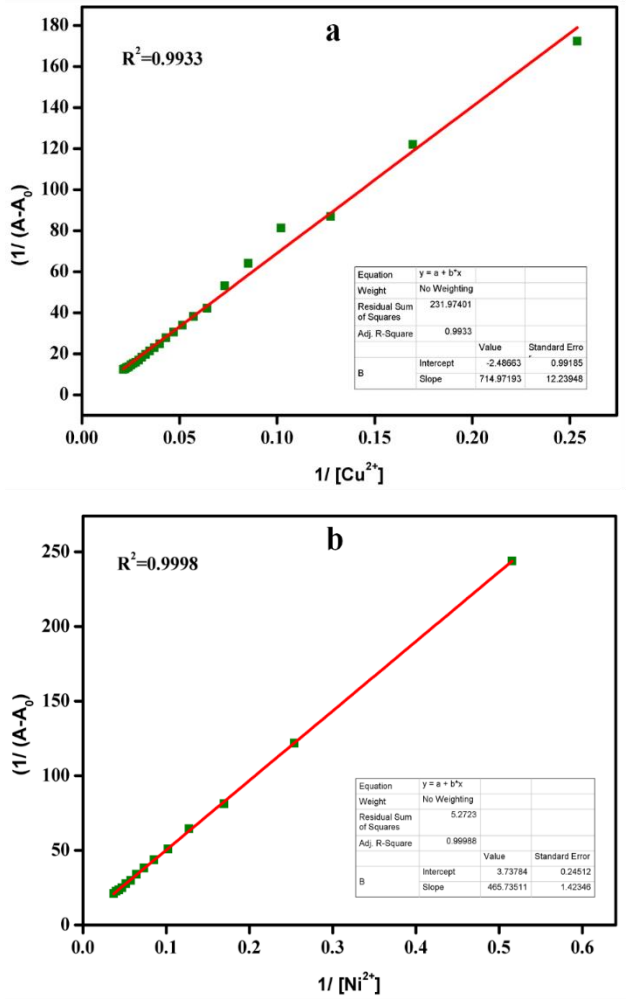

Fig.6 *Benesi-Hildebrand plot of PMB3 with (**a**) Cu^{2+} (**b**) Ni^{2+} metal ions*

To validate the enhanced selectivity of PMB3 toward Cu^{2+} and Ni^{2+}, the sensing performance in the presence of other competitive metal ions was conducted. Various metal ions, including Al^{3+}, Zn^{2+}, Co^{2+}, Fe^{3+}, Cr^{3+}, Cd^{2+}, Hg^{2+}, Ag^{+}, Mn^{2+}, Mg^{2+}, Pb^{2+}, Ba^{2+}, $Ca^{2+,}$ and Na^{+}, which could potentially interact with PMB3, were examined. In **Fig.7a**, the proportional changes in PMB3 absorbance induced by the addition of various metal ions are depicted, and the figure clearly illustrates that the sensing characteristics of PMB3 for Cu^{2+} and Ni^{2+} remained largely unaffected by the addition of

different metal ions. Additionally, the interaction between PMB3 and Cu^{2+} or Ni^{2+} in the presence of diverse anions was examined, and the resultant shifts in absorption are illustrated in **Fig.7b**. PMB3 manifested a pink colour upon the introduction of anions such as fluoride, cyanide, and acetate, followed by a transition to yellow upon the subsequent addition of Cu^{2+} and Ni^{2+}. This observation distinctly underscores the selectivity of PMB3 in the presence of competing anions.

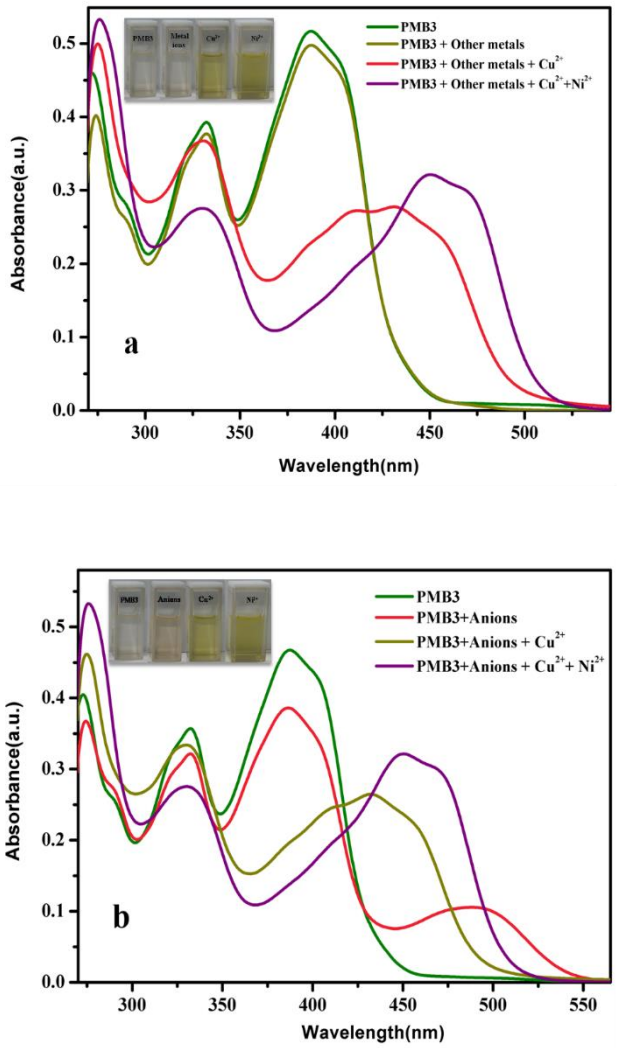

Fig.7 *Selectivity PMB3(10μM) (**a**) in presence of metal ions (**b**) in presence of anions*

3.4.3.6 Selectivity and reversibility of the complexation reaction

The reversible sensing behaviour stands as a pivotal characteristic of the sensor, in enhancing the practical utility of novel sensors. To prove the regeneration and reversibility of complexation of PMB3 with Cu^{2+} and Ni^{2+}, interaction with a potent chelator, the disodium salt of EDTA was studied. The absorbance bands at 454nm and 472nm corresponding to the PMB3-Cu^{2+} and PMB3-Ni^{2+} complex, respectively, disappeared upon the addition of Na_2EDTA to the mixtures, confirming restoration and regeneration of free PMB3. Furthermore, reintroducing Cu^{2+} and Ni^{2+} ions into the solution mixture reinstated the absorption bands (**Fig.8**). Consequently, the PMB3 sensor proves to be effective and reusable for real-time applications owing to its regeneration capability.

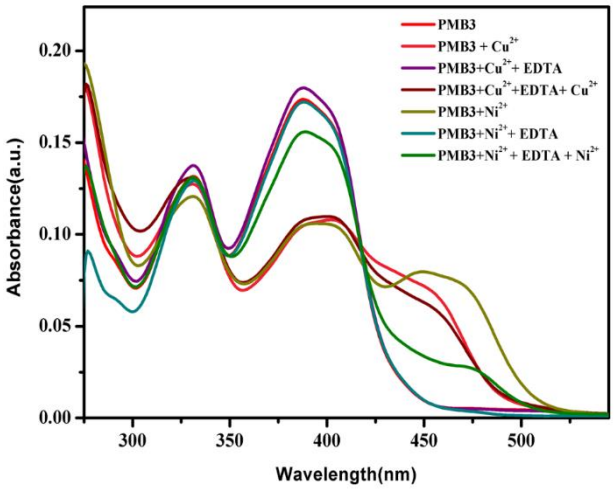

Fig.8 *Reversibility study of the PMB3(10 µM) towards Cu^{2+} and Ni^{2+} with addition of EDTA.*

3.4.3.7 Effect of pH on sensing behaviour of PMB3

The effect of pH on the sensing behaviour of PMB3 towards Cu^{2+} and Ni^{2+} was investigated. The absorption spectra of PMB3, PMB3 with the addition of Cu^{2+}, and PMB3 with the addition of Ni^{2+} were recorded at different pH values and depicted in **Fig.9**. The absorbance of PMB3 at

387nm has almost similar absorbance value from pH 3 to 10 and after it goes decreasing. With the addition of Cu^{2+} ion the absorbance value at 454nm and with the addition of Ni^{2+} the absorbance value at 472nm shows similar trends and hence PMB3 can be used for sensing Cu^{2+} and Ni^{2+} ions at a biological pH range also.

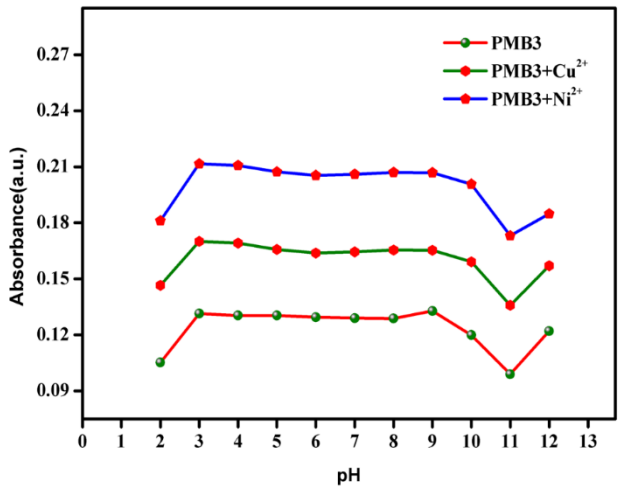

Fig.9 *Change in the absorption spectra of PMB3 (10 μM) at different pH*

3.4.3.8 Distinction of PMB3-Cu^{2+} and PMB3-Ni^{2+}

It is essential to figure out how to differentiate between PMB3-Cu^{2+} and PMB3-Ni^{2+} because both displayed the same yellow colour with a slight difference in wavelength. It is commonly known that amino acids and peptides containing thiols bind strongly to Cu^{2+}ion[9, 18-20]. Thus, to address the issue, we employed glutathione as a selective complexing agent. Upon addition of glutathione to PMB3-Cu^{2+} and PMB3-Ni^{2+} complex, only PMB3-Cu^{2+} complex demonstrated spectral and discernible colour changes from yellow to colourless as displayed in **Fig.10** and PMB3-Ni^{2+} complex did not show any spectral and noticeable colour change. This finding showed that the chelation of Cu^{2+} with glutathione caused PMB3-Cu^{2+} to return to free PMB3.

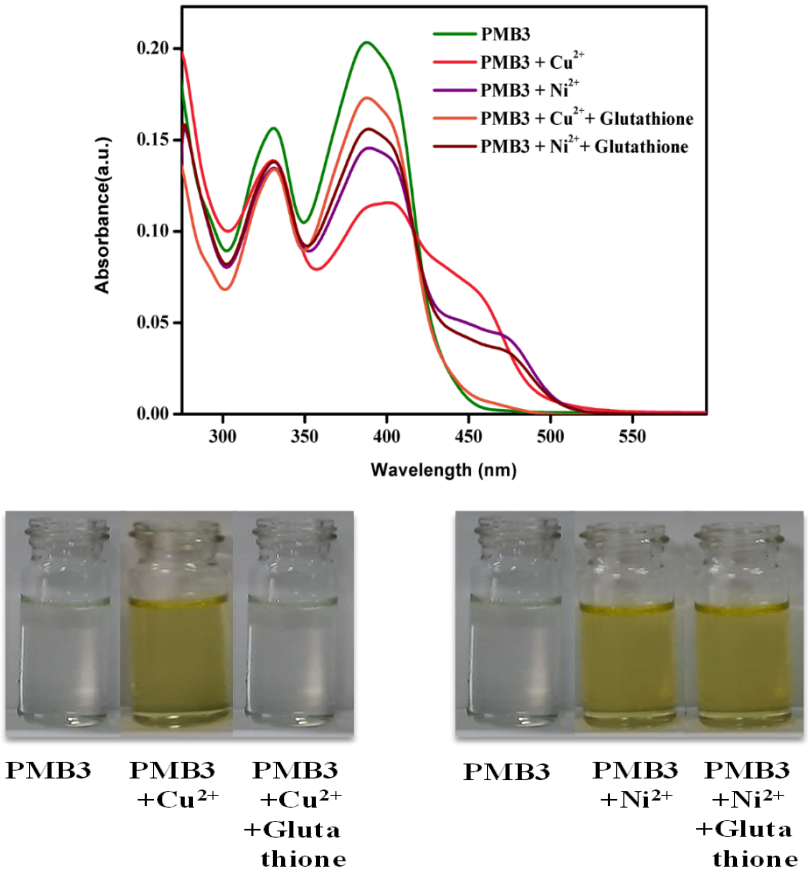

Fig.10 *Distinction between PMB3-Cu^{2+} and PMB3-Ni^{2+}*

3.4.3.9 Analysis of Real Sample

To demonstrate the practical applicability of PMB3 in quantifying Cu^{2+} and Ni^{2+}, these metal ions were scrutinized in real samples sourced from the natural environment. The assessment of metal ion recovery involved the examination of real samples spiked with varying concentrations of the metal ions, facilitating an evaluation of the accuracy of the procedure. The presented results in **Tables 2** and **3** indicated successful recovery for both analytes, affirming the practical viability of PMB3 for the precise detection of Cu^{2+} and Ni^{2+} in real environmental samples.

Table 2 *Detection of Copper in real samples*

Water sample	Added Cu^{2+} (µM)	Found (µM)	Error (%)	Recovery (%)
Well Water	5.90	5.89	0.16	99.83
	7.85	7.83	0.25	99.74
	9.80	9.76	0.40	99.59
Tap Water	5.90	5.87	0.50	99.49
	7.85	7.86	0.12	100.12
	9.80	9.86	0.61	100.61
River Water	5.90	5.93	0.50	100.50
	7.85	7.87	0.25	100.25
	9.80	9.82	0.20	100.20

Table 3 *Detection of Nickel in real samples*

Water sample	Added Ni^{2+} (µM)	Found (µM)	Error (%)	Recovery (%)
Well Water	3.94	3.96	1.01	101.01
	5.90	5.86	0.67	99.32
	7.85	7.84	0.12	99.87
Tap Water	3.94	4.00	1.52	101.50
	5.90	5.87	0.50	99.49
	7.85	7.83	0.25	99.74
River Water	3.94	4.00	1.52	101.50
	5.90	5.89	0.16	99.83
	7.85	7.82	0.38	99.60

3.4.4. Conclusion

We have designed and synthesized a facile colorimetric sensor PMB3 that showed efficient selectivity towards Cu^{2+} and Ni^{2+} ions compared to other heavy and trace metal ions in aqueous medium. Visual inspection and UV-visible experimental analysis were used to examine the sensing ability of PMB3. Amid various metal ions, the sensor PMB3 demonstrated remarkable selectivity and sensitivity toward Cu^{2+} and Ni^{2+} with a colour shift from colourless to yellow. Based on Job's plot, it was suggested that the stoichiometry of Cu^{2+} and Ni^{2+} complexes would be 1:1. The formation of the PMB3-metal complex is reversible and the LOD was calculated to be 4.56 μM and 2.68 μM for Cu^{2+}, and Ni^{2+} respectively using standard deviations and the linear fittings methods. These findings demonstrate that PMB3, may be successfully employed for on-site, real-time, naked-eye detection of bivalent copper and nickel in aqueous media.

References

1. Ghorai, A., et al., *Solvent-dependent fluorescent-colorimetric probe for dual monitoring of Al 3+ and Cu 2+ in aqueous solution: an application to bio-imaging.* Dalton Transactions, 2016. **45**(28): p. 11540-11553.
2. Askim, J.R., M. Mahmoudi, and K.S. Suslick, *Optical sensor arrays for chemical sensing: the optoelectronic nose.* Chemical Society Reviews, 2013. **42**(22): p. 8649-8682.
3. Zhu, H., et al., *Fluorescent, MRI, and colorimetric chemical sensors for the first-row d-block metal ions.* Chemical Society Reviews, 2015. **44**(13): p. 4337-4366.
4. Mulrooney, S.B. and R.P. Hausinger, *Nickel uptake and utilization by microorganisms.* FEMS microbiology reviews, 2003. **27**(2-3): p. 239-261.
5. Ragsdale, S.W., *Nickel-based enzyme systems.* Journal of Biological Chemistry, 2009. **284**(28): p. 18571-18575.
6. Denkhaus, E. and K. Salnikow, *Nickel essentiality, toxicity, and carcinogenicity.* Critical reviews in oncology/hematology, 2002. **42**(1): p. 35-56.
7. Feng, L., et al., *Colorimetric filtrations of metal chelate precipitations for the quantitative determination of nickel (II) and lead (II).* Analyst, 2011. **136**(20): p. 4197-4203.

8. Jiang, J., et al., *A novel highly selective colorimetric sensor for Ni (II) ion using coumarin derivatives.* Inorganic Chemistry Communications, 2012. **15**: p. 12-15.
9. Kim, P.A., et al., *A chelated-type colorimetric chemosensor for sensing Co2+ and Cu2+.* Inorganica Chimica Acta, 2020. **505**: p. 119502.
10. Anbu Durai, W. and A. Ramu, *Hydrazone Based Dual–Responsive Colorimetric and Ratiometric Chemosensor for the Detection of Cu 2+/F– Ions: DNA Tracking, Practical Performance in Environmental Samples and Tooth Paste.* Journal of Fluorescence, 2020. **30**: p. 275-289.
11. Roy, D., A. Chakraborty, and R. Ghosh, *Coumarin based colorimetric and fluorescence on-off chemosensor for F–, CN– and Cu2+ ions.* Spectrochimica Acta Part A: Molecular and Biomolecular Spectroscopy, 2018. **191**: p. 69-78.
12. Soufeena, P., T. Nibila, and K. Aravindakshan, *Coumarin based yellow emissive AIEE active probe: A colorimetric sensor for Cu2+ and fluorescent sensor for picric acid.* Spectrochimica Acta Part A: Molecular and Biomolecular Spectroscopy, 2019. **223**: p. 117201.
13. Ryu, K.Y., et al., *Colorimetric chemosensor for multiple targets, Cu 2+, CN– and S 2–.* RSC advances, 2016. **6**(20): p. 16586-16597.
14. Manna, A.K., et al., *A dual-mode highly selective and sensitive Schiff base chemosensor for fluorescent colorimetric detection of Ni 2+ and colorimetric detection of Cu 2+.* Photochemical & Photobiological Sciences, 2019. **18**: p. 1512-1525.
15. Manna, A.K., S. Chowdhury, and G.K. Patra, *A novel hydrazide-based selective and sensitive optical chemosensor for the detection of Ni 2+ ions: Applications in live cell imaging, molecular logic gates and smart phone-based analysis.* Dalton Transactions, 2019. **48**(32): p. 12336-12348.
16. Goswami, S., et al., *A simple quinoxaline-based highly sensitive colorimetric and ratiometric sensor, selective for nickel and effective in very high dilution.* Tetrahedron Letters, 2013. **54**(37): p. 5075-5077.
17. Bawa, R., et al., *A pyridine dicarboxylate based hydrazone Schiff base for reversible colorimetric recognition of Ni 2+ and PPi.* RSC advances, 2023. **13**(23): p. 15391-15400.
18. Peng, R., et al., *Fluorescent sensor based on BINOL for recognition of cysteine, homocysteine, and glutathione.* The Journal of Organic Chemistry, 2013. **78**(22): p. 11602-11605.
19. Meng, Q., et al., *A highly selective and sensitive ON–OFF–ON fluorescence chemosensor for cysteine detection in endoplasmic reticulum.* Biosensors and Bioelectronics, 2015. **74**: p. 461-468.
20. Li, Q., Y. Guo, and S. Shao, *A BODIPY based fluorescent chemosensor for Cu (II) ions and homocysteine/cysteine.* Sensors and Actuators B: Chemical, 2012. **171**: p. 872-877.

Journal of Fluorescence
https://doi.org/10.1007/s10895-024-03895-3

RESEARCH

2-hydroxy-1- Naphthaldehyde Based Colorimetric Probe for the Simultaneous Detection of Bivalent Copper and Nickel with High Sensitivity and Selectivity

Muhammed Arshad[1] · Linda Williams[1] · Athira Ajayan[1] · Abraham Joseph[1]

Received: 14 June 2024 / Accepted: 2 August 2024

Abstract
A neoteric colorimetric probe based on 2-hydroxy-1-naphthaldehyde (PMB3) was designed and synthesized for the real-time as well as on-site naked-eye detection of Cu^{2+}/Ni^{2+} ions. Various physicochemical methods were employed to characterize the probe, and its colorimetric response to different metal ions was meticulously investigated. The probe, PMB3, exhibited a sensitive colorimetric response to Cu^{2+}/Ni^{2+} ions among other competing metal ions, culminating in a prominent colour change from colourless to yellow. The stoichiometry of the ligand metal complexes was ascertained to be in a 1:1 ratio using Job's plot analysis, which was further corroborated by ESI–MS data. With detection limits of 4.56 µM for Cu^{2+} and 2.68 µM for Ni^{2+}, the method was effectively extended to real sample analysis, ensuring propitious results that closely aligned with the actual values.

Keywords Colorimetric probe · Naked eye · Job's plot · Naphthaldehyde

Introduction

A colorimetric sensor is an ingenious device that undergoes a visible colour change immediately when it detects specific substances, facilitating swift and simple sensing without the demand for intricate apparatus. The primary allure of colorimetric strategies lies in their simplicity, combined with sensitivity and selectivity (SSS). Additionally, this method perpetually carves out a unique niche on account of its distinctive characteristics, including naked eye detection under visible light, rapid response, and inexpensive instrumental facilities. Formulating a colorimetric sensor with exceptional selectivity for the detection and estimation of cations has consistently been an acute challenge for researchers. The achievement of efficient and simultaneous detection of multiple target ions with a single sensor seems more appealing and cost-effective than one-to-one testing methods, as it alleviates the hurdles associated with using multiple indicators [1–3].

Within the biological system, copper ranks as the third most abundant trace metal, and its significance stems from its vital role and crucial involvement in the formation, development, and maintenance of critical human organs, such as bones, muscle tissues, the brain, and the heart. Moreover, apart from its function as a catalytic co-factor for various metalloenzymes like superoxide dismutase (SOD), cytochrome-c-oxidase, tyrosinase, nuclease, and others [4–11]. Copper seems to be responsible for neurological disorders, including 'Menkes and Wilson illnesses', 'familial amyotrophic lateral sclerosis', 'Alzheimer's disease', and 'prion disorders' [12–20]. The widespread use and applications of Cu^{2+} ions in chemistry, and medicine have emerged as one of the most important environmental contaminants due to its excess accumulation in the environment, which creates a serious imbalance in the release and consumption cycle of the metal ion. The World Health Organisation (WHO) mandates that the concentration of Cu^{2+} ions in drinking water should not exceed 31.3 µM [21]. Considering the pervasive recognition of the multifaceted significance of copper in diverse physiological and pathological contexts, and its crucial role in maintaining human organs, the development of a selective colorimetric sensor for the naked-eye detection of Cu^{2+} is quite imperative.

✉ Abraham Joseph
abrahamjoseph@uoc.ac.in

[1] Department of Chemistry, University of Calicut, Calicut University, P O-673 635, Malappuram, Kerala, India

Published online: 19 August 2024

Chapter 4

Applications of BBHN as sensor

Chapter 4 presents an in-depth exploration of the Schiff base BBHN's versatile sensing capabilities, divided into two sections. Firstly, BBHN demonstrates selective fluorescence "Turn off" behavior for copper ions in aqueous medium, exhibiting high selectivity and sensitivity with a detection limit of 35.52 nM. Secondly, its Aggregation-Induced Emission Enhancement (AIEE) property is harnessed for the sensitive detection of picric acid (PA) in aqueous medium, showcasing a detection limit of 4.04μM and employing π-π interactions and other non-covalent interactions for fluorescence quenching. These observations underscore BBHN's potential as a robust sensor for various analytes, offering valuable insights into its applicability in environmental monitoring and analysis.

SECTION 4.1

Nanoscale detection of copper using BBHN as AIEE fluorescent sensor

4.1.1 Introduction

The development of an efficient fluorescent sensor for the sensitive and selective detection of biologically important metal ions has received great attention in the present scenario due to their simplicity, economic viability, sensitivity, easy visualization, and fast response for detection [1-6]. Recently, luminescent material research has focused on the development of organic molecules with the feature of Aggregation Induced Emission Enhancement (AIEE) [7]. As of today, many kinds of fluorophores such as quinoline, coumarin, fluorescein, and rhodamine-based fluorescent chemosensors [8-14] have been developed for the detection of copper ions. But some of the probes have serious limitations, including poor water solubility, low fluorescence intensity, poor selectivity and sensitivity, and long response times [15]. More significantly, there are very few fluorescent probes that can detect Cu^{2+} in both aqueous and organic systems. Hence, the growing concern has impelled the development of suitable fluorescent sensors for the rapid and selective detection of cations at trace levels. Conventional instrumental methods [16-20], used for the detection of bivalent copper, demand expensive equipment, carefully monitored experimental conditions, multi-step, challenging sample preparations, etc. On the other hand, fluorometric methods have many advantages such as simplicity, rapid response, low cost, high sensitivity, and reproducibility. Hence, the design and development of a novel fluorescent

chemosensor having a very low detection limit is still very challenging and significant.

Herein, we have introduced a novel AIEE active Schiff base BBHN, derived from 2-hydroxy-1-naphthaldehyde and 4-benzyloxybenz aldehyde as a selective fluorescence "turn off" sensor for copper ion in aqueous medium. The aggregates of BBHN exhibit strong green emission and demonstrate fluorescence "turn off" behaviour on interaction with Cu^{2+} ions, which could be very well applied for the instant "naked eye" detection of the metal ion.

4.1.2 Experimental section

4.1.2.1 Method of Preparation of BBHN Aggregates

A stock solution of BBHN in DMSO (1 mM) was prepared. An aliquot of 100µl of this solution was transferred into a 10ml standard flask using a micropipette and diluted to get a final concentration of 10µM using DMSO-Water solvent mixture of appropriate water fractions (fw) ratio of 0 to 99 volume percentage under vigorous stirring. The above solution was then sonicated for 20 minutes and UV-visible and emission spectra of resultant solution mixtures were recorded immediately.

4.1.2.2 Fluorescence activity measurements

A stock solution of BBHN of 1mM concentration was prepared in DMSO and the stock solutions of different metal ions of 1mM concentration were prepared in double-distilled water. Fluorescence sensing studies were performed using aggregates of BBHN in a DMSO-Water mixture (1:9) and 1 equivalent of different metal ions at room temperature at an excitation wavelength of 410

nm. Using the equation, 3σ/slope, the detection limit (LOD) was determined from the fluorescence titration profile.

4.1.2.3 Fluorescence Quantum Yield

Fluorescence quantum yield was determined using rhodamine (Φ_r = 0.95) as standard at an excitation wavelength of 537 nm. The quantum yield is calculated using the following equation,

$$\Phi_s = \Phi_r (A_r/A_s) (F_s/F_r) (\eta_s/\eta_r)^2$$

where A_s and A_r are the absorbance of the sample and reference solutions, F_s and F_r are the corresponding relative integrated fluorescence intensities, and η is the refractive index of the solvents.

4.1.3 Results and Discussion

A novel Schiff base BBHN was synthesized as detailed in the synthetic route shown in **Scheme 3** in chapter 2. BBHN has good solubility in organic solvents like DMF, DMSO, CH_3CN, THF, $CHCl_3$, and DCM.

4.1.3.1 Aggregation-Induced Emission Enhancement (AIEE)

The AIE characteristics of BBHN were investigated at room temperature by recording the UV-Visible and fluorescence spectra by adding poor solvent such as water with different water fractions to a solution of BBHN in DMSO. The concentration of the Schiff base BBHN was kept at 10μM throughout the studies.

4.1.3.1.1 UV-Visible Spectral Study

UV-Visible absorption spectra of BBHN in pure DMSO and DMSO-Water mixture of water fraction 90% are shown in **Fig.1**. The absorption spectra of BBHN in DMSO showed an intense band at 332, 409, and 432nm, which can be assigned to π-π* transitions of

the 2-hydroxy-1-naphthaldehyde moiety, n-π* transition of imine bonds and π-π* transitions originating from the extended conjugation between the nitrogen atom and aromatic ring respectively. However, the absorption spectral profile shows significant changes in increasing the water fraction from 0 to 99%. With increasing water fraction, aggregates begin to form, and the intensity of the absorption band at 409nm decreased followed by a slight red shift of 15nm. In addition, an additional peak at 453nm was detected in spectra of BBHN in DMSO with 90% water fraction, which indicated the change of a single molecule into aggregates *via* intermolecular interaction. Meanwhile, there was a level-off tail phenomenon in the long absorption wavelength in the visible region, which was attributed to Mie scattering caused by nanoparticles [21]. Furthermore, the red shift in absorption generally originated from J-type aggregates(head-tail) [22].

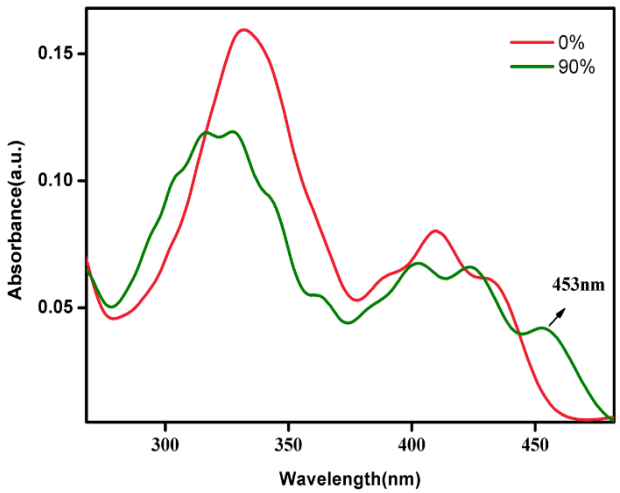

Fig.1 *UV–visible spectra of BBHN (10μM) in solution state in pure DMSO and in DMSO-Water mixed solvent with water fraction of 90% (aggregated state)*

4.1.3.1.2 Fluorescence Spectral Study

The fluorescence spectra were recorded with an excitation wavelength of 410 nm and emission behaviour was monitored by varying the water fraction(fw) from 0 to 99% in DMSO-Water mixture, keeping the overall concentration of the solution to 10μM. In the DMSO solution, BBHN (10μM) was feebly emissive and exhibited a weakly structured emission band at 510nm. Interestingly, as the water fraction increases the emission intensity was enhanced, and bright green emission is observed at 531nm with a redshift of about 21nm. It was clear from the fluorescence spectra of BBHN (**Fig.2**), that when the water fraction increased from 0 to 30%, BBHN had no significant fluorescence emission which could be due to intramolecular rotation[23]. However, as the water fraction reaches 40%, the emission intensity increases drastically and the intensity of emission continuously increased as the water fraction increased to 60%, 70%, 80%, 90%, and 99%, which indicated the AIE effect. It was observed from the emission profile **Fig.2**, that along with emission enhancement, there was a red shift of emission maxima, which could be attributed to the change of a single molecule into aggregates *via* intermolecular interaction between them. Up to 30% of water fraction, there was the active involvement of N-N and C=N intramolecular rotation in the excited state, which weakens the fluorescence emission of BBHN. However, when the water fraction reaches 40% aggregation starts, which blocks the intramolecular rotation due to C=N isomerization and results in strong fluorescence emission (**Scheme 1**).

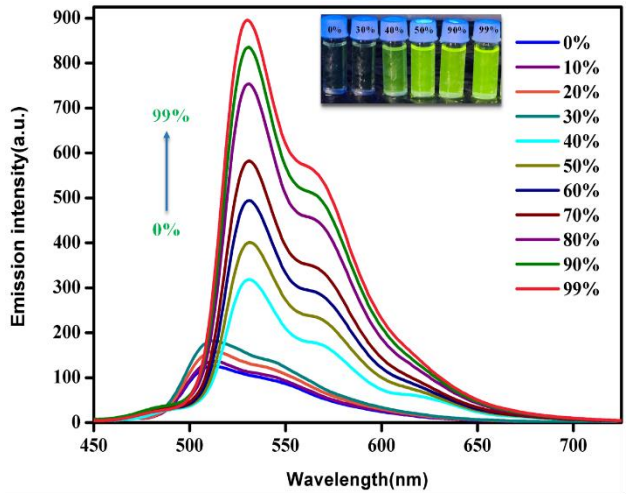

Fig.2 *Change in fluorescence emission spectra of BBHN (10μM, λ_{ex}= 410 nm, λ_{em}= 530 nm) in presence of increasing volume of water fraction(fw) percentage from 0 to 99%*

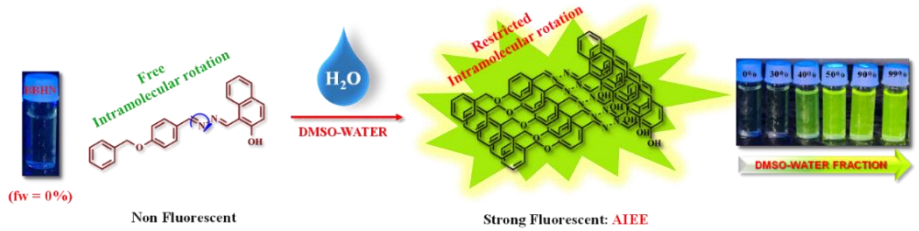

Scheme 1 *Proposed mechanism for AIEE behaviour of BBHN*

4.1.3.1.3 Optical microscopy

To gather more insights into AIEE and optical properties of BBHN, an optical microscopic study was done at room temperature, and the corresponding image is depicted in **Fig.3**. This optical microscopic image showed that there was no noticeable number of particles with fluorescence when BBHN is in the isolated state, whereas with increasing the water fraction, the particles were visible and show greenish yellow emission due to aggregation upon UV light excitation at 365nm. Thus, the optical microscopic images support

the formation of nanoparticles in the aggregated state which results in fluorescence behaviour.

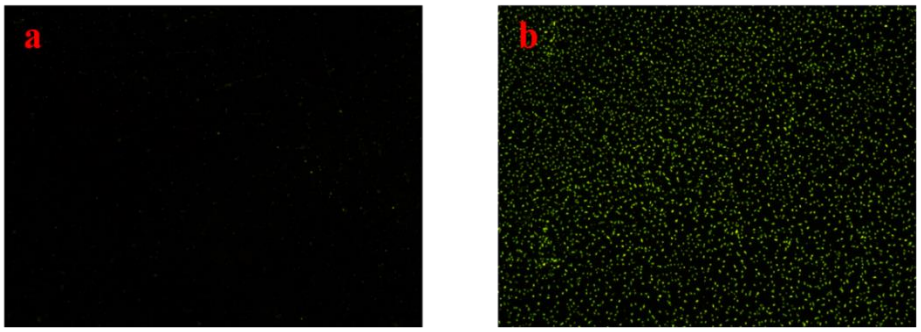

Fig.3 *Optical microscopy images (under UV excitation) of (**a**) BBHN in pure DMSO with water fraction(fw) a percentage of 0 in solution state (fw = 0%) and (**b**) BBHN in DMSO-Water mixed solvent with water fraction(fw) a percentage of 90 in the aggregated state (fw = 90%)*

4.1.3.1.4 Fluorescence decay study

The luminescence lifetime measurements were carried out to get further information about the AIEE property of BBHN. The lifetime decay profile of the BBHN in pure DMSO and DMSO-Water mixture

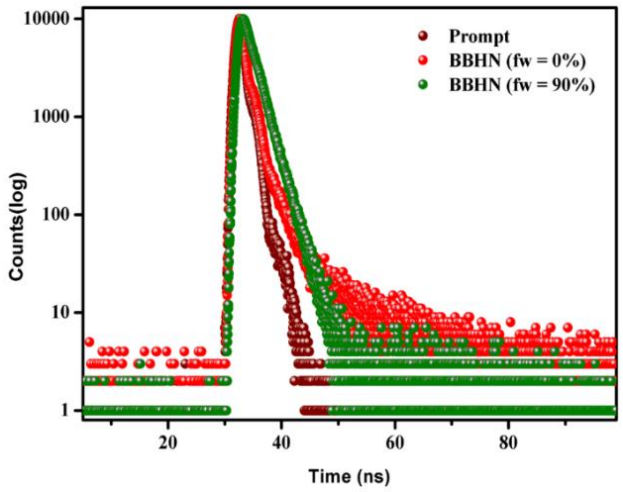

Fig.4 *Fluorescence decay profile of BBHN (10 μM) in pure DMSO with water fraction(fw) of 0% in solution state (fw = 0%) and in DMSO-Water mixed solvent with water fraction(fw) of 90% in the aggregated state (fw = 90%)*

of water fraction 90% is depicted in **Fig.4** which is well fitted with a single-exponential decay curve and BBHN in pure DMSO, shows an average fluorescence lifetime value of 1.177ns which is significantly increased (2.108ns) with an increase in water fraction. The increase in fluorescence lifetime in the DMSO-Water mixture is due to suppression of the intramolecular rotation due to aggregation of BBHN, which results in longer fluorescence lifetime.

4.1.3.1.5 The effect of viscosity on AIE

In addition, the solvent viscosity effect on the AIE property of BBHN was inspected in a viscous glycerol-methanol solvent mixture by blending methanol with glycerol, and the viscosity of the solvent mixture was varied by changing the ratio of glycerol to methanol. It is observed from **Fig.5** that the emission intensity of BBHN was increased with increasing the viscosity of the solution and this emission enhancement is attributed to the hindrance of intramolecular rotation which results in a decrease in non-radiative

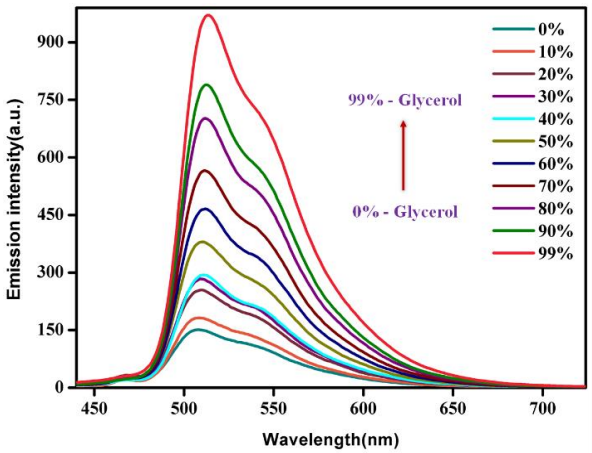

Fig.5 *Change in the fluorescence emission spectra of BBHN (10 μM, λ_{ex}= 410 nm, λ_{em}= 530 nm) with change in viscosity of the solvent mixture by varying the solvent ratio of glycerol to methanol*

decay, thereby enhancing the emission intensity. The outcomes specify that the restriction of intramolecular rotation has a significant effect on the AIE property of BBHN and has a key role in stimulating the emission characteristics of the molecule.

4.1.3.1.6 The effect of pH on AIE

To further evaluate the practical applications of the aggregate of BBHN, the pH dependence of the aggregate of BBHN in DMSO-Water mixture with a water fraction of 90% using buffers were investigated. It can be seen from **Fig.6**, that the fluorescence emission intensity of aggregate increased on increasing the pH from 2 to 7, and above pH 7 it is decreased. The emission intensity is stable over the pH range of 2-7, which covers the physiological pH range and increases the potential applications of the aggregates of BBHN in such environments.

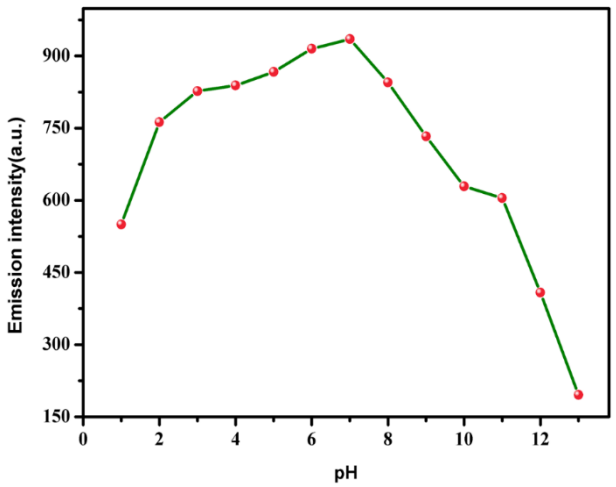

Fig.6 *Change in the emission spectra of BBHN (10 μM), λ_{ex}= 410 nm, λ_{em}= 530nm) in DMSO-Water mixture with water fraction 90% (fw = 90%) at different pH.*

4.1.3.2 Sensing of Cu^{2+} ions in aqueous media

In order to investigate the metal ion binding property and the sensing ability of aggregate of BBHN formed in DMSO-Water (1:9) mixture, towards various metal ions such as Cd^{2+}, Hg^{2+}, Zn^{2+}, Ag^{+}, Al^{3+}, Co^{2+}, Cr^{3+}, Cu^{2+}, Fe^{3+}, Ni^{2+}, Mn^{2+}, Ca^{2+}, Mg^{2+}, Ba^{2+}, Na^{+}, Pb^{2+}, K^{+}, a series of sensing experiments were performed by recording fluorescence spectra at an excitation wavelength of 410 nm as shown in **Fig.7**. The fluorescence emission profile of aggregate of BBHN decreases drastically with the addition of Cu^{2+} ion, while other metal ions gave no distinct response which implied the ability of aggregate of BBHN to selectively detect Cu^{2+} in aqueous medium. To further evaluate the sensing property and the selectivity of the aggregate of BBHN toward Cu^{2+}, the fluorescence titration experiments were performed by the incremental addition of Cu^{2+} ions (**Fig.8**). Upon the incremental addition of Cu^{2+} ions to the

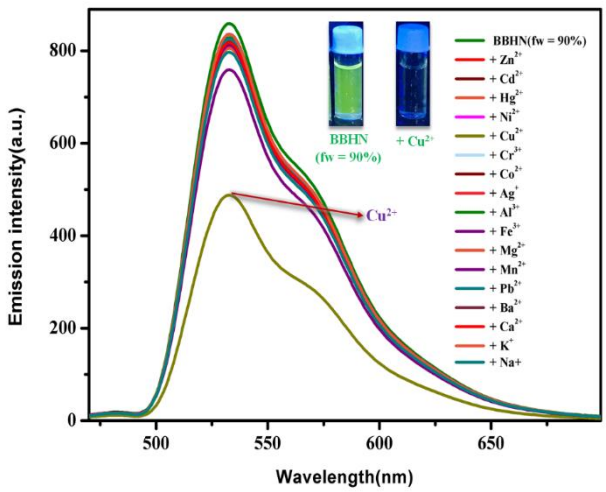

Fig.7 *Change in the fluorescence emission spectra of BBHN (10 μM, λ_{ex}= 410 nm, λ_{em}= 530 nm) with water fraction 90% (fw = 90%) in the presence of different metal ions*

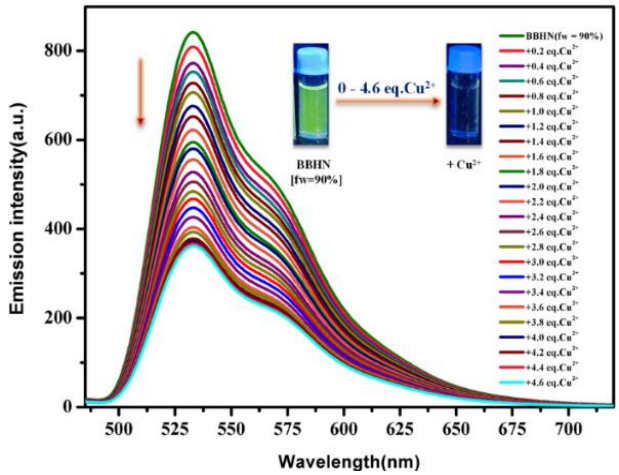

Fig.8 *Changes in the fluorescence emission spectra of BBHN (10 μM, λ_{ex}= 410 nm, λ_{em}= 530 nm) with water fraction 90% (fw = 90%) up on the increase in the concentration of Cu^{2+} from 0 - 4.6 equivalent*

aggregate of BBHN, an efficient quenching of fluorescence emission was observed and a complete fluorescence turn off was noticed when the Cu^{2+} ion concentration reaches to 4.6 equivalents, suggesting that there is a strong association between Cu^{2+} ions and aggregates of BBHN.

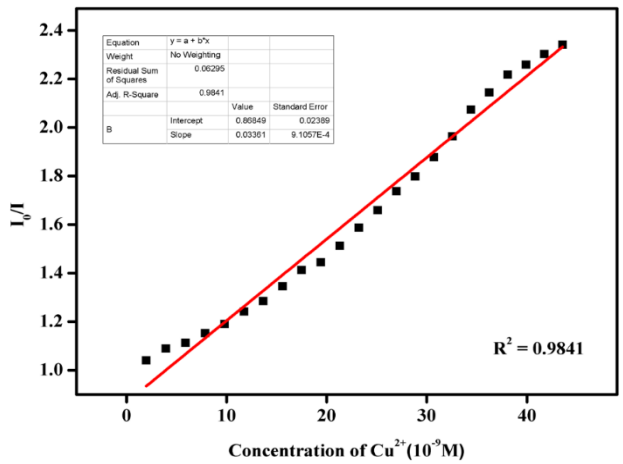

Fig. 9 *Stern-Volmer plot of BBHN aggregate in DMSO (10 μM, λ_{ex}= 410 nm, λ_{em}= 530 nm) with water fraction 90% (fw = 90%)*

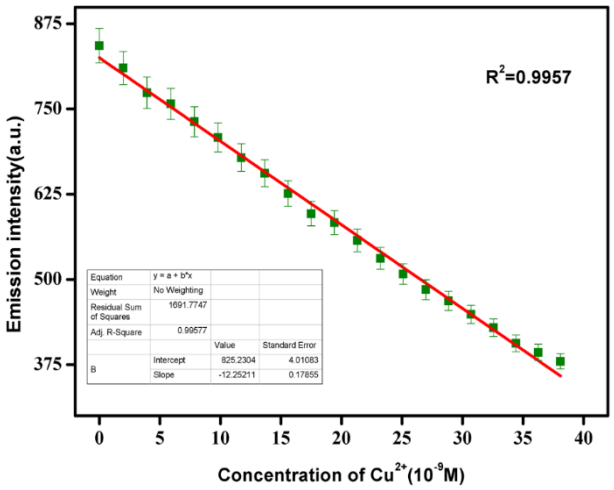

Fig.10 *Limit of detection (LOD) of BBHN in DMSO with water fraction 90% with* Cu^{2+}

The efficiency of the fluorescence quenching was calculated from the Stern-Volmer plot (**Fig.9**) and was found to be 2.58×10^{8} M^{-1}. The detection limit was calculated by the 3σ method as shown in **Fig.10** using the equation **3σ/k** and was calculated to be 35.52nM. The comparison of BBHN with other reported probes in the literature was shown in **Table 1**.

Table 1 *Comparison of BBHN with other reported probes*

Probe	Sensing analyte	LOD	Ref
Probe-1	Cu^{2+}	8.68μM	[24]
Probe-2	Cu^{2+}	0.27 μM	[25]
Probe-3	Cu^{2+}	6.0 μM	[26]
Probe-4	Cu^{2+}	9.6 μM	[27]
Probe-5	Cu^{2+}	0.036 μM	[28]
Probe-6	Cu^{2+}	0.18 μM	[29]
Probe-7	Cu^{2+}	2.4×10^{-8}M	[30]
Probe-8	Cu^{2+}	1.8 μM	[31]
BBHN	**Cu^{2+}**	**35.52nM**	**Present study**

Further, the strong fluorescence quenching behaviour of aggregates of BBHN in the presence of Cu^{2+} ions in an excited state has been investigated by the excited state fluorescence lifetime measurements. **Fig.11** shows the fluorescence lifetime decay profile of aggregates of BBHN in the presence and absence of Cu^{2+}ions. In the absence of Cu^{2+}ions, aggregates of BBHN show a single exponential decay with a lifetime value of 2.108ns. After the addition of Cu^{2+} ions to the aggregates of BBHN the lifetime value changed to 1.614ns. The change in fluorescence lifetime value suggests the involvement of the dynamic quenching process. Furthermore, the fluorescence quenching mechanism of aggregates of BBHN in the presence of Cu^{2+} ions may be attributed to the chelation between the imine-N atom, phenolic -O atom, and Cu^{2+} ions[32]. The possible quenching mechanism is depicted in **Scheme 2**. The quantum yield of BBHN aggregates was calculated to be 54.89% which is significantly reduced to 41.77% with the addition of Cu^{2+} ion. The

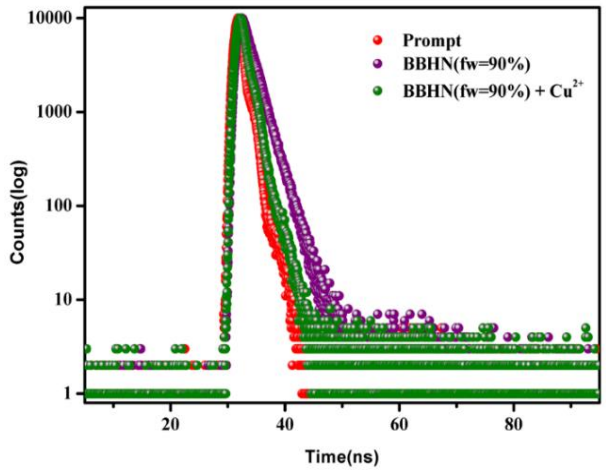

Fig. 11 *Fluorescence decay profile of BBHN in DMSO (10μM) with water fraction(fw) percentage of 90% in aggregated state (fw = 90%) in absence and presence of* Cu^{2+}

stoichiometry of the complex formed between BBHN and Cu^{2+} was examined by using Job's plot analysis and is found to be 1:1 (**Fig.12**).

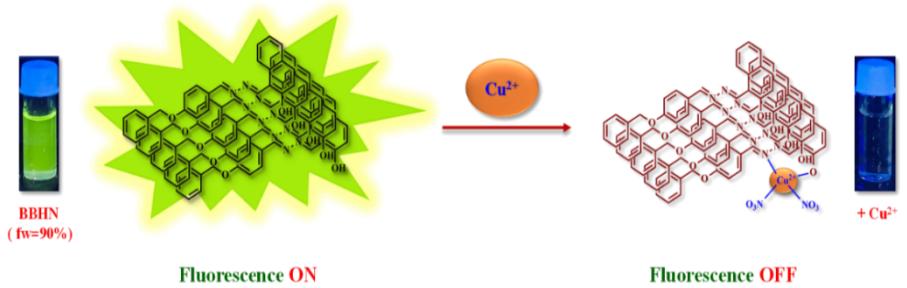

Scheme 2 *Proposed mechanism for BBHN aggregate (fw = 90%) with* Cu^{2+}

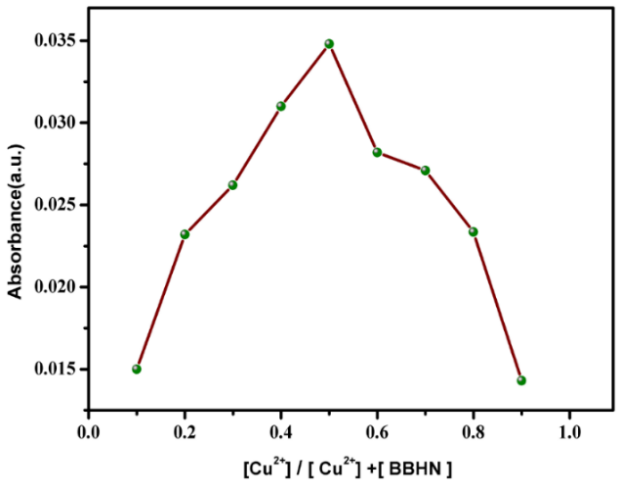

Fig.12 *Job's plot of BBHN in DMSO solvent*

To establish the specificity of aggregates of BBHN towards Cu^{2+}ions, metal competitive analysis was carried out by recording the fluorescence spectra of aggregates of BBHN in the presence of 1 equivalent of Cu^{2+} ions and an equivalent amount of other metal ions, as shown in **Fig.13**. When 1 equivalent of Cu^{2+} ions were added to the aggregates of BBHN in the presence of 1 equivalent of other metal ions, the fluorescence emission profile exhibited a similar

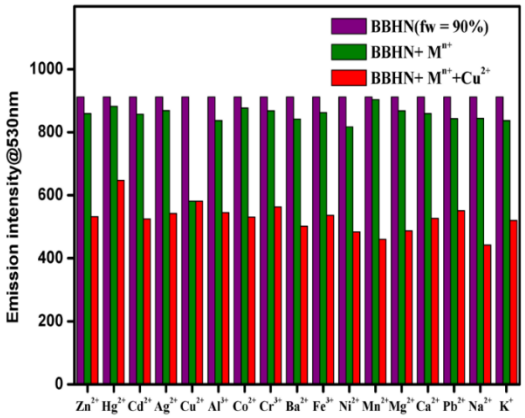

Fig.13 *The selectivity of BBHN (10 μM, λ_{ex}= 410 nm, λ_{em}= 530 nm) with water fraction 90% (fw = 90%) towards Cu^{2+} (1 equivalent) in the presence of other metal ions (1 equivalent)*

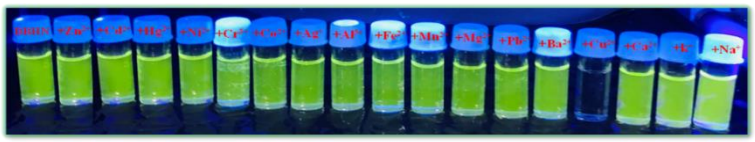

Fig.14 *Fluorescence emission of BBHN (10 μM) with water fraction 90% (fw =90%) in the presence of fixed concentration (10 μM) of different metal ions under UV lamp*

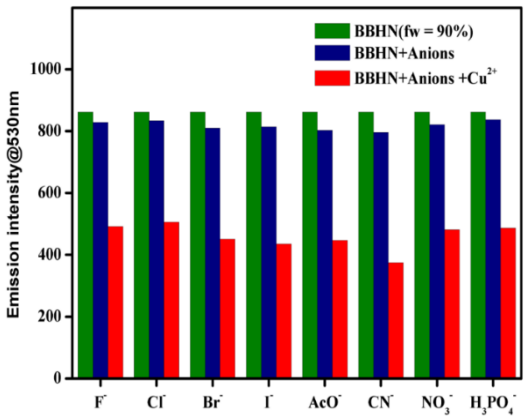

Fig.15 *The selectivity of BBHN (10 μM, λ_{ex}= 410 nm, λ_{em}= 530 nm) with water fraction 90% (fw = 90%) towards Cu^{2+} (1 equivalent) in the presence of anions (1 equivalent).*

pattern to that with Cu^{2+}ions. The photographs of aggregates of BBHN with different metal ions under a UV lamp is given in **Fig.14**,

verified the exceptional sensitivity and selectivity of the aggregate of BBHN to distinguish Cu^{2+} ions in the presence of various environmentally and biologically important competing metal ions with very high accuracy.

The analysis of aggregates of BBHN towards Cu^{2+} ions in the presence of biologically significant anions such as F^-, Cl^-, Br^-, I^-, CH_3COO^-, CN^-, NO_3^-, and $H_3PO_4^-$ was also carried out and found that there are no significant changes in the fluorescence emission profile in the presence of these anions (**Fig.15**). The reversibility and reusability were monitored using Na_2EDTA. Upon the addition of Na_2EDTA solution to BBHN aggregates with Cu^{2+} ion, the fluorescence regains and reach back to the original state of the free aggregates which indicates the regeneration of aggregates of BBHN (**Fig.16**) and hence can be reused.

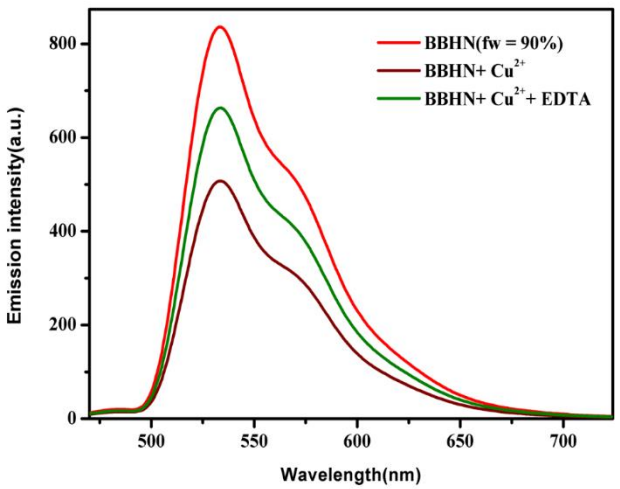

Fig.16 *Reversibility study of the BBHN in DMSO (10 μM, λ_{ex}= 410 nm, λ_{em}= 530 nm)) with water fraction 90% (fw = 90%) towards Cu^{2+} with addition of EDTA.*

4.1.3.3 Application of BBHN aggregates in real sample analysis

The property of BBHN aggregates to distinguish Cu^{2+} ions in the presence of other ions was further extended to real samples such as well water, tap water, and river water by the standard addition method. The results obtained are presented in **Table 2**. The recoveries varied in the 100.50-104.56% range, which demonstrates the applicability and reliability of BBHN aggregates in Cu^{2+} detection.

Table 2 *Detection of copper in real samples*

Water sample	Added Cu^{2+} (μM)	Found (μM)	Error (%)	Recovery (%)
Well Water	1.97	2.00	1.52	101.52
	3.94`	3.96	0.52	100.50
	5.90	6.02	2.03	102.03
Tap Water	1.97	2.02	2.53	102.53
	3.94	3.97	0.76	100.76
	5.90	6.08	3.05	103.05
River Water	1.97	2.06	4.56	104.56
	3.94	3.99	1.26	101.26
	5.90	6.11	3.55	103.55

4.1.4. Conclusions

A novel cost-effective Schiff base sensor BBHN having AIEE activity was synthesized, and used for the sensitive detection of Cu^{2+} ion for the first time. The aggregates of BBHN exhibited a green emission in DMSO-Water mixture and displayed a fluorescence switch-off response for Cu^{2+} ion with a low detection limit of 35.52nM. The

change in the fluorescence emission in the presence of Cu^{2+} demonstrated that the aggregate of BBHN could be useful for naked-eye detection of Cu^{2+} ions under UV lamp. The fluorescence quenching was calculated from the fluorescence titration profile and was found to be 2.58×10^{8} M^{-1}. The mechanism of quenching was further confirmed by a time-resolved emission study which revealed the involvement dynamic quenching process.

References

1. Huerta-Aguilar, C.A., et al., *Simultaneous recognition of cysteine and cytosine using thiophene-based organic nanoparticles decorated with Au NPs and bio-imaging of cells.* Photochemical & Photobiological Sciences, 2019. **18**(7): p. 1761-1772.
2. Huerta-Aguilar, C., et al., *Three novel input logic gates supported by fluorescence studies: Organic nanoparticles (ONPs) as chemo-sensor for detection of Zn2+ and Al3+ in aqueous medium.* Spectrochimica Acta Part A: Molecular and Biomolecular Spectroscopy, 2015. **146**: p. 142-150.
3. Huerta-José, D.S., et al., *Novel insight of indium (III) complex of N, N-bis (salicylidene) ethylenediamine as chemo-sensor for selective recognition of HSO4– and hemolytic toxicity (Red Blood Cells) studies: Experimental and theoretical studies.* Sensors and Actuators B: Chemical, 2019. **293**: p. 357-365.
4. Anbu, S., et al., *Differentially selective chemosensor with fluorescence off–on responses on Cu2+ and Zn2+ ions in aqueous media and applications in pyrophosphate sensing, live cell imaging, and cytotoxicity.* Inorganic Chemistry, 2014. **53**(13): p. 6655-6664.
5. Anbu, S., et al., *Naphthylhydrazone based selective and sensitive chemosensors for Cu 2+ and their application in bioimaging.* Dalton Transactions, 2012. **41**(43): p. 13330-13337.
6. Anbu, S., et al., *Phenyl carbohydrazone conjugated 2-oxoindoline as a new scaffold that augments the DNA and BSA binding affinity and anti-proliferative activity of a 1, 10-phenanthroline based copper (II) complex.* Inorganica Chimica Acta, 2014. **423**: p. 183-193.
7. Mei, J., et al., *Aggregation-induced emission: together we shine, united we soar!* Chemical reviews, 2015. **115**(21): p. 11718-11940.
8. Jung, H.S., et al., *Coumarin-derived Cu2+-selective fluorescence sensor: synthesis, mechanisms, and applications in living cells.* Journal of the American Chemical Society, 2009. **131**(5): p. 2008-2012.

9. Liu, Z., et al., *Design and synthesis of a ratiometric fluorescent chemosensor for Cu (II) with a fluorophore hybridization approach.* Organic letters, 2012. **14**(17): p. 4378-4381.
10. Muthuraj, B., et al., *Highly selective probe detects Cu2+ and endogenous NO gas in living cell.* ACS Applied Materials & Interfaces, 2014. **6**(9): p. 6562-6569.
11. Udhayakumari, D., S. Naha, and S. Velmathi, *Colorimetric and fluorescent chemosensors for Cu 2+. A comprehensive review from the years 2013–15.* Analytical Methods, 2017. **9**(4): p. 552-578.
12. García-Beltrán, O., et al., *Design and synthesis of a new coumarin-based 'turn-on'fluorescent probe selective for Cu+ 2.* Tetrahedron Letters, 2012. **53**(39): p. 5280-5283.
13. Fang, Y., et al., *Rhodamine–ferrocene conjugate chemosensor for selectively sensing copper (II) with multisignals: chromaticity, fluorescence, and electrochemistry and its application in living cell imaging.* Organometallics, 2015. **34**(12): p. 2962-2970.
14. Ge, F., et al., *A new fluorescent and colorimetric chemosensor for Cu (II) based on rhodamine hydrazone and ferrocene unit.* Sensors and Actuators B: Chemical, 2013. **181**: p. 215-220.
15. Xiong, J.-J., et al., *A highly selective and sensitive "turn-on" fluorescent probe of Cu2+ by p-dimethylaminobenzamide-based derivative and its bioimaging in living cells.* Sensors and Actuators B: Chemical, 2016. **232**: p. 673-679.
16. Becker, J.S., et al., *Quantitative imaging of selenium, copper, and zinc in thin sections of biological tissues (Slugs− Genus Arion) measured by laser ablation inductively coupled plasma mass spectrometry.* Analytical chemistry, 2007. **79**(16): p. 6074-6080.
17. Otero-Romaní, J., et al., *Evaluation of commercial C18 cartridges for trace elements solid phase extraction from seawater followed by inductively coupled plasma-optical emission spectrometry determination.* Analytica chimica acta, 2005. **536**(1-2): p. 213-218.
18. Gonzales, A., et al., *Peat as a natural solid-phase for copper preconcentration and determination in a multicommuted flow system coupled to flame atomic absorption spectrometry.* Analytica chimica acta, 2009. **636**(2): p. 198-204.
19. Mashhadizadeh, M., et al., *Solid phase extraction of lead (II), copper (II), cadmium (II) and nickel (II) using gallic acid-modified silica gel prior to determination by flame atomic absorption spectrometry.* Spectrochim. Acta B, 2008. **63**: p. 885-888.
20. Pathirathna, P., et al., *Fast-scan deposition-stripping voltammetry at carbon-fiber microelectrodes: real-time, subsecond, mercury free measurements of copper.* Analytical chemistry, 2012. **84**(15): p. 6298-6302.
21. Zhao, J., et al., *Excited state intramolecular proton transfer (ESIPT): from principal photophysics to the development of new chromophores and*

applications in fluorescent molecular probes and luminescent materials. Physical Chemistry Chemical Physics, 2012. **14**(25): p. 8803-8817.
22. Zhao, J.-S., et al., *Memory of chirality in J-type aggregates of an achiral perylene dianhydride dye created in a chiral asymmetric catalytic synthesis.* Chemical Science, 2011. **2**(5): p. 937-944.
23. Soufeena, P., T. Nibila, and K. Aravindakshan, *Coumarin based yellow emissive AIEE active probe: A colorimetric sensor for Cu2+ and fluorescent sensor for picric acid.* Spectrochimica Acta Part A: Molecular and Biomolecular Spectroscopy, 2019. **223**: p. 117201.
24. Gao, C., et al., *A retrievable and highly selective fluorescent sensor for detecting copper and sulfide.* Sensors and Actuators B: Chemical, 2013. **185**: p. 125-131.
25. Yeh, J.-T., et al., *A coumarin-based sensitive and selective fluorescent sensor for copper (II) ions.* New Journal of Chemistry, 2014. **38**(9): p. 4434-4439.
26. He, G., et al., *Synthesis and application of a highly selective copper ions fluorescent probe based on the coumarin group.* Spectrochimica Acta Part A: Molecular and Biomolecular Spectroscopy, 2018. **190**: p. 116-120.
27. Liu, S.-R. and S.-P. Wu, *An NBD-based sensitive and selective fluorescent sensor for copper (II) ion.* Journal of fluorescence, 2011. **21**: p. 1599-1605.
28. dos Santos Carlos, F., et al., *A novel fluorene-derivative Schiff-base fluorescent sensor for copper (II) in organic media.* Journal of Photochemistry and Photobiology A: Chemistry, 2017. **348**: p. 41-46.
29. Wang, X., et al., *A highly selective and sensitive Schiff-base based turn-on optical sensor for Cu2+ in aqueous medium and acetonitrile.* Inorganic Chemistry Communications, 2017. **79**: p. 50-54.
30. Wang, Z.-G., et al., *The development of coumarin Schiff base system applied as highly selective fluorescent/colorimetric probes for Cu2+ and tumor biomarker glutathione detection.* Dyes and Pigments, 2020. **175**: p. 108156.
31. Manna, A.K., et al., *A highly selective novel multiple amide based Schiff base optical chemosensor for rapid detection of Cu2+ and its applications in real sample analysis, molecular logic gate and smart phone.* Microchemical Journal, 2020. **157**: p. 104860.
32. Shellaiah, M., Y.C. Rajan, and H.-C. Lin, *Synthesis of novel triarylamine-based dendrimers with N 4, N 6-dibutyl-1, 3, 5-triazine-4, 6-diamine probe for electron/energy transfers in H-bonded donor–acceptor–donor triads and as efficient Cu 2+ sensors.* Journal of Materials Chemistry, 2012. **22**(18): p. 8976-8987.

Journal of Photochemistry & Photobiology, A: Chemistry 444 (2023) 114983

Contents lists available at ScienceDirect

Journal of Photochemistry & Photobiology, A: Chemistry

journal homepage: www.elsevier.com/locate/jphotochem

Nanoscale detection of copper using an aggregation induced emission enhancement fluorescent sensor derived from hydroxy naphthaldehyde and benzyloxy benzaldehyde

Muhammed Arshad, Anila Paul, Abraham Joseph *

Department of Chemistry, University of Calicut, Calicut University P O-673 635, India

ARTICLE INFO

Keywords:
Aggregation
DMSO
Dynamic quenching
Turn off fluorescence

ABSTRACT

A novel Schiff base 1-((E)-((E)-(4-(benzyloxy) benzylidene) hydrazono) methyl) naphthalen-2-ol [BBHN] having aggregation induced emission enhancement (AIEE) behaviour in DMSO/water mixture have been designed, synthesized, and characterized using spectral methods. The aggregate of BBHN shows relatively high Cu^{2+} ion selectivity and sensitivity among various metal ions through fluorescence "turn off" response with a very high detection limit of 35.52 nM and a quenching constant value of $2.58 \times 10^8\ M^{-1}$. These observations suggest that the synthesized Schiff base, BBHN could effectively function as a nano sensor for the detection of Cu^{2+} ion in aqueous media. The fluorescence quenching behaviour of BBHN in the presence of Cu^{2+} ions is taking place through dynamic quenching which was evident from the steady state fluorescence lifetime measurement study.

1. Introduction

The development of an efficient fluorescent chemosensor for the sensitive and selective detection of biologically important metal ions has received great attention in the present scenario due to their simplicity, economic viability, sensitivity, easy visualization, and fast response for detection [1–6]. Recently, luminescent material research has focused on the development of organic molecules with the feature of aggregation induced emission enhancement (AIEE) [7]. Since in dilute solution, most of the organic molecules are highly emissive and become weakly or feebly emissive when aggregated in pure solvents and this phenomenon is known as aggregation-caused quenching (ACQ) [8]. To overcome the ACQ effect, a new photophysical property of aggregation-induced emission (AIE) was observed by Tang and co-workers in 2001 [9,10]. AIE is the phenomenon in which the molecules which are non-emissive in pure solvent become strongly emissive in the aggregated form [11,12]. Hence, these unique AIEE characteristics increase their potential applications in different fields, such as optoelectronic devices including organic light-emitting diodes (OLEDs) and chemosensors [13–16]. The mechanism of AIEE activity involves the restriction of intramolecular rotation (RIR) [17,18], restriction of intramolecular charge transfer (ICT) [19], twisted intramolecular charge transfer (TICT) [20,21], and cis–trans isomerization [22]. There is no common mechanism that can be applied to all systems, each mechanism is distinctive to a given system.

Among the biologically important cations, copper is a crucial divalent cation, which is used as a catalytic cofactor for many metalloenzymes, including superoxide, tyrosinase, dismutase, cytochrome c oxidase, and nuclease [23–25]. However, Uncontrolled over-loading of copper ions can have detrimental health consequences, including gastrointestinal disturbances, liver or kidney damage, neurodegenerative diseases including Parkinson's, Alzheimer's, Wilson disease, and prion diseases [26–29]. Cu^{2+} ions have become one of the most significant environmental contaminants as a result of their extensive use and applications in chemistry, medicine, biology, and biotechnology. Hence, the development of selective fluorescent chemosensors for the selective quick detection of nanomolar levels of Cu^{2+} ions in environmental systems with high sensitivity is of great significance and challenging.

As of today, many kinds of fluorophores such as quinoline, coumarin, fluorescein, and rhodamine-based fluorescent chemosensors [30–36] have been developed for the detection of copper ions. But some of the probes have serious limitations, including poor water solubility, low fluorescence intensity, poor selectivity and sensitivity, and long response times [37]. More significantly, there are very few fluorescent probes that can detect Cu^{2+} in both aqueous and organic systems. Hence, the growing concern has impelled the development of suitable

* Corresponding author.
E-mail address: abrahamjoseph@uoc.ac.in (A. Joseph).

https://doi.org/10.1016/j.jphotochem.2023.114983
Received 25 April 2023; Received in revised form 17 June 2023; Accepted 23 June 2023
Available online 24 June 2023

SECTION 4.2

Sensing of picric acid using BBHN as an AIEE active “turn off” fluorescent probe

4.2.1. Introduction

A fluorescent sensor having aggregation-based enhancement in emission characteristics with excellent selectivity and sensitivity to picric acid (PA) has been synthesized, and characterized as the sensing and determination of aromatic nitro compounds got great attraction globally in recent times due to security and safety reasons [1-3]. The designing of a proper chemosensor for the detection of PA follows the essential criteria that, the molecule contains a π-electron cloud that can combine with the electron-poor PA efficiently through π-π interactions and Lewis basic sites to interact through noncovalent hydrogen bonding interactions. Considering these challenges, herein this work, AIEE active fluorescent sensor was synthesized from 1-(hydrazonomethyl) naphthan-2-ol and 4-benzyloxybenzaldehyde by simple condensation reaction.

4.2.2. Experimental section

4.2.2.1. Development of BBHN Aggregates

In DMSO, a 1mM solution of BBHN was prepared. 100 µl of this stock solution was transferred into a 10ml flask, diluted to a final concentration of 10µM using a DMSO/Water solvent mixture with the water fractions (fw) ratios of 0 to 99 volume percentage under vigorously stirring conditions. After 20-minutes of sonication, UV-visible and emission spectra of solution mixtures were recorded.

4.2.2.2. Fluorescence activity studies

A 1mM solution of BBHN was prepared in DMSO, and a 1mM nitro aromatic compound stock solutions was prepared in double-distilled water. Fluorescence sensing experiments were carried out

at an excitation wavelength of 410 nm using aggregates of BBHN in a DMSO/Water solution combination (1:9) and 1 equivalent of the standard solution of nitro compounds at room temperature. The LOD was calculated from the titration fluorescence profile using the equation 3σ/slope.

4.2.3. Results and Discussion

The method of synthesis of BBHN is shown in **Scheme 3** in chapter 2. BBHN has good solubility in some organic solvents including DMF, DMSO, CH_3CN, THF, $CHCl_3$, and DCM.

4.2.3.1 AIE Properties

The BBHN was water insoluble compound with a strong tendency to dissolve in solvents like DMF, DMSO, CH_3CN, THF, $CHCl_3$, and DCM. The AIE properties of BBHN were examined at room temperature by recording the absorption spectrum and fluorescence spectrum of the solution mixture after adding water with various water fractions to a solution of BBHN dissolved in DMSO. The concentration of BBHN was kept at 10μM.

4.2.3.2. Absorption- Emission Spectra

In **Fig.1**, absorption spectra of BBHN in DMSO and DMSO with 90% water content are given. The UV-visible spectra of BBHN in DMSO register an intense bands at 332, 409, and 432 nm, due to π to π* transition of substituted naphthaldehyde, n to π* transition of imine bonds, and π to π* transition from the extended conjugation between the nitrogen atom and aromatic ring, respectively. However, as the water percentage increased from 0 to 99, the absorption spectral profile exhibited noticeable changes. Aggregates

start to develop as the water fraction rises, and as a result, the intensity of the absorption band at 409nm was reduced with a slight red shift of 15nm. Also, a new peak at 453nm was found in the spectra of BBHN in DMSO with a 90% water fraction, suggesting the formation of aggregates from a single molecule through intermolecular interaction. A level-off tail phenomenon was also observed in the visible region at long absorption wavelengths due to Mie scattering by nanoparticles [4] and the red shift in absorption[5] is formed to be the result of J-type aggregates.

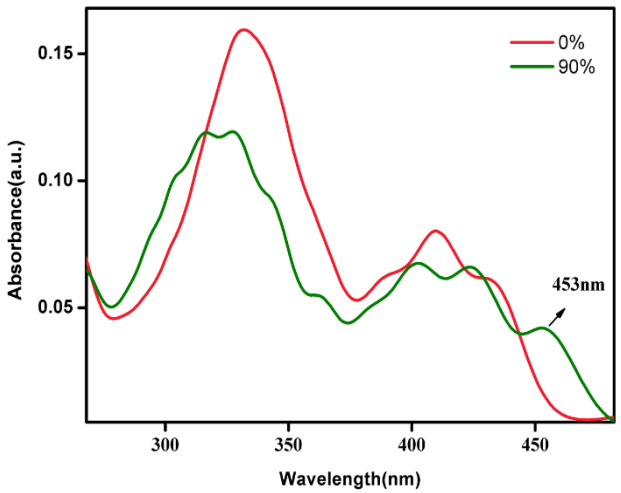

Fig.1 *UV–visible spectra of BBHN (10μM) in solution state in pure DMSO and in DMSO-Water mixed solvent with water fraction of 90% (aggregated state)*

4.2.3.3. Fluorescence Spectra

The fluorescence spectra were recorded by varying the water fraction in a DMSO-Water mixture from 0 to 99%, maintaining the overall concentration of the solution to 10μM using an excitation wavelength of 410 nm. BBHN (10 μM) was weekly emissive and registered an emission band at 510 nm in DMSO solution.

Interestingly, the emission intensity was increased as the water fraction increased, and green emission was observed at 531nm with a red shift of 21nm. The fluorescence spectra of BBHN (**Fig.2**) clearly show that no detectable fluorescence emission is reported as the water fraction increased from 0 to 30%, which might be due to the intramolecular rotation.

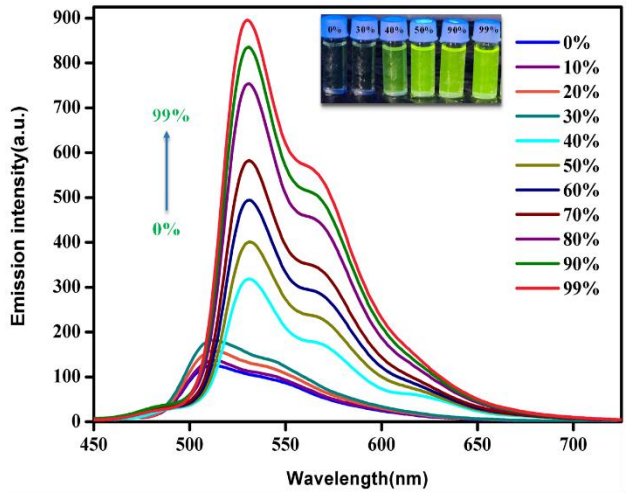

Fig.2 *Fluorescence emission spectra of BBHN in DMSO (10μM) in presence of increasing the presence of water fraction(fw) from 0 to 99%*

However, as the water fraction increases to 40%, the intensity of the emission significantly increases, and this trend continues as the water fraction increases to 60% - 99%, indicating the AIE effect (**Fig.3**). It can be noticed from the emission profile in **Fig. 2** that there was a red shift of emission maxima along with emission enhancement, which could be explained by formation of aggregates through intermolecular interaction between molecules. The intramolecular C=N and N-N bond rotation were actively involved up to 30% of water fraction in the excited state, which diminishes

the fluorescence emission of BBHN. However, once the water content reaches 40%, aggregation begins, which prevents intramolecular rotation brought on by C=N isomerization and triggers a significant increase in fluorescence emission (**Scheme 1**).

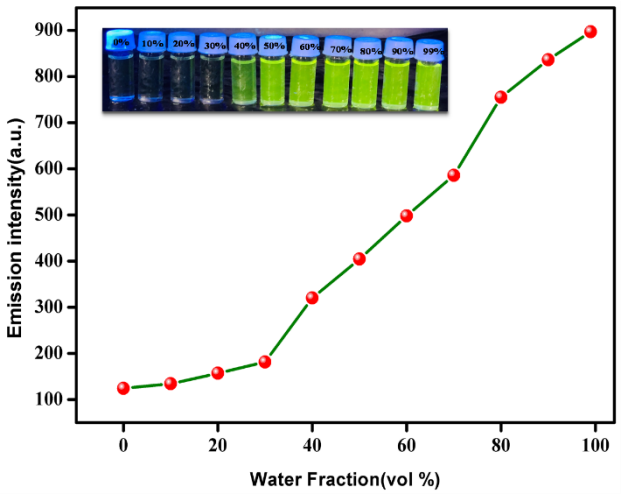

Fig.3 *Change in fluorescence intensity of BBHN with water fraction in DMSO (fw varies from 0% to 99%). Inset Fluorescence emission of aggregates of BBHN under UV-lamp*

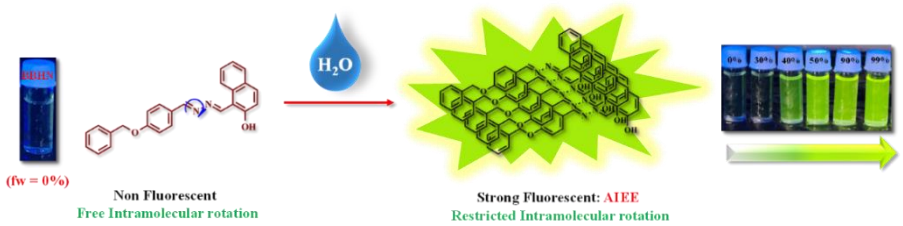

Scheme 1 *Proposed mechanism for AIEE behaviour of BBHN*

4.2.3.4. Microscopic study

The optical microscopic image was recorded at room temperature to gather more information into the AIEE and optical characteristics of BBHN, and the results are shown in **Fig.4**. It was clear from the image that BBHN in the isolated state had no discernible particles

that fluoresce, but on increasing water percentage, the particles became visible and emitted a greenish yellow colour due to aggregation in response to 365 nm UV light excitation. Thus, optical microscopic images obtained are consistent with the formation of nanoparticles in their aggregated state, which results in fluorescence behaviour.

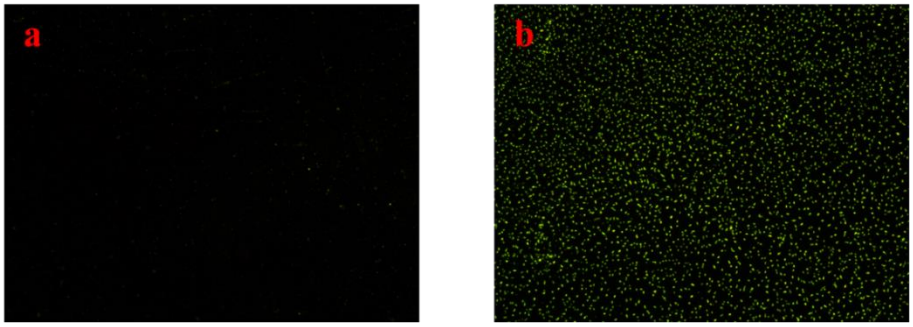

Fig.4 *Optical fluorescence microscopic images (under UV excitation) of (**a**) BBHN in solution state (fw = 0%) and (**b**) BBHN in aggregated state (fw = 90%)*

4.2.3.5. Fluorescence decay study

To explore the emission enhancement property of BBHN further, luminescence lifetime studies were performed. **Figure 5** illustrates

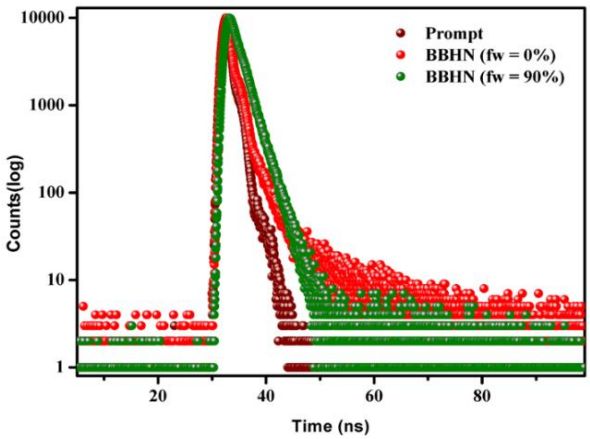

Fig.5 *Fluorescence decay profile of BBHN (10 μM) in pure DMSO (fw = 0%) and in DMSO/Water mixture (1:9) (fw = 90%)*

the lifetime decay profile of the BBHN in DMSO and DMSO with 90% water content which is well-fitted with a single-exponential decay curve. The decay profile of BBHN in DMSO exhibits an average fluorescence lifetime value of 1.177ns, which is substantially increased in the presence of aggregates (2.108ns). The increase in fluorescence lifetime is believed to be the consequence of the suppression of intramolecular rotation.

4.2.3.6. Fluorescence emission and viscosity effect

To understand the impact of solvent viscosity on the AIE property of BBHN, the system was examined in a viscous glycerol-methanol solvent mixture by blending the two substances, and the viscosity of the mixture was varied by adjusting the proportion of glycerol and methanol. As seen in **Fig. 6**, the emission intensity of BBHN increases with an increase in viscosity. This emission enhancement of BBHN at higher viscosity is attributed to the restricted intramolecular rotation, which causes a decrease in non-radiative decay and

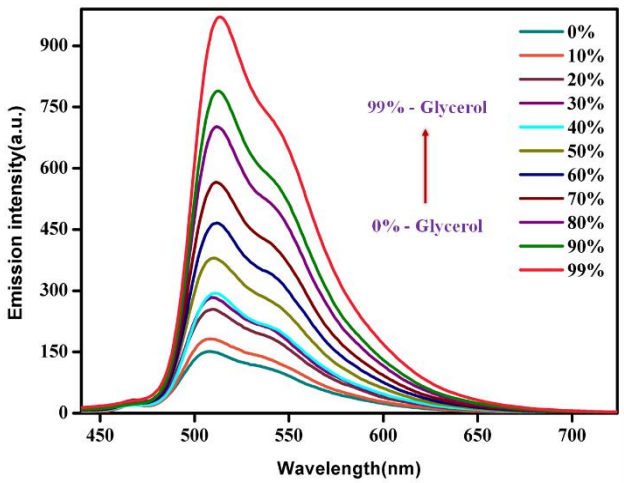

Fig.6 *Fluorescence emission spectra of aggregates of BBHN (10 μM) with change in viscosity of the solvent mixture by varying the solvent ratio of glycerol to methanol*

increases the emission intensity. The outcomes specify that the restricted intramolecular rotation affects the AIEE property of BBHN significantly and plays a prominent role in triggering the light emission properties of the molecule.

4.2.3.7. Emission enhancement and pH influence

The influence of pH on BBHN aggregates in DMSO with 90% water using HEPES buffer was studied to explore the practical applications. It is evident from **Fig.7**, that the fluorescence emission intensity of aggregates increased with pH between 2 and 7 and decreased further above pH 7. Since the emission intensity is stable over the pH range of 2 to 7, the sensor system may be extended to bio-environments for similar applications.

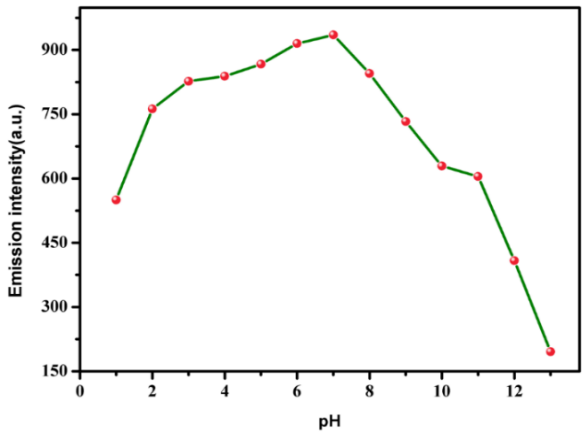

Fig.7 *Emission spectra of BBHN (10 μM) in DMSO-Water mixture (fw = 90%) at different pH*

4.2.3.8. Sensing of Picric acid

2,4,6-trinitrophenol (PA) is one of the most used explosives among other nitroaromatic compounds and fluorescence techniques have emerged as an effective tool for picric acid sensing due to fast response, high sensitivity, and easy visualization. Taking advantage

of the easiness of the method of synthesis and enhanced AIE property of BBHN, we investigated its application for the sensing and quantification of picric acid from among other nitroaromatics in aqueous media.

For the sensing of various nitro aromatics, the respective compounds was mixed with the aggregates of BBHN formed in DMSO-Water (1:9) mixture and then the fluorescence emission profile was recorded and which does not show any significant change on adding different nitroaromatic compounds except PA (**Fig.8**). With the addition of PA, the emission was quenched significantly which implied that the aggregate of BBHN could selectively detect PA in aqueous medium. The photographic image of the aggregates of BBHN with different nitroaromatic compounds under a UV lamp is given in **Fig.9**, verifying its sensitivity and selectivity. To explore the sensitivity of BBHN aggregate to PA, the titration experiments were carried out by the addition of PA into

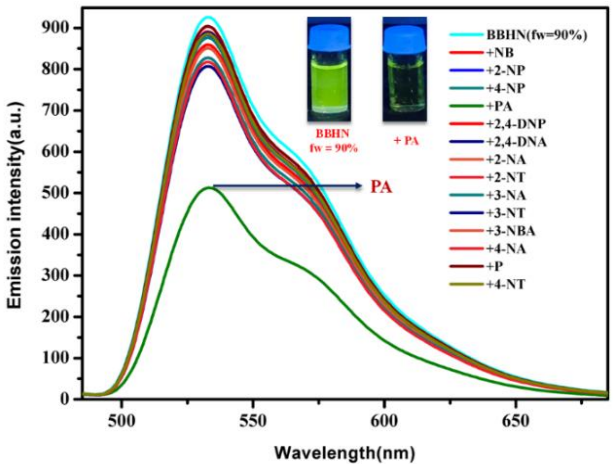

Fig.8 *Fluorescence emission spectra of aggregate of BBHN (10 μM) with water fraction 90% (fw = 90%) in presence of different Nitro compounds*

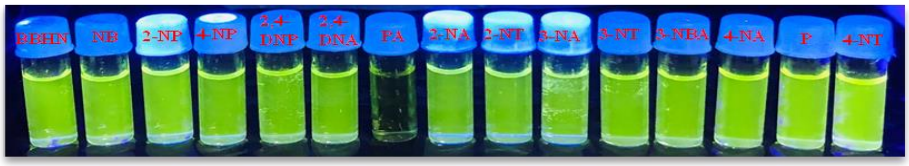

Fig.9 *Fluorescence emission of aggregate of BBHN (10 μM) with water fraction 90% (fw = 90%) in presence of different nitro compounds under UV lamp*

BBHN aggregate, and changes in the emission intensity were recorded (**Fig.10**). Upon addition of PA to the aggregate of BBHN, quenching of fluorescence emission was observed and fluorescence emission turned off completely when the PA concentration reaches to 9.6 equivalent. The quenching efficiency was calculated using the Stern-Volmer method (**Fig.11**) and was found to be $2.03\times10^{6}\ M^{-1}$. On further increasing the concentration of PA, the stern-Volmer curve shows an upward bending which indicates that the efficiency of quenching increased with PA concentration which suggests the

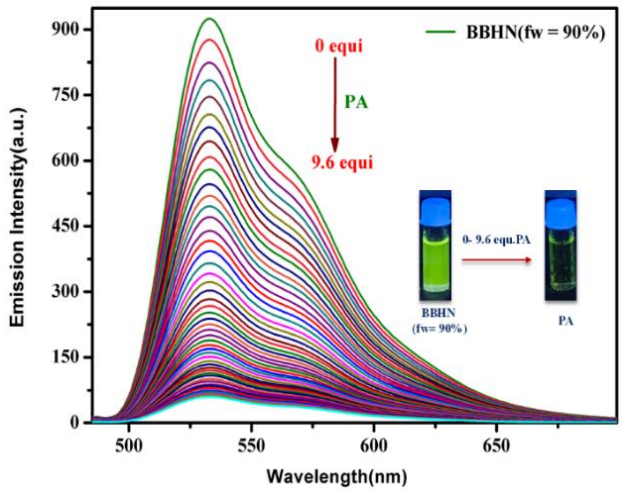

Fig.10 *Fluorescence emission spectra of aggregate of BBHN in DMSO (10 μM) with water fraction 90% (fw = 90%) up on the gradual increase in the concentration of PA from 0-9.6 equivalent*

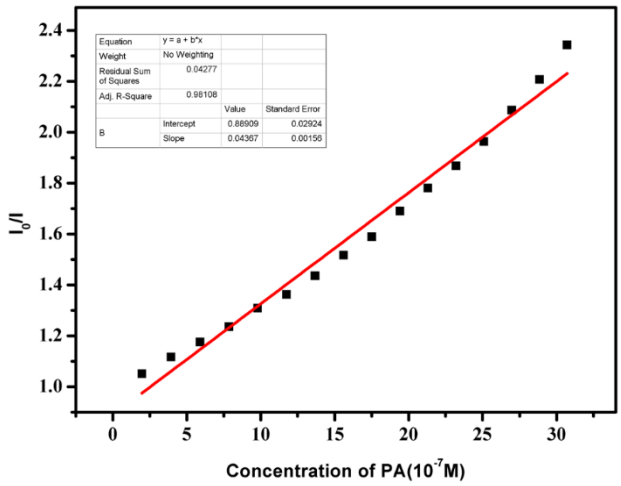

Fig.11 *Stern-Volmer plot of aggregate of BBHN with PA*

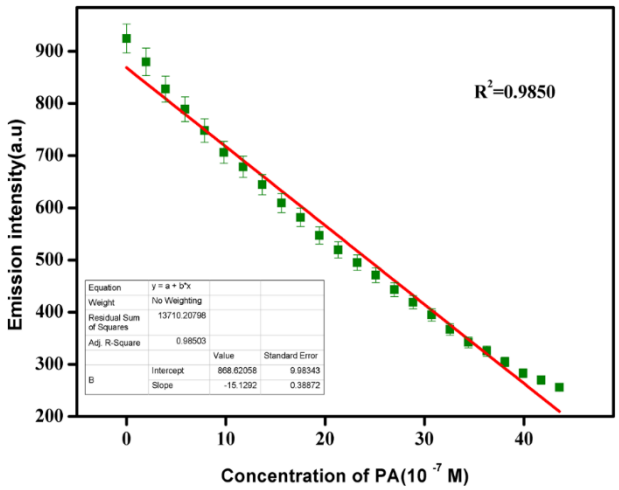

Fig.12 *Limit of detection (LOD)*

super amplified quenching effect[6]. The Limit of detection, 4.04μM, was calculated from the slope of the calibration curve (**Fig.12**) using the equation 3σ/k.

To understand further the interaction between BBHN aggregates and PA and the strong fluorescence quenching process, the fluorescence lifetime measurements were carried out in the excited state. The decay (lifetime) of BBHN aggregates in the presence and absence of PA is depicted in **Fig.13**. From the decay profile, the lifetime value of the aggregate of BBHN was found to be 2.108ns which remains almost constant in the presence of PA (2.083ns) and this constancy in the fluorescence lifetime value strongly suggests the involvement of static quenching processes. The non-linearity observed in the Stern-Volmer plot further supports the combined effect of both static and dynamic quenching processes (**Fig.14**)[7]. The linearity of the plot in the lower concentration of PA indicated the static quenching process which was confirmed by excited state lifetime measurements and an upward bending at a higher concentration of PA indicated a dynamic quenching process. It is

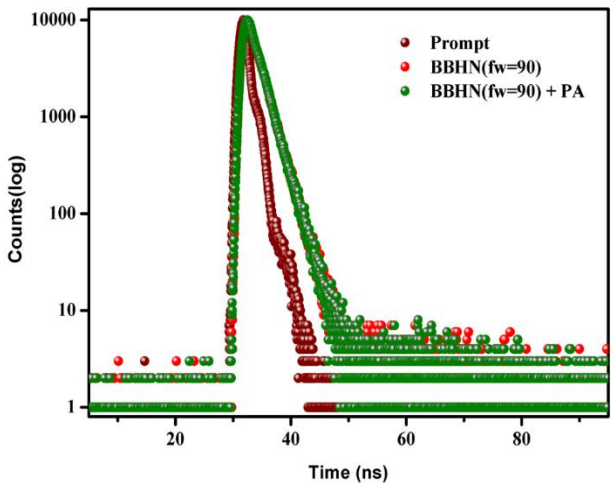

Fig.13 *Fluorescence decay profile of BBHN in DMSO (10μM) with water fraction (fw) percentage of 90 in aggregated state (fw = 90%) in the absence and presence of PA*

therefore concluded that fluorescence quenching is followed by both static and dynamic processes. Moreover, the quenching of fluorescence is due to ground-state complexation between electron-rich fluorescent aggregates of BBHN and electron-deficient picric acid through noncovalent interactions like charge transfer mechanism and π−π interactions (**Scheme 2**).

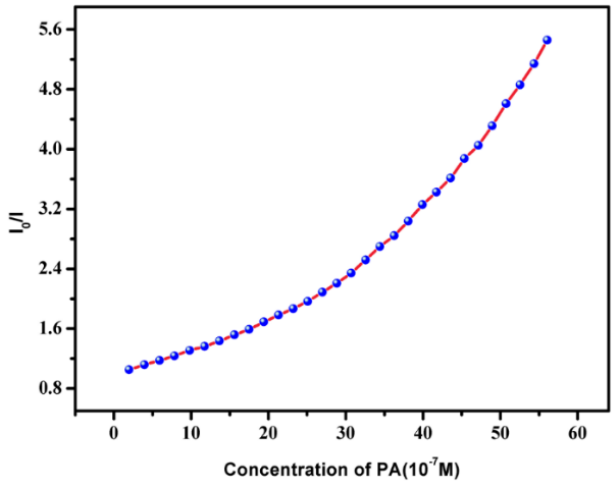

Fig.14 *Stern-Volmer plot of aggregate of BBHN with increasing of concentration of PA*

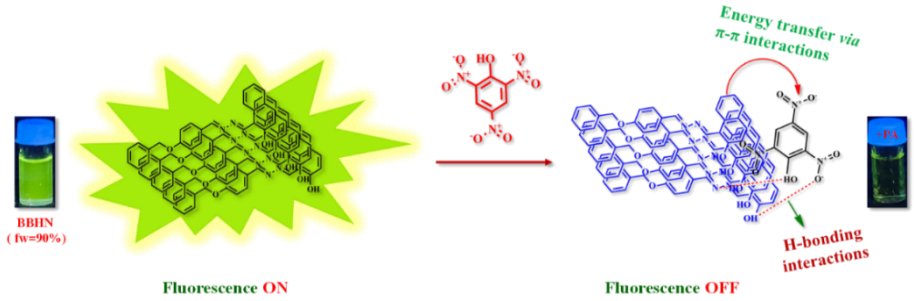

Scheme 2 *Proposed mechanism for BBHN aggregate (fw = 90%) with PA*

To understand the high selectivity of BBHN aggregates towards PA, among other nitroaromatics, competitive selectivity experiments

were conducted by recording the fluorescence spectra of BBHN aggregates in the presence of 1 equivalent of PA and an equivalent amount of other nitro compounds. It was clear from **Fig.15**, that the quenching efficiency of PA is much higher compared to other nitro aromatics which suggests the exceptional selectivity and sensitivity of BBHN towards PA. The comparison of BBHN with other reported probes was done and the data are shown in **Table 1**.

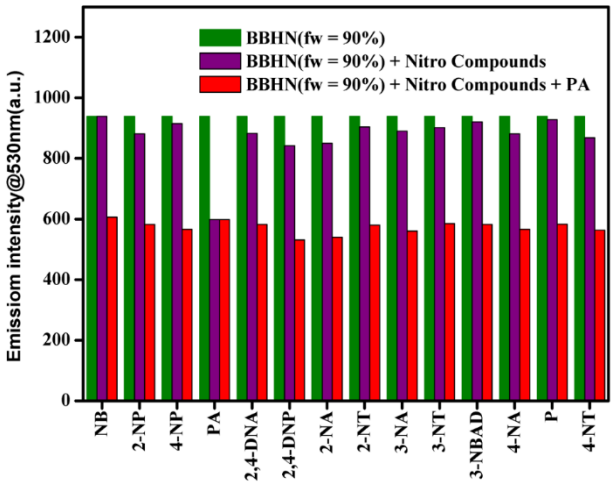

Fig.15 *The selectivity of aggregate of BBHN in DMSO (10 μM) with water fraction 90% (fw = 90%) towards PA (1 equivalent) in the presence of other nitro compounds (1 equivalent)*

Table 1 *Comparison of BBHN with other reported probes*

Probe	Sensing analyte	LOD [M]	Quenching Constant [M^{-1}]	AIEE Property	Ref
Probe-1	PA	9.5×10^{-6}	1.59×10^{5}	yes	[8]
Probe-2	PA	0.11×10^{-6}	1.91×10^{5}	yes	[9]
Probe-3	PA	1.96×10^{-6}	2.37×10^{4}	yes	[10]
Probe-4	PA	2.85×10^{-7}	3.36×10^{5}	yes	10]
Probe-5	PA	1.74×10^{-6}	4.14×10^{5}	yes	[11]
Probe-6	PA	1.22×10^{-4}	Not found	No	[12]
Probe-7	PA	4.32×10^{-6}	10.5×10^{3}	No	[13]
Probe-8	PA	4.15×10^{-6}	29.4×10^{3}	No	[13]
Probe-9	PA	0.4×10^{-6}	1.2×10^{3}	No	[14]
Probe-10	PA	1.7×10^{-5}	Not found	No	[15]
Probe-11	PA	1.5×10^{-6}	Not found	No	[16]
BBHN	**PA**	**40.4×10^{-7}M**	**2.03×10^{6}**	**Yes**	**Present work**

4.2.4. Conclusions

A novel chemosensor, BBHN is designed and synthesized with AIEE properties *via* a condensation reaction. The AIEE activity of BBHN was used as a sensor probe for picric acid (PA) in the aqueous medium. The aggregate of BBHN exhibited excellent sensitivity towards PA with fluorescence "turn off" response among various other nitroaromatics. The fluorescence quenching of BBHN was due to π-π interactions, and non-covalent hydrogen bonding interactions. The steady-state fluorescence lifetime measurement and Stern–Volmer plots confirm that the fluorescence quenching follows both static and dynamic processes. These results indicated that BBHN can act as a very reliable probe for the sensitive naked-eye detection of PA.

References

1. Banerjee, D., Z. Hu, and J. Li, *Luminescent metal–organic frameworks as explosive sensors.* Dalton transactions, 2014. **43**(28): p. 10668-10685.
2. Peng, Y., et al., *A colorimetric and fluorescent chemosensor for the detection of an explosive—2, 4, 6-trinitrophenol (TNP).* Chemical communications, 2011. **47**(15): p. 4505-4507.
3. Lustig, W.P., et al., *Metal–organic frameworks: functional luminescent and photonic materials for sensing applications.* Chemical Society Reviews, 2017. **46**(11): p. 3242-3285.
4. Zhao, J., et al., *Excited state intramolecular proton transfer (ESIPT): from principal photophysics to the development of new chromophores and applications in fluorescent molecular probes and luminescent materials.* Physical Chemistry Chemical Physics, 2012. **14**(25): p. 8803-8817.
5. Zhao, J.-S., et al., *Memory of chirality in J-type aggregates of an achiral perylene dianhydride dye created in a chiral asymmetric catalytic synthesis.* Chemical Science, 2011. **2**(5): p. 937-944.
6. Chen, T., et al., *Monodisperse AIE-active conjugated polymer nanoparticles via dispersion polymerization using geminal cross-coupling of 1, 1-dibromoolefins.* Small, 2016. **12**(47): p. 6547-6552.
7. Zhao, D. and T.M. Swager, *Sensory responses in solution vs solid state: a fluorescence quenching study of poly (iptycenebutadiynylene) s.* Macromolecules, 2005. **38**(22): p. 9377-9384.

8. Soufeena, P., T. Nibila, and K. Aravindakshan, *Coumarin based yellow emissive AIEE active probe: A colorimetric sensor for Cu2+ and fluorescent sensor for picric acid.* Spectrochimica Acta Part A: Molecular and Biomolecular Spectroscopy, 2019. **223**: p. 117201.
9. Maity, S., et al., *Aggregation induced emission enhancement from antipyrine-based schiff base and its selective sensing towards picric acid.* Sensors and Actuators B: Chemical, 2017. **248**: p. 223-233.
10. Ding, A., et al., *Complex-formation-enhanced fluorescence quenching effect for efficient detection of picric acid.* Chemistry–A European Journal, 2014. **20**(38): p. 12215-12222.
11. Dey, S., et al., *An antipyrine based fluorescence "turn-on" dual sensor for Zn 2+ and Al 3+ and its selective fluorescence "turn-off" sensing towards 2, 4, 6-trinitrophenol (TNP) in the aggregated state.* Photochemical & Photobiological Sciences, 2019. **18**: p. 2717-2729.
12. Saha, S., et al., *Pyridine-pyrazole based Al (III)'turn on'sensor for MCF7 cancer cell imaging and detection of picric acid.* RSC advances, 2021. **11**(17): p. 10094-10109.
13. Moral, R., O.A. Pegu, and G. Das, *Probing the aggregation potential and picric acid recognition aptitude by altering aromatic core substitution in a series of cinnamaldehyde-based receptors.* Dyes and Pigments, 2023. **218**: p. 111502.
14. Rahman, Z., et al., *A 4-aminophthalimide derive smart molecule for sequential detection of aluminum ions and picric acid.* Journal of Photochemistry and Photobiology A: Chemistry, 2023. **439**: p. 114593.
15. Ghosh, S., N. Baildya, and K. Ghosh, *A new 1, 2, 3-triazole-decorated imino-phenol: selective sensing of Zn 2+, Cu 2+ and picric acid under different experimental conditions.* New Journal of Chemistry, 2021. **45**(24): p. 10923-10929.
16. Halder, S., et al., *A quinoline-based compound for explosive 2, 4, 6-trinitrophenol sensing: experimental and DFT-D3 studies.* New Journal of Chemistry, 2018. **42**(11): p. 8408-8414.

Spectrochimica Acta Part A: Molecular and Biomolecular Spectroscopy 305 (2024) 123465

Contents lists available at ScienceDirect

Spectrochimica Acta Part A:
Molecular and Biomolecular Spectroscopy

journal homepage: www.journals.elsevier.com/spectrochimica-acta-part-a-molecular-and-biomolecular-spectroscopy

Sensing of picric acid using an AIEE active "Turn Off" fluorescent probe derived from hydroxy naphthaldehyde and benzyloxy benzaldehyde

Muhammed Arshad, P. Sowmya, Anila Paul, Abraham Joseph *

Department of Chemistry, University of Calicut, Calicut University P O-673 635, India

HIGHLIGHTS

- A fluorescent probe, BBHN with AIEE properties has been developed for sensing PA.
- The fluorescent emission happens in DMSO/H_2O system due to RIM rotation.
- Naked eye detection of Picric acid in low level is possible under UV irradiation.
- The detection limit was 4.04 μM with a quenching constant value of 2.03 × 10^6 M^{-1}.
- DFQ takes place in the presence of Picric acid.

GRAPHICAL ABSTRACT

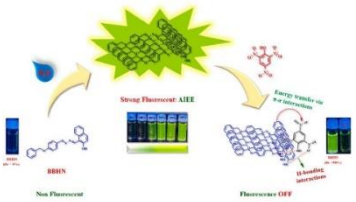

ARTICLE INFO

Keywords:
Induced emission
DMSO
Picric acid
Mixed quenching

ABSTRACT

A novel Schiff base with AIEE characteristics has been developed and used as a chemosensor for picric acid in aqueous media. The Schiff base 1-((E)-((E)-(4-(benzyloxy) benzylidene) hydrazono) methyl) naphthalen-2-ol [BBHN] with strong fluorescence emission was obtained by the simple condensation of 1-(hydrazonomethyl) naphthan-2-ol and 4-benzoxy benzaldehyde. The characterization of BBHN was done using Fourier Transfer Infra-Red, UV–visible, Magnetic Resonance (^{1}H and ^{13}C) spectroscopy, and HRMS. The sensing behaviour of BBHN aggregates towards nitro explosive was then investigated. The aggregates of BBHN showed a quick, highly selective, and sensitive fluorescence 'Turn Off' response towards picric acid (PA) in an aqueous medium among various other nitroaromatics. The limit of detection was 4.04 μM with 2.03 × 10^6 M^{-1} as the quenching constant. The fluorescence "Turn Off" response in the presence of PA is mainly due to π-π interactions, and non-covalent hydrogen bonding interactions. Moreover, steady-state fluorescence lifetime measurement and Stern – Volmer plots reveal that the fluorescence quenching followed mixed quenching strategies.

1. Introduction

A fluorescent sensor having aggregation-based enhancement in emission characteristics with excellent selectivity and sensitivity to picric acid (PA) has been synthesized, and characterized as the sensing and determination of aromatic nitro compounds got great attraction globally in recent times due to security and safety reasons[1–3]. Also, the synthesis of pesticides, dyes, plastics, polymers, medicines, and

* Corresponding author.
E-mail address: abrahamjoseph@uoc.ac.in (A. Joseph).

https://doi.org/10.1016/j.saa.2023.123465
Received 6 June 2023; Received in revised form 17 September 2023; Accepted 25 September 2023
Available online 27 September 2023

Chapter 5

Applications of AHN as sensor

AHN functions as a fluorescent sensor for PA, exhibiting a fluorescence switch-off response with a detection limit of 2.45 μM, and as a colourimetric sensor for Cu^{2+} in aqueous media, showing a colour change from colourless to yellow with a detection limit of 3.16 μM. The fluorescence quenching mechanism for PA involves both static and dynamic processes, mediated by π-π interactions and intramolecular hydrogen bonding, as indicated by Stern-Volmer plots and lifetime measurements. For Cu^{2+}, the colourimetric response is due to the complexation of AHN with Cu^{2+} in a 2:1 stoichiometry, confirmed by Job's plot method. These findings underscore AHN's potential as a versatile sensor for environmental analytes, providing significant insights for practical applications in environmental monitoring and analysis.

5.1 Introduction

Simultaneous detection of multiple target ions using facile chemosensors has garnered great attention on account of their simplicity and it has often succeeded in triumphing over the difficulties of employing multiple indicators by one-to-one analysis. Among the array of sensing methods, fluorescence, and colourimetric approaches have captivated considerable interest owing to their numerous advantages, such as simplicity, selectivity, visual detectability, non-destructive nature, cost-effectiveness, and quick real-time monitoring capabilities [1-4].

Herein we reported a novel 9-anthraldehyde based Schiff base, 1-((E)-((E)-(anthracen-9-ylmethylene) hydrazono) methyl) naphthalen-2-ol (AHN) with AIEE activity having responses to PA and bivalent copper in different contexts. The probe AHN with AIEEF (Aggregation Induced Emission Enhancement Fluorescence) property, acts as a fluorescent sensor for the selective detection of PA through fluorescence switch-off response and acts as a colourimetric sensor for Cu^{2+} in aqueous medium through a shift of colour from colourless to yellow. Hence, AHN is very useful for the selective detection of PA and Cu^{2+} through naked-eye for quick real-time monitoring.

5.2 Results and Discussion

The Schiff base AHN was synthesized through a facile condensation reaction between 9-anthraldehyde and (E)-1-(hydrazonomethyl) naphthalen-2-ol (**Scheme 4** in chapter 2) and was soluble in organic solvents like DMSO and DMF.

5.2.1 Aggregation-Induced Emission Characteristics of AHN

AHN was readily soluble in DMSO and was insoluble in pure water. The AIEE activity of AHN was studied by fluorescence spectrometry by varying the water percentage in DMSO solvent from 0 to 99. The fluorescence spectra of AHN depicted in **Fig.1** embody that as the water fraction increases from 0% to 70% the fluorescence intensity increases slightly. Later, when the water fraction reaches 80% the system shows a drastic enhancement in fluorescence intensity, and red emission was observed at 570nm with a shift of 60nm. Further, as the water fraction varies from 80% to 90% and then to 99%, the fluorescence emission intensity increases considerably which indicates the AIEE activity of AHN. Along with emission enhancement, there was a red shift in emission maxima which implies the transformation of a single molecule into aggregates by intramolecular association. Up to 70% of the water fraction there is

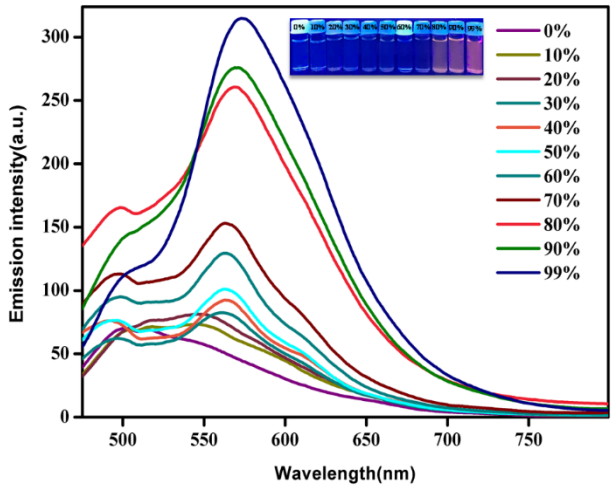

Fig.1 *Change in the fluorescence emission spectra of AHN in DMSO (10μM, λ_{ex}=425 nm, λ_{em}= 570 nm) in presence of increasing water fraction (fw) from 0% to 99%*

an active involvement of C=N isomerization and intramolecular rotation about the N-N bond which suppresses the fluorescence emission of AHN and as the water fraction reaches 80% aggregation starts and blocks the intramolecular rotations and hence increases the fluorescence emission (**Scheme 1**).

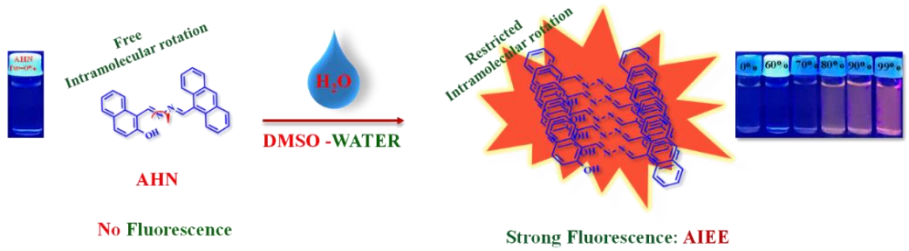

Scheme 1 *Proposed mechanism for AIEE behaviour of AHN aggregate*

Besides, the fluorescence emission property was studied using an optical microscope, and the optical microscopic image of AHN with 0% water fraction and 90% water fraction is shown in **Fig.2**. The obtained images clearly show that there are no noticeable particles at 0% water fraction with fluorescence and as the water fraction

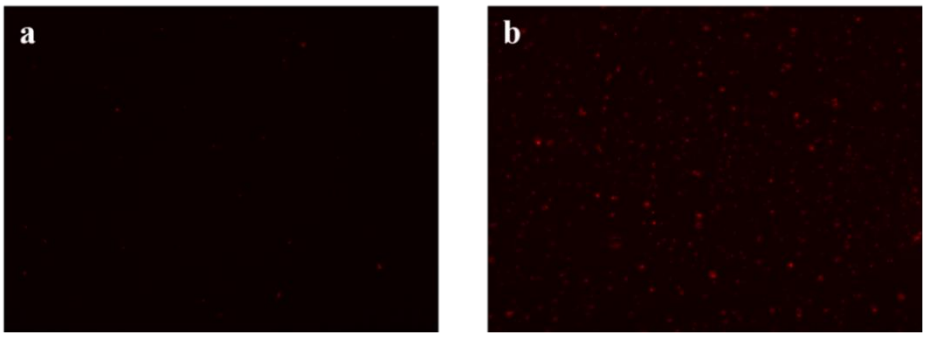

Fig.2 *Optical fluorescence microscopic images (under UV excitation) of (**a**) AHN in pure DMSO with percentage water fraction(fw) of 0 in solution state (fw = 0%) and (**b**) AHN in DMSO-Water mixed solvent with percentage water fraction(fw) of 90 in the aggregated state (fw = 90%)*

increases the number of particles with fluorescence also increases, which supports the nanoparticle formation in the aggregated state. The dynamic light scattering (DLS) measurement of AHN aggregates supports that the size of AHN aggregates is in the nano range (**Fig.3**).

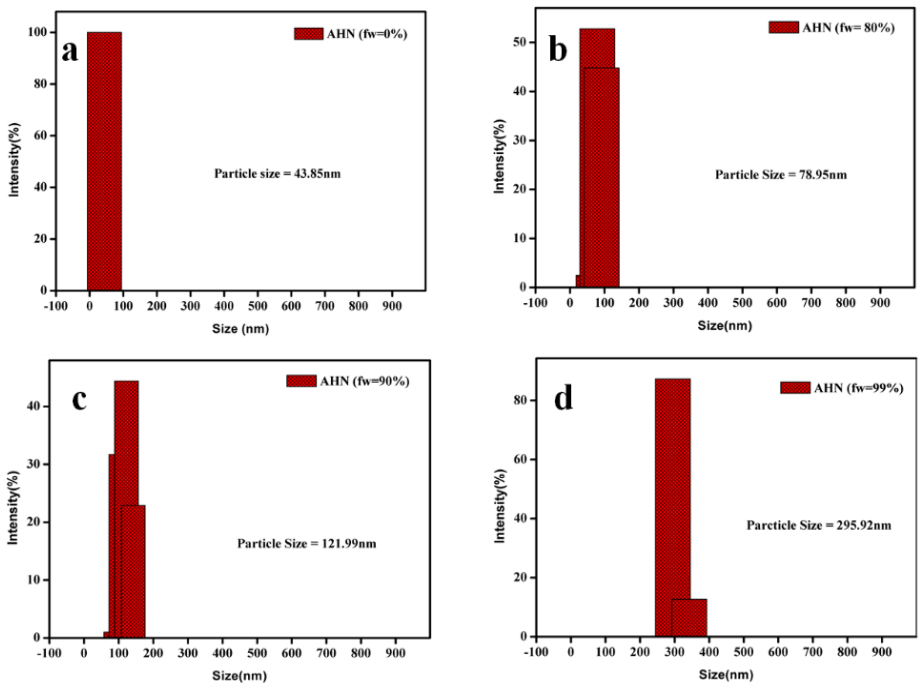

Fig.3 *The dynamic light scattering (DLS) measurements of AHN (**a**) with 0% water fraction, (**b**) with 80% water fraction, (**c**) with 90% water fraction, (**d**) with 99% water fraction.*

To investigate the AIEE property of AHN, the absorption spectra of AHN in DMSO with 0% water fraction and with 90% water fraction were studied. From the absorption spectra depicted in **Fig.4**, AHN in DMSO shows two broad bands at 330nm and 425nm corresponding to π - π* and n - π* transitions in the 2-hydroxy-1-naphthaldehyde moiety. As the water fraction increases from 0% to 70% there are no remarkable changes in absorption spectra. However, as the water fraction reaches 80% the intensity of the band decreases with the

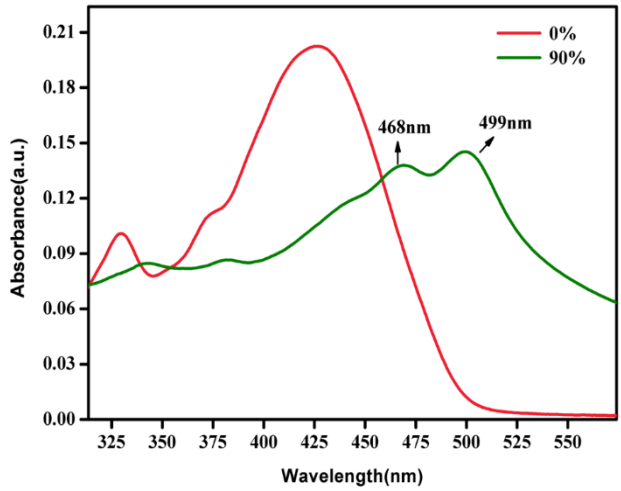

Fig.4 *UV–visible spectra of AHN (10μM) in solution state in pure DMSO and in DMSO-Water mixed solvent with water fraction of 90% (aggregated state)*

formation of new peaks at 468nm and 499nm in the visible region. The new peaks with levelled-off tails at the visible region are due to the formation Mie scattering effect by nanoparticle aggregates of AHN suspension [5]. Generally, aggregates of J-type (head-tail type)

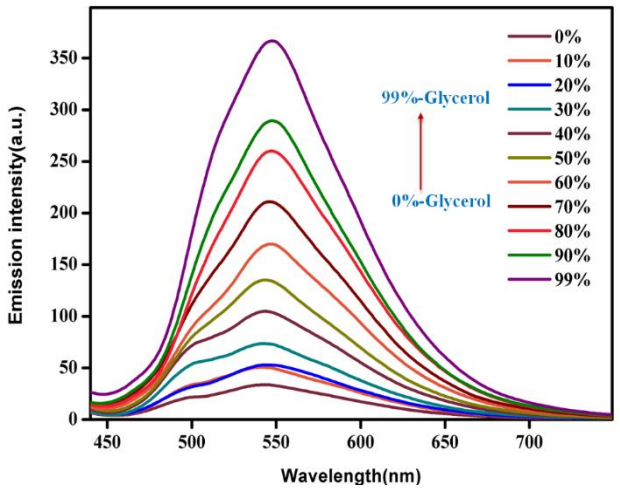

Fig.5 *Change in the fluorescence emission spectra of AHN in DMSO (10 μM, λ_{ex}= 425 nm, λ_{em}= 570 nm) with change in viscosity of the solvent mixture by varying the solvent ratio of glycerol to methanol*

are responsible for the red shift in the absorption spectra which significantly enhances the emission intensity [6, 7].

To validate the mechanism of fluorescence enhancement, the effect of viscosity is also studied by using methanol glycerol mixture. The viscosity of the mixture is varied by increasing the percentage of glycerol to methanol. It is evident from **Fig.5**, that as the glycerol percentage increases, the emission intensity also increases and this enhancement in emission is due to the viscosity effect. The significant enhancement in emission at higher glycerol fraction is due to suppression of intramolecular rotations.

Moreover, the photostability of AHN aggregate was studied by recording emission spectra periodically for 0 to 240 minutes and the results obtained are given in **Fig.6**. It is clear from **Fig.6**, that the emission intensity of AHN aggregate was stable over the time range and which indicates its photostability.

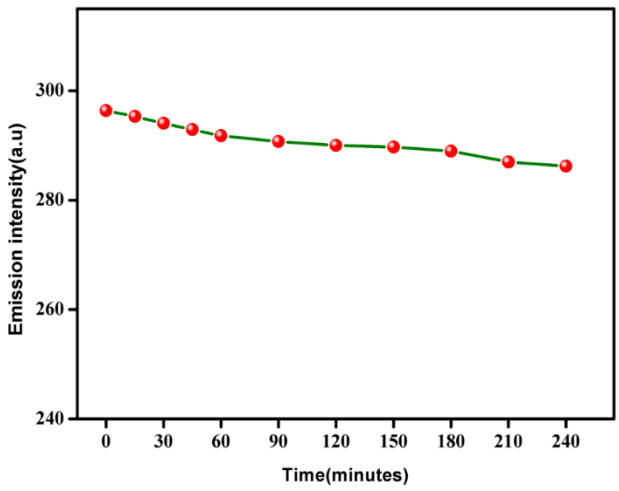

Fig.6 *Time-dependent emission intensity of AHN aggregates*

To understand more about AIEE activity, the fluorescence lifetime measurements are also studied. **Fig.7** shows the fluorescence decay profile of AHN in DMSO with 0% water fraction and with 90% water fraction. It was observed from the decay profile, that the lifetime value obtained for AHN with 0% water fraction (1.191ns) is significantly increased to 2.108ns as the water fraction reaches 90% due to aggregate formation.

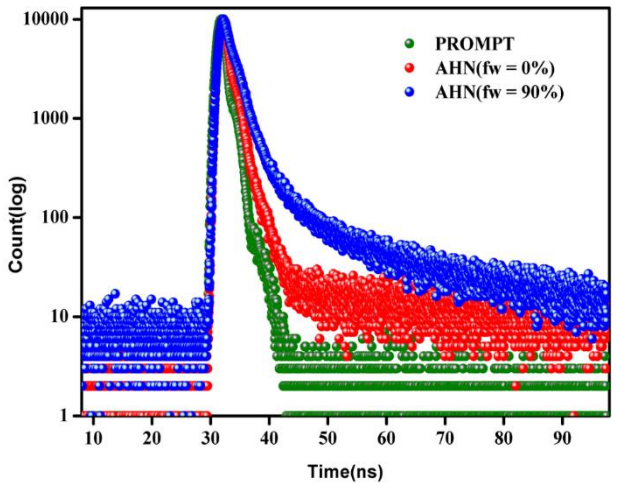

Fig.7 *Fluorescence decay profile of AHN (10 μM) in pure DMSO (fw = 0%) and in DMSO-Water mixed solvent in the aggregated state (fw = 90%)*

The influence of pH on emission intensity was carried out to extend the application of AHN aggregates in practical situations. As illustrated in **Fig.8**, it was clear that the emission intensity of AHN in DMSO with 90% water fraction increased from pH 2 to 7 and then decreased. The emission intensity is almost similar in the range of 2-7, which indicates its potential application in the physiological pH range.

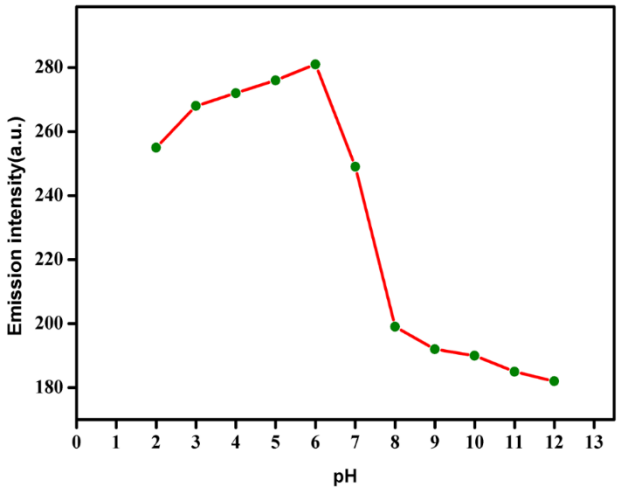

Fig.8 *Change in the emission spectra of AHN (10 μM), λ_{ex}= 425 nm, λ_{em}= 570nm) in DMSO/Water mixture with water fraction 90% (fw = 90%) at different pH*

5.2.2 Detection of picric acid (PA)

The AHN aggregates in DMSO with 90 % water fraction were tested for the sensing of PA, 2,4- dinitrophenol (2,4-DNP), 2,4,6-trinitrotoluene (TNT), nitrobenzene (NB), 2-nitrophenol (2-NP), 4-nitrophenol (4-NP), 4-nitroaniline (4-NA), 2-nitrotoluene (2-NT), 4-nitrotoluene (4-NT), 3-nitroaniline (3-NA), 3- nitrobenzoic acid(3-NBA) 2-nitroaniline (2-NA), 3-nitrotoluene (3-NT), and 2,4-dinitroaniline (2,4-DNA). The fluorescence emission profile of AHN aggregates with different nitro compounds is delineated in **Fig.9**. It is ascertained from **Fig .9**, that the emission intensity was quenched significantly on the addition of PA while other nitro compounds do not affect the intensity of the emission of AHN aggregate, which indicates the selectivity of AHN aggregates towards PA. Furthermore, to investigate the sensitivity of AHN aggregates towards PA, the fluorescence titration experiments were carried out

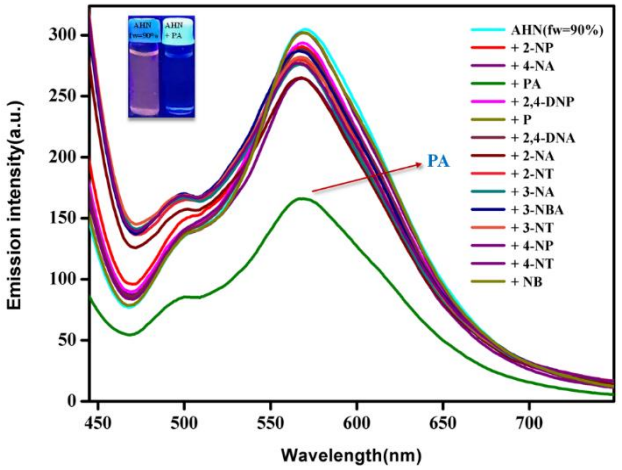

Fig.9 *Change in the fluorescence emission spectra of AHN in DMSO (10 μM, λ_{ex}= 425 nm, λ_{em}= 570 nm) with water fraction 90% (fw = 90%) in the presence of different nitro compounds*

by the incremental addition of PA (**Fig.10**). Up on the gradual addition of PA, the fluorescence intensity also decreased gradually and the fluorescence completely switched off when the concentration of PA reaches 5.2 equivalents.

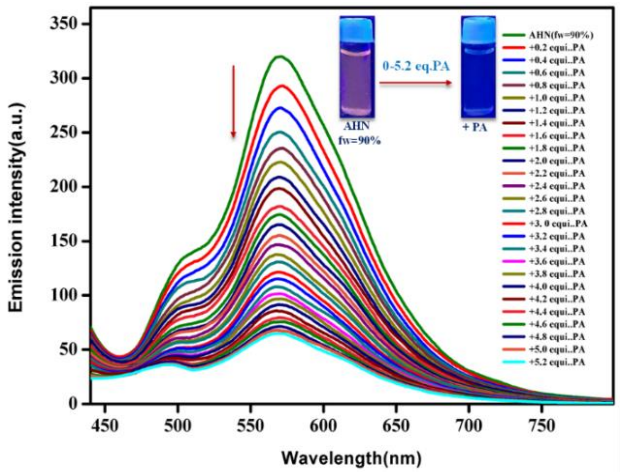

Fig.10 *Changes in the fluorescence emission spectra of AHN in DMSO (10 μM, λ_{ex}= 425 nm, λ_{em}= 570 nm) with water fraction 90% (fw = 90%) up on the gradual increase in the concentration of PA from 0 – 5.2 equivalent*

The quenching constant value is calculated from the Stern-Volmer plot (**Fig.11**) and was found to be $6.21\times10^{7}M^{-1}$. The limit of detection was calculated from the calibration curve (**Fig.12**) using the equation $3\sigma/k$ and was found to be 2.45µM. The comparison of AHN with other reported probes was done and the data are shown in **Table 1**.

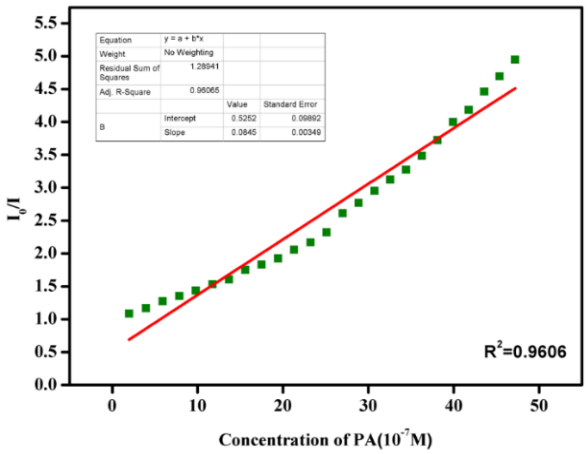

Fig. 11 *Stern-Volmer plot of AHN in DMSO (10 µM, λ_{ex}= 425 nm, λ_{em}= 570 nm) aggregate with water fraction 90% (fw = 90%)*

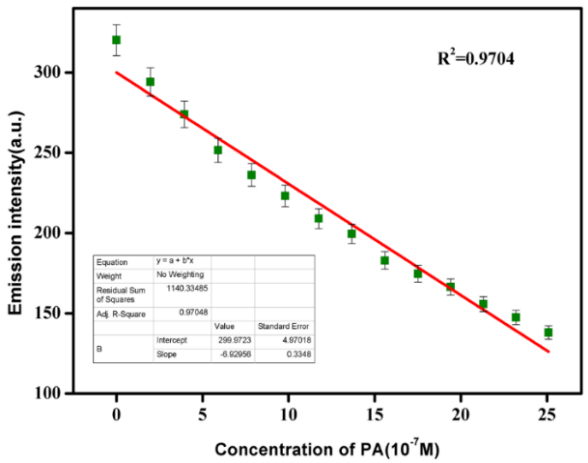

Fig.12 *Limit of detection (LOD) of AHN in DMSO with water fraction 90% with PA*

Table 1 *Comparison of AHN with other reported probes*

Probe	Sensing analyte	LOD [M]	Quenching constant [M^{-1}]	AIEE Property	Ref
Probe-1	PA	9.5×10^{-6}	1.59×10^{5}	yes	[8]
Probe-2	PA	0.11×10^{-6}	1.91×10^{5}	yes	[9]
Probe-3	PA	1.96×10^{-6}	2.37×10^{4}	yes	[10]
Probe-4	PA	2.85×10^{-7}	3.36×10^{5}	yes	[10]
Probe-5	PA	1.74×10^{-6}	4.14×10^{5}	yes	[11]
Probe-6	PA	4.32×10^{-6}	10.5×10^{3}	No	[12]
Probe-7	PA	4.15×10^{-6}	29.4×10^{3}	No	[12]
Probe-8	PA	0.4×10^{-6}	1.2×10^{3}	No	[13]
Probe-9	PA	1.7×10^{-5}	Not Found	No	[14]
Probe-10	PA	1.5×10^{-6}	Not Found	No	[15]
AHN	**PA**	$\mathbf{24.57\times10^{-7}}$	$\mathbf{6.215\times10^{7}}$	**Yes**	**Present work**

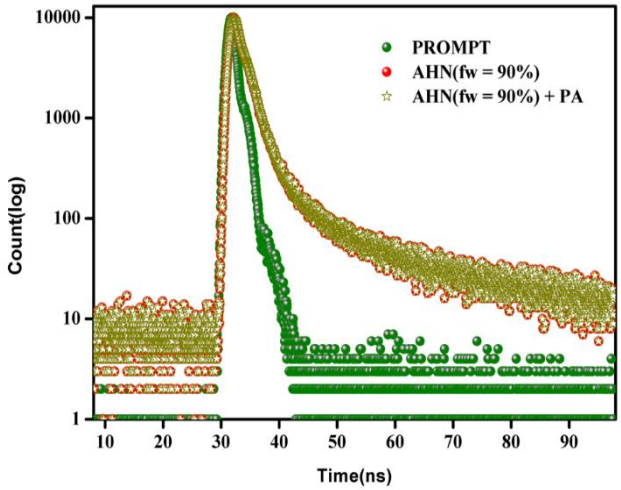

Fig. 13 *Fluorescence decay profile of AHN in DMSO (10μM) with percentage water fraction(fw) of 90 in aggregated state (fw = 90%) in absence and presence of PA*

To investigate further the interactions and the quenching process, lifetime measurements were carried out. **Figure 13** shows the lifetime decay profile of AHN aggregate both with and without PA. The lifetime value of the aggregate of AHN was determined from the decay profile to be 2.108ns, which remains almost constant in the presence of PA (2.009ns). The unchanging fluorescence lifetime

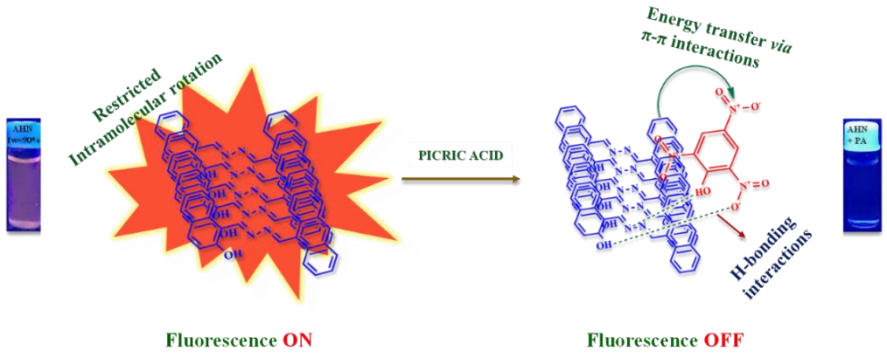

Scheme 3 *Proposed mechanism of the interaction of AHN aggregate (fw = 90%) with PA*

value of the aggregate and aggregate PA system shows that the mechanism of the quenching process is more or less static. Additionally, the combined effect of static and dynamic quenching was shown by the non-linearity seen in the Stern-Volmer plot (**Fig. 11**). An upward bending at a higher concentration of PA indicated a

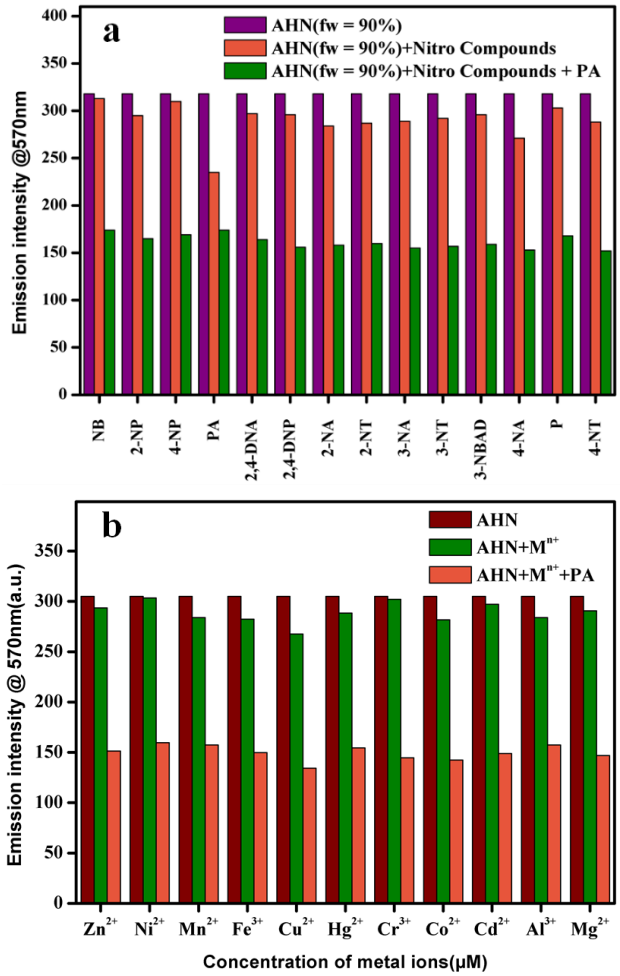

Fig.14 *The selectivity of AHN in DMSO (10 μM, λ_{ex}= 425 nm, λ_{em}= 570 nm) with water fraction 90% (fw = 90%) towards* ***(a)*** *PA (10 μM) (1 equivalent) in the presence of other nitro compounds (10 μM) (1 equivalent),* ***(b)*** *PA (1 equivalent) in the presence of other metal ions (10 μM) (1 equivalent)*

dynamic quenching process, whereas the linearity of the curve in the lower concentration of PA showed a static quenching process, which was supported by excited state lifetime measurements. As a result of the above observations and findings, it is clear that both static and dynamic quenching processes were involved in the present case of fluorescence quenching[16]. Additionally, the static quenching is due to ground-state complexation between electron-rich fluorescent AHN aggregates and electron-deficient PA and the dynamic quenching is due to energy transfer through π-π interactions and intramolecular hydrogen bonding interaction between AHN and PA (**Scheme 3**)[17, 18].

A series of competitive selectivity studies were conducted by recording the fluorescence spectra of AHN aggregates in the presence of 1 equivalent of PA and an equivalent quantity of other nitro compounds. It was evident from **Fig.14a**, that the quenching efficiency of PA is obviously much higher than that of other nitro compounds, and this fact shows that the aggregate of AHN exhibits excellent sensitivity and selectivity towards PA, even in the presence of other nitro compounds in aqueous solution. In addition to that selectivity of AHN aggregates were investigated in the presence of diverse metal ions (**Fig.14b**). It is clear from **Fig.14b**, that the selectivity of AHN aggregates towards PA was not affected by the presence of other metal ions.

5.2.3 Colourimetric Sensing of Copper

The colour change of AHN in DMSO upon the addition of various metal ions such as Al^{3+}, Hg^{2+}, Zn^{2+}, Co^{2+}, Fe^{3+}, Cd^{2+}, Mn^{2+}, Mg^{2+}, Cr^{3+},

$Cu^{2+}$and Ni^{2+} nitrates in aqueous medium was investigated. Only the Cu^{2+} ion induced an immediate visible colour change to light yellow. This result demonstrated the high selectivity of AHN in DMSO towards Cu^{2+} and the usefulness of AHN for recognizing Cu^{2+} in aqueous media with naked eye (**Fig.15**).

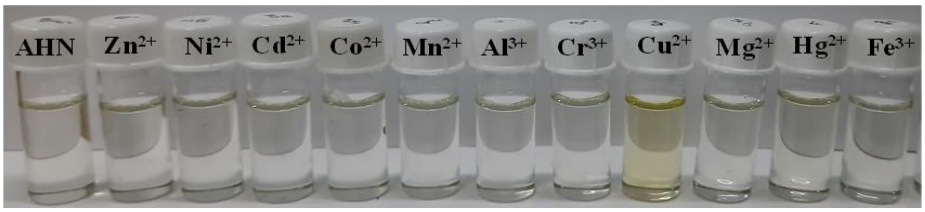

Fig.15 *Colour change of AHN in DMSO (10 μM) in the presence of fixed concentration (10 μM) of different metal ions*

Furthermore, using the UV-visible absorption studies, the binding affinity of AHN of 10μM concertation towards different metal ions in aqueous solution was investigated. The AHN in DMSO solvent shows two broad bands at 330nm and 425nm corresponding to π - π* and n - π* transitions in the 2-hydroxy-1-naphthaldehyde moiety. With

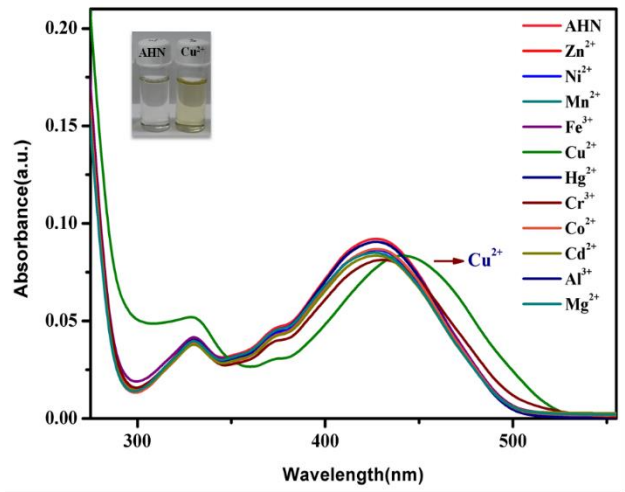

Fig.16 *Change in the Absorption spectra of AHN in DMSO in the presence of different metal ions*

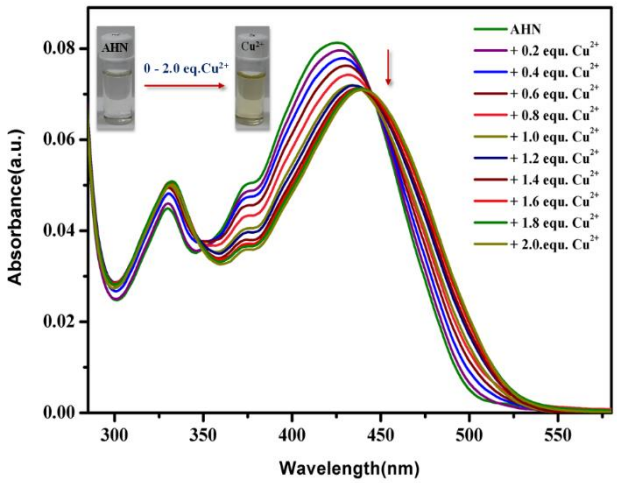

Fig.17 *Changes in the Absorption spectra of AHN in DMSO (10 μM) up on the increase in the concentration of Cu^{2+} from 0 – 2.0 equivalent*

the addition of Cu^{2+} ion, the intensity of the peak at 425nm gets shifted to 447nm region, which indicates an extensive complexation of AHN with Cu^{2+}. However, the addition of other metal ions did not produce any change in the intensity of absorption of AHN as shown in **Fig.16.** To examine the selectivity of AHN with Cu^{2+}, the titration experiments were done by increasing the concentration of Cu^{2+}. The changes in the absorption titration profile of AHN are shown in **Fig. 17.** The titration profile clearly shows that the absorption intensity of AHN at 425 nm steadily decreases as the concentration of Cu^{2+} was increased, followed by the shift of the absorption band to 447 nm with a distinct isosbestic point at 444 nm. Intriguingly, during the titration studies, the colour of the AHN solution changed to yellow, and the intensity of the colour increased with increasing Cu^{2+} concentration, indicating the development of the AHN-Cu^{2+} complex in the solution (**Scheme 4**).

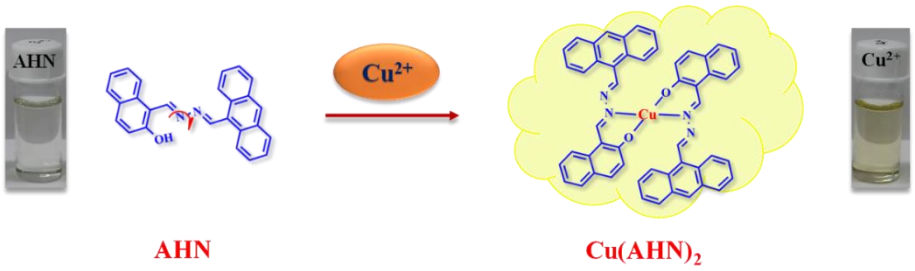

Scheme 4 *Proposed mechanism of interaction of AHN with Cu^{2+}*

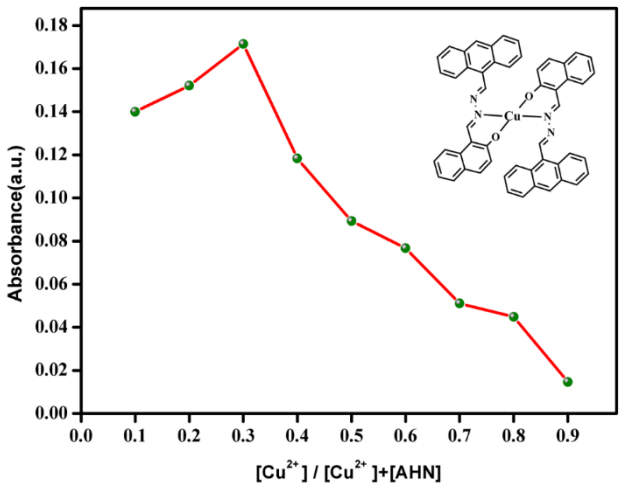

Fig.18 *Job's plot of AHN with addition of Cu^{2+}*

Using Job's plot analysis, the stoichiometry of the complex formed between AHN and Cu^{2+} was investigated, and a 2:1 binding stoichiometry was identified (**Fig.18**).Using the equation 3σ/k, the limit of detection was estimated from the absorption titration profile (**Fig.19**) and was found to be 3.16μM which is far below the acceptable limit of copper recommended by the World Health Organisation in drinking water[19]. The association constant (K_a) for AHN with Cu^{2+} was calculated using Benesi-Hildebrand equation was found to be $2.4\times 10^{4}M^{-1}$ (**Fig.20**).

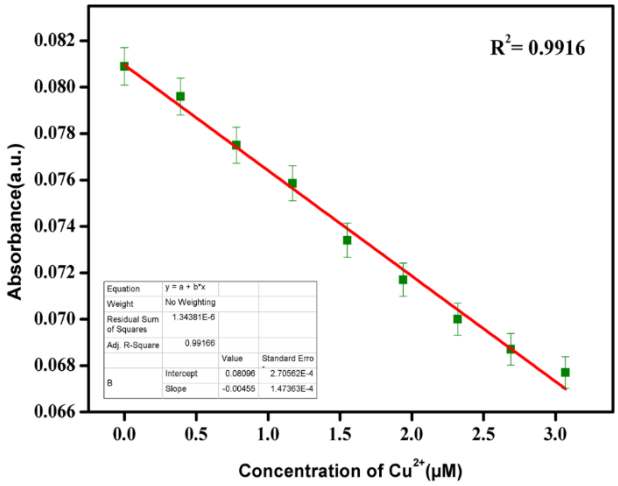

Fig.19 *Limit of detection* ***(****LOD) for* Cu^{2+}

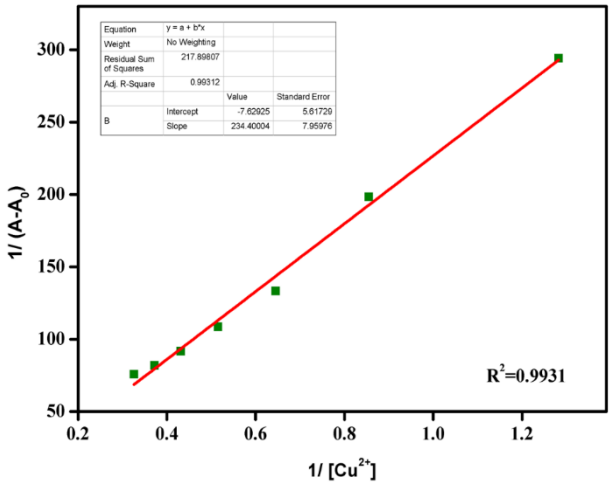

Fig.20 *Benesi-Hildebrand plot of AHN with* Cu^{2+}

Moreover, competitive experiments were carried out both in the presence and absence of metal ions to investigate the selectivity of AHN towards the Cu^{2+} ion. It is evident from **Fig.21a** that AHN exhibits high selectivity with Cu^{2+} in the presence of competing metal ions. Furthermore, the selectivity of AHN towards Cu^{2+} in the presence of anions was investigated. The addition of anions did not

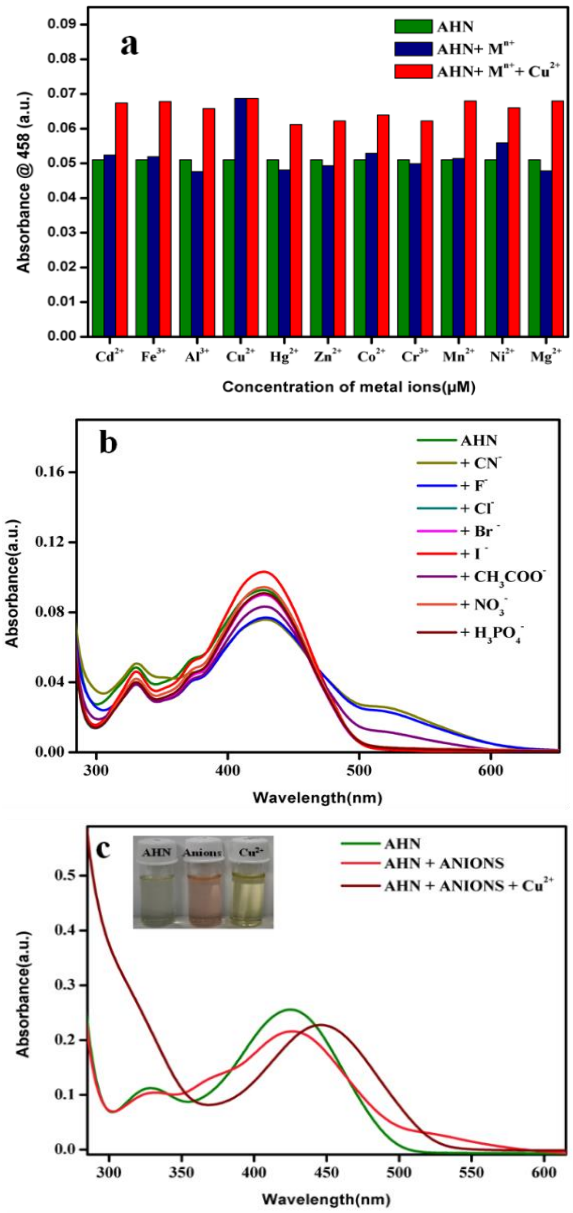

Fig.21 *(**a**) The selectivity of AHN in DMSO (10 μM) towards Cu^{2+}(10 μM) (1 equivalent) in the presence of other metal ions (1 equivalent) (**b**) Sensing ability of AHN with addition of anions (10 μM), (**c**) Selectivity of AHN towards Cu^{2+} in presence of anions*

show any observable change in the absorption spectrum of AHN except for F^-, CN^-, and CH_3COO^- ions. With the addition of F^-, CN^-, and

CH_3COO^- ions absorption peak significantly changed and the colour of the AHN solution shifted from colourless to pink (**Fig.21b**). To prove the selectivity of AHN towards copper, the competing experiments in the presence of F^-, CN^-, and CH_3COO^- ions were also conducted, and the result obtained is shown in **Fig.21c.** As it is clear from **Fig.21c**, that the addition of Cu^{2+} ion to the AHN solution containing a mixture of anions such as F^-, CN^-, and CH_3COO^- ions, results in the change of colour from pale pink to yellow with a significant change in the absorption spectrum profile. Therefore, the results obtained revealed that the absorption spectral response of AHN towards Cu^{2+} is better and is highly useful for the selective detection of Cu^{2+} in aqueous medium.

The reversibility of complexation between AHN and Cu^{2+} was examined by the addition of disodium salt of EDTA to the solution mixture. The addition of EDTA results in the regeneration of the AHN

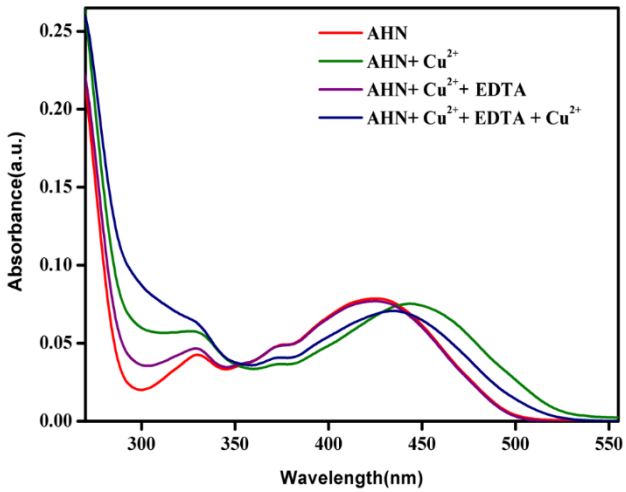

Fig.22 *The reversibility of AHN in DMSO (10μM) towards Cu^{2+} (1 equivalent) in the presence of EDTA (1 equivalent)*

peak at 425nm with a shift of colour from yellow to colourless. Moreover, the AHN-Cu^{2+} peak was further regenerated with the addition of metal salt solution to the same solution mixture (**Fig.22**). This result proves AHN regeneration and its applicability in subsequent sensing analysis.

5.2.4. Application of AHN for the detection of PA and Cu^{2+} in real samples

The practical application of AHN aggregates was investigated by employing the AHN aggregates for the detection of the picric acid in real samples made from natural resources such as well water, tap water, and river water by the standard addition method. The results obtained are presented in Table 2. The recoveries varied in 101-

Table 2 Detection of PA in real samples

Water sample	Added PA (µM)	Found (µM)	Error (%)	Recovery (%)
Well Water	3.94	3.98	1.05	101.01
	5.90	5.98	1.35	101.35
	7.85	7.89	0.50	100.52
Tap Water	3.94	4.01	1.77	101.77
	5.90	6.02	2.03	102.03
	7.85	7.93	1.09	101.01
River Water	3.94	4.05	2.79	102.79
	5.90	6.09	3.22	103.22
	7.85	8.06	2.67	102.67

Table 3 Detection of Cu^{2+} in real samples				
Water sample	**Added Cu^{2+} (μM)**	**Found (μM)**	**Error (%)**	**Recovery (%)**
Well Water	5.90	5.95	0.84	100.84
	7.85	7.91	0.76	100.76
	9.80	9.83	0.30	100.30
Tap Water	5.90	5.98	1.35	101.35
	7.85	7.96	1.40	101.40
	9.80	9.88	0.81	100.81
River Water	5.90	6.03	2.20	102.20
	7.85	8.04	2.42	102.42
	9.80	9.93	1.32	101.32

103% range, which demonstrates the applicability and reliability of AHN aggregates in PA detection. Moreover, the AHN is also employed for the detection of copper in real samples through colourimetric responses and the results obtained are presented in Table 3. The recoveries varied in 100 - 102% range, which demonstrates the applicability of AHN for Cu^{2+} detection.

5.2.5 AHN aggregate-coated test strips

The on-site detection of PA has great attention and hence this method has been extended to the development of a paper sensor for PA. To explore this, we have prepared a TLC plate coated with AHN aggregates and PA solution dropped onto the test plate. The changes obtained are depicted in **Fig.23**. These changes in the emission

colour can be easily visualized when exposed to UV light with naked eye. So, this method can be well extended to the development of paper strip sensors for PA with excellent sensitivity.

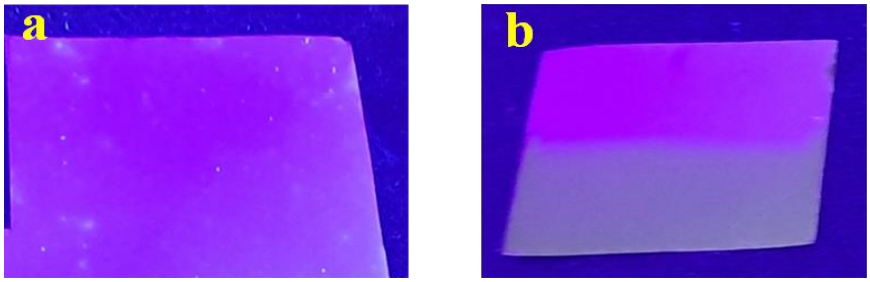

Fig. 23 *Test strips of TLC plate (**a**) coated with AHN aggregate only (10 μM) and (**b**) AHN aggregate dropped with PA solution under UV light*

5.3 Conclusions

A novel chemosensor (AHN) with dual functionality has been designed and synthesized. The AIEE activity of AHN has been explored for the selective detection of PA through a fluorescence switch-off response (fluorescence probe) and serving as a colourimetric sensor for selective detection of Cu^{2+} (colourimetric probe) among other biologically and environmentally important metal cations. The AHN aggregate exhibited a fluorescence switch-off response to PA with a detection limit of 2.45μM, resulting from ground-state complexation between the electron-rich fluorescent aggregates of AHN and electron-deficient PA through π-π interactions and intramolecular hydrogen bonding interactions, as determined from a Stern-Volmer plot with a quenching constant of $6.21\times10^{7}M^{-1}$. The ligand, AHN additionally displayed selectivity for Cu^{2+} with a distinct colour change from colourless to yellow with a 2:1 stoichiometry, alleging a low limit of detection for Cu^{2+} at

3.16μM, significantly below the acceptable limit recommended by the WHO.

References

1. Wang, F., et al., *A new rhodamine derivative bearing benzothiazole and thiocarbonyl moieties as a highly selective fluorescent and colorimetric chemodosimeter for Hg2+.* Sensors and Actuators B: Chemical, 2012. **161**(1): p. 948-953.
2. Liu, Y., et al., *A naphthalimide–rhodamine ratiometric fluorescent probe for Hg2+ based on fluorescence resonance energy transfer.* Dyes and pigments, 2012. **92**(3): p. 909-915.
3. Arshad, M., A. Paul, and A. Joseph, *Nanoscale detection of copper using an aggregation induced emission enhancement fluorescent sensor derived from hydroxy naphthaldehyde and benzyloxy benzaldehyde.* Journal of Photochemistry and Photobiology A: Chemistry, 2023: p. 114983.
4. Arshad, M., et al., *Successive detection of bivalent zinc and picric acid using an organo-fluorescent sensor derived from 2-hydroxy-1-naphthaldehyde.* Sensors and Actuators A: Physical, 2023. **358**: p. 114418.
5. Kathiravan, A., et al., *Pyrene Schiff base: photophysics, aggregation induced emission, and antimicrobial properties.* The Journal of Physical Chemistry B, 2014. **118**(47): p. 13573-13581.
6. Zhao, J.-S., et al., *Memory of chirality in J-type aggregates of an achiral perylene dianhydride dye created in a chiral asymmetric catalytic synthesis.* Chemical Science, 2011. **2**(5): p. 937-944.
7. Irshad, H., et al., *AIEE active J-aggregates of naphthalimide based fluorescent probe for detection of Nitrobenzene: Combined experimental and theoretical approaches for Non-covalent interaction analysis.* Spectrochimica Acta Part A: Molecular and Biomolecular Spectroscopy, 2023. **290**: p. 122273.
8. Soufeena, P., T. Nibila, and K. Aravindakshan, *Coumarin based yellow emissive AIEE active probe: A colorimetric sensor for Cu2+ and fluorescent sensor for picric acid.* Spectrochimica Acta Part A: Molecular and Biomolecular Spectroscopy, 2019. **223**: p. 117201.
9. Maity, S., et al., *Aggregation induced emission enhancement from antipyrine-based schiff base and its selective sensing towards picric acid.* Sensors and Actuators B: Chemical, 2017. **248**: p. 223-233.
10. Ding, A., et al., *Complex-formation-enhanced fluorescence quenching effect for efficient detection of picric acid.* Chemistry–A European Journal, 2014. **20**(38): p. 12215-12222.

11. Dey, S., et al., *An antipyrine based fluorescence "turn-on" dual sensor for Zn 2+ and Al 3+ and its selective fluorescence "turn-off" sensing towards 2, 4, 6-trinitrophenol (TNP) in the aggregated state.* Photochemical & Photobiological Sciences, 2019. **18**: p. 2717-2729.
12. Moral, R., O.A. Pegu, and G. Das, *Probing the aggregation potential and picric acid recognition aptitude by altering aromatic core substitution in a series of cinnamaldehyde-based receptors.* Dyes and Pigments, 2023. **218**: p. 111502.
13. Rahman, Z., et al., *A 4-aminophthalimide derive smart molecule for sequential detection of aluminum ions and picric acid.* Journal of Photochemistry and Photobiology A: Chemistry, 2023. **439**: p. 114593.
14. Ghosh, S., N. Baildya, and K. Ghosh, *A new 1, 2, 3-triazole-decorated imino-phenol: selective sensing of Zn 2+, Cu 2+ and picric acid under different experimental conditions.* New Journal of Chemistry, 2021. **45**(24): p. 10923-10929.
15. Halder, S., et al., *A quinoline-based compound for explosive 2, 4, 6-trinitrophenol sensing: experimental and DFT-D3 studies.* New Journal of Chemistry, 2018. **42**(11): p. 8408-8414.
16. Zhao, D. and T.M. Swager, *Sensory responses in solution vs solid state: a fluorescence quenching study of poly (iptycenebutadiynylene) s.* Macromolecules, 2005. **38**(22): p. 9377-9384.
17. Waseem, M.T., et al., *Fluorene based fluorescent and colorimetric sensors for ultrasensitive detection of nitroaromatics in aqueous medium.* Journal of Photochemistry and Photobiology A: Chemistry, 2022. **425**: p. 113660.
18. Majeed, S., et al., *Mechanochromic and AIE active fluorescent probes for solution and vapor phase detection of picric acid: Application of logic gate.* Journal of Photochemistry and Photobiology A: Chemistry, 2022. **432**: p. 114057.
19. Ma, X., et al., *Solvent controlled sugar–rhodamine fluorescence sensor for Cu 2+ detection.* Analyst, 2012. **137**(6): p. 1436-1439.

Sensors & Actuators: A. Physical 364 (2023) 114787

Contents lists available at ScienceDirect

Sensors and Actuators: A. Physical

journal homepage: www.journals.elsevier.com/sensors-and-actuators-a-physical

Exploring the dual sensing properties of an anthraldehyde based Schiff base for the successive determination of picric acid using AIEEF and copper using colorimetric methods

Muhammed Arshad, Athira Ajayan, Abraham Joseph *

Department of Chemistry, University of Calicut, Calicut University, P O 673635, India

ARTICLE INFO

Keywords:
Aggregation induced emission
Picric acid
Bivalent copper
WHO

ABSTRACT

A novel and lucid Schiff base, designated as AHN, exhibiting multiple analytical responses comprising AIEE (Aggregation Induced Emission Enhancement) and colorimetric activity towards distinct analytes has been designed and synthesized. The probe, AHN, effectively leverages AIEE activity to selectively detect picric acid (PA) on behalf of fluorescence switch-off response amidst other nitro chemicals. Additionally, it offers remarkable colorimetric selectivity to bivalent copper ions (Cu^{2+}) via a distinct colour change from colourless to yellow. The multi-response characteristics of AHN propel its practicality for naked-eye detection of these analytes. The addition of PA to the aggregate of AHN in DMSO with a 90% water fraction induces a quenching in the fluorescence intensity of the AHN aggregate and the limit of detection of PA was found to be 24.5×10^{-7} M with a quenching constant value of 6.21×10^{7} M^{-1}. Stern Volmer plots and lifetime measurements, clearly indicate that both static and dynamic processes were involved in the quenching mechanism. It is also evident that ground-state complexation between electron-rich fluorescent aggregates of AHN and electron-deficient PA takes place through π-π interactions and intramolecular hydrogen bonding interactions. Further, AHN in DMSO exhibits a selective colorimetric response to bivalent copper among various metal ions with a detection limit of 3.16 μM which is substantially below the permitted limit recommended by WHO in drinking water. The mechanism of colorimetric response is the complexation of AHN with Cu^{2+} in the 2:1 stoichiometry, as confirmed by Job's plot method. Consequently, the versatility of probe AHN in detecting PA and Cu^{2+} through distinct mechanisms fosters its significance in the field of sensing and opens promising avenues for practical sensing applications.

1. Introduction

Simultaneous detection of multiple target ions using facile chemosensors has garnered great attention on account of their simplicity and it has often succeeded in triumphing over the difficulties of employing multiple indicators by one-to-one analysis. Among the array of sensing methods, fluorescence, and colorimetric approaches have captivated considerable interest owing to their numerous advantages, such as simplicity, selectivity, visual detectability, non-destructive nature, cost-effectiveness, and quick real-time monitoring capabilities, making them highly sought-after in realm of sensing[1–4].

Picric acid (PA), an aromatic nitro compound of paramount significance, finds extensive applications in the dye industry, pharmaceuticals, and chemical laboratories, in addition to its crucial role in the manufacturing of explosives, rocket fuel, and propellants[5–7]. However, its explosive nature and widespread application contribute to innate risks and environmental pollution[8–11]. Prolonged exposure to PA can lead to acute health effects such as cyanosis, aplastic anaemia, liver damage, gastritis, and skin and eye irritation, while its high solubility in water and electron-accepting properties create challenges for its degradation, resulting in soil and water contaminations [12–15]. Regarding these concerns, there is an imminent need for selective detectors capable of accurately identifying PA. The existing methods employed for detecting aromatic nitro compounds rely on chromatography coupled with energy-dispersive X-ray diffraction [16,17], surface-enhanced Raman spectroscopy[18], mass spectrometry[19,20], nuclear quadruple resonance spectroscopy [21], etc., entail high costs, necessitate specialized technical expertise, and can only be operated by trained personnel, posing limitations to their widespread accessibility. There are also fluorescence-based detection approaches employing

* Corresponding author.
E-mail address: abrahamjoseph@uoc.ac.in (A. Joseph).

https://doi.org/10.1016/j.sna.2023.114787
Received 18 August 2023; Received in revised form 19 October 2023; Accepted 29 October 2023
Available online 31 October 2023

Summary and future outlook

In this piece of work, three Schiff base receptors PMB3, BBHN, and AHN have been designed and synthesized, and their chemosensing activity has been investigated using colourimetric and fluorometric techniques in the presence of different analytes. The efficient and simultaneous detection of multiple target ions with a single sensor molecule having different characteristics would be more attractive and less expensive than a one-to-one analysis. This novel feature is the highlight of this work. The Schiff bases synthesized are possessing different characteristics and thus can be utilized for the detection of various analytes.

The Schiff base PMB3 acts as an organo-fluorescent sensor for successive detection of bivalent Zinc and Picric acid through an "OFF-ON-OFF" response. The PMB3 exhibits a significant emission enhancement in intensity with Zn^{2+} with a limit of detection of 11.12×10^{-7}M, however, the intensity of emission of the *in-situ* produced complex PMB3-Zn^{2+} ensemble is quenched selectively upon the progressive addition of PA with a detection limit of 42.4×10^{-15}M. PMB3 has shown AIEE characteristics which are applied for the detection of Cu^{2+} with a detection limit of 16.08 fM and picric acid (PA) with a detection limit of 2.43μM. PMB3, exhibited a sensitive colourimetric response to Cu^{2+} and Ni^{2+} ions too among other competing metal ions with a detection limits of 4.56μM and 2.68μM.

Schiff base BBHN possesses AIEE characteristics and is applied for the selective fluorescence "Turn off" sensing studies for copper and PA with a detection limit of 35.52 nM and 4.04μM. The fluorescence quenching behaviour of BBHN in the presence of Cu^{2+} ions take place through dynamic quenching whereas the fluorescence "Turn off" response in the presence of PA is mainly due to π-π interactions, and non-covalent hydrogen bonding interactions.

Schiff base AHN, exhibiting multiple analytical responses comprising AIEE and colourimetric activity towards distinct analytes. The probe AHN with AIEE property acts as a fluorescent sensor for the selective detection of PA through fluorescence switch-off response with a detection limit of 2.45μM and as a colourimetric sensor for Cu^{2+} in aqueous medium with a detection limit of 3.16μM through a change in colour from colourless to yellow.

SCOPE FOR FUTURE WORK

The current investigation focussed only on the designing and synthesis of three novel Schiff base ligands that have great potential for use in environmental applications. Our research revealed a number of interesting directions for further investigation, such as:

1. Metal-organic frameworks functionalized with Schiff bases can act as effective adsorbent for the removal of heavy metals from water. This method of heavy metal removal is more energy-efficient and cost-effective technique. This method has many advantages including low cost, ease of use, quick separation, and simple recycling of adsorbents and hence is to be explored.

2. Metal complexes of Schiff bases can act as effective catalyst which enhances the yield and selectivity of the different chemical processes. Schiff base metallo-systems can attract industry because of their high efficiency, excellent selectivity, mild reaction conditions, reusability, and simple operation conditions.

3. Metal complexes of these Schiff bases do offer anti-corrosive properties and hence can be used as corrosion inhibitors and for coating purposes with polymer support to prevent metal corrosion.

4. Schiff bases and their complexes find lots of applications in the field of medicinal chemistry and pharmaceutical chemistry as potential metallodrug, anticancer drugs, DNA cleavage agents, therapeutics sensors, enzyme mimics, artificial enzyme cofactors, etc. and hence is to be explored.

5. Schiff bases with optical properties can be used for the development of optoelectronic devices (OLED and thin film organic solar cells) and photonic devices since they provide cheaper and simpler routes to optoelectronic materials and hence open new avenues.

6. Entrapping of polymeric Schiff bases with metal oxide nanoparticles will serve as a good candidate for the removal dye and other pollutants and hence may open new environmental remediation strategies.

List of publications

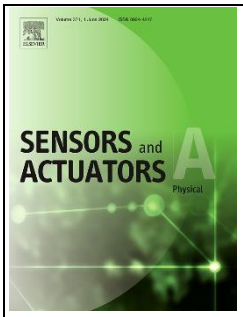	**Muhammed Arshad**, Athira Ajayan, Vismaya Joseph, Abraham Joseph. Highly sensitive detection of copper in aqueous media using a fluorescent probe developed from Isophthaldehyde and (E)-1-(hydrazonomethyl) naphthlen-2-ol, **Sensors and ActuatorsA:Physical,2024,**115436.https://doi.org/10.1016/j.sna.2024.115436.
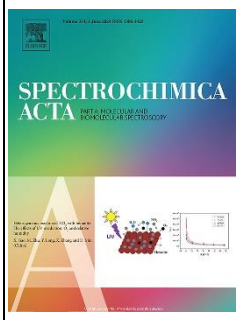	**Muhammed Arshad**, Soumya P, Anila Paul, Abraham Joseph. Sensing of picric acid using an AIEE active "Turn Off" fluorescent probe derived from hydroxy naphthaldehyde and benzyloxy benzaldehyde. **Spectrochimica Acta Part A: Molecular and Biomolecular Spectroscopy 2024**,305,123465. https://doi.org/10.1016/j.saa.2023.123465.
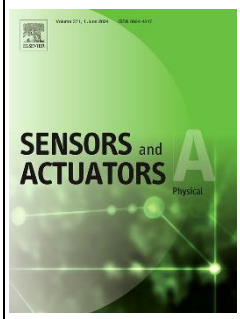	**Muhammed Arshad**, Athira Ajayan, Abraham Joseph. Exploring the dual sensing properties of an anthraldehyde based Schiff base for the successive determination of picric acid using AIEEF and copper using colorimetric methods. **Sensors and Actuators A:Physical 2023**,364,114787. https://doi.org/10.1016/j.sna.2023.114787.
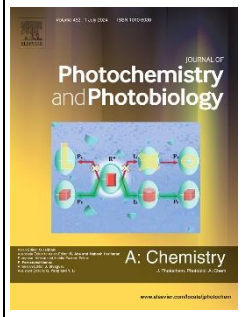	**Muhammed Arshad**, Anila Paul, Abraham Joseph. Nanoscale detection of copper using an aggregation induced emission enhancement fluorescent sensor derived from hydroxy naphthaldehyde and benzyloxy benzaldehyde. **Journal of Photochemistry and Photobiology A: Chemistry 2023**,444,114983. https://doi.org/10.1016/j.jphotochem.2023.114983

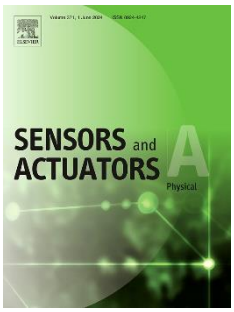	**Muhammed Arshad**, A.T. Jeejarani, Athira Ajayan, C.D. Sebastian, Abraham Joseph. Successive detection of bivalent zinc and picric acid using an organo-fluorescent sensor derived from 2-hydroxy-1- naphthaldehyde. **Sensors and Actuators A: Physical 2023**, 358, 114418. https://doi.org/10.1016/j.sna.2023.114418
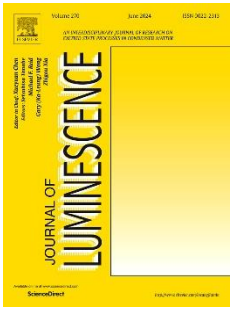	**Muhammed Arshad,** A.T. Jeejarani, Vismaya Joseph, Abraham Joseph**.** Selective detection of picric acid in aqueous medium using a novel naphthaldehyde-based aggregation induced emission enhancement (AIEE) active "turn-off" fluorescent sensor. **Journal of Luminescence 2023**, 258,119818. https://doi.org/10.1016/j.jlumin.2023.119818
	**Muhammed Arshad,** Linda Williams, Athira Ajayan, Abraham Joseph. 2-hydroxy-1-Naphthaldehyde Based Colorimetric Probe for the Simultaneous Detection of Bivalent Copper and Nickel with High Sensitivity and Selectivity. **Journal of Fluorescence 2024**. https://doi.org/10.1007/s10895-024-03895-3

List of other publications

	AT Jeeja Rani, **Muhammed Arshad**, Mathew Kuruvilla & Abraham Joseph. Computational modelling and correlation of physical parameters of 1-heptatriacotanol, phytol and 3, 7, 11, 15-tetra methyl-2-hexadecen-1-ol with the corrosion inhibition efficiency of CIW for mild steel in HCl. **Corrosion Engineering, Science and Technology 2023**,58(3),243-258. https://doi.org/10.1080/1478422X.2023.2165238
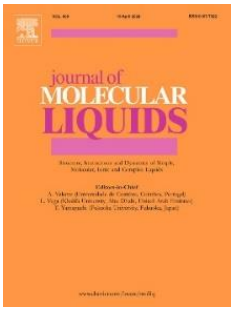	Jeeja Rani, A. T, Asha Thomas, **Muhammed Arshad**, M.; Joseph, A. The influence of aqueous and alcoholic extracts of Garcinia cambogia fruit rind in the management of mild steel corrosion in hydrochloric acid: Theoretical and electroanalytical studies. **Journal of Molecular Liquids 2022,** 346, 117873. https://doi.org/10.1016/j.molliq.2021.117873.
	Jeeja Rani A.T, Asha Thomas, Mathew Kuruvilla, **Muhammed Arshad**, Abraham Joseph. The co-adsorption of thymohydroquinone dimethyl ether (THQ) and coumarin present in the aqueous extract of Ayapana triplinervis on mild steel and its protection in hydrochloric acid up to 323 K: computational and physicochemical studies. **RSC Advances.2022**,12,14328-14341. https://doi.org/10.1039/D2RA02109A.

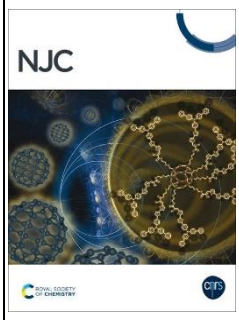	Linda Williams, **Muhammed Arshad**, Jeeja Rani A.T, Abraham Joseph. Biogenic MnO2 nanoparticles derived from a Cedrus deodara pine needle extract and their composites with polyaniline/activated charcoal as an electrode material for supercapacitor applications. **New J. Chem.2022**,46,4325-4333. https://doi.org/10.1039/D1NJ05380A
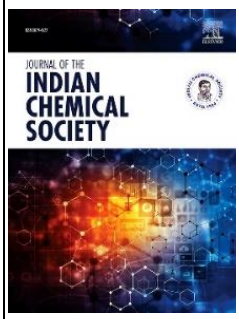	Shamsheera K. O, Anupama R Prasad, **Muhammed Arshad**, Abraham Joseph. A sustainable method of mitigating acid corrosion of mild steel using jackfruit pectin (JP) as green inhibitor: Theoretical and electrochemical studies. **Journal of the Indian ChemicalSociety.2021**,99. https://doi.org/10.1016/j.jics.2021.100271

List of presentations

1. Aggregation-Induced Emission Enhancement (AIEE) fluorescent probe for the nanoscale detection of copper, derived from 2-hydroxy-1-naphthaldehyde and benzyloxybenzaldehyde. ***National Seminar, Frontiers in Chemical Science (FCS 2024***) organised by the department of chemistry, university of Calicut during 13th-15th February 2024.
2. Successive detection of Zn^{2+} and PA using Fluorescent Sensor derived from 2-hydroxy-1- naphthaldehyde. ***International Conference on Advanced Materials for Sustainability (ICAMS 2023)*** organized by the School of Physical Science, University of Calicut during 21th-23rd December, 2023. **Secured best poster award**.
3. Synthesis, characterization and sensing applications of naphthaldehyde based dithiosemicarbazone. ***National Conference Emerging Frontiers in Chemical Science (EFCS-2020)*** organised by the department of chemistry, Farook college (Autonomous) during 4-5, December 2020. **Secured best paper award (oral)**.